COLLEGE SCIENCES
DOCTORAL DE L'INGENIERIE
PAYS DE LA LOIRE ET DES SYSTEMES

Nantes Université

THESE DE DOCTORAT

NANTES UNIVERSITE

ECOLE DOCTORALE N° 602
Sciences de l'Ingénierie et des Systèmes
Spécialité : *Energétique-Thermique-Combustion*

Par
Luc AMEDEWOVO

Study of Thermoplastic Matrix Composites Deconsolidation Phenomenon by Considering the Consolidation Process

Thèse présentée et soutenue à Nantes Université, le 18 Avril 2023
Unité de recherche : Laboratoire de Thermique et Energie de Nantes (LTEN), UMR 6607
IRT Jules Verne

Rapporteurs :

Xavier Colin	Professeur, Laboratoire PIMM, ENSAM Paris
Julien Bruchon	Professeur, Laboratoire Georges Friedel, MINES Saint-Etienne

Composition du Jury :

Président :	James Kratz	Professeur, Institut des composites de Bristol, Univ. Bristol, Angleterre
Examinateurs :	Anaïs Barasinski	Enseignante-chercheuse, Laboratoire IPREM, Univ. Pau et Pays de l'Adour
	Basile de Parscau du Plessix	Docteur, IRT Jules Verne
Dir. de thèse :	Steven Le Corre	Professeur, LTeN, Nantes Université
Co-dir. de thèse :	Laurent Orgéas	Directeur de recherche CNRS, 3SR, Univ. Grenoble Alpes
Co-en. de thèse :	Arthur Levy	Maître de conférences, LTeN, Nantes Université

"This page left intentionally blank"

To

my wife, my mother

and

in memory of my father,

Kossi Robert AMEDEWOVO.

"Don't listen to the person who has the answers,
listen to the person who has the questions."

«N'écoutez pas la personne qui a les réponses,
écoutez la personne qui a les questions. »

Albert Einstein

REMERCIEMENTS

Les remerciements, cette fameuse partie ni corrigée, ni supervisée mais en même temps la partie la plus lue de ce document. Pour une fois que le manque de rigueur est toléré dans le monde scientifique :) Ok1e remark sur cè fote d'ortograf et tjrs lè mèm kèstion : y serais-je ? Qu'a-t-il dit sur moi, sur elle ou sur lui ? On y va !

18 Avril 2023, 12h00, un Mardi, je viens de finir ma soutenance de thèse de doctorat. Avant de lâcher les démons de l'absurdité, essayons de garder encore un ton sérieux pour un moment. Commençons par remercier les membres du jury.

Je remercie chaleureusement Messieurs Xavier Colin et Julien Bruchon pour avoir accepté la charge d'évaluer mes travaux de thèse puis Mr. James Kratz pour avoir accepté de présider ce jury et Mme. Anaïs Barazinski pour avoir accepté d'y participer. Je vous remercie de l'intérêt que vous avez porté à mes travaux et les discussions riches qu'on a pu avoir durant la soutenance.

Retournons à présent au bercail, l'IRT Jules Verne et le LTEN à Nantes, là où toute la magie s'est opérée. Ouvrons le bal avec Messieurs Steven Le Corre, Arthur Lévy, Basile de Parscau du Plessix et Laurent Orgéas, mes encadrants de thèse. Je vous remercie de m'avoir donné la possibilité de travailler sur un sujet de thèse aussi intéressant. Je tiens à vous exprimer ma profonde gratitude pour votre disponibilité, votre aide, votre forte implication, vos critiques et remarques très constructives qui ont conduit à la bonne réussite de cette thèse. Je peux vous assurer que j'ai beaucoup apprécié nos échanges et dicussions scientifiques. C'était très formateur et très riche. Ce fût un réel plaisir de travailler avec vous !

Parlons maintenant de toutes ces personnes extérieures à ce projet de thèse mais qui d'une certaine manière ont apporté une pierre à l'édifice. Je remercie toute l'équipe SEF du LTEN, en particulier Arnaud, Julien et Nicolas. Merci également à Amandine, Michelle-Anne et Nathalie. Sans vous, mes bancs expérimentaux n'auraient très probablement pas vu le jour. Un grand MERCI pour votre disponibilité sans faille, votre professionnalisme, votre enthousiasme et tout le support que vous apporté aux doctorants tout au long de leur thèse. Je remercie également Julien pour toute l'aide qu'il m'a apporté sur la caractérisation de mon matériau d'étude et Florent pour son aide sur le traitement des images tomographiques. Je n'oublie pas Théo, Rima, Maxime, Violaine ainsi que tous les autres collègues chercheurs, ingénieurs, techniciens, post-doctorants et doctorants avec qui j'ai pu échanger durant cette thèse. Je profite pour adresser mes encouragements aux nouveaux doctorants et ceux qui soutiennent leur thèse prochainement.

Du côté de l'IRT Jules Verne, je remercie Mr. Yannick Amosse ainsi que toute l'équipe Procédés Matériaux Composites (PMC) pour l'accueil et l'intégration. Un grand MERCI à Thomas, l'expert en consolidation de composites, qui m'a initié à l'art de l'habillage thermoplastique. Je remercie également Henry-Pierre, Franck, Alexandre et Thomas pour leur disponibilité et leur aide durant la consolidation de mes plaques. Je n'oublie pas non plus l'équipe SIM, en particulier Yvan pour nos échanges et aussi pour le temps que tu as bien voulu consacrer au modèle thermoméca qui n'a malheureusement pas pu voir le jour dans les temps. Mes remerciements vont ensuite aux Mesdames Nathalie Guerrin, Valérie Donald pour leur disponibilité et support aux doctorants PERFORM.

Je tiens à remercier également l'équipe du 3SR à Grenoble pour leur acceuil, en particulier Clara, François et Antoine pour leur aide sur le traitement de mes images tomo. Merci à Guillaume et Sofiane de la société Novitom pour leur accompagnement durant les essais à l'ESRF et pour la reconstruction des images. Enfin, comme dirait l'autre, le meilleur pour la fin.

Mes pensées vont d'abord à mon Père que j'aurais aimé voir un peu plus longtemps, puis à ma Mère et à ma Femme qui m'ont toujours soutenu. Vous avez toujours été là depuis le début et vous serez encore là même après la fin.

CONTENTS

LIST OF TABLES

List of Figures

LIST OF ABBREVIATIONS

Notation	Description
1SH	one-Sided Heating
2SH	two-Sided Heating
AN	Annealed
AS	Ambient Storage sample
ATP	Automated Tape Placement
CCC	Carbon-Carbon Composite
CF	Carbon Fiber
CFRP	Carbon Fiber-Reinforced Plastic
CFRTP	Carbon Fiber-Reinforced ThermoPlastic
CMC	Ceramic Matrix Composite
CODEC	COmposite DEconsolidation Characterization
CP	Cross-Ply
CT	Computed Tomography
CTE	Coefficient of Thermal Expansion
DS	Dried Sample
DSC	Differential Scanning Calorimetry
DTS	Deconsolidation's Thermal Sensitivity

Notation	Description
DVS	Dynamic Vapor Sorption
FAW	Fiber Areal Weight
FRC	Fiber-Reinforced Composite
GF	Glass Fiber
GFRTP	Glass Fiber-Reinforced ThermoPlastic
HP	Hot Press
HPC	Hot Press Consolidation
ILSS	InterLaminar Shear Strength
InCODETO	*In situ* COmposite DEconsolidation Tomography Observation
IPSS	In-Plane Shear Strength
ISC	*In Situ* Consolidation
MMC	Metal Matrix Composite
NAP	No Applied Pressure
NCF	Non-Crimp Fabrics
NCP	No Counter Pressure
OMICHA	Online Moisture Ingress CHAracterization
OOA	Out Of Autoclave
PA	PolyAmide
PAEK	PolyArylEtherKetone
PAN	PolyAcryloNitrile
PEEK	PolyEtherEtherKetone
PEG	PolyEthylene Glycol

Notation	Description
PEI	PolyEtherImide
PEKK	PolyEtherKetoneKetone
PMC	Polymer Matrix Composite
PP	PolyPropylene
PPS	PolyPhenylene Sulfide
PRC	Particle-Reinforced Composite
QI	Quasi Isotropic
RGA	Residual Gas Analysis
RH	Relative Humidity
ROI	Region Of Interest
SFT	Stress Free Temperature
T_c	crystallization temperature
T_g	glass transition temperature
TGA	ThermoGravimetric Analysis
T_m	melting temperature
TMA	ThermoMechanical Analysis
TPC	ThermoPlastic Composite
UD	UniDirectional
VBO	Vacuum Bag Only
VBOC	Vacuum Bag Only Consolidation
WI	Water Immersed

"This page left intentionally blank"

CHAPTER 1

INTRODUCTION

Contents

1.1 Background and motivation

CO_2 emissions from commercial aviation have been growing steadily in recent years, approaching 1 billion tons of CO_2 per year [1]. This represents about 2 % of all man-made emissions. Between 2004 and 2022 (before COVID[1]), the sector's emissions have increased by almost 50 % [1]. In a context of growing activity in the world, these emissions could further increase by more than 50 % in 2050, reaching about 2 billion tons of CO_2 if no action is taken [2]. The main challenge for aviation in next years thus lies in its decarbonization, in order to meet the ecological transition challenges and the expectations of passengers in terms of sustainable mobility. With this in mind, the aircraft industry and airlines companies decided to take the bull by the horns several years ago by committing to reduce their contribution to global warming, with an extremely ambitious goal for 2050: to halve the sector's carbon emissions compared to 2005, *i.e.* net zero emissions (balance between the amount of greenhouse gas produced and the amount removed from the atmosphere).

In addition to Sustainable Aviation Fuels (SAFs) or new engine and aircraft technologies, weight reduction is a non negligible factor in reducing fuel consumption and CO_2 emissions. This has led to an increased popularity (despite their generally high cost) of *composite materials* in high-performance products that need to be lightweight. Compared to the more conventional materials such as aluminum or titanium alloys, composite materials have better specific properties (ratio between mechanical properties and density). The continuous improvement of the composite components (matrix and reinforcement) resulted in high-performance composite materials with improved thermo-mechanical properties and chemical resistance able to replace the conventional materials in primary structures. This is reflected in the latest generation of aircraft such as the Airbus A350 XWB [3] and Boeing 787 Dreamliner [4] in which half of the total weight is made of composite materials.

In addition to the environmental aspect, the use of composite materials also has a significant economic benefit. For instance, assembly costs can account for up to 50 % of the cost of an airframe. Composites offer the opportunity to significantly reduce the amount of assembly labor and fasteners because detail parts can be combined into a single mold assembly [5]. Moreover, composites do not corrode and their fatigue resistance is outstanding. Corrosion of aluminum alloys is a major cost and a constant

[1] COVID is an epidemic that the world experienced towards the end of 2019 and is ongoing to this date.

maintenance problem for commercial aircraft. The corrosion resistance of composites can thus result in major savings in maintenance costs. However, composites have high raw material costs and usually high manufacturing and assembly costs. Consequently, to meet the growing demand for composite materials, their manufacturing processes must be optimized by reducing cycle times, energy costs, *etc.*

1.2 Thermoplastic composites for structural aircraft applications

Composite materials, especially Carbon Fiber-Reinforced Plastics (CFRPs) are classified into two categories according to the type of polymer matrix (thermoset or thermoplastic). Toughened thermoset epoxies are currently the traditional polymer matrix used in many high-performance structures, particularly for aircraft or aerospace applications. However, there is an increased interest from manufacturers to introduce more ThermoPlastic Composites (TPCs) in the aircraft structures over the past few years. This interest is illustrated by the thermoplastic Multi-Functional Fuselage Demonstrator (MFFD) which is one of the world's largest (8 m $\times$ 4 m) TPC aerostructures, developed within the framework of the Clean Sky 2 STUNNING project led by Airbus [6] (Figure 1.1). In fact, TPCs offer significant advantages in terms of assembly, repairability and automated high-rate manufacturing.

On the one hand, consolidation of thermoset matrix composite parts requires several hours of curing in an autoclave. The consolidated parts are then assembled by adhesive bonding and mechanical assembly (riveting). The adhesive bonding process is time-consuming and require significant surface preparation. Mechanical assembly implies quite long quality control times, since each rivet on the structure has to be checked. It also induces stress concentration zones in the structure that can be a source of crack propagation. Finally, autoclave consolidation is very energy-consuming.

On the other hand, TPCs does not require lengthy cure schedules as thermoset matrix composites, allowing to reduce consolidation times. Instead, they can be reheated and reprocessed in short cycles repeatedly without significant degradation of their properties. This has lead to the development of rapid (few minutes) Out Of Autoclave (OOA) consolidation processes, such as thermostamping, *In Situ* Consolidation (ISC) and Vacuum Bag Only Consolidation (VBOC). Moreover, the reversible thermal behavior of TPCs enables fastener and adhesive-free joining methods that rely on

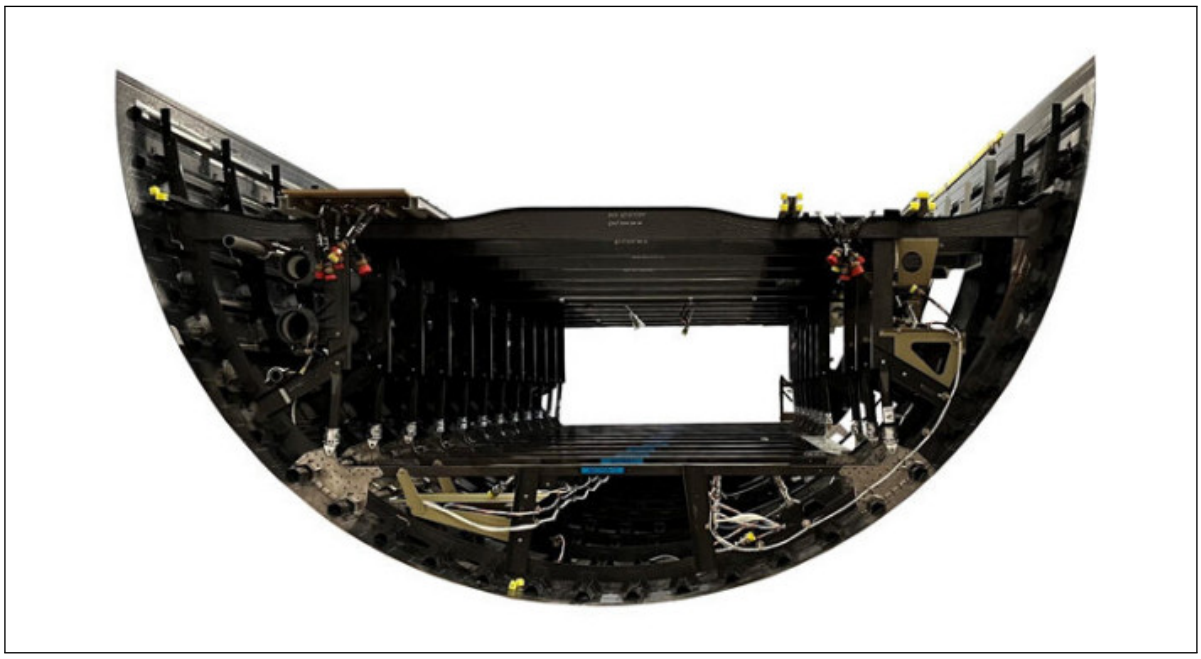

Figure 1.1: Clean Sky 2 thermoplastic Multi-Functional Fuselage Demonstrator (MFFD) [6].

fusion bonding, such as overmolding and induction, resistance or ultrasonic welding. Another advantages of TPCs are their unlimited shelf life at room temperature, a high fracture toughness, a good chemical resistance, and a possible recyclability. However, high-performance thermoplastics are very expensive materials compared to most thermoset such as epoxies and polyesters. Processing of high-performance TPCs also requires high temperature and pressure due to their high melt viscosity, leading to a higher tooling costs. Consequently, to enable a transition from the use of thermoset matrix composites to high-performance TPCs, the production costs of TPCs must be reduced.

Most consolidation processes for high-performance TPCs are still undergoing development. Thermo-stamping of parts with complex geometry is not yet fully mastered. ISC is not totally mastered yet and often requires subsequent consolidation step in autoclave. Consolidation of thick parts by VBOC is also under investigations. Regarding welding which represents the major benefit of TPCs, most welding processes are not yet mature enough for industrialization. However, several research and development efforts are devoted to achieve a good mastering of high-rate manufacturing of TPCs, in particular the welding processes.

1.3 Deconsolidation issue

TPC laminates post-processing (shaping or welding) includes re-heating, re-consolidation and cooling. During the first stage, pre-consolidated laminates are re-heated above their melting temperature (T_m). The re-heating can be *global* (thermostamping or co-consolidation), or *localized* only at the weld interface (welding). During re-consolidation, counter pressure is applied to shape the composite or to provide intimate contact at the weld interface. The composite parts are then cooled to freeze their condition. Although the principle looks simple, the applicability of TPC laminates post-processing is currently limited by the phenomenon of *deconsolidation*.

Deconsolidation refers to the appearance and growth of pores during re-heating of the laminates. It occurs when no or low counter pressure is applied during re-heating, which is the case for most welding or thermoforming processes. Therefore, it is sometimes necessary to apply a counter pressure of generally unknown value throughout the process, in order to prevent deconsolidation. This significantly complicates the application of thermostamping or welding on thick parts or parts with complex geometry. The problem is that the presence of pores in composites severely degrades their mechanical strength [7–9]. For this reason, parts with a porosity content exceeding a defined threshold (1 % in aerospace) are generally rejected.

1.4 Research objective

Although the deconsolidation issue is well identified industrially, its modeling and the optimal solutions to prevent it are little study today. In order to prevent deconsolidation and optimize the quality of the produced parts, it is necessary to improve our understanding of the causes and mechanisms that govern the phenomenon. The objective of this thesis is thus to provide an in-depth understanding of the physical origin of deconsolidation and its driving mechanisms. In order to achieve this objective, the thermo-mechanical conditions of consolidation and deconsolidation must be carefully controlled and analyzed at the macroscopic (or laminate) and microscopic (or fibers) scales. New experimental techniques will thus be developed in this study to finely characterize the conditions of deconsolidation (temperature, counter pressure, moisture content, heating rate, *etc.*) at macroscopic and microscopic scales. The impact of the manufacturing conditions of the laminates (consolidation process, preconditioning) will also be analyzed to understand the effect of a possible residual

stress redistribution/relaxation on deconsolidation. The investigation will focus on a high-performance TPC used industrially in the aerospace sector. The material used in this thesis is thus a UniDirectional (UD) Carbon Fiber (CF) reinforced PolyEtherKetoneKetone (PEKK) prepreg tape with a Fiber Areal Weight (FAW) of 194 g/m^2 and a theoretical thickness of 0.185 mm, provided by Toray Advanced Composites.

This research work was funded by the french Institute of Technological Research (IRT) Jules Verne in the framework of the fundamental research and resourcing on manufacturing program (PERFORM in french). This program allows manufacturers in the aircraft sector in particular, to initiate and follow thesis projects through IRT Jules Verne. This thesis, for example, has been followed by manufacturers such as Airbus and Safran.

1.5 Outline

Chapter 2 synthesizes the basic but fundamental knowledge on the processing of prepreg-based TPCs. It is mainly intended for non-initiated on the processing of TPCs for a better understanding of the physical phenomena further discussed in the other chapters. This chapter introduces in a first time the basic concepts of composite materials (definition, role of reinforcements and matrix, manufacturing techniques of TPCs, *etc.*). It then deals with the physical mechanisms occurring during the laminates consolidation and leading to the formation of *residual stresses* in the composite. It briefly introduces the deconsolidation phenomenon and its detrimental impact on the composites mechanical properties.

Chapter 3 reviews our current knowledge of deconsolidation based on studies performed in the literature. It first discusses the hypotheses on the physical origin of deconsolidation and the existing models to predict the phenomenon. It then describes the different techniques used to characterize deconsolidation in order to determine the most suitable for the needs of this work. Finally, it ends with a positioning of the thesis in relation to the literature and describes the methodology adopted to achieve the objectives.

Chapters 4 to 7 present the results of the different experimental investigations carried out in this work. Each chapter is reproduced from a scientific research paper. This means that these chapters can be read independently, while each part is integrated into a more global view of this work. Consequently, some major elements are repeated

throughout the chapters, for which the author apologizes beforehand. In the bibliographic chapters 2 and 3 mentioned earlier, the presence of moisture and/or residual stresses are identified as the main potential origin of deconsolidation.

Chapter 4 thus addresses the characterization of moisture transport in Carbon Fiber-Reinforced ThermoPlastic (CFRTP) laminates. It presents a new ThermoGravimetric Analysis (TGA) device named OMICHA and developed to continuously measure weight variation of large composite samples under controlled and high temperature and/or humid environment. The identified moisture diffusivities of CF/PEKK after sorption and desorption tests at several temperatures are mentioned. A complex dual stage macroscopic diffusive behavior is highlighted, modeled and discussed in this chapter. The results of this first study allowed, on the one hand, to establish the preconditioning strategy of the samples in order to better decouple the effect of moisture from residual stresses. On the other hand, the hygrothermal behavior characterized allows to better understand the contribution of moisture during deconsolidation.

Chapter 5 is devoted to the development of a new experimental technique to characterize *in situ*, deconsolidation at a macroscopic scale. This chapter presents a new ThermoMechanical Analysis (TMA) device named CODEC and developed for online characterization of CFRTP laminates deconsolidation, by continuously measuring the strain of samples with large size (several centimeters) under representative heating conditions. The validation and illustration of the device capability is demonstrated with CF/PEKK laminates. This chapter also highlights the critical importance of *in situ* measurements for a better understanding of the deconsolidation phenomenon.

Chapter 6 aims at understanding the mechanisms involved in the formation of pores at a microscopic scale. It also presents a new device named InCODETO and developed to observe in three dimensions and *in situ* at a microscopic scale, the appearance and growth of pores during the processing of CFRTPs. This chapter analyzes the evolution of the pore morphology, spatial distribution and content before, during and after the deconsolidation of CF/PEKK laminates. The results highlight the contribution of moisture and residual stresses on the micro-structural changes occurring during deconsolidation.

However, the study performed in Chapter 6 does not fully provide insight into the phenomenology of deconsolidation (kinetics, conditions of appearance and collapse). Therefore, a parametric study is carried out in Chapter 7 on the effect of moisture,

residual stresses, pre-consolidation process and processing conditions (counter pressure, heating rate and ply orientation) on deconsolidation, using the CODEC device developed in Chapter 5. The results of this study clearly reveal the phenomenology of deconsolidation in CF/PEKK laminates.

Chapter 8 concludes this manuscript and provides recommendations for future work. A complete description of the deconsolidation phenomenon and the industrial application of this work are provided.

References

[1] IATA. "Carbon dioxide emissions from commercial aviation worldwide from 2004 to 2022 (in million metric tons)." (2023), [Online]. Available: https://www.statista.com/statistics/1186820/co2-emissions-commercial-aviation-worldwide/ (visited on 2023) (cit. on p. 2).

[2] O. Wyman. "Projected CO_2 emissions from the aviation industry between 2022 and 2050, by scenario (in billion metric tons)." (2022), [Online]. Available: https://www.statista.com/statistics/1189613/projected-co2-emission-aviation-worldwide/ (visited on 2023) (cit. on p. 2).

[3] "Airbus A350 Family." (2013), [Online]. Available: https://www.airbus.com/en/products-services/commercial-aircraft/passenger-aircraft/a350-family (visited on 2022) (cit. on p. 2).

[4] "Boeing 787 Family." (2013), [Online]. Available: https://www.boeing.com/commercial/787/by-design/#/advanced-composite-use (visited on 2022) (cit. on p. 2).

[5] F. C. Campbell, *Lightweight materials: understanding the basics*. ASM international, 2012 (cit. on p. 2).

[6] "Multi-Functional Fuselage Demonstrator." (2023), [Online]. Available: https://www.jeccomposites.com/news/the-largest-thermoplastic-aerostructures-successfully-manufactured-as-part-of-the-multi-functional-fuselage-demonstrator-project/ (visited on 2023) (cit. on pp. 3–4).

[7] D. Saenz-Castillo, M. Martín, S. Calvo, F. Rodriguez-Lence, and A. Güemes, "Effect of processing parameters and void content on mechanical properties and NDI of thermoplastic composites," *Composites Part A: Applied Science and Manufacturing*, vol. 121, pp. 308–320, 2019 (cit. on p. 5).

[8] M. L. Costa, S. f. M. De Almeida, and M. C. Rezende, "The influence of porosity on the interlaminar shear strength of carbon/epoxy and carbon/bismaleimide fabric laminates," *Composites Science and Technology*, vol. 61, no. 14, pp. 2101–2108, 2001 (cit. on p. 5).

[9] M. R. Wisnom, T. Reynolds, and N. Gwilliam, "Reduction in interlaminar shear strength by discrete and distributed voids," *Composites Science and Technology*, vol. 56, no. 1, pp. 93–101, 1996 (cit. on p. 5).

"This page left intentionally blank"

CHAPTER 2

SYNTHESIS OF THERMOPLASTIC COMPOSITES PROCESSING FUNDAMENTALS

Contents

This chapter gives an overview of ThermoPlastic Composite (TPC) processing. It reviews the elementary but essential notions to better understand the issue of deconsolidation and the physical phenomena that will be discussed in the next chapters. It also allows to better apprehend the stakes of this research work. The concepts are introduced in a question–answer format. The questions were raised through the author own thought process at the beginning of this research work. This format was inspired from the A. K. Kaw's book on mechanics of composite materials [1].

2.1 Thermoplastic composite materials processing

This section presents TPCs and their processing techniques. First, some basic knowledge on composites in general and on Carbon Fiber-Reinforced ThermoPlastic (CFRTP) in particular are presented, in order to understand the potential of CFRTPs for structural applications in aircraft industry and the challenge of deconsolidation. Second, CFRTPs consolidation techniques are reported. Finally, deconsolidation issue encountered during the shaping or welding of pre-consolidated laminates is briefly introduced.

2.1.1 Composite materials

What is a composite material ?

A composite material can be defined as a combination of two or more non-miscible (but having a strong adhesion capacity) materials, with different properties and distinct boundaries between the components, that results in a single material with better properties than those of the individual components used alone. However, not all the properties and characteristics of the single material are advantageous when composites are made. Some of the properties that can be improved by forming a composite material are: strength, stiffness, corrosion resistance, weight, fatigue life, *etc*. Some of the properties that can be damaged by forming a composite are: fracture toughness, ductility, thermal conductivity, *etc*. Nevertheless, in many cases, the use of composites is more efficient. For each application the advantages and disadvantages should be merely well-weighed. The objective is to create a single material that has the best characteristics needed to suit the design requirements. For example, in aeronautics, the overall mass of the airplanes are significantly reduced, without a decrease of the components stiffness and strength, by replacing the conventional metal alloys with

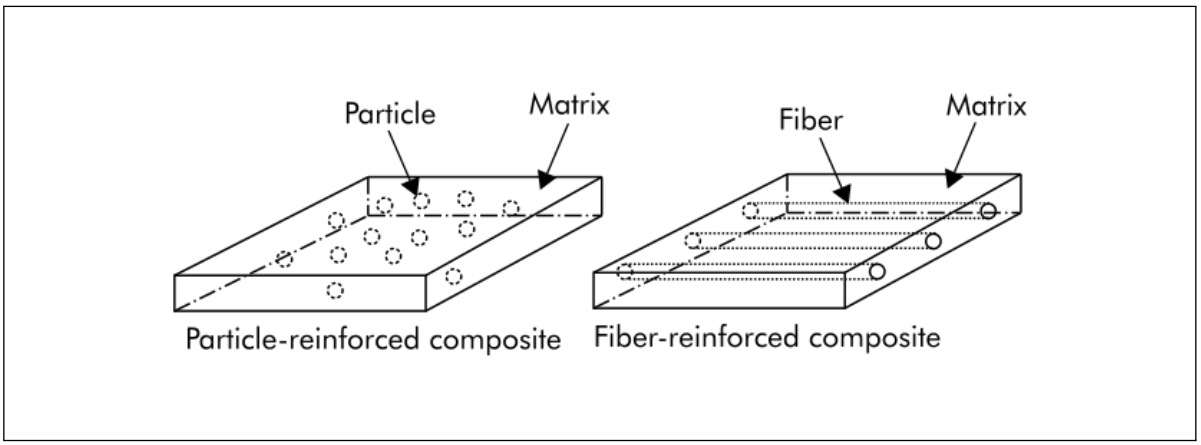

Figure 2.1: Type of composites based on the reinforcement geometry.

composite materials [1]. Given their advantages over metals and other materials group, composites are used in several sectors such as transportation, aerospace, medical, sports, *etc*.

What are the different types of composite materials ?

A composite material is generally made up of two elements: *a reinforcement phase* and *a matrix phase*. Composites are classified by the reinforcement geometry (fiber or particle) or by the matrix type (polymer, metal, ceramic or carbon). According to the reinforcement geometry, one distinguishes *Particle-Reinforced Composites (PRCs)* and *Fiber-Reinforced Composites (FRCs)*. In PRCs, the particles are immersed in matrices such as metallic alloys and ceramics for example (Figure 2.1). These composites are usually *isotropic* because the particles are randomly added and their dimensions are roughly equal in all directions. In FRCs, the matrices are reinforced by *short* (discontinuous) or *long* (continuous) fibers. These type of composites are usually *anistropic* because the fibers length are much greater than their diameter.
According to the matrix type, there are *Polymer Matrix Composites (PMCs)*, *Metal Matrix Composites (MMCs)*, *Ceramic Matrix Composites (CMCs)* and *Carbon-Carbon Composites (CCCs)*. The matrices are generally continuous, homogeneous and isotropic media.

What are the roles of the reinforcement and the matrix ?

Reinforcements are the important component of composites because they contribute the main mechanical strength to the composites. The main function of reinforcements is to carry the load applied to the composite. Thus, they provide the major mechanical

properties to the composites such as stiffness, hardness, fracture toughness, *etc*. The reinforcement can also contribute to improve some physical properties like thermal conductivity, abrasive resistance, electrical properties, *etc*.

The matrix, on the other hand, give the shape to the composite structure. It surrounds and covers the reinforcements. It thus protect the reinforcements from external damage and environnemental attak (humidity, fire, *etc*.). When a composite experiences a certain force, the load is transferred to the reinforcements by the matrix through shear loading at the interfaces. Although matrices by themselves generally have low mechanical properties compared to those of reinforcements, the matrix influences also many mechanical properties of the composite. These properties include transverse modulus and strength, shear modulus and strength, compressive strength, interlaminar shear strength, thermal expansion coefficient, and fatigue strength.

What factors contribute to the mechanical performances of a composite material ?

A composite material mechanical performances depend on a first level on the reinforcement type (fiber or particle) and the matrix type (polymer, metal, *etc*.). According to the fiber type, FRCs produce more high-strength composites than PRCs, in general. In fact, PRCs contain usually less reinforcement due to processing difficulties. Moreover, fibers provide larger contact area with the matrix than particles. In FRCs, the mechanical strength of the composite depend on the fibers material, length, orientation, spatial distribution, and volume fraction. With respect to orientation and length, the fibers can be long (continuous) and aligned parallel to their principal axis in a single direction, or short (discontinuous) and randomly aligned. Continuous fibers provide many benefits over discontinuous fibers such as impact resistance, low shrinkage, and dimensional stability. However, short fibers provide low cost, are easy to work with, and have fast cycle time fabrication procedures. Therefore, continuous fibers composites are used where higher strength and stiffness are required (but at a higher cost), and discontinuous fiber composites are used where cost is the main driver and strength and stiffness are less important [2].

With regard to the fibers volume fraction, a higher volume fraction gives better mechanical properties. However, there is a practical limit. When the fiber content is too high, the amount of matrix is too little to support the fibers effectively and can lead

to poor mechanical performances of the composite. Finally, the material of the fiber directly affects the mechanical performance of the composite. The materials of the fibers are generally expected to have high elastic moduli and strengths.

The composite mechanical performances also depend on the type of matrix used. Polymer matrices have a low strength and stiffness compared to metallic and ceramic matrices. However, they are more easy to process and provide strong adhesion at fiber-matrix interface and a low density to the composite, compared to metals and ceramics. The processing of MMCs, CMCs and CCCs requires higher temperatures and pressures which make them very expensive to manufacture. Their applications are limited in very few industrial sectors such as aerospace, military, transportation and machining. In light of their specific properties, ease of fabrication, and cost, PMCs are the commonly used in the greatest diversity of composite applications, as well as in the largest quantities.

On a second level, the composite material mechanical performances depend on the strong bonding at the matrix-fiber interface because it determines how well the matrix transfers the load to the fibers. The effectiveness of load transfer is one of the most important keys to the proper performance of the composite. The overall composite performances arise, to some extent, from the interaction of both the matrix and the reinforcement. Even, when one component prevails, both components must work together to achieve optimal performances [3].

What is the particularity of high-performance PMCs ?

According to the performance requirements, the PMCs can be divided in two groups, *advanced composites* and *engineering composites*. The main difference between these two groups is the length and type of fiber reinforcement, and the materials properties of the matrix used. The engineering composites are characterized by short fibers with low mechanical properties. Generally, they are made with low-cost polymers. In contrast, the advanced composites are generally characterized by long fibers with high mechanical properties and by high-performance polymers with superior thermal and mechanical properties. Consequently, they cost more than the engineering composites. Advanced composites are the mainly used composites in aerospace and aeronautics structure due to the high mechanical performance requirements. The commonly used

fiber reinforcement in advanced or high-performance PMCs is the *carbon fiber*. Composites made of the combination of the carbon fiber and a polymer matrix are called Carbon Fiber-Reinforced Plastics (CFRPs).

2.1.2 Carbon Fiber Reinforced Plastics (CFRPs) composites

Describe the carbon fiber ?

CFRPs composites consist of a polymer resin reinforced with a carbon fiber as the reinforcement. Carbon fibers are the commonly used reinforcement in high-performance PMCs because they have the highest specific modulus and specific strength of all reinforcing fiber materials [4]. They also retain their high specific properties at elevated temperatures. They are not affected by moisture or a wide variety of solvents, acids, and bases, at room temperature. They have multiple physical characteristics (good thermal conductivity, low thermal expansion, *etc*.) which allow composites incorporating these fibers to have specific engineered properties.
All these high properties come from the internal structure of the carbon fibers. Carbon fibers actually consist of graphite and non-graphitic carbonaceous material. The graphitic phase is in the form of crystallites that can be oriented differently from each other. A graphite structure consists of carbon atoms arranged in a lamellar structure of hexagonal layers (Figure 2.2).

The high specific properties of the carbon fibers are the products of the strong covalent bonds ($\approx 525\,\mathrm{kJ/mol}$) along the basal planes. These covalent bonds are strongly resistant to the tensile force, when the fibers are pulled in tension. Hence, the fiber strength and stiffness increased, as the graphitic phase content is higher and oriented along the fiber principal axis. However, it is important to mention that carbon fibers are extremely anisotropic. The basal planes are held together by weak Van der Waals forces ($\approx 10\,\mathrm{kJ/mol}$). Thus, the transverse strength and modulus of the fiber are much less than the longitudinal values. The carbon fibers manufacturing techniques are relatively complex and will not be discussed. They are generally made from three different organic precursor such as: rayon, PolyAcryloNitrile (PAN) and pitch. The processing techniques and the resultant fiber properties will depend on the precursor used. PAN-based carbon fibers are the predominant type commonly used, accounting for 80 % of the world's total output [5].

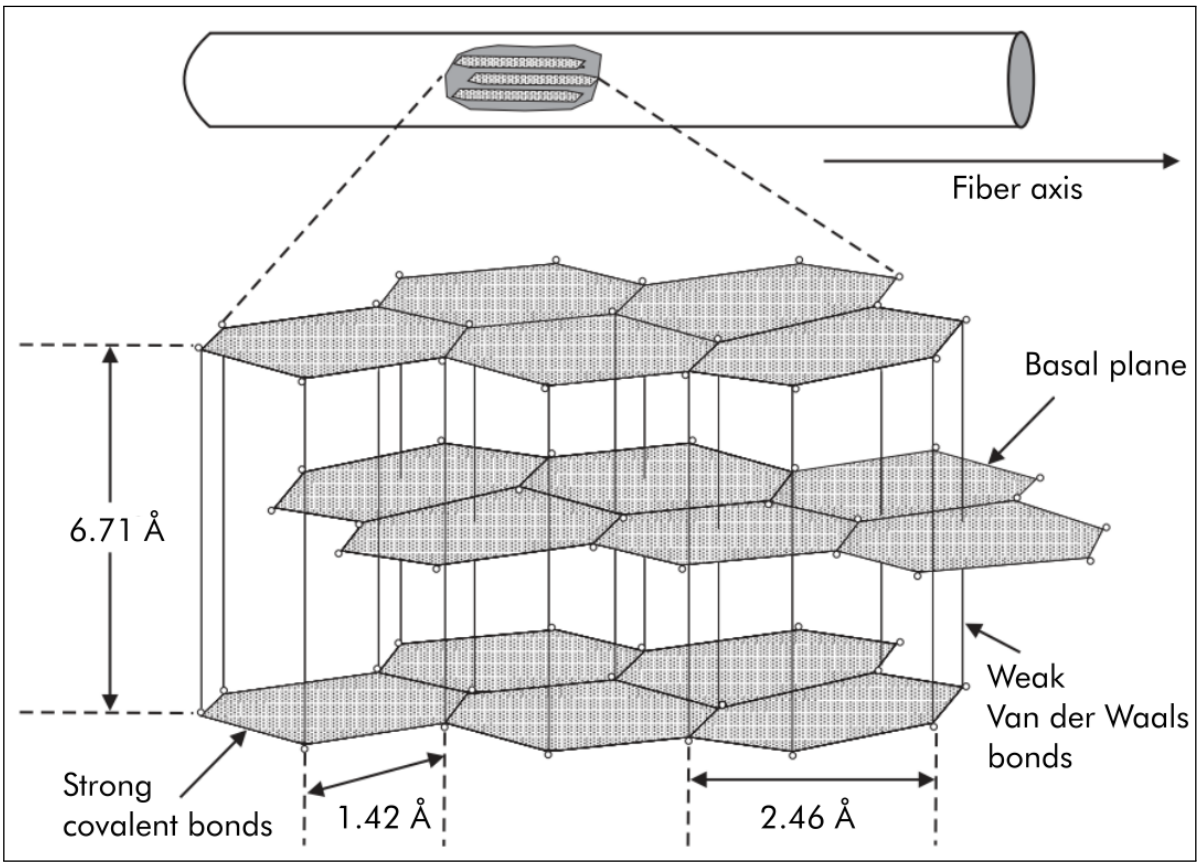

Figure 2.2: Three-dimensional representation of the carbon fiber structure [3].

What is a polymeric material ?

In high-performance CFRPs, the use of a high strength carbon fiber is not enough. The matrix determine the maximum usage temperature, the impact and abrasion resistance, fracture toughness. Therefore, the polymeric material combined with the carbon fiber must also have superior properties. A *polymer* is defined as a macromolecular composed by the assembly of individual molecular units called *monomer* into a chain-like structure where each monomer is like a link in the chain. A *polymeric material* is a collection of a large number of polymer chains of similar chemical structure [6]. The atoms in the polymeric material are held together by different types of bonds: covalent bond, hydrogen bond, dipole interaction, Van der Waals bond and ionic bond. Except the covalent bonds, all the other bonds are known as weak bonds. In the polymeric material, the different polymer chains are generally held together by weak bonds

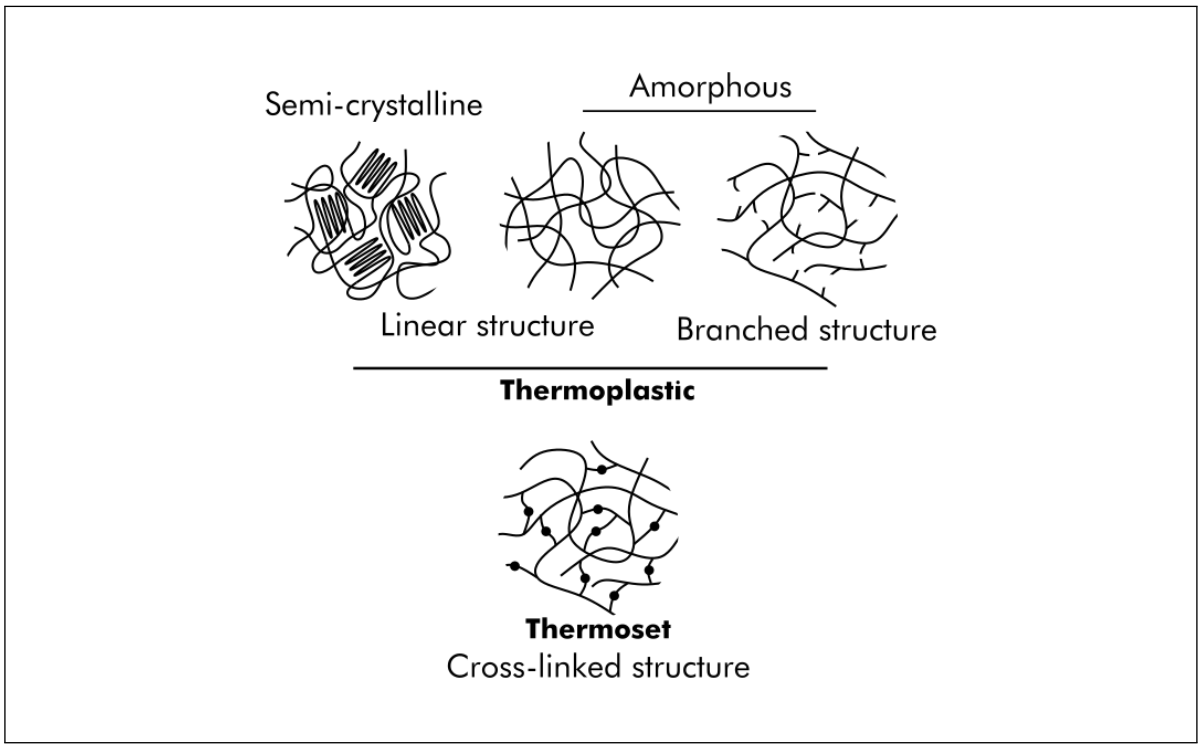

Figure 2.3: Schematic representation of polymer structures.

(intermolecular bonds) while the internal units of the polymer chain are held by relatively strong covalent bonds (intramolecular bonds) [7]. Polymeric materials can have three different structure: linear, branched or cross-linked (Figure 2.3) [8].

The linear structure consists of long chains of connected monomers in a linear fashion. The length of the chain is usually characterized by a quantity called *molecular weight* [3]. The polymer is branched when side chains of the same polymer are attached to the main polymer chain. These side chains form branches along the main polymer chain and are not connect to another polymer chain in the polymeric material. As the length and frequency of the branches increase, the probability that the branches reach from one polymer chain to another increases. The polymer is cross-linked when the polymer chains are linked together through the branches by strong covalent bonds. In a polymeric material, the interactions between the polymer chains determine its behavior during processing.

What polymeric materials are used in CFRPs ?

In composites, polymeric materials also called *resins*, are generally classified in two categories: *thermoplastics* and *thermosets*. In a thermoplastic resin, the linear or branched individual polymer chains are held together by weak bonds (Van der Waals, hydrogen bonds, *etc.*). When the thermoplastic polymer is heated, these weak bonds can be temporarily broken and the polymer chains are free to slide past one another or flow to a new configuration if pressure is applied. On cooling, the polymer chains can be locked in their new configuration and the weak bonds are restored, resulting in a new solid shape. For this reason, thermoplastics can be softened or melted and reshaped many times [6].

According to the structural arrangement of the polymer chains, thermoplastic resins are further subdivided in two groups: *amorphous* thermoplastics and *semi-crystalline* thermoplastics (Figure 2.3). In amorphous thermoplastics, on the one hand, the polymer chains have a more-or-less random, twisted and entangled configuration as in the bowl of cooked spaghetti. During heating, they softened from a solid glassy state to a rubbery state around the glass transition temperature (T_g) range and finally to a viscous state (viscoelastic fluid behavior) as a smooth transition. As they lose their mechanical stability above T_g, the service temperature of amorphous thermoplastics is below T_g and their processing temperature above T_g.

Semi-crystalline thermoplastics, on the other hand are composed of amorphous region (random arrangement) linked to *crystalline* region where the polymer chains have a regular and ordered arrangement. In contrary to amorphous thermoplastics, semi-crystalline thermoplastics retain some of their stiffness above T_g due to the presence of *crystallites* which remain above T_g. Until the crystallites completely melt above the melting temperature (T_m), semi-crystalline thermoplastics exhibit a viscoelastic solid behavior. Hence, the service temperature of semi-crystalline thermoplastics is below T_m and processing temperature above T_m [9]. Thanks to the crystallites present in semi-crystalline thermoplastics, they provide good solvent resistance, higher strength and stiffness than amorphous thermoplastics. Nevertheless, amorphous thermoplastics provide good toughness and impact resistance.

In a thermoset resin, the branched individual polymer chains cross-linked when heat is applied. The chains are then held together by strong covalent bonds. Once the cross-links are formed during the heating or *curing*, the thermoset polymer cannot be

melted by the application of heat; because when the thermal energy is superior to the dissociation energy of the covalent bonds, both the internal units of the polymer chains and the cross-links randomly fail and the polymer degrade. Thus, thermosets cannot be melted and reshaped twice. All post-forming attempts will lead to the structure degradation. Since the thermal energy needed to activate the formation of cross-links during the curing of thermosets is low, the processing temperatures of thermosets are usually lower than thermoplastics ones. The service temperatures of thermoset are also higher than thermoplastics ones because of the cross-linking mechanism irreversibility.

When used as composite matrices, high-performance resins must meet the applications requirements such as processing ability, thermal, physical and mechanical properties. The processing performance includes the resins melting viscosity (flow ability) and change in viscosity behavior (processing windows). The resin thermal properties will determine the service temperature ranges. The resins physical properties such as electrical conductivity, chemical resistance and anti-corrosion properties will determine the service environments. Finally, the maximum loads under service conditions are given by the resins mechanical properties (tensile strength, fracture toughness, impact resistance, *etc.*).
Both thermoset and thermoplastic resins are used in CFRPs. Each resin has its advantages and drawbacks in its use. The majority of CFRPs currently used, in aeronautic structures, contain a thermoset resin as matrix. However, the development of high-performance thermoplastics offers promising possibilities to reverse the trend.

What are the advantages and drawbacks of thermoset and thermoplastic resins ?

Prior to curing, thermoset resins are usually low molecular weight liquid chemicals with a very low viscosity (1 - 10 $Pa \cdot s$). Since the viscosity is very low before processing, it is easy to achieve a good wet-out between the fibers and matrix without high pressure or high temperature. Thermoplastic resins, in contrast, have high viscosity prior to processing (for example 10^3 $Pa \cdot s$ - 10^6 $Pa \cdot s$) [2]. Thus, the coating and wetting of the fibers are much more difficult and require high temperature (260 °C to 400 °C) and high pressure.

Although the curing of thermoset resin require low temperatures (120 °C to 175 °C), the curing reaction can take hours before the resin is fully cross-linked. Processing with thermoplastic resins, in contrast, can be faster (few minutes), since no curing reaction is required. In fact, TPCs only require heating, shaping and cooling.

In terms of mechanical properties, thermoplastic are inherently much tougher than thermosets. However, the toughness exhibit by thermoset today are comparable to that of thermoplastic. In fact, the thermoset resins are now toughened by adding thermoplastics to the thermoset resin. Nevertheless, thermoplastics have higher tensile strain-at-failure, higher impact energy absorption and greater resistance to crack propagation [10].

With respect to thermal and physical properties, thermosets have in general higher T_g than thermoplastics. Due to the presence of cross-links, thermosets have a great thermal stability and good resistance to solvents. They can be used for high temperature applications. However, high-performance semi-crystalline thermoplastics such as PolyEtherEtherKetone (PEEK), PolyEtherKetoneKetone (PEKK) and PolyPhenylene Sulfide (PPS) also have high T_g and good resistance to solvents but they are more expensive than most thermosets, such as epoxies and polyesters. Moreover, high-performance thermoplastics have a low moisture uptake compared to thermosets.

In terms of processability, thermoplastics can be reprocessed in contrary to thermoset which will degrade and eventually char if heated to high enough temperatures. However, Thermoplastics cannot be reprocessed indefinitely. Indeed, the processing temperatures of thermoplastics are often close to the polymer degradation temperature. Thus, many reprocessing will eventually lead to the resin degradation or in some cases, the thermoplastic resin may cross-link.

Other advantages of using thermoplastics is their unlimited storage (shelf) life (before processing) at room temperature compared to thermoset which have a limited storage life and require refrigeration. The use of thermoplastics also offers a number of attractive joining options such as melt fusion, resistance welding, ultrasonic welding, and induction welding, in addition to conventional adhesive bonding and mechanical fastening.

Thermoplastics, therefore, offer many advantages over thermosets in terms of production time, raw material storage time, and recyclability at the end of the composite's life. They also offer better alternatives in terms of assembly and exhibit very good mechanical properties and thermal stability.

What limits the application of TPCs ?

In spite of such distinct advantages of thermoplastics, toughened thermosets are still dominating in aeronautic applications. Several factors limit the application of TPCs. First, the raw material is expensive and the high temperatures and pressures required, to process TPCs, lead to high tooling costs. Second, due to their high melt viscosity, the processing of thermoplastics is difficult. For large structures, the heating step and the pressure required for consolidation become challenging. Press forming processes, for example, are often limited to relatively simple geometric shapes. Finally, the welding of thermoplastics, which is their great potential, is not yet fully mastered. The TPCs welding processes are still facing several issues. Nevertheless, TPCs are still of great interest for future structural composites. However, a better mastering of TPCs processing is required.

2.1.3 ThermoPlastic Composite (TPC) laminates processing

The basic processing steps of TPCs include fiber treatment, combination of fibers with the thermoplastic resin (impregnation) and processing techniques to produce laminates and to form shaped parts.

The raw carbon fiber is chemically inert (non-polar surface, less adsorption characteristics, *etc.*) [11]. This makes difficult to have a strong adhesion between carbon fiber and a polymer resin. The fibers treatment help to promote and improve a good adhesion at the fiber-matrix interface during impregnation processes with polymer resins. As mentioned earlier, a load applied to a composite is transferred to the fibers mainly through shear stresses at the fiber-matrix interface. Thus, strong bonds at the fiber-matrix interface improve the composite strength (transverse tensile strength and interlaminar shear strength). Damage development in the composite is also influenced by the bonding between the fibers and the matrix [10]. Finally, the robustness of the fiber-matrix adhesion depend on the type of interactions at the interfaces.

What are the bonding types at fiber-matrix interface ?

Adhesion mechanisms can be divided into three groups, according to the type of interaction forces in presence: physical, chemical and mechanical (Figure 2.4) [12].

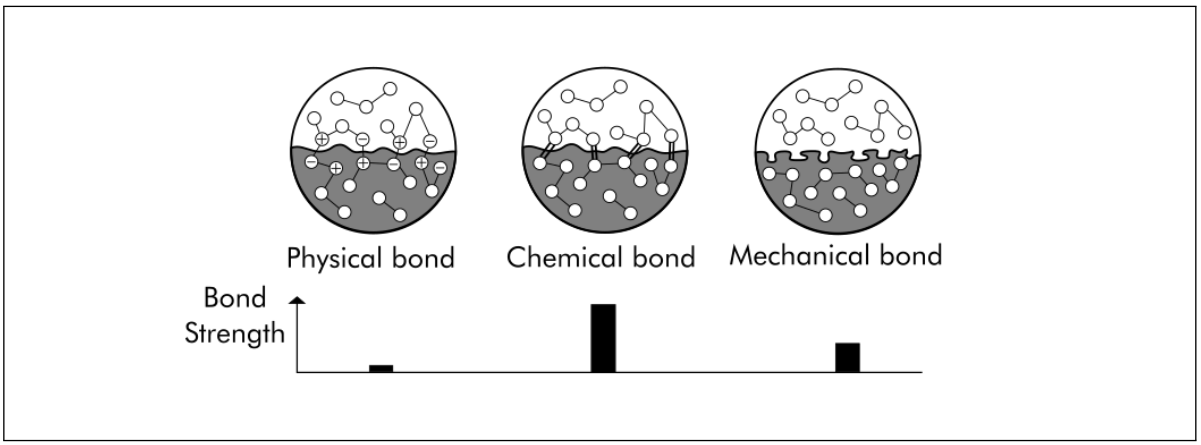

Figure 2.4: Schematic representation of different type of adhesion mechanisms and their bonding strength: physical, chemical and mechanical.

Physical interactions are any bonding involving weak, Van der Walls forces, dipolar interactions and hydrogen bonding. The bond energy is very low in physical bonds ($\approx$ 8 - 16 kJ/mol).

Chemical bonds include all types of covalent, ionic and metallic bonding. They involve transport of atoms or molecules trough diffusion. There are two main types of chemical bonding know as *dissolution bonding* which occurs at an electronic scale (require an intimate contact of both surfaces at an atomic scale) and *reaction bonding* which involve atoms, molecules or ions transport from one or both surface to the reaction site (interface). Chemical bonds are much stronger than physical bonds ($\approx$ 40 - 400 kJ/mol). They can be achieved in CFRP by grafting a reactive group at the fiber-matrix interface.

Mechanical bonds consist of interlocking effects between two phases in contact. It occurs when one phase can penetrate into the topological roughness of the second phase surface. Mechanical bonds are, in general, lower than chemical bonds. In CFRPs, the addition of mechanical bonding to chemical bonding is often desirable.

In the case of high-performance TPCs, most of the fiber-matrix interactions are of physical and mechanical type [13]. Modifications are performed on the carbon fibers surface, through several surface treatments, to promote these interactions with the thermoplastic resin [14].

Give some types of carbon fiber surface treatment ?

The carbon fibers surface treatments include wet chemical modification, dry modifications and multi-scale modifications. The "wet" methods (non-oxidative treatment) consist in applications of polymer sizings, chemical modifications with acids and electrochemical modifications. The "dry" methods (oxidative treatment) include the plasma treatments, high-energy irradiation and thermal treatments. The "Multi-scale" coating consists of nano-particles/carbon and nano-tubes/graphene modifications [15]. These treatments enhance the fiber-matrix adhesion by improving the carbon fiber surface reactivity and adhesion potential; by increasing the surface roughness; and by removing the carbonaceous impurities. The treatments are often done in line with the fiber manufacturing process.

What make the fibers impregnation with thermoplastic resins difficult ?

The impregnation of the fibers with the matrix resin is one of the critical step in TPC processing, as it creates the reinforcing synergy in the final composite structure. The high melt viscosity of high-performance thermoplastic make the impregnation difficult. The average flow velocity of a fluid into a porous media (*e.g.*, fiber bed) can be related to the applied pressure P, the fluid viscosity η, the fiber bed permeability K, and the depth of impregnation a, through the Darcy law,

$$\frac{da}{dt} = \frac{KP}{\eta a} \tag{2.1}$$

By integrating Equation 2.1, and assuming constant permeability during the impregnation process, the time required to completely impregnate the fiber bed can be estimated,

$$t = \frac{\eta \cdot a^2}{2K \cdot P} \tag{2.2}$$

It follows from Equation 2.2 that the impregnation time is proportional to the resin viscosity. Since, high-performance thermoplastic resins melt viscosity are very high, the same impregnation techniques used with thermoset resins are not suitable. The application of high pressure to accelerate the impregnation process is not an effective solution, since a high pressure may lead to a fiber damage. Moreover, the fiber bed permeability, K, decrease when the applied pressure is high, making the impregnation more difficult [13]. Therefore, specific impregnation techniques need to be applied to process high-performance thermoplastic resins at intermediate pressures.

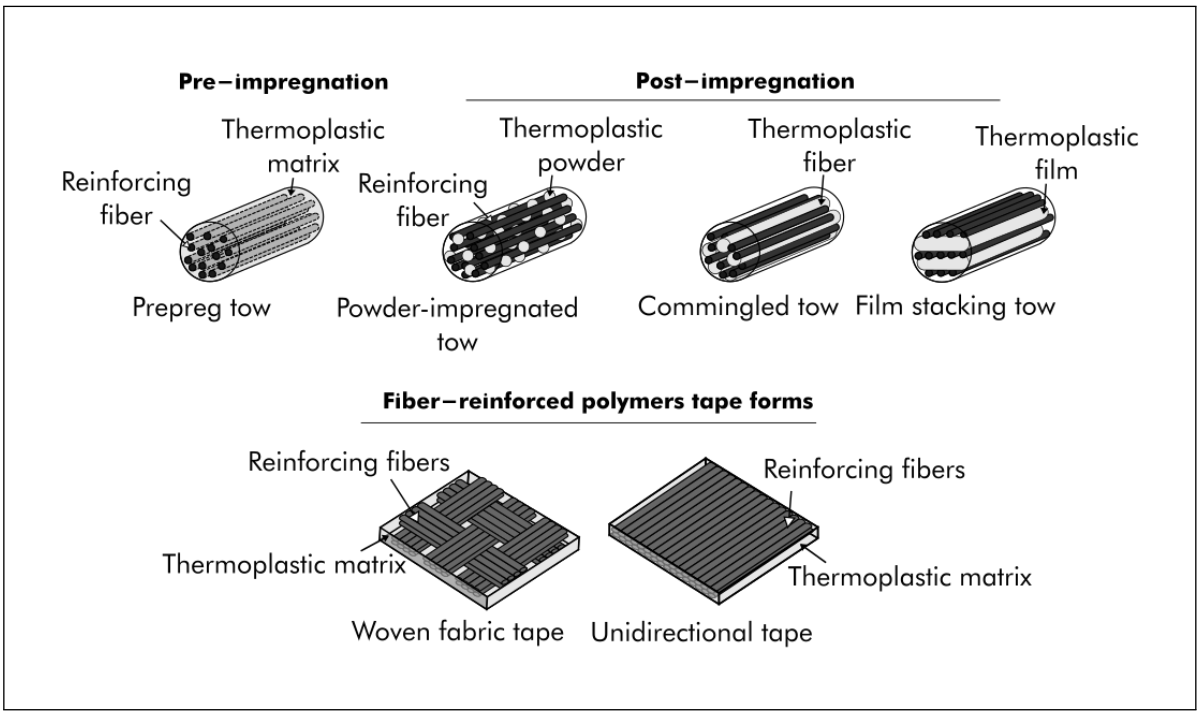

Figure 2.5: Schematic representation of intermediate product forms for thermoplastic composites.

Give some impregnation methods of carbon fibers with high-performance thermoplastic resins ?

The impregnation methods of carbon fibers by high-performance thermoplastic resins are classified as post-impregnation and pre-impregnation methods [16].

In *post-impregnation* methods, the resin is not initially melt to impregnate the fibers. The resin is rather in form of film, filament or powder and brought into intimate contact with the fibers to form towpregs. The impregnation itself is postponed until the part fabrication. This method is based on reducing the distance to flow a (in Equation 2.2) of the resin, to completely impregnate the fibers during shaping operations. Three major techniques are used in post-impregnation such as *film stacking*, *cowoven* or *commingled towpregs*, and *powder impregnated towpregs*. Figure 2.5 illustrates the structure of these three preform types.

The post-impregnation methods help to overcome the difficulty of working with high melt viscosities resins with poor solubility. The towpregs obtained by these methods

are readily drapable into complex forms which is suitable for complex shape parts. However, high pressures, high temperatures and long dwell times are required, to achieve a good impregnation during the shaping operations.

The key problem of these techniques is to achieve a fine enough dispersion of the matrix in the fiber bed. Moreover, the air gap between the fibers and resins is a significant concern. At high temperatures, the air and more specifically the oxygen may interact both with the fiber surface and with the resin. Since oxidative surface treatments are already performed on the carbon fiber to enhance their surface reactivity, further oxidation may alter that surface (de-treatment, loss of functional groups, and so loss of adhesion capability). With regard to the resin, high-performance resins such as PEEK or PEKK may cross-link in the presence of oxygen, at high temperatures. This cross-link will necessarily occur at the resin free surface [17]. Consequently, it is desirable to make the fiber-matrix bonding in the absence of air and as quickly as possible. This requirement is the primary motivation of pre-impregnation methods.

In *pre-impregnation* methods, the fibers are wetted and impregnated by the thermoplastic resin in one step. This method is based on reducing the resin viscosity η (in Equation 2.2) to promote good impregnation. Three major techniques are used in pre-impregnation such as solution impregnation, *in situ* polymerization and hot melt impregnation.

Solution impregnation consists of dissolving the thermoplastic resin in a suitable solvent, to reduce the resin viscosity, and wetting the fibers with the solution. The obtained product is dry later to remove the solvent. This technique makes the impregnation easy, as the the resin viscosity is low. However, removing of the solvent used is a real challenge, as the presence of residual solvents may compromise processing (risk of pore formation) and reduce service performance [13]. This techniques is not suitable for high-performance thermoplastic resins because they exhibit a good resistance to solvent and thus cannot be dissolved in many solvents at room temperature [18].

In situ polymerization consists of pre-impregnating the fiber bed with a low molecular weight monomers or pre-polymer in solution followed by *in situ* polymerization. This technique is suitable for a limited range of polymers called thermosetting thermoplastic or pseudo-thermoplastic. These materials are processed like thermosets. Consequently, the fast processing advantage of thermoplastic is lost.

Hot melt impregnation consists of forcing molten resin into a fiber bed. The melt resin is often provide by extruders. Considerable pressure is required to ensure a complete impregnation of the fibers. This technique is suitable for high-performance thermoplastics because no solvents are needed. The wet out is generally excellent with a low void content but the obtained prepreg is stiff and tackless. Moreover, there is some danger of thermally degrading the polymer during the heating to lower its viscosity [18]. However, this technique is probably the most commonly used to combine carbon fibers with high-performance thermoplastic resins. The resulting product from hot melt impregnation is called *prepreg* (Figure 2.5). The term prepreg is a contraction of "pre-impregnated". The prepregs are delivered to the manufacturer, in tape rolls form. The fibers are often directly impregnated to make UniDirectional (UD) tapes or they can be transformed first into fabric products, such as woven fabrics or Non-Crimp Fabrics (NCF) to create multi-directional prepregs [19]. Due to the homogeneous and straighter fiber arrangement in prepregs, they provide higher mechanical strength and stiffness to the composite. Prepregs are the semi-finished product widely used for structural applications [4].

How are the TPC prepreg tapes processed ?

Most thermoplastic prepregs do not possess enough drape to be readily laid-up against a contoured shape. They are instead laid-up or stack as a flat panel which is subsequently thermoformed into the desired three dimensional shape ("3D shape"). The objective is to form a laminate with individual tape or ply oriented in the required directions and bonded together. The UD plies are oriented so that the fibers main axis (high-strength direction) is aligned with the load direction. Hence, a laminar composite has relatively high-strength in a number of directions in the 2D plane according to the plies orientation. For example, a laminate with all plies oriented at 0° will be extremely strong and stiff in this direction but very weak in the 90° direction. The stacking can be done manually or automatically by Automated Tape Placement (ATP).

In the case of manual stacking, the prepregs are just stacked on top of each other without any link, according to the defined stacking sequence. With respect to ATP, the placement is done by a robot equipped with a placement head, a compaction roller and a heating element. The heating element and compaction roller allow to melt and pressurize the resin locally, in order to promote adhesion with the bottom ply. This

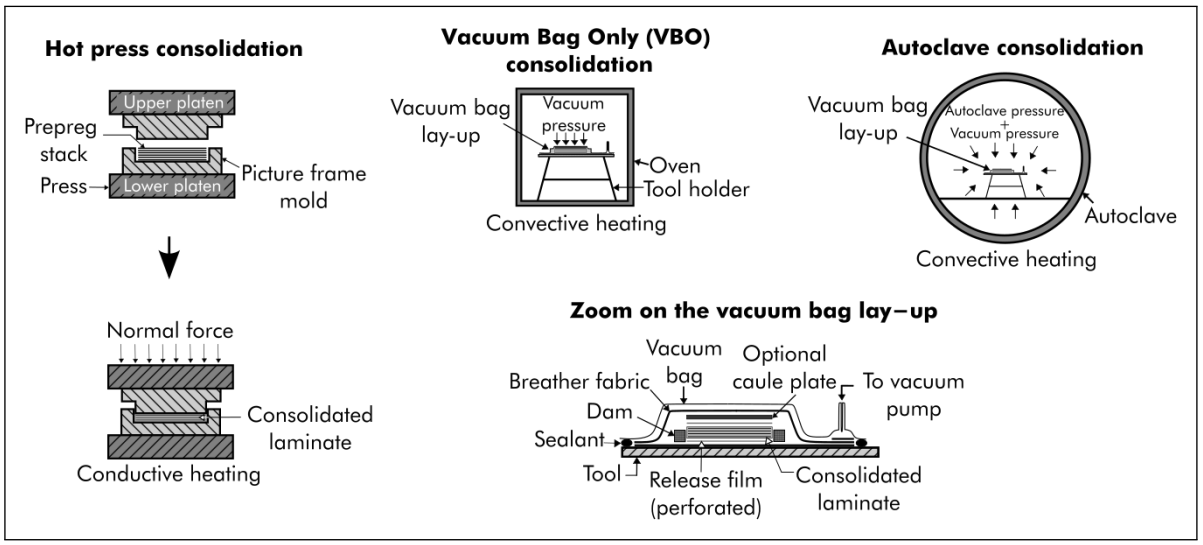

Figure 2.6: Some thermoplastic composites consolidation processes.

lay-up technique is used for large parts with tailored stacking sequence. The resulting stack is then consolidated by the application of pressure and heat through different consolidation process.

Describe some prepreg based TPC consolidation processes ?

Different techniques are used to consolidate thermoplastic prepregs tapes. They include Hot Press Consolidation (HPC), Vacuum Bag Only Consolidation (VBOC), and autoclave consolidation (Figure 2.6).

Hot Press Consolidation consists of placing the prepreg stack inside a picture frame mold located between two platen of a hot hydraulic press. First, the hot platens of the press heated the mold by thermal conduction. The heat is then transferred to the prepregs. A small pressure can be applied during the heating to promote a good thermal contact between the mold and the prepregs stack. The stack is heated at a constant rate up to the resin melting temperature (T_m). The melting temperature is selected such that the thermoplastic resin becomes a low viscosity fluid which will flow under the consolidation pressure. The decrease of viscosity after T_m also helps to promote the fiber wetting by the liquid resin; and to remove air from both inside the fiber bundles and between the stacked prepregs. The consolidation pressure ($\approx$ 1 MPa - 4 MPa) is applied once T_m is reached. The stack is maintained under the consolidation pressure

during a few minutes, in order to achieve a good fiber wetting and consolidation of the plies. The obtained laminate is subsequently cooled down below the resin T_g, after the consolidation is complete. The consolidation pressure is maintained during the cooling to prevent defects occurrence. In HPC, the applied pressure is high but not hydrostatic. This factor sometimes leads to a resin squeeze-out during the consolidation. HPC is often use to make laminate sheets. The consolidated laminates are further used as the starting material in shaping operations like thermo-stamping.

In *Vacuum Bag Only Consolidation*, the prepreg layers are stacked on a thick steel tool. The lay-up are covered by high-temperature thermalimide release films (Kapton) then a breather (porous glass cloth). Thermalimide films are placed between the stacking and the breather, in order to facilitate the demolding of the final part. An optional caul plate or pressure plate can be placed over the breather to provide a smoother part surface. The stacking, films and breather together are covered by a high-temperature thermalimide vacuum bag which is sealed to the periphery of the tool with a ultra-high temperature (up to 426 °C) silicone rubber sealant.

The vacuum bag provides the membrane pressure to the laminate during consolidation. The breather allow a better distribution of the vacuum pressure and facilitate the evacuation of residual gases and released solvents during the heating. Since the vacuum pressure is not hydrostatic, for thick laminates, dams can be used to prevent excess pressure on the laminates edge. The whole setup is placed in an oven for the consolidation process. The oven ensures a homogeneous temperature and therefore limits thermal gradients within the prepreg layers during the consolidation.

The whole setup is heated by thermal convection at low heating rates ($\approx 2\,^{\circ}\mathrm{C/min}$) up to the resin T_m and held at this temperature for several minutes. Then, the laminate is cooled by forced or natural convection below the resin T_g, before demolding. Full vacuum is maintained during the whole cycle. Due to the low heating rates and pressure, VBOC lasts longer than HPC but the risk of resin squeeze-out is significantly reduce. VBOC can not only be used to make laminates sheets but also to directly consolidated part with relatively simple geometry. In the latter case, the tapes are directly laid-up by ATP on the mold corresponding to the part geometry.

In *autoclave consolidation*, the setup employed is identical to the one used in VBOC. The only difference is that instead of placing the setup in an oven, the setup is placed in an autoclave. The autoclave provides an external gas pressure to the part. The autoclave

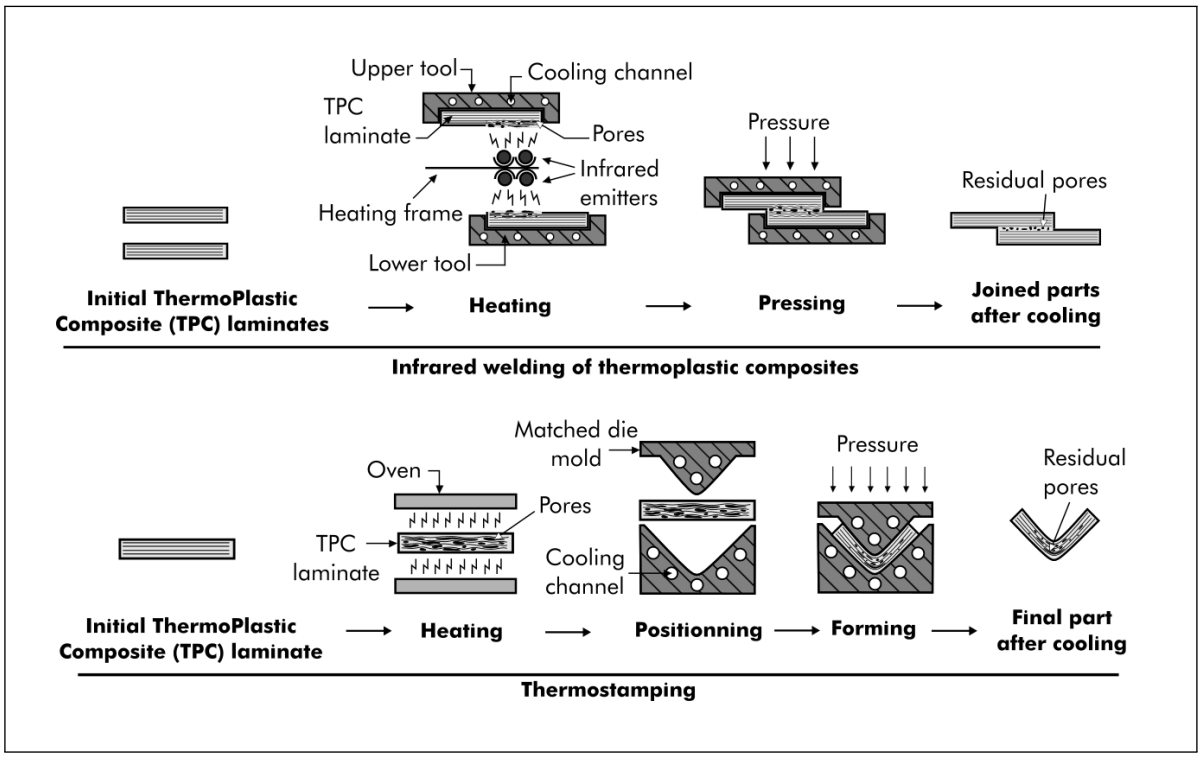

Figure 2.7: Example of thermoplastic welding and forming process.

are generally pressurized with inert gas to prevent fire risk during heating. The prepreg layers are heated and cooled by forced thermal convection like in VBOC. Although, the dwell time during heating is the same as that of HPC and VBOC, autoclave lasts very longer than both HPC and VBOC, because of the large tools generally employed. The time required to heat up and cool down a large autoclave is very long ($\approx$ 5 to 15 hours). However, it is suitable for large parts with complex geometry, since the applied pressure is hydrostatic.
The resulting laminates sheets or parts, from the mentioned consolidation processes, are further used in forming operations or joining applications.

Give some forming and joining processes of pre-consolidated TPC laminates ?

TPC laminates are usually shaped by thermoforming. A thermoforming process consists of heating a flat pre-consolidated laminate sheet in an external oven to the forming temperature (Figure 2.7). The heating can be done by convection oven, infrared radiation or conduction between two hot platens. The pre-consolidated laminate is then transferred into a forming system where it is shaped to the geometry imposed by the

die. At the end of the forming, the composite part is cooled under pressure below its T_g before it is removed from the forming system [18]. Several forming techniques are used to form TPC laminates. They include thermo-stamping, rubber pad press forming, diaphragm forming, hydro-forming, and autoclave/vacuum forming (similar to diaphragm forming).

Contrary to the assembly techniques traditionally used for thermoset composites, such as mechanical fastening and adhesive bonding, the use of TPC makes assembly by fusion bonding (welding) possible. Several problems are encountered when using mechanical fasteners. They include stress concentration due to the presence of holes and cut-outs; delamination during the drilling; possible galvanic corrosion at fastened joints, *etc* [20]. Moreover, the use of mechanical fasteners adds an extra weight to the composite structure. Although the use of adhesives eliminates the issues encountered with mechanical fastening, adhesive bonding requires extensive surface preparation and long curing times for the thermoset-based adhesives, which make the process labor intensive. In contrast, welding do not require any adhesives and the surface preparation requirements are less laborious.

Several welding techniques are available. They all involve five basic steps to build a good bond between the TPC parts: surface preparation, heating, pressing, molecular diffusion, and cooling. The surface preparation is performed to remove any impurities and mold release agent at the surfaces. Since welding process can tolerate materials with low surface energy, a sanding of the surfaces is often sufficient. The heating allow to melt the thermoplastic resin in order to promote molecular chains mobility. There are many techniques to supply the heat energy (*e.g.*, infrared heating, induction heating, resistance heating, electromagnetic heating, mechanical vibration). The heating rates involved in these techniques are often very high (1 °C/s - 75 °C/s).

In most of the welding techniques, the heat is applied locally around the bond surfaces. Pressure is then applied on the heated zones to bring the surface into contact (Figure 2.7). The applied pressure must be sufficient to promote the resin flow, a good intimate contact and the squeeze out of air trapped at the interface. As the two melt surfaces are in contact, the thermoplastic macromolecular chains at the interface diffuse in each other resulting in a gradual vanishing of the interface. At the end of inter-diffusion process, the joined parts are cooled down under pressure to solidify the weld line.

Given that TPCs welding and shaping principles are relatively simple, what then limits the application of TPCs in aeronautical structures ?

Welding techniques can make composite parts joining faster and even more easily automated. However, TPCs welding and thermoforming are confronted with several issues that are still under investigation. With regard to forming, these issues include *defects occurrence* during forming such as deconsolidation, matrix cracking, plies delamination, part warpage, fibers buckling and wrinkling; or *part deformation* after forming like part spring-back and part distortion. With respect to welding, the process parameters are not always well mastered. Master the intimate contact and healing is a real challenge. However, the central issue that is encountered in both forming and joining processes is deconsolidation. The research work presented in this dissertation focuses on deconsolidation because there are still many mysteries around this phenomenon.

What is deconsolidation ?

Deconsolidation is the appearance and growth of pores during the processing of pre-consolidated laminates. Deconsolidation occurs during heating of a pre-consolidated laminate, when no or low pressure is applied, leading to detrimental pores or delaminations. As reported by many authors [21–23], pores severely affect the mechanical properties of the composite. These properties include shear stiffness and strength, compressive strengths, transverse tensile strength, interlaminar shear strength, flexural strength, and fatigue resistance.

An example is shown on Figure 2.8, where mechanical tests were performed on Carbon Fiber (CF)/PEEK laminates consolidated by different consolidation techniques (VBOC, HPC, *In Situ* Consolidation (ISC)) with different void (or pore) contents [24]. The tests results show that a 64 % reduction in In-Plane Shear Strength (IPSS) can be observed with void volume fraction ranging between 1.2 % and 3.8 % in VBOC samples. Another example of porosity content effect on InterLaminar Shear Strength (ILSS) of CF/PEKK can be found in [25]. In fact, depending on the voids volume fraction, distribution and size, they become high stress concentrations zones. Hence, they initiate cracks or delaminations formation which expand under load and lead to the part failure. Deconsolidation is thus a critical issue to avoid during CFRTP processing.

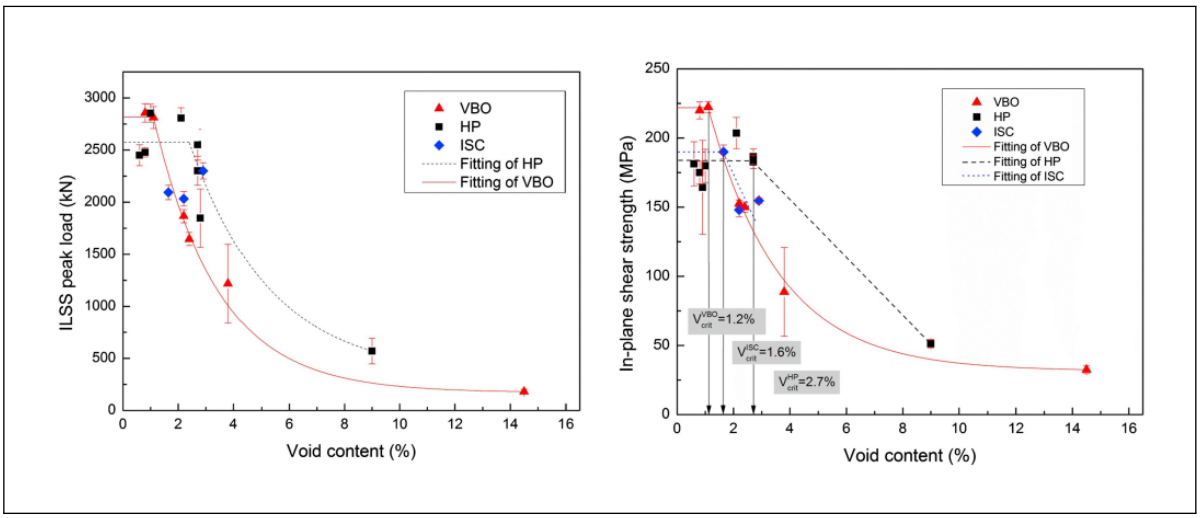

Figure 2.8: Effect of void content on (left) InterLaminar Shear Strength (ILSS) and (right) In-Plane Shear Strength (IPSS) for CF/PEEK laminates manufactured by different technologies [24].

Since the pre-consolidated laminates behavior during forming or joining depend on their process history, to understand the origin of deconsolidation, the laminates behavior during consolidation must be analyzed.

2.2 Mechanisms involved during TPC laminates consolidation

The objectives of the composite manufacturing processes are to achieve a consistent product by controlling fiber content and orientation, minimize voids, reduce internal residual stresses and process in the most cost-effective way. To reach these objectives, the processing techniques, espacially the consolidation steps need to be well mastered. The consolidation of CFRTP involves a combination of complex fluid flow, adhesion and thermomechanical phenomena that determines the quality of the composite part [26]. CFRTP consolidation process can be divided in three steps: heating, consolidation, and cooling.

2.2.1 Heating

The state of a polymer depends on the temperature. At room temperature, the prepregs are stiff due to the thermoplastic resin which is in a glassy state. At this stage, the polymer chains movement are somewhat frozen and their motion is restricted. Heat energy is provide during the heating to promote molecular mobility.

What are the molecular mechanisms during the prepreg stack heating ?

Molecular motion are divided into four categories. In order of increasing activation energy (as well as increasing number of atoms involved in the motion), there are (1) vibrations of atoms about equilibrium positions; (2) motions of a few atoms or side groups, along the main chain; (3) cooperative wriggling and jumping of segments of molecules approximately 40 - 50 carbon atoms in length, permitting flexing and uncoiling, that lead to elasticity; and (4) translational motion of entire molecular chain that permits flow [7]. Since the activation energy of the motion type (1) and (2) are low, during heating the motion type (3) and (4) are "frozen out" until T_g is reached. When the temperature exceeds T_g, the motion type (3) and (4) are activated.

T_g thus characterizes the polymer transition from a glassy state to a rubbery state with a viscoelastic behavior. This transition is reflected by the observed variation of certain thermodynamic properties with temperature like the specific volume for example. As the temperature arise above T_g, the free volume (*i.e.* space that is not occupied by polymer molecules) increased allowing molecular motions to take place. Since, entangled polymer chains cannot respond instantaneously to temperature changes, T_g may depend on the heating rate.

Only the amorphous region of the semi-crystalline resin is affected by these chain motions above T_g. More heat energy is needed to overcome the crystalline bonding forces. The prepregs layers are, therefore, heated above T_m. T_m is usually taken as the temperature at which the last trace of crystallinity disappears [27]. The processing temperature is usually higher than T_m in order to effectively erase all the crystallites. The goal is to increase the chains ability to slip past one another and thus reduce the resin viscosity which characterizes its resistance to flow under stress.

However, viscosity depend not only on temperature but also on the molecular weight. High-performance thermoplastic resins have usually high molecular weight. The chains are thus long enough to be significantly entangled. The resistance to flow

caused by theses entanglements explains the high melt viscosities of these resins. Fo this reason, heating the prepregs layers above T_m promotes molecular mobility but it is no enough to generate a resin flow.

2.2.2 Consolidation

As the prepregs are heated above T_m, a consolidation pressure is applied to the stack. Pressure plays many roles, during consolidation step, such as remove the air lying between the prepregs, bring the prepregs layers into intimate contact to promote molecular interdiffusion, and finally force the resin to squeeze out of the prepregs.

How the air gap between the prepregs layers are removed ?

There are mainly two methods to remove air between the prepregs layers. The first method is to apply enough pressure *to dissolve the air* into the melt resin by adsorption-diffusion. In fact, the molecules contained in air are small molecules when compared to polymers. Due to Wan der Waals forces, the air molecules are absorbed on the surface of the melt resin. Then, due to the air molecules concentration gradient between the melt resin surface and core, the molecules adsorbed on the resin surface are diffused into the resin melt [28]. Since, the free volume content of the melt resin is high, the small molecules will fit in these free volume until equilibrium is achieved. This mechanism is called *diffusion*. The diffusion mechanism of fluids in polymers is further discussed later in Chapter 4. This first method, based on air dissolution, is the one used in HPC.

Instead of dissolving the air into the melt resin, the second method consists of *extracting the air* between the prepregs by vacuum. This method is the one used in autoclave consolidation and VBOC.

Describe the prepregs layers autohesion process ?

In addition to evacuating air, pressure also allows intimate contact between the prepregs layers and force the resin to flow. As the melt resins of each prepreg layer are brought together, the interface between the layers gradually disappears through a healing process. The healing process involves five stages described by Wool *et al.* [29, 30]: (1) surface rearrangement, (2) surface approach, (3) wetting, (4) diffusion, and (5) randomization.

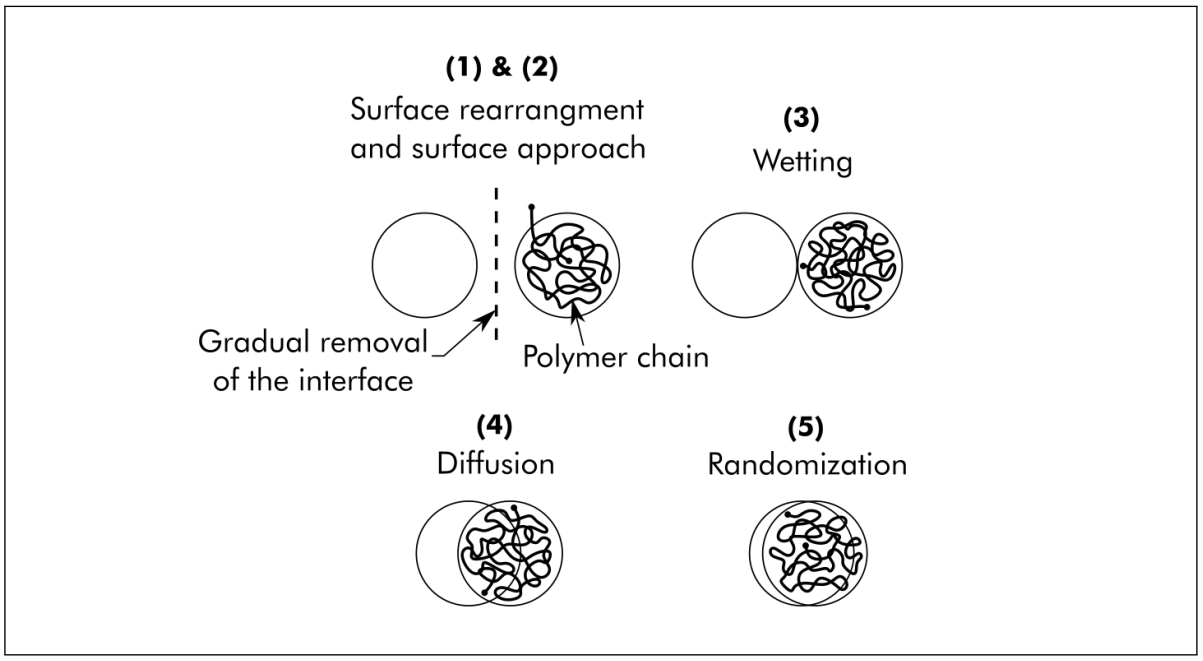

Figure 2.9: Schematic diagram showing two random polymer chains on opposite surfaces during the five steps of the healing process. A single polymer chain is shown for better clarity. Adapted from Ref. [30].

In stages (1) and (2), the barriers at the interface disappear gradually as the surface are getting closer and rearrange (Figure 2.9). In stage (3) the intimate contact is effective as all potential barriers due to inhomogeneities at the interface have disappeared. In stage (4), the polymer chains are free to move across the interface by interdiffusion , also called autohesion. In stage (5), the chains entangled after inter-diffusion.

The autohesion process description is based on the reptation theory first stated by de Gennes [31]. The reptation theory describes the motion of polymer chains in entangled polymer network. According to this theory, a single polymeric chain is trapped inside a three-dimensional network of a set of fixed obstacles (Figure 2.10). The polymer chain can move around the obstacles in a snake-like fashion but it cannot cross any of these obstacles.

The chain is assumed to have certain "defects" which migrate along it. The reptation motion produces a forward motion when a defect leaves the chain at the extremity. The chain is therefore assumed to be actually confined in a permanent and non-deformable tube which have a similar shape to the random-coil configuration of the polymer chain. The tube represents topological constraints to the lateral motion of monomers, imposed

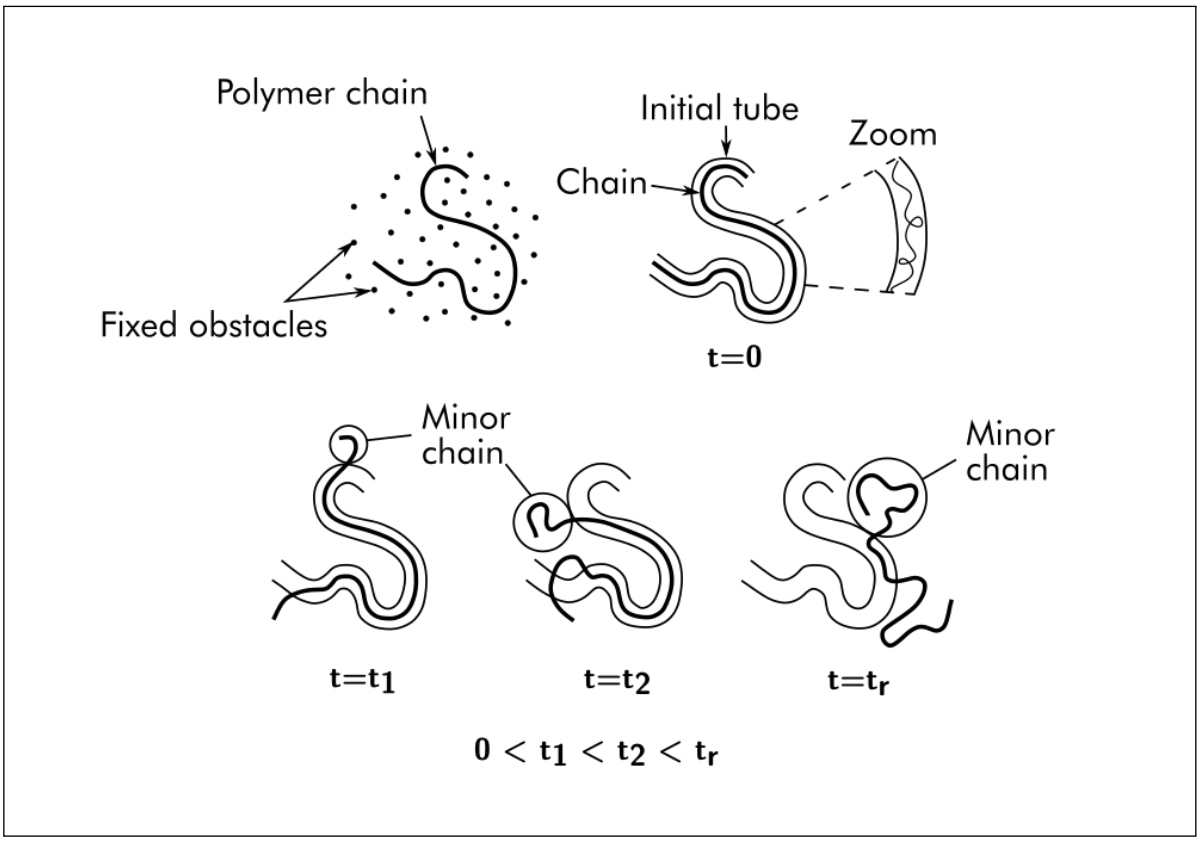

Figure 2.10: Schematic representation of a polymer chain migration as described in the reptation theory. First, the polymeric chain is surrounded by obstacles. The same chain is in an equivalent tube, showing details of the conformation of the molecule in the tube (zoom). Second, the chain gradually moves out of the tube by reptation until the reptation time when it is completely out of the initial tube. Adapted from Ref. [20].

by neighboring chains via entanglements. The chain exhibits Brownian motion back and forth in the tube and the only way for it to leave the tube is to get out at the tube extremity. As the chain is moving out of the tube at the extremity, it gradually forgets the initial position of the tube in space.

Finally, the chain escapes from the tube and forgets its initial configuration when the reptation time elapses. The reptation time is the time after which the chain completely diffuses out of the initial tube. Repetition of the reptation movement throughout the polymer network explains the interdiffusion at the interfaces [20]. The rate of inter-diffusion depends directly on the resin molecular weight [32], material viscosity [33], the degree of chain segregation, cross-linking and chain entanglement [34].

What is the dwell time effect during consolidation ?

The primary function of the dwell time is to allow temperature homogenization in the laminate. This time depends on the thermal properties of the mold and the composite layers. Since, the interdiffusion process is time-temperature dependent, the dwell time also allows enough time to achieve complete interdiffusion at interfaces [35]. However, the autohesion time is usually low compared to the temperature homogenization time. Furthermore, as it will be discussed in the following section, the dwell time also have an effect on the final composite degree of crystallinity.

2.2.3 Cooling

As soon as the autohesion process is completed, the laminate is cooled from the consolidation temperature to a temperature below T_g. The thermoplastic resin transforms from a liquid state to a solid state. This transformation takes place at the crystallization temperature (T_c). T_c is the temperature at which the polymer chains are mobile enough to rearrange into ordered arrangements (crystalline regions). This phenomenon is called *crystallization*.

Describe the molecular mechanisms of crystallization ?

Crystallization is the process whereby the ordered structure of the semi-crystalline thermoplastic crystallites are produced from a disordered structure of the polymer chains in the melt resin. Crystallization takes place in two distinct stages: *nucleation* and *growth*.

In the first stage, the random entangled chains in the melt resin tend to become aligned and form small ordered regions, when the temperature is reduced to T_c. The small ordered regions are called *nuclei*. These nuclei are stable only below T_m and are disrupted by thermal motion above T_m. When the small nuclei forms randomly throughout the melt resin, the nucleation is *homogeneous*. The nucleation is *heterogeneous*, when the nuclei forms on foreign matter such as dust particles, nucleating agents; or forms on the walls of a foreign bodies such as a fiber or impurities (Figure 2.11). During CFRTP processing, the nucleation is heterogeneous due to the presence of fibers.

During the second stage, the crystal nuclei grow by addition of further chains [36]. As the chains are incorporate in the crystal, they form individual lamellae. The lamellae

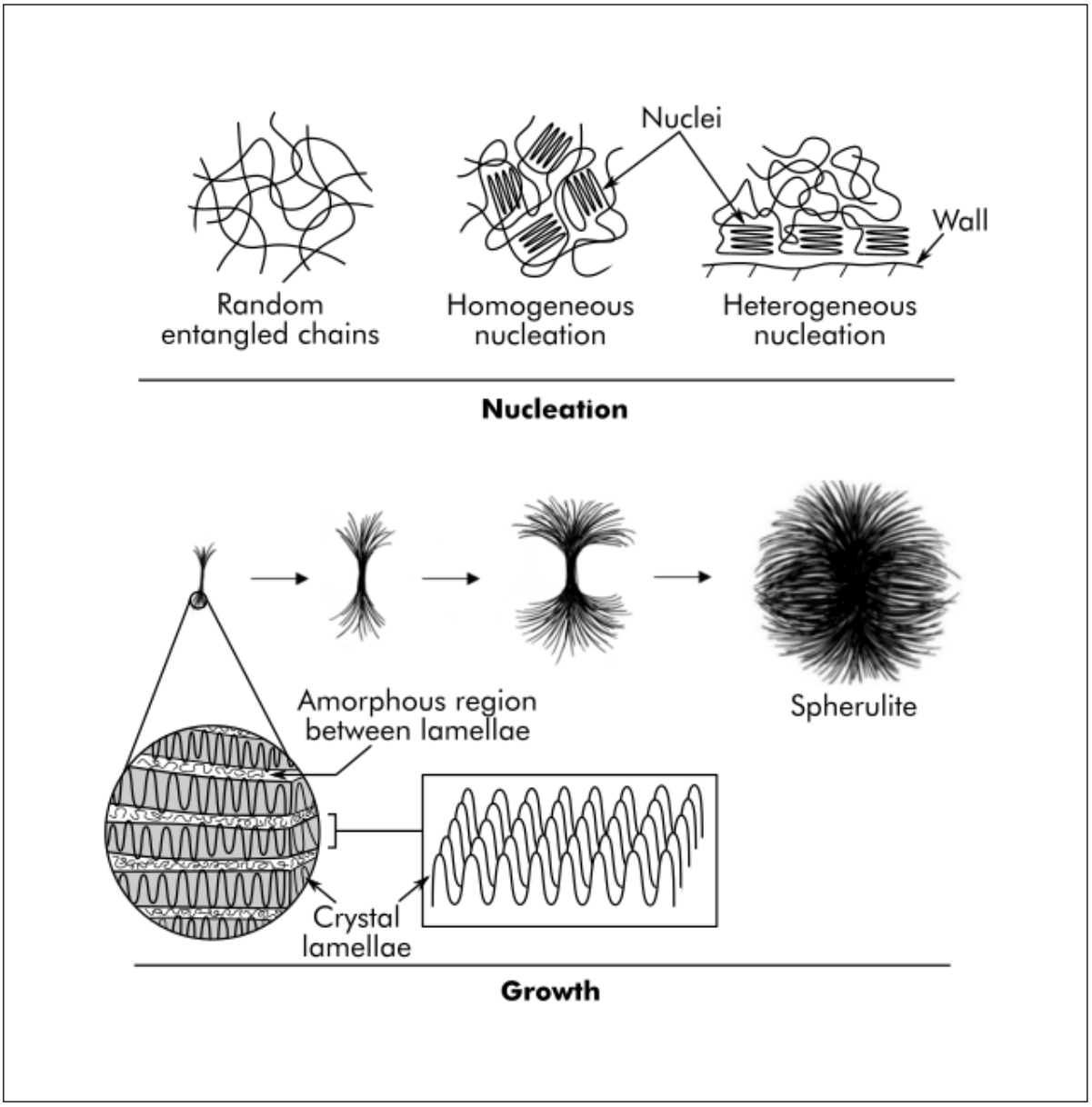

Figure 2.11: A schematic showing the two type of nucleation and the spherulite formation steps, with a zoom on the crystalline morphology.

then develop into sheaf-like structures and grow further in and out of plane to form spherulites. The spherulites grow as long as the resin is held at T_c or until two or more spherulites fronts meet and impinge [37–39].

What factors influence the crystallization ?

The spherulites nucleation and growth depend first on the initial state of the melt resin. If all the crystallites initially present in the thermoplastic resin are not melt during the heating, the residual traces of the unmelted crystallites become nuclei during the crystallization. Hence, if the polymer is held in the melt for a sufficient period of time to destroy any pre-existing nucleation sites, a low nucleation density and therefore large spherulites can be obtained. Alternatively, high initial nucleation sites content in the resin melt leads to numerous small spherulites.

The presence of carbon fibers in the melt resin also influences the crystallization process. Experimental observations show that spherulites nucleate preferentially along the carbon fibers. Thus, carbon fibers act like nucleation sites. Since stresses are also nucleating factor for crystallization, the reason for this preferred growth along the fibers is probably that shrinkage stresses during cooling and solidification of the matrix will be high at the fiber-matrix interface.

Furthermore, Blundell *et al.* [37] divided nucleation sites in the CFRTP into three types: nucleation from contact points between fibers (regions where the fibers are almost in contact), nucleation at free fiber-matrix interface and nucleation from within the polymer matrix. The relative abundance of each type of nucleation depends on the processing conditions. For example, a longer melt holding times will favor crystallization on the carbon fibers surfaces [40]. In all cases, nucleation around the carbon fibers is not of critical importance to the performance of composite materials [17]. It is a necessary condition for good bonding but it does not imply that good fiber-matrix bonding is guaranteed.

Finally, the main factor that affects crystallization is the cooling rate. The rate at which the melted resin is cooled below T_g controls the final degree of crystallinity and the spherulites morphology (size and distribution) in the composite laminate [41]. The degree of crystallinity characterizes the fraction of crystalline regions in the resin. A high cooling rate leads to lower crystalline contents because the spherulites will not

have enough time to grow before the resin structure is frozen below T_g. However, small spherulites can be obtained by fast cooling while large spherulites can be formed by a low cooling.

Other factors such as molecular structure, molecular weight of the melt resin or applied stress during cooling can influence crystallization process. A branched or cross-linked structure for example, is not favorable to the formation of an ordered region and therefore can prevent crystallization. Stretching the resin orients the chains in the direction of the stress, and increases the alignment of the amorphous region which lead to higher degree of crystallinity [7].

What is the impact of crystallinity on the laminate mechanical properties ?

The mechanical properties of semi-crystalline thermoplastics depend not only on their degree of crystallinity but also on the spherulites size and distribution, the crystalline structure and orientation. The crystallites orientation in one specific direction can lead to an anisotropy in the mechanical properties [42]. Larger spherulites will promote stiffness with a loss in ductility. In general, a low degree of crystallinity will produce higher elongation and better toughness but with a lower stiffness, lower thermal stability and lower chemical resistance [43]. Alternatively, higher crystallinity improve stiffness (by limiting molecular mobility) [44], thermal stability and chemical resistance and reduce toughness.

Regardind the spherulites size and distribution, Cebe *et al.* [45] have studied morphology and mechanical properties of PEEK samples with different thermal histories and show that depending on the cooling rate during processing, samples with the same degree of crystallinity have different tensile properties. This result was attributed to the differences in the resin morphology (spherulites size and distribution). Hence, they noted that the degree of crystallinity is not the primary factor influencing the resin room temperature mechanical properties but the resin processing history [18]. It is, therefore, important to know how the thermoplastic resin characteristics (morphology and structure) is affected by the processing conditions and how the consolidated laminate behavior is affected by the resin characteristics.

Why is the consolidation pressure maintained during cooling ?

In general, the consolidation pressure is maintained during cooling to prevent defects (voids, delamination) appearance in the laminates and to control the dimensional stability of the laminate. A decrease in the temperature during cooling result in a volumetric contraction of the thermoplastic resin, called thermal shrinkage. At any temperature, polymer chains always tend to adopt the most favorable conformations and increase chain packing, to reach thermodynamic equilibrium [46]. Thermal shrinkage is due to the rearrangement of the polymer chains into more compact configuration. When the polymer is semi-crystalline, additional shrinkage occurs due to crystallization (formation and growth of spherulites). Depending on the type of polymer and the cooling rate, the crystallization shrinkage can be an order of magnitude greater than the thermal shrinkage [10]. Resin shrinkage can promote dimensional variation in laminates. The pressure holding during cooling offsets the shrinkage until the resin solidification below T_g. Unfortunately, this pressure holding during cooling, lead to *residual stresses* trapped in the laminates.

At this level, one knows how the CFRTP prepregs stack behaves during consolidation to form laminates and how the processing conditions determine the consolidated laminate mechanical properties and its behavior after processing. Now the question is what are the phenomena induced by consolidation that can be a source of deconsolidation during post-processing of the pre-consolidated laminates. This question is addressed in the next section.

2.2.4 Residual stresses induced by consolidation

Given their high melt viscosities and high T_m, consolidation of high-performance CFRTP often require high pressure and/or high consolidation temperature. However, cooling from high temperature under pressure can lead to residual stresses in the consolidated laminate. Residual stresses are internal stresses that remain trapped in the laminate even in the absence of external loading or thermal gradient [47].

What are the effects of residual stresses on the consolidated laminates ?

Residual stresses can cause several defects in the composite laminates and structures such as fiber waviness, transverse cracking, delamination, and warpage (Figure 2.12) [48].

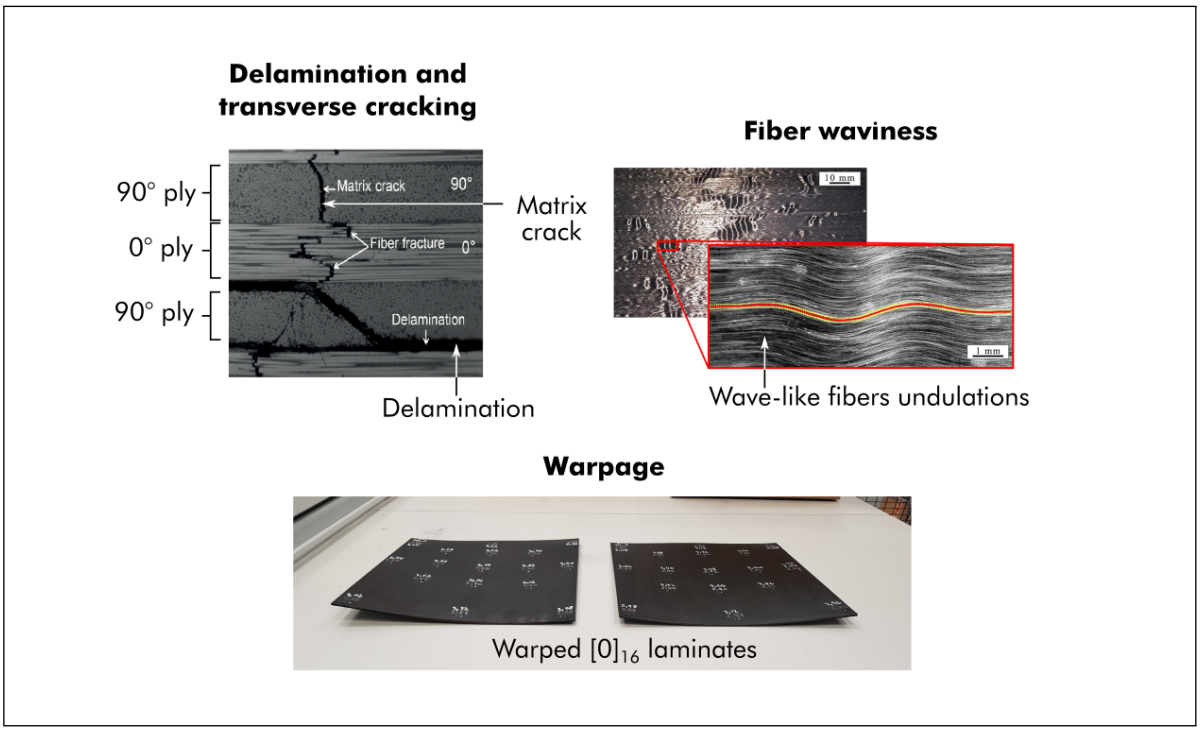

Figure 2.12: Several defects caused by residual stresses: transverse cracking and delamination [49], fiber waviness [50], and warpage.

Fiber waviness in UD laminates consists of a deviation of the fibers from the main direction imposed by the UD ply, causing wave-like undulations. It occurs mostly in the surface plies of the laminate, during cooling [50]. Fiber waviness have shown detrimental effects on mechanical behavior like stiffness and strength (tensile, compressive, flexural, and fatigue) of the composite materials [51]. The other defects often occurs in service or after the laminate consolidation. They also significantly deteriorate the composite mechanical properties and can lead to the part failure in service [49, 52].

Transverse cracking occurs when the residual stresses in the laminates exceeds the yield strength of the resin and/or the fiber-matrix interface bond strength [53]. Delamination is an interlaminar failure characterized by progressive debonding of plies of a composite laminate, resulting in a loss of stiffness and strength of the structure [54–56]. It can occur around any geometric stress concentration arising due to holes, cut-outs or changes in section [48]. Finally, warpage is a macroscopic deformation of the composite part resulting in a geometric distortion of the part. It can be related to a non-symmetrical thermal residual stress gradients in-plane or through the thickness of the laminate, and/or to interlaminar residual stresses [57, 58].

Due to the detrimental effect of residual stresses, it is important to minimize them during processing. This requires a good understanding of how the residual stresses are formed in the laminates during processing.

What are the origins of residual stresses in the consolidated laminate ?

Residual stresses in composite laminates are often associated with the difference in thermal expansion of their components (fiber and matrix), the organization of those components (stacking sequence), and the processing history of the laminate [13]. Residual stresses are produced in three different levels [59, 60].

On the *micromechanical level*, the mismatch in Coefficient of Thermal Expansion (CTE) between the fibers and the matrix CTE induces stresses during the laminate cooling. For example, carbon fibers such as Hercules AS4 have a CTE of around $-0.22 \times 10^{-6}\,°C^{-1}$, parallel to their long axis, and a CTE in the range of 10-20 $\times\, 10^{-6}\,°C^{-1}$ across the primary direction [61]. Compared to high-performance thermoplastics, these values are much lower. High-performance PEEK resin, for example, exhibits a CTE in the range of 50-400 $\times\, 10^{-6}\,°C^{-1}$ between room temperature and the melt [61]. As the composite laminate is cooled from the melt, the resin tries to shrink (as mentioned earlier). Assuming that there is no fiber-matrix bonding, the resin will slip, as it shrink, along the fibers without any resistance (Figure 2.13). This case is almost never encountered in composites. In fact, there are usually a fiber-matrix bonding during processing of prepregs. Thus, the rigid and inextensible fibers resist the resin shrinkage, resulting in a residual *compressive* stress in the fibers and residual *tensile* stress in the matrix, in the longitudinal and radial direction.

On the *macromechanical level*, the residual stresses are formed on a ply-to-ply scale due to a difference in the transverse and longitudinal ply CTE [62]. According to the low CTE of the fibers in longitudinal direction, the CTE of the prepreg ply along the fibers direction are much lower than that in the transverse direction. Thus in a cross ply laminate, for example, the plies in 90° and 0° will have different thermal shrinkage direction. This differential shrinkage of the individual plies in different direction are source of residual stresses. In the cross ply laminate, the plies in 90° will impose a mechanical constraint on the 0° plies and vice versa resulting in a residual compressive stresses on the 90° plies and residual tensile stresses on the 0° plies (Figure 2.13) [63].

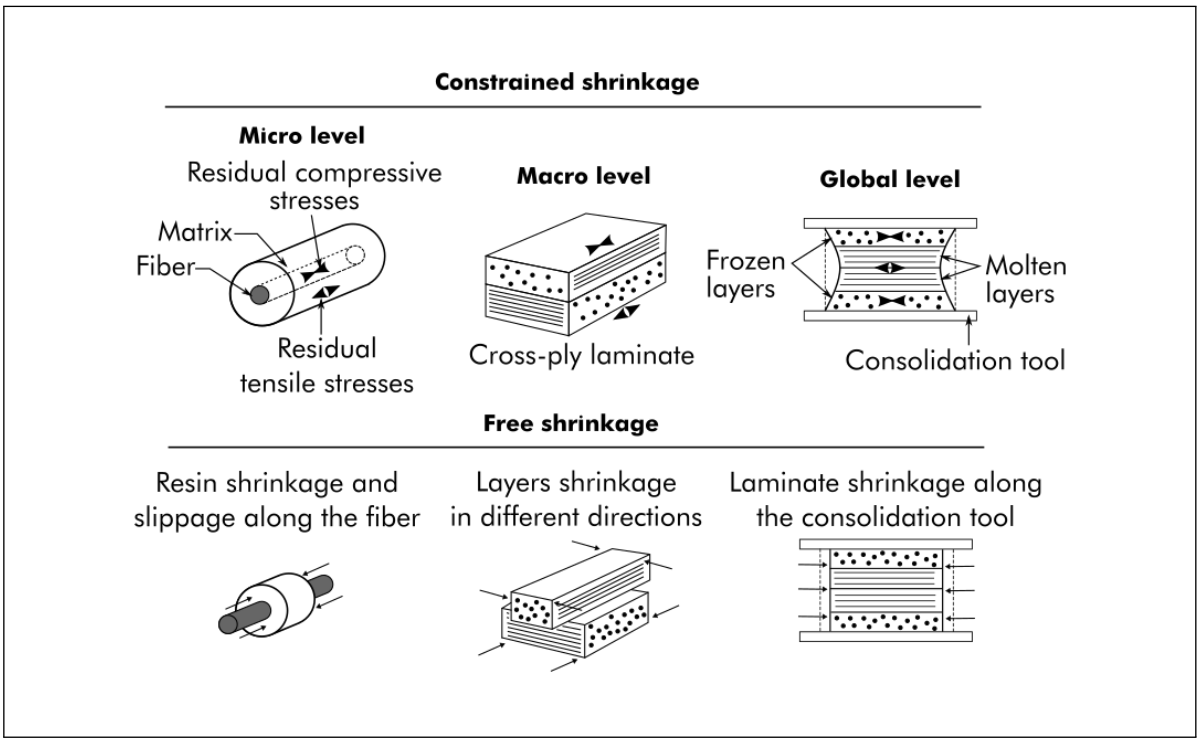

Figure 2.13: Schematic representation of residual stresses formation at different level. The free shrinkage case represents the behavior that would have been observed, assuming that the composite components (or plies) are not bonded together. This case is, in fact, never encountered during the processing of composite materials.

On a "*global*" level, depending on the imposed cooling rate, residual stresses can arise due to a thermal gradient throughout the laminate thickness [61]. Generally, during cooling of thick laminate, the middle plies experience a slower cooling rate than the plies near the surface. During the cooling, the first plies near the surface in contact with the mold will cool and solidify early while the center plies will still need to solidify. The surface plies then constrain the middle plies shrinkage resulting in a parabolic distribution of compressive residual stresses in the surface plies and tensile residual stresses in the middle plies (Figure 2.13) [64]. This residual stress is also named as "skin-core" residual stress. As mentioned earlier, this type of residual stress significantly depend on the cooling rate. Higher cooling rate lead to high skin-core residual stresses with a significant distribution.

Another source of global residual stresses is the interaction between the consolidation tool and the laminate part. The tool-part interaction can be thermal or mechanical. Thermal interaction consists of heat transfer properties between the consolidation

tool and the laminate part through the tool-part interface. For example, a poor heat transfer at the tool-part interface due to a low thermal contact resistance, can generate thermal gradients through the laminate thickness, and thus lead to the formation of residual stresses. The mechanical interaction consists of the difference between the tool and the laminate part CTE. The in-plane CTE of high-performance CFRTP (fiber dominate), is often lower than that of the tool (steel and aluminum) [65]. This means that, during cooling, the tool may forced additional shrinkage of the composite laminate, resulting in compressive residual stresses in the plies located at the tool-interface. This stress transfer at the tool-part interface is determined by the friction behavior between the tool and the composite laminate. While this effect of tool-part interactions on the formation of residual stresses has been, widely, highlighted for thermoset composites [66–71], only few studies mentioned this phenomenon during the processing of high-performance CFRTPs [65, 72, 73].

The three levels of residual stresses enumerated, would result in *a complex three-dimensional residual stress state* within the laminate [74]. As the resin-fiber distribution is non uniform in the composite, as also will be the residual stresses [13].

What factors influence the residual stresses magnitude ?

The magnitude of residual stresses will depend on four parameters, according to Favre [59]: *thermal gradients* through the laminate thickness, difference in Coefficient of Thermal Expansion/Shrinkage of the composite components (or plies), the components (or plies) *elastic coefficients*, and fiber volume fraction. These parameters are, in turn, largely dependent on the thermoplastic *resin morphology* (semi-crystalline or amorphous), the *type of fibers*, the fiber-matrix *interface properties*, the *fibers morphology* or *architecture* (woven or unidirectional prepregs), and *processing conditions* [75].

With respect to resin morphology, semi-crystalline resins will have a crystallization shrinkage in addition to the thermal shrinkage, during cooling. Residual stresses in high-performance CFRTPs are thus higher than in most other TPCs. Moreover, The resin morphology also influences the onset of the residual stresses formation. The temperature at which the thermal stresses start building up in the composite is called Stress Free Temperature (SFT).

During cooling, the semi-crystalline is in a fluid viscoelastic state, between the processing temperature and crystallization temperature (T_c). Therefore, the eventual stress

build up due to thermal shrinkage can still be relaxed above this temperature (T_c), because the polymer chains possess enough energy for motion, especially at low cooling rates. When T_c is reached, the thermoplastic resin becomes a viscoelastic solid and residual stresses are formed and "frozen in" upon subsequent cooling of the laminate. It can, therefore, be conclude that the thermal transition properties of the thermoplastic resin are the governing parameters for SFT. In general, the further the cool-down temperature from the SFT, the more residual stress reside in the composite. This is one of the reasons why residual stresses in amorphous matrix composites are lower compared to semi-crystalline matrix composites. Amorphous resin SFT was found to be around T_g and around T_c for semi-crystalline polymers [76, 77].

Another resin property that affects the formation of residual stresses in composites, is the resin elastic or Young's modulus [59]. Barnes and Byerly [61] ranked the calculated stress levels for different composite material systems and showed that the stress level increases with increasing transverse stiffness of the laminates. Since the transverse stiffness depends among other things on the matrix modulus, it can be said that if the Young's modulus of the matrix is higher, the residual stresses will increase [78].

According to the fiber type, some fibers like Carbon Fiber (CF) or aramid fiber, for example, exhibit highly anisotropic thermal expansion with small shrinkage in the fiber longitudinal direction when cooled. As mentioned earlier, this results in higher residual stresses in the longitudinal fibers direction than the radial direction [61]. Other fibers like Glass Fiber (GF) show isotropic thermal expansion behavior and there is therefore, no such difference in residual stress distribution. Another factor related to the reinforcements that has an impact on the residual stresses is the fiber volume fraction. For higher fiber volume fractions the compressive residual stresses in the fibers were found to be lower [79]. This can be attributed to a lower proportion of contracting resin and the distribution of the strains over more fibers. However, for cross-ply composites the interlaminar residual stresses increase with increasing fiber volume fraction [80] and with increasing number of plies [81–84].

Besides the fibers and resin characteristics, the fiber-matrix interface properties also play a major role on the residual stresses magnitude. During cooling, the fibers are loaded in compression along their length due to the resin shrinkage. Hence, the tendency for fiber buckling increases and interfacial shear stresses are produced. This can lead to interface debonding and eventually microcracking [62]. A higher

fiber-matrix interfacial bond strength will prevent this debonding from occurring but will increase the residual stresses [85, 86], because the residual stresses could not be relieved by interfacial debonding. A weak interface bonding strength would allow for fiber-matrix slippage in the longitudinal direction relieving partially the stress build-up. This reduces the residual stresses in the fibers, preventing the fibers from buckling and interfacial debonding. However, this is not very desirable, as it will eventually result in a composite with lower mechanical properties [86, 87].

With regard to fibers architecture, some studies performed on woven fabric composites shows that additional constrains in the fiber network might lead to significant levels of residual stresses [88, 89]. Hence, woven laminates may provide higher residual stresses than UD laminates, after the same processing conditions.

Another factors that influence residual stresses magnitude are the processing conditions. The most studied processing parameter effect on the magnitude of residual stresses is the cooling rate. Some authors even stated that it is the most important processing conditions that affect the formation of residual stresses [75]. In fact, as mentioned earlier, the cooling rate has a significant effect on the crystallization behavior of the semi-crystalline thermoplastic polymer. A higher cooling rate leads to a lower peak T_c which in turn results in a lower SFT and less shrinkage [90]. Higher cooling rate, can therefore reduce the residual stresses due to crystallization shrinkage [57, 91, 92]. However, higher cooling rate also leads to a low degree of crystallinity which is often unwanted in composite processing, because of the crystallinity impact on mechanical properties [93] and chemical resistance.

According to pressure, only few studies mentioned its effect on the residual stresses during processing of CFRTP [76, 94]. For some authors [75], pressure may only affect the SFT because of its influence on the thermal properties and crystallization kinetics of high-performance CFRTP [36, 95–97]. White *et al.* [98] showed that pressure has no effect on residual stresses during thermoset curing, after curvature measurement on unsymmetric CF/Epoxy laminates cooled under different pressure (0.35 MPa, 0.7 MPa, and 1.05 MPa). In the case of high-performance CFRTP, there is currently no available studies which highlighted the effect of pressure on residual stresses, at the best of the author knowledge. The exact influence of pressure, thus need to be investigated.

By considering the origin of residual stresses and the factors influencing their magnitude, the consolidation processes can be optimized to minimize them. However, due to the intrinsic properties of high-performance composites, residual stresses will always remain in the composite.

2.3 Conclusion

This first bibliographic study presented the fundamental concepts concerning Thermo-Plastic Composite (TPC) laminates and their processing. First, a general presentation of composite materials highlighted the interest of high-performance Polymer Matrix Composite (PMC) for aerospace applications. A focus was then made on Carbon Fiber-Reinforced ThermoPlastic (CFRTP) with a discussion on the advantages of TPCs compared to thermoset matrix composites which are currently the most used in aircraft structures. It appears from this literature review that TPCs are a good alternative to thermoset matrix composites in the aerospace sector, not only in terms of reduction of production time but also because TPCs enable new possibilities of composites assembly.

However, the application of TPCs is currently limited because most of their processing techniques (presented in this review) are not mature yet. Deconsolidation appears to be a central issue that faces both TPC laminates forming and joining processes. In order to understand the effect of the process history of the laminates on their post-processing behavior, a review has been carried out on the physical mechanisms involved during the laminates consolidation cycle. The review revealed that residual stresses can result from consolidation and may lead to several defects (warpage, delamination, cracks, *etc.*) in the composite laminates. They are formed at three levels (fiber scale, ply scale and laminate scale) during cooling of the polymer matrix from the melt to solid state, resulting in a *complex three-dimensional residual stress state* within the laminate.

The temperature at which the residual stresses start building up in the composite is called Stress Free Temperature (SFT). This temperature is driven by the thermal transition properties of the thermoplastic matrix. SFT is around the crystallization temperature (T_c) for semi-crystalline thermoplastics and the glass transition temperature (T_g) for amorphous ones. In general, the further the cooling temperature from the SFT, the more residual stresses reside in the composite. The amount of residual stresses stored in the laminates depends on several factors such as the *thermal gradients*

through the laminate thickness during consolidation, difference in Coefficient of Thermal Expansion/Shrinkage of the composite components (or plies), the components (or plies) *elastic coefficients*, and fiber volume fraction.

The thermomechanical history of the laminates thus have an effect on their behavior after consolidation. With this in mind, a second review is performed on our current understanding of deconsolidation: its physical origin, its modeling as well as the experimental techniques allowing its characterization. This is the topic of the next chapter.

References

[1] A. K. Kaw, *Mechanics of composite materials*. CRC press, 2005 (cit. on pp. 12–13).

[2] F. C. Campbell, *Structural composite materials*. ASM international, 2010 (cit. on pp. 14, 20).

[3] A. B. Strong, *Fundamentals of composites manufacturing: materials, methods and applications*. Society of manufacturing engineers, 2008 (cit. on pp. 15, 17–18).

[4] W. D. Callister, D. G. Rethwisch, *et al.*, *Materials science and engineering: an introduction*. Wiley New York, 2010, vol. 8 (cit. on pp. 16, 27).

[5] X.-S. Yi, S. Du, and L. Zhang, *Composite Materials Engineering, Volume 1*. Springer, 2018 (cit. on p. 16).

[6] P. K. Mallick, *Fiber-reinforced composites: materials, manufacturing, and design*. CRC press, 2007 (cit. on pp. 17, 19).

[7] C. S. Brazel and S. L. Rosen, *Fundamental principles of polymeric materials*. John Wiley & Sons, 2012 (cit. on pp. 18, 34, 41).

[8] L. W. McKeen, *The effect of sterilization on plastics and elastomers*. William Andrew, 2018 (cit. on p. 18).

[9] S. Ropers, *Bending behavior of thermoplastic composite sheets*. Springer, 2017 (cit. on p. 19).

[10] P. Mallick, *Processing of polymer matrix composites*. CRC Press, 2017 (cit. on pp. 21–22, 42).

[11] M. Paiva, C. Bernardo, and M. Nardin, "Mechanical, surface and interfacial characterisation of pitch and PAN-based carbon fibres," *Carbon*, vol. 38, no. 9, pp. 1323–1337, 2000 (cit. on p. 22).

[12] K. K. Chawla, *Composite materials: science and engineering*. Springer Science & Business Media, 2012 (cit. on p. 22).

[13] M. T. Connor, "Consolidation mechanisms and interfacial phenomena in thermoplastic powder impregnated composites," Ph.D. dissertation, EPFL, 1995 (cit. on pp. 23–24, 26, 44, 46).

[14] L.-G. Tang and J. L. Kardos, "A review of methods for improving the interfacial adhesion between carbon fiber and polymer matrix," *Polymer composites*, vol. 18, no. 1, pp. 100–113, 1997 (cit. on p. 23).

[15] M. Sharma, S. Gao, E. Mäder, H. Sharma, L. Y. Wei, and J. Bijwe, "Carbon fiber surfaces and composite interphases," *Composites Science and Technology*, vol. 102, pp. 35–50, 2014 (cit. on p. 24).

[16] U. Vaidya and K. Chawla, "Processing of fibre reinforced thermoplastic composites," *International Materials Reviews*, vol. 53, no. 4, pp. 185–218, 2008 (cit. on p. 25).

[17] F. N. Cogswell, *Thermoplastic aromatic polymer composites: a study of the structure, processing and properties of carbon fibre reinforced polyetheretherketone and related materials*. Elsevier, 2013 (cit. on pp. 26, 40).

[18] S. Beland, *High performance thermoplastic resins and their composites*. William Andrew, 1990 (cit. on pp. 26–27, 31, 41).

[19] J. Bai, *Advanced fibre-reinforced polymer (FRP) composites for structural applications*. Elsevier, 2013 (cit. on p. 27).

[20] C. Ageorges, L. Ye, and M. Hou, "Advances in fusion bonding techniques for joining thermoplastic matrix composites: a review," *Composites Part A: applied science and manufacturing*, vol. 32, no. 6, pp. 839–857, 2001 (cit. on pp. 31, 37).

[21] M. L. Costa, S. f. M. De Almeida, and M. C. Rezende, "The influence of porosity on the interlaminar shear strength of carbon/epoxy and carbon/bismaleimide fabric laminates," *Composites Science and Technology*, vol. 61, no. 14, pp. 2101–2108, 2001 (cit. on p. 32).

[22] M. R. Wisnom, T. Reynolds, and N. Gwilliam, "Reduction in interlaminar shear strength by discrete and distributed voids," *Composites Science and Technology*, vol. 56, no. 1, pp. 93–101, 1996 (cit. on p. 32).

[23] J. Suarez, F. Molleda, and A. Guemes, "Void content in carbon fibre/epoxy resin composites and its effects on compressive properties," *ICCM/9. Composites: Properties and Applications.*, vol. 6, pp. 589–596, 1993 (cit. on p. 32).

[24] D. Saenz-Castillo, M. Martín, S. Calvo, F. Rodriguez-Lence, and A. Güemes, "Effect of processing parameters and void content on mechanical properties and NDI of thermoplastic composites," *Composites Part A: Applied Science and Manufacturing*, vol. 121, pp. 308–320, 2019 (cit. on pp. 32–33).

[25] V.-T. Hoang, B.-S. Kwon, J.-W. Sung, H.-S. Choe, S.-W. Oh, S.-M. Lee, J.-H. Kweon, and Y.-W. Nam, "Postprocessing method-induced mechanical properties of carbon fiber-reinforced thermoplastic composites," *Journal of Thermoplastic Composite Materials*, vol. 36, no. 1, pp. 432–447, 2020 (cit. on p. 32).

[26] R. A. Brooks, H. Wang, Z. Ding, J. Xu, Q. Song, H. Liu, J. P. Dear, and N. Li, "A review on stamp forming of continuous fibre-reinforced thermoplastics," *International Journal of Lightweight Materials and Manufacture*, vol. 5, no. 3, pp. 411–430, 2022 (cit. on p. 33).

[27] L. H. Sperling, *Introduction to physical polymer science*. John Wiley & Sons, 2005 (cit. on p. 34).

[28] D. Wang, Z. Cai, X. Huang, and L. Wang, "Study on the dissolution and diffusion of supercritical carbon dioxide in polystyrene melts based on adsorption and diffusion mechanism," *ACS omega*, vol. 6, no. 3, pp. 1971–1984, 2021 (cit. on p. 35).

[29] R. Wool and K. O'Connor, "A theory crack healing in polymers," *Journal of applied physics*, vol. 52, no. 10, pp. 5953–5963, 1981 (cit. on p. 35).

[30] R. Wool and K. O'Connor, "Time dependence of crack healing," *Journal of polymer science: Polymer letters edition*, vol. 20, no. 1, pp. 7–16, 1982 (cit. on pp. 35–36).

[31] P.-G. De Gennes, "Reptation of a polymer chain in the presence of fixed obstacles," *The journal of chemical physics*, vol. 55, no. 2, pp. 572–579, 1971 (cit. on p. 36).

[32] D. K. Owens and R. Wendt, "Estimation of the surface free energy of polymers," *Journal of applied polymer science*, vol. 13, no. 8, pp. 1741–1747, 1969 (cit. on p. 37).

[33] R. P. Wool, "Adhesion at polymer–polymer interfaces: a rigidity percolation approach," *Comptes Rendus Chimie*, vol. 9, no. 1, pp. 25–44, 2006 (cit. on p. 37).

[34] F. Awaja, "Autohesion of polymers," *Polymer*, vol. 97, pp. 387–407, 2016 (cit. on p. 37).

[35] C. Ageorges and L. Ye, *Fusion bonding of polymer composites*. Springer Science & Business Media, 2002 (cit. on p. 38).

[36] R. J. Young and P. A. Lovell, *Introduction to polymers*. CRC press, 2011 (cit. on pp. 38, 48).

[37] D. Blundell, R. Crick, B. Fife, J. Peacock, A. Keller, and A. Waddon, "Spherulitic morphology of the matrix of thermoplastic PEEK/carbon fibre aromatic polymer composites," *Journal of materials science*, vol. 24, no. 6, pp. 2057–2064, 1989 (cit. on p. 40).

[38] L. Jin, J. Ball, T. Bremner, and H.-J. Sue, "Crystallization behavior and morphological characterization of poly (ether ether ketone)," *Polymer*, vol. 55, no. 20, pp. 5255–5265, 2014 (cit. on p. 40).

[39] P. Painter and M. Coleman, "Polymer morphology. fundam. polym. sci. introd. text," 1997 (cit. on p. 40).

[40] Y. Lee and R. S. Porter, "Crystallization of poly (etheretherketone)(PEEK) in carbon fiber composites," *Polymer engineering & science*, vol. 26, no. 9, pp. 633–639, 1986 (cit. on p. 40).

[41] S.-L. Gao and J.-K. Kim, "Cooling rate influences in carbon fibre/PEEK composites. Part 1. Crystallinity and interface adhesion," *Composites Part A: Applied science and manufacturing*, vol. 31, no. 6, pp. 517–530, 2000 (cit. on p. 40).

[42] W. H. Beever and J. E. O'Connor, *Ryton®-PPS carbon fiber reinforced composites: the how, when, and why of molding*. ASTM International, 1987 (cit. on p. 41).

[43] S.-L. Gao and J.-K. Kim, "Cooling rate influences in carbon fibre/PEEK composites. Part II: interlaminar fracture toughness," *Composites Part A: Applied science and manufacturing*, vol. 32, no. 6, pp. 763–774, 2001 (cit. on p. 41).

[44] H.-J. Um, Y.-T. Hwang, K.-H. Choi, and H.-S. Kim, "Effect of crystallinity on the mechanical behavior of carbon fiber reinforced polyethylene-terephthalate (CF/PET) composites considering temperature conditions," *Composites Science and Technology*, vol. 207, p. 108 745, 2021 (cit. on p. 41).

[45] P. Cebe, S.-D. Hong, S. Chung, and A. Gupta, "Mechanical properties and morphology of poly (etheretherketone)," in *Toughened composites*, ASTM International, 1987 (cit. on p. 41).

[46] M. Trznadel and M. Kryszewski, "Thermal shrinkage of oriented polymers," *Journal of Macromolecular Science, Part C: Polymer Reviews*, vol. 32, no. 3-4, pp. 259–300, 1992 (cit. on p. 42).

[47] W. D. Callister, *Materials science and engineering, an introduction*. John Wiley & Sons, Inc., 1994 (cit. on p. 42).

[48] P. P. Parlevliet, H. E. Bersee, and A. Beukers, "Residual stresses in thermoplastic composites–a study of the literature. Part III: Effects of thermal residual stresses," *Composites Part A: Applied Science and Manufacturing*, vol. 38, no. 6, pp. 1581–1596, 2007 (cit. on pp. 42–43).

[49] M. Loukil, "Microcracking in fiber composites and degradation of thermo-elastic properties of laminates," Ph.D. dissertation, Luleå tekniska universitet, 2011 (cit. on p. 43).

[50] E. Krämer, W. J. B. Grouve, S. Koussios, L. Warnet, and R. Akkerman, "Real-time observation of waviness formation during C/PEEK consolidation," *Composites Part A: Applied Science and Manufacturing*, vol. 133, p. 105 872, 2020 (cit. on p. 43).

[51] P. Kulkarni, K. D. Mali, and S. Singh, "An overview of the formation of fibre waviness and its effect on the mechanical performance of fibre reinforced polymer composites," *Composites Part A: Applied Science and Manufacturing*, vol. 137, p. 106 013, 2020 (cit. on p. 43).

[52] S. Abrate, "Matrix cracking in laminated composites: a review," *Composites engineering*, vol. 1, no. 6, pp. 337–353, 1991 (cit. on p. 43).

[53] A. Abedian and W. Szyszkowski, "Influence of the free surface on the thermal stresses in unidirectional composites," *Composites Part A: Applied Science and Manufacturing*, vol. 28, no. 6, pp. 573–579, 1997 (cit. on p. 43).

[54] W. Unger and J. Hansen, "A method to predict the effect of thermal residual stresses on the free-edge delamination behavior of fibre reinforced composite laminates," *Journal of composite materials*, vol. 32, no. 5, pp. 431–459, 1998 (cit. on p. 43).

[55] C.-H. Hsueh, S. Lee, and H.-Y. Lin, "Analyses of mode I edge delamination by thermal stresses in multilayer systems," *Composites Part B: Engineering*, vol. 37, no. 1, pp. 1–9, 2006 (cit. on p. 43).

[56] L. Lagunegrand, T. Lorriot, R. Harry, H. Wargnier, and J. Quenisset, "Initiation of free-edge delamination in composite laminates," *Composites Science and Technology*, vol. 66, no. 10, pp. 1315–1327, 2006 (cit. on p. 43).

[57] W. E. Lawrence, J. C. Seferis, and J. W. Gillespie Jr, "Material response of a semicrystalline thermoplastic polymer and composite in relation to process cooling history," *Polymer composites*, vol. 13, no. 2, pp. 86–96, 1992 (cit. on pp. 43, 48).

[58] S. Wijskamp, "Shape distortions in composites forming," *Mechanical Engineering*, 2005 (cit. on p. 43).

[59] J. Favre, "Residual thermal stresses in fibre reinforced composite materials, a review," vol. 1, no. 1, pp. 37–53, 1988 (cit. on pp. 44, 46–47).

[60] A. Trende, B. Åström, and G. Nilsson, "Modelling of residual stresses in compression moulded glass-mat reinforced thermoplastics," *Composites Part A: Applied Science and Manufacturing*, vol. 31, no. 11, pp. 1241–1254, 2000 (cit. on p. 44).

[61] J. Barnes and G. Byerly, "The formation of residual stresses in laminated thermoplastic composites," *Composites Science and Technology*, vol. 51, no. 4, pp. 479–494, 1994 (cit. on pp. 44–45, 47).

[62] J.-K. Kim and Y.-W. Mai, *Engineered interfaces in fiber reinforced composites*. Elsevier, 1998 (cit. on pp. 44, 47).

[63] B. Harris *et al.*, "Engineering composite materials," 1999 (cit. on p. 44).

[64] J.-A. E. Månson and J. C. Seferis, "Process simulated laminate (PSL): a methodology to internal stress characterization in advanced composite materials," *Journal of composite materials*, vol. 26, no. 3, pp. 405–431, 1992 (cit. on p. 45).

[65] D. Kugler and T. J. Moon, "Identification of the most significant processing parameters on the development of fiber waviness in thin laminates," *Journal of composite Materials*, vol. 36, no. 12, pp. 1451–1479, 2002 (cit. on p. 46).

[66] G. Twigg, A. Poursartip, and G. Fernlund, "Tool–part interaction in composites processing. Part I: experimental investigation and analytical model," *Composites Part A: Applied Science and Manufacturing*, vol. 35, no. 1, pp. 121–133, 2004 (cit. on p. 46).

[67] N. Ersoy, K. Potter, M. R. Wisnom, and M. J. Clegg, "An experimental method to study the frictional processes during composites manufacturing," *Composites Part A: Applied science and manufacturing*, vol. 36, no. 11, pp. 1536–1544, 2005 (cit. on p. 46).

[68] M. Wisnom, M. Gigliotti, N. Ersoy, M. Campbell, and K. Potter, "Mechanisms generating residual stresses and distortion during manufacture of polymer–matrix composite structures," *Composites Part A: Applied Science and Manufacturing*, vol. 37, no. 4, pp. 522–529, 2006 (cit. on p. 46).

[69] X. Zeng and J. Raghavan, "Role of tool-part interaction in process-induced warpage of autoclave-manufactured composite structures," *Composites Part A: Applied Science and Manufacturing*, vol. 41, no. 9, pp. 1174–1183, 2010 (cit. on p. 46).

[70] V. Kaushik and J. Raghavan, "Experimental study of tool–part interaction during autoclave processing of thermoset polymer composite structures," *Composites Part A: Applied Science and Manufacturing*, vol. 41, no. 9, pp. 1210–1218, 2010 (cit. on p. 46).

[71] E. Hörberg, T. Nyman, M. Åkermo, and S. Hallström, "Thickness effect on spring-in of prepreg composite L-profiles–An experimental study," *Composite Structures*, vol. 209, pp. 499–507, 2019 (cit. on p. 46).

[72] C. Brauner, C. Peters, F. Brandwein, and A. S. Herrmann, "Analysis of process-induced deformations in thermoplastic composite materials," *Journal of Composite Materials*, vol. 48, no. 22, pp. 2779–2791, 2014 (cit. on p. 46).

[73] T. Tsukada, S. Minakuchi, and N. Takeda, "Identification of process-induced residual stress/strain distribution in thick thermoplastic composites based on in situ strain monitoring using optical fiber sensors," *Journal of Composite Materials*, vol. 53, no. 24, pp. 3445–3458, 2019 (cit. on p. 46).

[74] M. M. Shokrieh, *Residual stresses in composite materials*. Woodhead publishing, 2014 (cit. on p. 46).

[75] P. P. Parlevliet, H. E. Bersee, and A. Beukers, "Residual stresses in thermoplastic composites—A study of the literature—Part I: Formation of residual stresses," *Composites Part A: Applied Science and Manufacturing*, vol. 37, no. 11, pp. 1847–1857, 2006 (cit. on pp. 46, 48).

[76] J. A. Nairn and P. Zoller, "Matrix solidification and the resulting residual thermal stresses in composites," *Journal of Materials Science*, vol. 20, no. 1, pp. 355–367, 1985 (cit. on pp. 47–48).

[77] Y. Youssef and J. Denault, "Residual stresses in continuous glass fiber/polypropylene composite thermoformed parts," Proceedings of International Sampe Symposium Conference, 2006 (cit. on p. 47).

[78] S. White, "Processing-induced residual stresses in composites," 2000 (cit. on p. 47).

[79] H. Wagner and J. Nairn, "Residual thermal stresses in three concentric transversely isotropic cylinders: application to thermoplastic-matrix composites containing a transcrystalline interphase," *Composites Science and Technology*, vol. 57, no. 9-10, pp. 1289–1302, 1997 (cit. on p. 47).

[80] S. Wang, D. P. Kowalik, and D. Chung, "Self-sensing attained in carbon-fiber–polymer-matrix structural composites by using the interlaminar interface as a sensor," *Smart materials and structures*, vol. 13, no. 3, p. 570, 2004 (cit. on p. 47).

[81] C. Filiou and C. Galiotis, "In situ monitoring of the fibre strain distribution in carbon-fibre thermoplastic composites1. Application of a tensile stress field," *Composites science and technology*, vol. 59, no. 14, pp. 2149–2161, 1999 (cit. on p. 47).

[82] C. Galiotis, N. Melanitis, D. Batchelder, I. Robinson, and J. Peacock, "Residual strain mapping in carbon fibre/PEEK composites," *Composites*, vol. 19, no. 4, pp. 321–324, 1988 (cit. on p. 47).

[83] A. S. Nielsen and R. Pyrz, "The effect of cooling rate on thermal residual strains in carbon/polypropylene microcomposites," *Science and engineering of composite materials*, vol. 7, no. 1-2, pp. 1–22, 1998 (cit. on p. 47).

[84] R. Young, R. Day, M. Zakikhani, and I. Robinson, "Fibre deformation and residual thermal stresses in carbon fibre reinforced PEEK," *Composites science and technology*, vol. 34, no. 3, pp. 243–258, 1989 (cit. on p. 47).

[85] L. Di Landro and M. Pegoraro, "Evaluation of residual stresses and adhesion in polymer composites," *Composites Part A: Applied Science and Manufacturing*, vol. 27, no. 9, pp. 847–853, 1996 (cit. on p. 48).

[86] Y. Youssef and J. Denault, "Thermoformed glass fiber reinforced polypropylene: microstructure, mechanical properties and residual stresses," *Polymer composites*, vol. 19, no. 3, pp. 301–309, 1998 (cit. on p. 48).

[87] L. Drzal and M. Madhukar, "Fibre-matrix adhesion and its relationship to composite mechanical properties," *Journal of materials science*, vol. 28, no. 3, pp. 569–610, 1993 (cit. on p. 48).

[88] K. Vasylevskyi, I. Tsukrov, B. Drach, H. Buntrock, and T. Gross, "Identification of process-induced residual stresses in 3d woven carbon/epoxy composites by combination of FEA and blind hole drilling," *Composites Part A: Applied Science and Manufacturing*, vol. 130, p. 105 734, 2020 (cit. on p. 48).

[89] X. Liu, X. Wang, Z. Guan, T. Jiang, K. Geng, and Z. Li, "Improvement and validation of residual stress measurement in composite laminates using the incremental hole-drilling method," *Mechanics of Materials*, vol. 154, p. 103 715, 2021 (cit. on p. 48).

[90] A. Sorrentino, F. De Santis, and G. Titomanlio, "Polymer crystallization under high cooling rate and pressure: a step towards polymer processing conditions," in *Progress in Understanding of Polymer Crystallization*, Springer, 2007, pp. 329–344 (cit. on p. 48).

[91] W. Unger and J. Hansen, "The effect of cooling rate and annealing on residual stress development in graphite fibre reinforced PEEK laminates," *Journal of Composite Materials*, vol. 27, no. 2, pp. 108–137, 1993 (cit. on p. 48).

[92] C. Wang and C. Sun, "Thermoelastic behavior of PEEK thermoplastic composite during cooling from forming temperatures," *Journal of composite materials*, vol. 31, no. 22, pp. 2230–2248, 1997 (cit. on p. 48).

[93] G. Dai, L. Zhan, C. Guan, and M. Huang, "The effect of cooling rate on crystallization behavior and tensile properties of CF/PEEK composites," *Journal of Polymer Engineering*, vol. 41, no. 6, pp. 423–430, 2021 (cit. on p. 48).

[94] M. E. Adams, G. A. Campbell, and A. Cohen, "Thermal stress induced damage in a thermoplastic matrix material for advanced composites," *Polymer Engineering & Science*, vol. 31, no. 18, pp. 1337–1343, 1991 (cit. on p. 48).

[95] X. Tardif, "Cristallisation et transferts thermiques dans un polymère thermoplastique semi-cristallin en refroidissement rapide sous pression," Ph.D. dissertation, Université de Nantes, 2012 (cit. on p. 48).

[96] X. Tardif, B. Pignon, N. Boyard, J. W. Schmelzer, V. Sobotka, D. Delaunay, and C. Schick, "Experimental study of crystallization of PolyEtherEtherKetone (PEEK) over a large temperature range using a nano-calorimeter," *Polymer Testing*, vol. 36, pp. 10–19, 2014 (cit. on p. 48).

[97] B. Pignon, X. Tardif, N. Lefèvre, V. Sobotka, N. Boyard, and D. Delaunay, "A new PvT device for high performance thermoplastics: Heat transfer analysis and crystallization kinetics identification," *Polymer Testing*, vol. 45, pp. 152–160, 2015 (cit. on p. 48).

[98] S. White and H. Hahn, "Cure cycle optimization for the reduction of processing-induced residual stresses in composite materials," *Journal of Composite Materials*, vol. 27, no. 14, pp. 1352–1378, 1993 (cit. on p. 48).

"This page left intentionally blank"

CHAPTER 3

CURRENT UNDERSTANDING OF THERMOPLASTIC COMPOSITES DECONSOLIDATION

Contents

In the previous chapter, the main advantages of high-performance Carbon Fiber-Reinforced ThermoPlastics (CFRTPs) for aircraft and aerospace applications have been discussed. The main physical mechanisms involved during CFRTPs consolidation and the induced residual stresses have also been discussed. Deconsolidation was identified as one of the major limiting factors of CFRTPs application in aircraft primary structures. This chapter reviews the current understanding of this phenomenon. As mentioned in the previous chapter, this manuscript focuses exclusively on unidirectional prepreg-based CFRTPs.

3.1 Introduction

High-performance CFRTPs materials are promising to replace in future the traditional thermoset composites which to date are still the most used in aeronautics. One of the major advantages of high-performance CFRTP is their weldability which enables new ways of Out Of Autoclave (OOA) shaping (thermoforming) and assembling (welding) of composite materials. The material used in most of these post-processes are pre-consolidated laminates either by autoclave consolidation, Hot Press Consolidation (HPC) or Vacuum Bag Only Consolidation (VBOC). The pre-consolidated laminates require a secondary re-heating and re-consolidation step, during shaping or assembling operations. When no or a low pressure is applied during the re-heating stage, the appearance and growth of pores can be observed. These pores may remain in the composite when the pressure applied during re-consolidation is weak. This phenomenon called *deconsolidation* and its detrimental effects on the composite parts were briefly introduced in the previous chapter. Although deconsolidation issue is well identified industrially, its understanding is still under investigation.

Pores appearance and growth during processing of prepreg-based composite materials have been reported in the literature by several authors. However, most of these works focuses either on the growth of pores during curing of thermoset composites, or during the processing of woven fabric ThermoPlastic Composite (TPC). In contrast to thermoset composites, the porosity issue in high-performance CFRTPs has been the subject of more recent works due to the fairly recent emergence of new continuous thermoplastic manufacturing techniques such as *In Situ* Consolidation (ISC) or fusion bonding. Nevertheless, the main hypotheses on the physical origin of high-performance CFRTPs deconsolidation are inspired by the results obtained from the

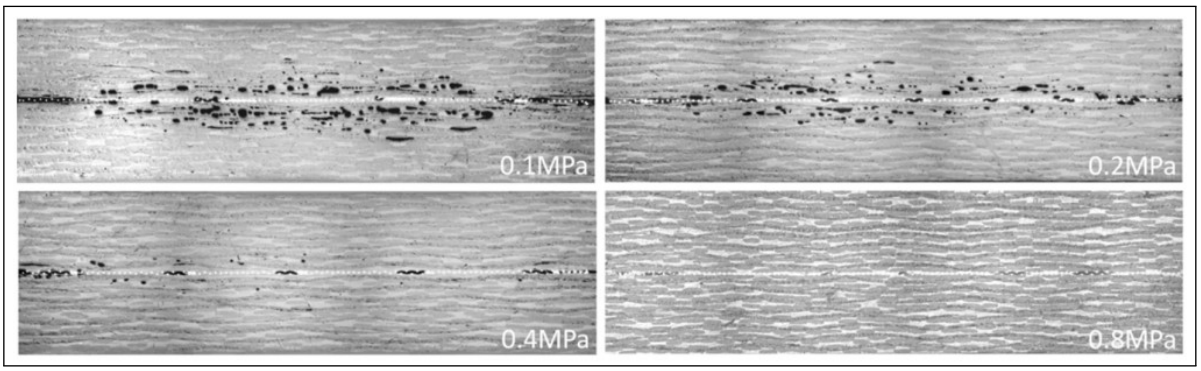

Figure 3.1: Cross section micrographs of GF/PEI joints welded with different pressure of 0.1 MPa, 0.2 MPa, 0.4 MPa, 0.8 MPa [1]. The black spots correspond to the pores.

studies carried out on thermoset and woven composites. First, this chapter reviews the main hypotheses on the origin of deconsolidation as well as the existing models used to predict pore growth during composites processing. Second, the techniques mainly used to characterize porosity in composites are discussed. Finally, this chapter concludes with the positioning of this thesis with respect to the literature and its main objectives.

3.2 Physical origin of deconsolidation

The deconsolidation of TPC laminates have been reported in the literature by several authors. An example is given in Figure 3.1 where pores are observed along the weld line, when low pressure is applied during resistance welding of 8HS Glass Fiber (GF) reinforced PolyEtherImide (PEI) woven fabric TPC laminates initially consolidated in Hot Press [1].

In the literature, there are mainly two hypotheses about the origin of deconsolidation: *volatiles* and *residual stresses*. On the one hand, the volatile hypothesis is inspired by the results obtained from the research carried out on thermoset composites which showed that volatiles such as moisture are responsible for the creation and growth of pores during composite processing. On the other hand, the residual stresses hypothesis is rather inspired by the findings of the studies performed on woven fabrics TPCs. The following sections describe the scenarios suggested by each hypothesis to explain deconsolidation of high-performance CFRTP laminates.

3.2.1 Volatiles induced porosity

Volatile substances are the most studied sources of porosity in composite materials. The volatiles usually come from the *additives* such as plasticizers used during prepreg manufacturing or *moisture*. All polymers, hydrophilic as well as hydrophobic, uptake a certain quantity of moisture when exposed to wet environment [2]. These volatiles can cause pre-existing pores growth or lead to the formation of new pores through a *nucleation* process.

Pre-existing pores usually result from air bubbles mechanically trapped in the laminates during consolidation. This may include air pockets at ply interfaces, ply gaps and ply terminations, wrinkles created during layup, and draping operations. In fact, it is difficult or even impossible to obtain a perfectly consolidated laminate with no initial porosity content during composites processing. With increasing temperature, the volatile substances may evaporate (if initially in a liquid state within the composite) and/or diffuse into the pre-existing pores to increase their interior pressure. This may lead to pore growth when the interior pressure of the pores is higher than the pressure applied by the composite. If the pores contains only vapor, then the interior pressure will be the sum of the partial pressures of the gases contained in the pore (Dalton's law).

Regarding pore nucleation, it can occur either by *boiling* or by *cavitation* [3]. Boiling is define as the nucleation process that occurs when the temperature is raised above the saturated vapor/liquid temperature and cavitation is when the pressure falls below the vapor pressure [3]. Increasing temperature or rapid decompression may cause volatiles evaporation and/or diffusion. The resulting gas may form clusters of critical size leading to the formation of micro-bubbles which are nuclei for pore growth. The pore nucleation is a *thermodynamic process* which mainly depend on temperature and pressure [4]. It can occur homogeneously in the polymer matrix or heterogeneously at the fiber/matrix or particles/matrix interfaces. Here, particles represent all the impurities in the polymer matrix such as dust for example.

The pore growth is rather a *kinetic process* which depends not only on temperature and pressure but also on volatiles diffusivity. In fact, once the pores are formed by nucleation, they grow whether when their interior pressure is above the applied pressure by the composite or by coalescing with neighboring micro-pores. Using the perfect gas law $P_g V = nR_g T$ (R_g is the universal gas constant) to describe the gas (air,

Table 3.1: Preconditioning treatments performed by Slange and coworkers [13].

Treatment	Method	Conditions	Duration
AS	Ambient storage	Lab (≈23 °C/50 %RH)	2 months
VOS	Vacuum oven storage	70°C/vacuum	2 months
HCS	Humidity chamber storage	80 °C/85 %RH	2 weeks
HT-3H@150C	Heat treatment	150 °C	3 h
HT-15M@250C	Heat treatment	250 °C	15 min
HT-3H@150C	Heat treatment	150 °C	3 h
HT-3H@250C + HCS	Heat treatment + Humidity chamber storage	250 °C + 80 °C/85 %RH	3 h + 5 days

water vapor, *etc.*) pressure P_g inside the pores, one realizes that the increase of P_g requires either an increase of the temperature T at constant volume V or an increase of the the number of moles of gas n. The latter depends on the concentration of diffusing substances in the composite and their diffusivity. Therefore, a high volatiles content or moisture uptake and diffusivity promotes pore growth during composites processing.

Volatiles evaporation and/or diffusion as the driving factor of pore appearance and growth during curing of thermoset matrix have been highlighted by several studies [5–7]. In the case of TPC laminates, this hypothesis was mainly highlighted for GF reinforced TPCs such as GF/PolyPropylene (PP), GF/PEI [2, 8, 9]. Although high-performance CFRTPs generally uptake less moisture than high-performance thermoset matrix composites [10–12], Slange *et al.* [13] recently (2018) showed that moisture evaporation and/or diffusion is the driving factor of CFRTP laminates deconsolidation. The authors performed deconsolidation experiments on 100 mm × 100 mm UniDirectional (UD) $[0/90]_{4s}$ Carbon Fiber (CF)/PolyEtherEtherKetone (PEEK) laminate samples pre-consolidated in Hot Press (under 1 MPa with a cooling rate of 2.5 °C/min). After consolidation, the laminates were subjected to different preconditioning treatments listed in Table 3.1. One group of samples were exposed to wet environment (ambient lab conditions, humidity chamber) and the other were dried during different heat treatments.

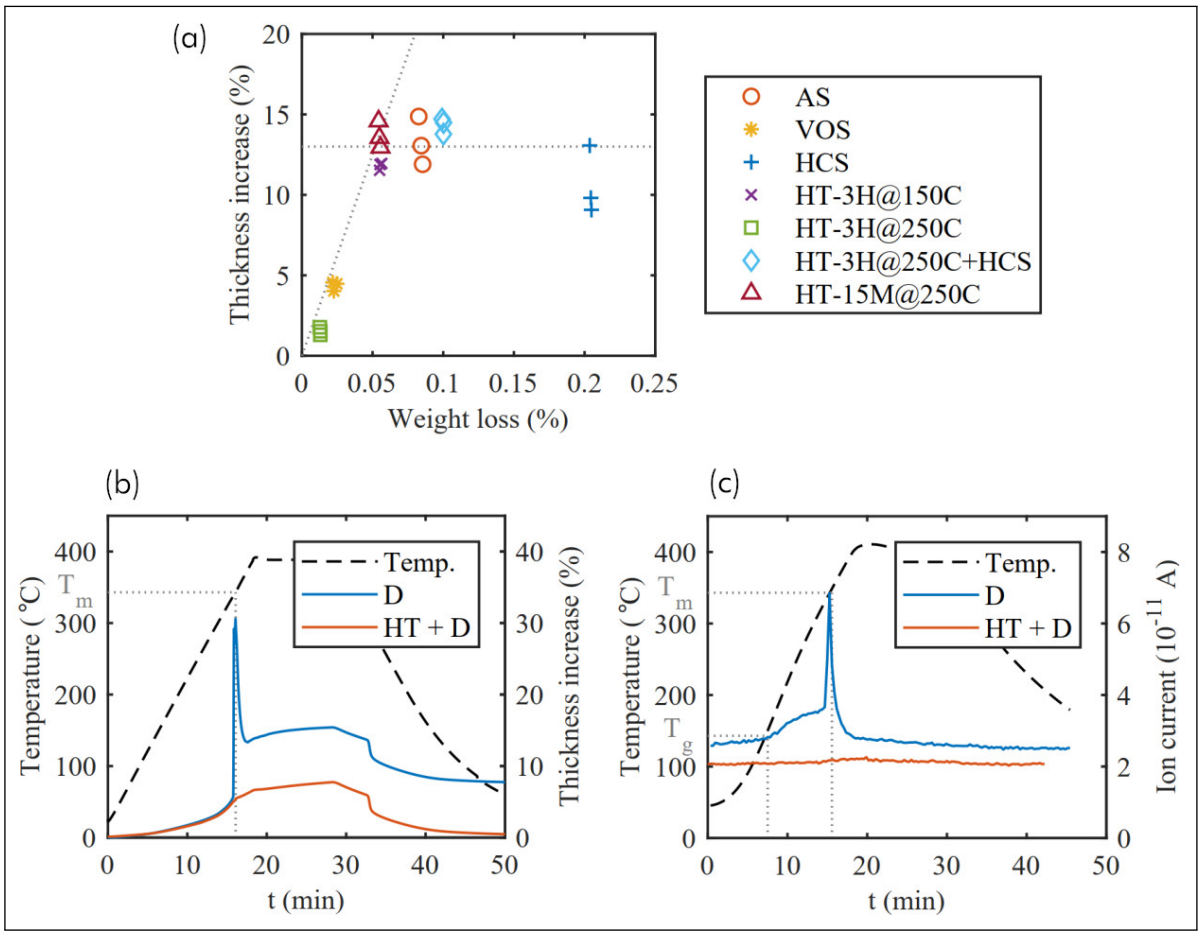

Figure 3.2: Relative thickness increase vs weight loss after deconsolidation [13].

The deconsolidation experiments consisted in heating the preconditioned samples in a pre-heated convection oven at 390 °C for 20 minutes. Deconsolidation was characterized after the experiments by thickness measurements. The authors assume that the relative thickness increase h_{rel} defined by Equation (3.1), after the experiments gives a quantitative measure for the amount of deconsolidation.

$$h_{rel}(\%) = \frac{h_1 - h_0}{h_0} \times 100 \tag{3.1}$$

where h_0 and h_1 are respectively the sample thickness before and after deconsolidation.

Figure 3.2 (a) shows the relative thickness increase of the samples as function of the relative weight loss after the deconsolidation experiments. The relative weight loss w_{rel} defined by Equation (3.2) corresponds to the moisture content in the samples prior to deconsolidation, by assuming no additional weight loss was caused by other

phenomena during the experiments.

$$w_{rel}(\%) = \frac{w_0 - w_1}{w_0} \times 100 \tag{3.2}$$

where w_0 and w_1 are respectively the sample weight before and after the deconsolidation experiment.

The results show that the heat treatment for 3 hours at 250 °C (HT-3H@250C) is most effective in reducing both moisture content and deconsolidation to 0.01 % and 1.5 %. Moreover, the rehumidifying of heat treated samples (HT-3H@250C + HCS) restore all the deconsolidation, showing that moisture is the driving factor of the laminates deconsolidation [13].

However, the final thickness of the samples may be affected by thermal and crystallization shrinkage during cooling. This characterization technique may therefore not correctly highlight the mechanisms leading to deconsolidation. Continuous measurements were thus performed by the authors, on 8 mm × 8 mm ambient storage (AS) and dried (HT-3H@250C) samples, using ThermoMechanical Analysis (TMA) on a Mettler Toledo TMA/SDTA840. Residual Gas Analysis (RGA) in a Netsch STA 449 F3 was also performed to detect the moisture molecules released during the samples heating, by measuring the ion current for a mass-to-charge ratio $m/z = 18$ for H_2O.

Figures 3.2 (b) and (c) show the results of the TMA and RGA experiments. The AS samples show a sudden drastic increase in thickness (deconsolidation peak) around the material melting temperature (T_m) which is correlated to a sudden increase in ion current (moisture release). The dried samples does not show a deconsolidation peak and the ion current remains constant during the heating cycle, suggesting that this heat treatment (HT-3H@250C) has removed almost all moisture in the sample.

The TMA and RGA results thus suggest that moisture is the main factor for press-consolidated CF/PEEK laminates. However, the experiments were performed on small-sized samples of 8 mm × 8 mm. Deconsolidation may be affected by free stress edges, if the sample size is not representative of a laminate structure. Moreover, residual stresses may relax during the heat treatments for 3 hours at 250 °C. Consequently, the deconsolidation peak observed in AS samples cannot be attributed to moisture effect solely. In contrast to dried samples, the AS samples does not relax their residual stresses before the deconsolidation experiments. Nevertheless, Slange *et al.* [13] work suggests that both moisture and residual stresses may be involved in the decon-

solidation phenomenon. It also appears as difficult to decorrelate these two effects, since drying and relaxing residual stresses are usually performed altogether during preconditioning.

3.2.2 Residual stresses induced porosity

The second hypothesis also used to explain CFRTPs laminates deconsolidation is the strain induced by residual stresses. The mechanisms of residual stresses formation during laminates consolidation has been discussed in the previous chapter (see Section 2.2.4 in Chapter 2). Residual stresses result from fiber-bed compaction and shrinkage phenomena during cooling. They are produced at three different scales [14, 15] (fiber, ply and laminate scale) resulting in a *complex three-dimensional residual stress* state within the composite laminate [16].

According to the residual stress hypothesis, deconsolidation might be a reverse process to consolidation [17]. In the consolidation process, the compaction of the fiber bed and the applied pressure control the laminate thickness while the fibers permeability and the melt resin viscosity control the consolidation time. Conversely, the laminate thickness during deconsolidation would be controlled by the amount of residual stresses and applied external pressure, while the time required to reach a stable state after deconsolidation would be influenced by the melt resin viscosity which is sensitive to processing temperature. This means that pores arise during heating, when the resin viscosity or the applied external pressure is low enough to allow strains due to residual stresses loading. The induced strains may cause pore nucleation and growth.

This hypothesis was mainly highlighted in woven and mat TPCs which are known for their ability to store elastic energy due to the fiber bed compressibility and undulating fiber bundels (woven fabric). Although less elastic energy is stored in the fiber bed of UD prepreg-based laminates compared to woven fabrics [18, 19], Donadei *et al.* [20] recently (2018) show that residual stresses are the driving factor of UD CFRTP laminates deconsolidation. The authors performed deconsolidation tests on 200 mm × 50 mm × 3.3 mm UD $[-45/90/45/0]_{3s}$ CF/PolyEtherKetoneKetone (PEKK) laminate samples initially consolidated in an autoclave (under 0.6 MPa with a cooling rate of ≈2 °C/min). After consolidation, one group of samples were dried (DS) for 16 hours at 150 °C and the other were annealed (AN) at 240 °C for several time period (0.5 h, 1 h, 2 h, 3 h, 6 h, 20 h). The deconsolidation tests were carried out in an infrared

Table 3.2: Relative thickness increase measured on blank laminates after IR heating as function of different heat treatments [20].

Heat treatment	Relative Thickness Increase (%)
16H@150C	7.67
0.5H@240C	6.15
1H@240C	5.35
2H@240C	2.67
3H@240C	1.63
6H@240C	0.83
20H@240C	0.45

oven where the samples were heated up to 410 °C, usually in 220 s-240 s. As in the Slang *et al.* [13] work, deconsolidation was also characterized by a relative thickness increase. The tests results are reported in Table 3.2.

On the material system studied by Donadei and coworkers, a high temperature drying at 240 °C for 3 hours was not sufficient to reduce the sample thickness increase after deconsolidation. Only a long time annealing at 240 °C for 20 hours allowed to prevent deconsolidation, suggesting that residual stresses loading is the driving mechanism of deconsolidation. The thickness measurements were supported by post-process micrographs as shown in Figure 3.3. Porosities were not detected after the long time annealing (20H@240C).

However, as mentioned in previous section, post-process thickness measurements may be affected by shrinkage phenomena during cooling. Moreover, significant microstructural changes may also occur during heating leading to a different final microstructure after cooling. Furthermore, the observations made on samples annealed at 240 °C for less than 20 hours can also be attributed to moisture effect, since no information was given about whether the heat treatments actually removed the moisture initially stored in the samples. Nevertheless, Donadei *et al.* [13] work also suggest that both moisture and residual stresses may be involved in deconsolidation. It also appears as difficult to decorrelate these two effects, since drying and relaxing residual stresses are usually performed altogether during preconditioning.

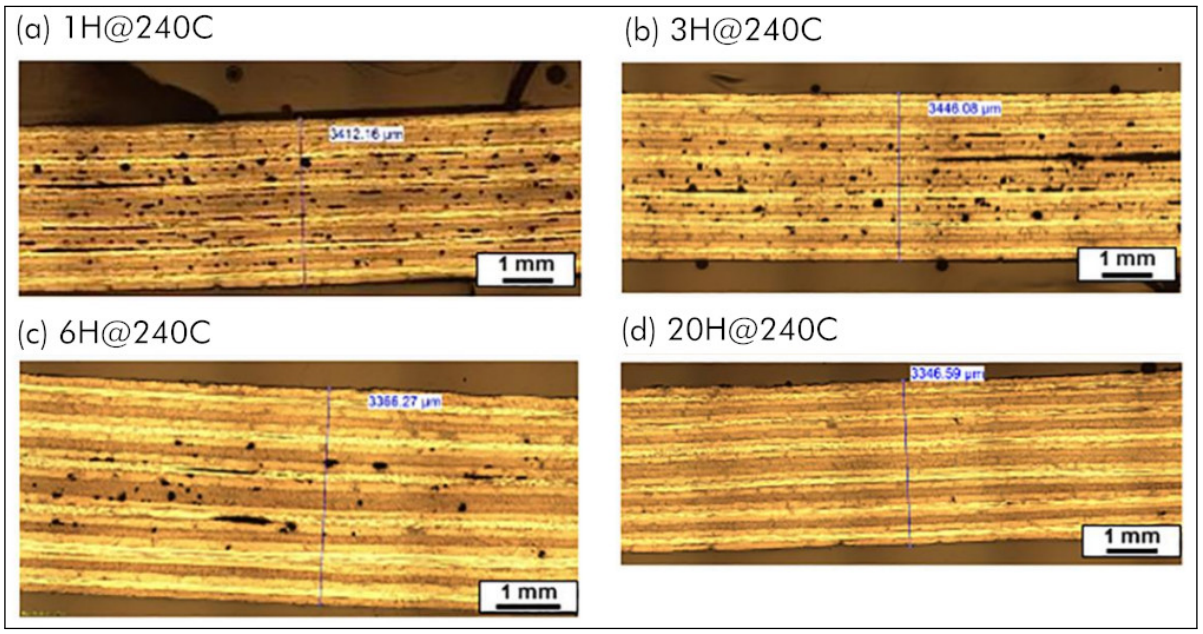

Figure 3.3: Optical micrographs of IR-heated blank laminates after annealing at 240 °C at different times [20]. The black spots correspond to the pores.

Although the material studied in both works [13, 20] are relatively different in terms of chemical structure, it is surprising that they have two different origins of deconsolidation. In fact, both materials are consolidated under similar conditions and they have similar moisture-related (moisture uptake and diffusivity) properties [21–23]. Therefore, it is quite difficult to conclude on the physical origin of deconsolidation from these studies.

3.3 Porosity growth prediction models

Two categories of predictive models are found in the literature: models based on the volatiles diffusion scenario and those based on residual stresses loading.

3.3.1 Models based on volatiles diffusion

Most of the volatiles diffusion models are based on the scenario described by Campbell [24]. The vapor pressure of the volatiles (including moisture) stored in the material increases with increasing temperature. When this vapor pressure inside the pores is higher than the pressure applied by the composite, then the pores grow. Conversely, when the interior vapor pressure is lower than the external pressure applied by the

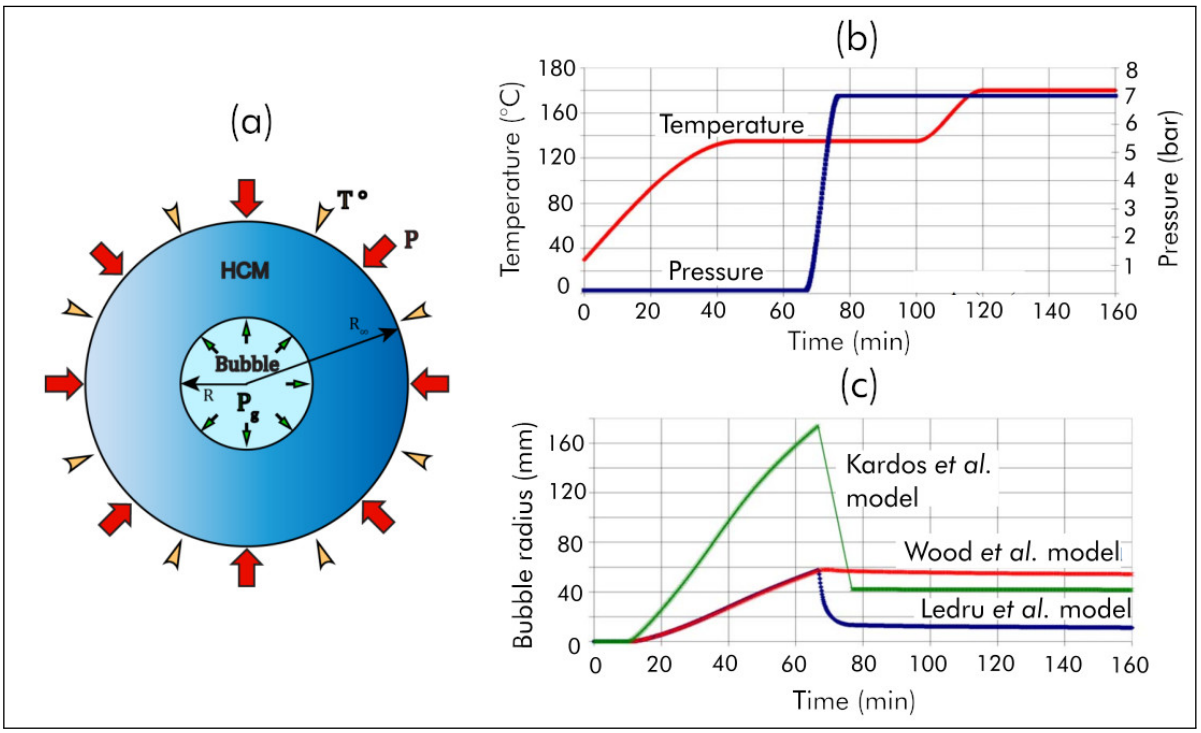

Figure 3.4: Models based on volatiles diffusion. (a) Porosity modeled by a spherical bubble surrounded by an isotropic homogeneous medium [7]; (b) Models application to a thermoset matrix composite curing cycle and (c) the bubble radius predict by Kardos *et al.* [26], Wood *et al.* [25] and Ledru *et al.* [27].

composite, the pores size decreases [25]. Among the volatiles, moisture is the most present in prepregs and the one with the highest saturation vapor pressure. The amount of moisture uptake in the material thus significantly affects its final porosity content.

The first model of pore growth in composites was proposed by Kardos *et al.* [26] in 1986. This model was used to describe the pore growth during curing of thermoset matrix composites. Like most pore growth models, they consider a spherical bubble surrounded by an isotropic homogeneous medium with a concentration of diffusing species (Figure 3.4 a). To simplify the model, they neglected the effect of fibers present in the resin. Coalescence and pore migration were also not taken into account. Temperature and moisture concentration were assumed to be uniform. The moisture concentration around the bubble does not decrease with increasing moisture diffusion in the bubble. The effects of viscosity and surface tensions were also neglected. Finally, the resin pressure was assumed to be equal to the pressure imposed on the material.

The bubble growth was thus estimated with the following equations:

$$\frac{d(d_B^2)}{dt} = 16D\beta^2 \tag{3.3}$$

with

$$\beta = \frac{C_\infty(S_0, W_R, \rho_R) - C_{sat}(P_{H_2O}, P, T)}{\rho_g(d_B, M, P, T)} \tag{3.4}$$

and

$$D = D_0 exp\left(\frac{-E_a}{R_g T}\right) \tag{3.5}$$

where d_B (m) is the bubble diameter, D (m^2/s) the moisture diffusivity and β is the driving force of the pore growth. C_∞ is the moisture concentration in the resin which depends on the solubility S_0 of moisture in the resin, W_R and ρ_R respectively the weight fraction of resin and its density. C_{sat} is the moisture concentration at the bubble interface which depends on the partial pressure of moisture P_{H_2O} within the bubble, the applied pressure by the resin P (N/m^2) and temperature T (K). ρ_g (kg/m^3) is the density of gas in the bubble which depends among other parameters mentioned in Equation 3.4 on molecular weight M (g/mole) of gas in the bubble.

D_0 (m^2/s) is a pre-exponential constant; E_a (J/mol) the activation energy for diffusion; and R_g ($J/(mol \cdot K)$) the universal gas constant. Given the assumptions made by Kardos *et al.*, their model overpredicted the pores size (Figure 3.4 c) for a given thermoset matrix composite curing cycle (Figure 3.4 b). For example, it predicts pore size higher than 20 mm diameter in 2 mm thick sample.

To improve the accuracy of Kardos *et al.* model, Wood *et al.* [25] take into account the effect of surface tension. Equations 3.3 and 3.4 were rewritten as follows:

$$\frac{dR}{dt} = -\frac{D(C_{sat} - C_\infty)}{\rho_g - (\tau/3R)}\left[\frac{1}{R} + \frac{1}{(\pi D)^{1/2}}\right] \tag{3.6}$$

with

$$\tau = \frac{2M\Gamma}{R_g T} \tag{3.7}$$

where R is the bubble radius and Γ the constant surface tension for the bubble/resin system.

Nevertheless, the predicted pore sizes were still overestimated (Figure 3.4 c). The main limitation of these models was that they do not consider the rheological behavior of

the polymer resin around the bubble. Regarding the sensitivity of these models with respect to the process parameters, Wood *et al.* model has a low sensitivity to pressure and Kardos *et al.* model a high sensitivity to temperature.

In 2010, Ledru *et al.* [27] proposed a new model by coupling the diffusion with the viscoelastic behavior of the resin. However, moisture diffusion was still assumed to be Fickian and moisture diffusivity was thus still expressed by the Arrhenius Equation 3.5. The bubble growth was described by the following differential equation:

$$\frac{dR}{dt} = \frac{P_g(R, m, T) - P}{4\eta(T, \alpha)} R + \frac{\Gamma}{2\eta(T, \alpha)} \tag{3.8}$$

with

$$\frac{dm}{dt} = 4\pi D(C_\infty - C_{sat})R\left(1 + \frac{R}{\sqrt{\pi D t}}\right) \tag{3.9}$$

where m is the mass of gas in the bubble and η is the resin viscosity which depends on temperature and crosslinking ratio α.

This new formulation allowed a decrease in the predicted pore size (Figure 3.4 c). However, the predicted size was still not representative of the pore growth during processing. For example, Ledru *et al.* model predicts a final pore radius close to 10 mm while the thickness of a prepreg ply is about 0.2 mm. It was not possible to validate these models given the predicted pore sizes.

de Parscau du Pessix *et al.* [28] (2016) explain the limitation of these models by an overestimation of moisture effect. The authors thus improved the model proposed by Ledru *et al.* by considering a "dual stage" diffusion of moisture and a slowing down of diffusion due to the resin polymerization. The "Dual-stage" diffusion is based on the principle that moisture diffusion in the material is governed by two phenomena which are respectively the filling of free volumes in the composites (free water) and the formation of chemical bonds between the water molecules and the polymer matrix (bonded water). Each of these two phenomena can be represented by a Fickian behavior and their sum allows to describe the global behavior of the material. The dual stage diffusion in composites is further discussed later in Chapter 4.

Equation 3.5 describing the moisture diffusivity was rewritten as follow:

$$\begin{cases} D_F = D_{0,1} \exp\left(-\dfrac{E_{a,1}}{R_g T}\right) \exp(-X_1 \alpha) & \\ D_B = D_{0,2} \exp\left(-\dfrac{E_{a,2}}{R_g T}\right) \left(\dfrac{\alpha_{rig} - \alpha}{\alpha}\right) & \text{if } (\alpha \leq \alpha_{rig}) \\ D_B = 0 & \text{if } (\alpha > \alpha_{rig}) \end{cases} \tag{3.10}$$

where D_F and D_B are respectively the moisture diffusivity of free and bonded water molecules. X_1 and α_{rig} are constants.

Moreover, they introduced an intermediate phase at the interface between the resin and the bubble (Figure 3.5 a). This intermediate phase, having different diffusive properties than the resin, also allowed a slowing down of the diffusion at the bubble interface. Equation 3.9 thus becomes:

$$\frac{dm}{dt} = -4\pi R^2 J_2 \tag{3.11}$$

with

$$\begin{cases} J_2 = J_{2,F} + J_{2,B} & \\ J_{2,i} = -D_{1,i} \dfrac{(C_{\infty,i} - C_{sat2,i})}{R} \dfrac{R_\infty (R + \delta)}{\gamma R_\infty \delta + R(R_\infty - R - \delta)} & , i = \{F, B\} \\ \gamma = \dfrac{D_1}{D_2} & \end{cases} \tag{3.12}$$

where $J_{2,F}$ and $J_{2,B}$ are respectively the density of free and bonded molecules flow at the bubble surface. γ is a dimensionless parameter which represents the increase in moisture diffusion resistance in the vicinity of the bubble. δ is a second parameter corresponding to the thickness of the intermediate phase (Figure 3.5 a).

The resolution of the system of equations (3.8), (3.11) and (3.12) allowed to predict more realistic pore sizes during a thermoset composite curing. However, this model includes several parameters whose identification is relatively complex. Moreover, the improvements provided by a slowdown of moisture diffusion due to the crosslinking are not applicable to TPCs. Further developments are thus required to adapted this model based on volatiles diffusion to high-performance CFRTPs processing.

3.3.2 Models based on residual stresses

In addition to the models based on volatiles diffusion, predictive models have also been developed on the mechanism of residual stresses loading. Xiao *et al.* [17, 29] were

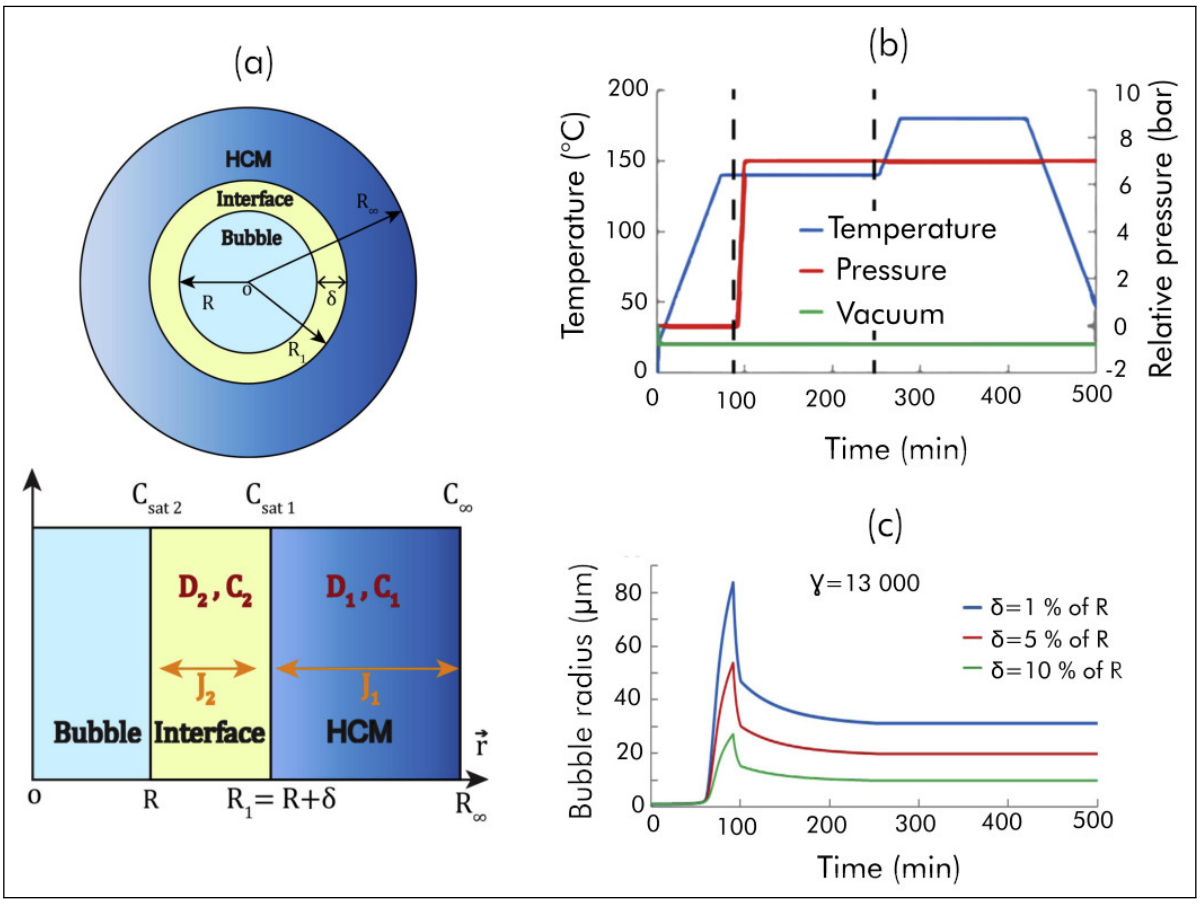

Figure 3.5: (a) Schematic view of the bubble growth model including an additional interface diffusion layer of radius $R + \delta$ with assumed different behavior. (b) Model application to a thermoset composite curing. (c) Model predictions of the bubble radius evolution for several values of δ and γ =13 000 during the curing cycle. The bubble initial radius is 1 µm. [28]

the first, in 1993, to put forward the idea of deconsolidation due to residual stress. However, they consider that the thickness increase observed during heating is due to interply decohesion. Therefore, their model did not describe a pore growth. Later in 1998, Henninger *et al.* [30] observed the same phenomenon of thickness increase during post-processing of woven fabric GF reinforced PolyAmide (PA12) sheets. They call this phenomenon thermal deconsolidation. Their experiments consisted in heating, at different temperatures and pressures, pre-consolidated blanks. Deconsolidation was then characterized by the final porosity content in the samples. According to their observations, deconsolidation would occur after T_m for semi-crystalline polymers (and

glass transition temperature (T_g) for amorphous ones). Then beyond this temperature, deconsolidation would be insensitive to any further increase in temperature. Their observations also point out that the porosity content is not sensitive to heating time.

Based on these observations, Ye *et al.* [17] proposed a scenario of deconsolidation which would be a reverse process to consolidation. According to the authors, in a first stage, increasing temperature leads to increasing thermal pressure inside the pores. This thermal pressure then generates a growth of micro-pores (gas thermal expansion). In a second stage, the micro-pores coalesce to form larger pores. Finally in the last stage, the de-compaction pressure (Figure 3.6 a) of the fiber bed due to residual stresses, leads to pore growth. However, the authors emphasized that gas thermal expansion (first stage) and pore coalescence (second stage) have a negligible impact on the final porosity content and that the de-compaction pressure (last stage) is the driving force of pore growth.

From the proposed scenario, the authors developed a model which consider a spherical bubble (of radius R_g) surrounded by a volume of polymer matrix (of radius R_M). The bubble and the matrix were immersed in a Representative Elementary Volume (REV) of the composite (Figure 3.6 a). Contrary to the volatiles diffusion-based approaches, the bubble in this case was subjected to a de-compaction pressure and not a compression exerted by the polymer matrix. The de-compaction pressure was assumed to be hydrostatic and the polymer matrix behavior was described by a viscoelastic model. The medium around the bubble was assumed to be incompressible. The bubble radius variation and the subsequent porosity content were estimated with the following equations:

$$\begin{cases} \dfrac{d^2(R_g)}{dt^2} = \kappa(P_{r=R_M} - P_{r=R_g}) + I_\varphi + E_\varphi + V_\varphi \\ \kappa = \dfrac{1}{\rho_M}\left[R_g\left(1 - \dfrac{R_g}{R_M}\right)\right]^{-1} \\ P_{r=R_M} = P_0 + \Delta P - P_{dec} \\ P_{r=R_g} = \left[\left(\dfrac{T}{T_0}\right)\left(\dfrac{R_g^0}{R_g}\right)^3 P_g^0 - \dfrac{2\Gamma}{R_g}\right] \\ I_\varphi = \kappa\rho_M\left\{-2\ln\dfrac{R_M}{R_g} + \dfrac{1}{2}\left[1 - \left(\dfrac{R_g}{R_M}\right)^4\right]\right\}\left(\dfrac{d(R_g)}{dt}\right) \end{cases} \tag{3.13}$$

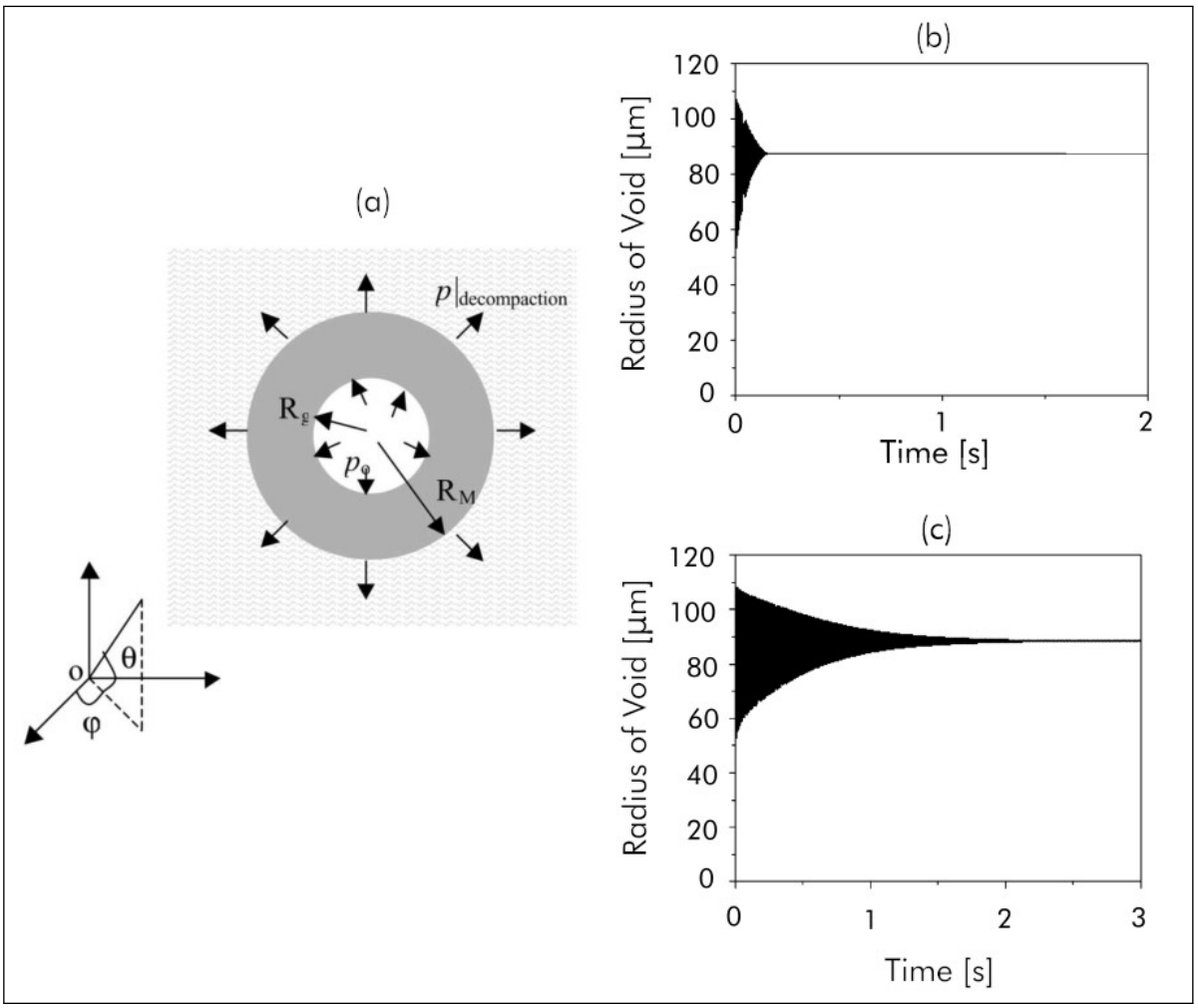

Figure 3.6: (a) Schematic illustration of the representative volume element. Dependence of the void (bubble) radius on time at (b) T =180 °C and (c) T =220 °C [17].

$$\begin{cases} E_\varphi = -2\kappa\rho_M\lambda\left[\left(\dfrac{R_g^0}{R_g}\right)^2 - \dfrac{(R_M^3 - R_g^3 + (R_g^0)^3)}{R_M^2}\right] \\ V_\varphi = -\dfrac{3\kappa\rho_M(\sqrt{6})^{n-1}\eta_0(T)}{2(3n+1)}\left[1 - \left(\dfrac{R_g}{R_M}\right)^{3n-1}\right]\left(\dfrac{|dR_g/dt|}{R_g}\right)^{n-1}\dfrac{dR_g}{dt} \end{cases} \tag{3.14}$$

where ρ_M is the polymer matrix density; P_0 corresponds to the pressure of the external circumstance (atmospheric pressure); ΔP is the controllable processing pressure; and P_{dec} is the traction due to the fiber de-compaction. R_g^0, T_0 and P_g^0 are respectively the initial radius, temperature and pressure of the gas inside the bubble. Γ is the surface tension, λ the elastic shear modulus of the polymer matrix, η_0 a temperature-dependent viscosity coefficient and n a material constant. This bubble growth equation

was obtained from the equations of mass and momentum conservation for the polymer matrix melt in spherical coordinates, in addition with the Kelvin–Voigt equation [31] in order to consider the viscoelastic effect.

The results obtained from this model on woven fabric GF/PolyAmide (PA)12 supported the observations made by Henninger *et al.* about the insensitivity of deconsolidation to the temperature above T_g. Furthermore, the stability of the pore size was achieved in a few seconds *i.e.* 0.2 s at 180 °C (Figure 3.6 b) and 2.5 s at 220 °C (Figure 3.6 c). However, even if the model predicts realistic pore sizes, the predicted radius evolution is not in agreement with the described deconsolidation scenario. According to the authors, this is related to the fact that they did not consider the temperature dependence of the elastic moduli of the polymer matrix. Other approaches based on residual stresses loading can be found in the literature with applications on woven [32] and mat [29, 33] composites or unimpregnated fibers [34].

3.4 Deconsolidation characterization techniques

One of the limiting factors in the development of physically motivated models of deconsolidation is the limited knowledge of the phenomenon. However, understanding the mechanisms of pore occurrence and growth requires a good characterization of the phenomenon. This section reviews most of the techniques commonly used to characterize porosity in composites. Qualitative methods for composite parts inspection are not concerned by this review. Only quantitative techniques are discussed. These techniques are divided into two groups namely *post-process* and *in situ* characterization.

3.4.1 Post-process characterization

The post-process techniques consist in characterizing the deconsolidation after the experiments (after cooling). The measurement method used can alter the sample condition (destructive) or not (nondestructive). The destructive measurement methods includes microscopy and density measurement. The non destructive techniques includes thickness measurements and ultrasonic testing.

Microscopy It is used to estimate the porosity content, sizes, shapes and distribution on a two-dimensional (2D) cross section. This technique is based on processing (segmentation, binarization, *etc.*) of a 2D image obtained by optical microscopy or Scanning Electron Microscopy (SEM). Like all techniques based on image processing,

the validity of the results (porosity content, sizes, *etc.*) depends significantly on the image quality. For this reason, close attention must be paid to the sample preparation step. Indeed, the preparation stage consists in encapsulating the sample in a resin. The 2D surface to be analyzed is then successively polished with several abrasives having smaller grain sizes, until a mirror surface is obtained. These steps can induce defects and biased porosity.

Microscopy allows to obtain 2D images with very good contrast between fibers, matrix and pores at low resolutions ($\approx 2^2$ µm^2/pixel). However, the sample preparation step is labor intensive and time consuming. The surface that can be analyzed is also limited due to the operating area of microscopes (about 100 mm $\times$ 100 mm). Moreover, microscopy does not provide quantitative 3D data of the internal structure of the composite. Several samples of the same composite part must thus be analyzed in order to be quantitative. Despite these limitations, microscopy is widely used in the literature for qualitative analysis of deconsolidation [7, 13, 20, 35–37].

Density measurements This technique allows to estimate the global porosity volume content of a composite sample. It consists in the evaluation of the composite density ρ_c (kg/m^3) then the weight fractions (%) of fibers w_f and polymer matrix w_m. The global porosity content is then estimated from the following equation [38]:

$$\%Porosity = 100 - \rho_c \left(\frac{w_m}{\rho_m} + \frac{w_f}{\rho_f} \right) \tag{3.15}$$

where ρ_f and ρ_m are respectively the density of fibers and matrix. The composite density can be evaluated using a hydrostatic weighing scale or by using the buoyancy exerted on the sample when it is immersed in distilled water (Archimedes's Principle) [39]. The weight fraction of fiber in the composite can be measured by degrading the resin through calcination or chemical attack [40].

Although this method allows to estimate the global porosity content on larger samples (compared to microscopy) [41, 42], it does not provide any information on the morphology (size, shape) and spatial distribution of pores. Moreover, it requires a precise knowledge of the fibers and matrix density because a small error on one of these properties may lead to a significant change of the obtained porosity content.

Thickness measurement It is a non destructive macroscopic analysis technique that can be used to estimate a sample strain after a deconsolidation experiment. It

consists in measuring the sample thickness before and after the test. The strain is then characterized by a relative thickness variation h_{rel} according to the Equation 3.1 already mentioned in Section 3.2.1. The sample thickness is usually measured with a micrometer of 0.01 mm accuracy.

The advantage of this technique lies in its rapidity and simplicity but the estimated strain may not correspond to the actual porosity content in the composite, due to shrinkage phenomena during cooling. Nevertheless, it is widely used in the literature to characterize deconsolidation [13, 20, 29, 43]. However, thickness measurement becomes more reliable when it is performed continuously and *in situ* during the whole deconsolidation experiment [44]. In this latter case, it can be classified in *in situ* characterization techniques.

Ultrasonic testing (UT) This technique is also non destructive and allows to identify the pores location and to approximate their global content [45]. It consists in sending an ultrasound signal through the composite part. The signal is sent from a transmitting transducer to a receiving transducer. The wave generated passes through the part at a particular frequency and speed. To enhance the wave transmission in the composite, coupling agents such as water, oil or gel are often used. The composite surfaces are thus partially wet or completely immersed in the coupling medium. The wave attenuation through the composite in its thickness is then measured, because of the attenuation variation in the presence of delamination or pores. Finally, it is possible to correlate the porosity content to the attenuation coefficient which is representative of the ratio between the amplitude of the emitted and transmitted wave. To establish this correlation, it is essential to also estimate the porosity content from another technique.

This method allows relatively fast measurements on very large parts (several meters). However, it requires a good knowledge of the material and its properties, to properly interpret the results. In addition, the discrepancy in the pore sizes require to perform the measurements at several frequencies. For example, the observation of delamination requires a different working frequency than the one used for the observation of micro-pores. Furthermore, this technique gives little information about the pores spatial distribution in the thickness and their morphology. Nevertheless, it is widely used in the industrial and academic field [20, 41, 46–49]. There are acceptance criteria for composite parts in attenuation that impose detection limits which correspond to defect sizes of a few microns to qualify a part as acceptable.

3.4.2 *In situ* characterization

In contrast to post-process techniques, *in situ* methods allow to characterize the studied phenomenon without necessarily waiting for the experiment ending. The characterization can be done continuously during the whole cycle or in a sequential manner by interrupting the test at periodic times.

Dilatometry This technique allows to characterize the sample strain during a temperature cycle. It consists in measuring the time evolution of the sample thickness. Dilatometry is generally performed on standard TMA devices (dilatometer) where the thickness is measured from the displacement of a piston in contact with the sample. The piston is usually made of ceramics which have a low Coefficient of Thermal Expansion (CTE), in order to minimize measurement errors related to its thermal expansion.

This technique is very simple to implement and allows to characterize the deconsolidation continuously during the whole heating cycle. However, it requires small sample sizes (around 10 mm) imposed by the dilatometer, which are not representative of the size of composite structures. This technique is rarely used for the characterization of pore growth [13].

Optical measurements This technique is based on the same principle as the dilatometer. It also involves the measurement of thickness variation during the whole heating cycle. The difference here is that the thickness is measured by optical means such as laser sensors (distance measurement) or Charge Coupled Device (CCD) cameras. In the first case, the laser sensors can be positioned in different directions and synchronized to obtain online the sample strain in several directions during the experiments. In the second case, only the lateral surface of the sample can be recorded by the camera. This last solution does not allow to have information on the strain at the sample core. It can therefore be used for the study of woven fabrics laminates where the deconsolidation is homogeneous in the samples [32]. In the case of UD laminates, laser sensors are more appropriate [44].

Unlike dilatometry which is limited in sample size, this technique can be used on relatively large samples (over 100 mm) which are more representative of composite structures. However, while it allows a continuous characterization, this technique does not provide any information on the micro-structure evolution of the samples

during the experiments. Since there is no standard machine that uses this technique, it requires the development of an experimental bench capable of applying a temperature and pressure cycle to the samples in a controlled environment.

X-ray transmission microtomography This technique also called X-ray micro Computed Tomography (CT) is a non destructive technique that enables a complete qualitative and quantitative analysis of a composite microstructure. It consists in measuring the linear absorption coefficient μ of X-ray passing through a sample in several directions. The absorption coefficient in turns depends on the density ρ, the atomic number Z of the investigated material, and the photon energy E [50]. To perform a measurement, the sample is placed on a rotating platform positioned between an X-ray source and a detector. Successive 2D projections of the sample on the detector are captured at each rotation increment [51]. The rotation angle and rate vary according to the type of device (tomograph) and the desired resolution. The series of 2D projections are then reconstructed into 3D density field through an inverse method called "reconstruction" [40] (Figure 3.7).

The time interval between the successive shots (projections) must be small enough to perform a continuous measurement during the experiments. Otherwise, interrupted tests between the different scans are performed. In the past, the acquisition time was too long to perform continuous measurements but with the recent development of large devices such as synchrotron X-ray technologies, this time is increasingly reduced allowing *in situ* investigations [53–55].

The difference in density between the components of the composite (fiber, matrix, pores or other defects) makes this technique very efficient to examine the composite microstructure in detail [39]. This technique provides a complete 3D distribution of the pores inside the composite, their morphology and their content, without any initial preparation of the samples. However, the measurements as well as the reconstructions can be time-consuming and may provide large digital files depending on the sample size and the scans resolution [7]. In addition, the use of tomographs requires significant investment and operating costs. Therefore, this technique is currently limited to small-sized (few millimeters) samples in order to have a sufficient resolution for the pores observation [55–57].

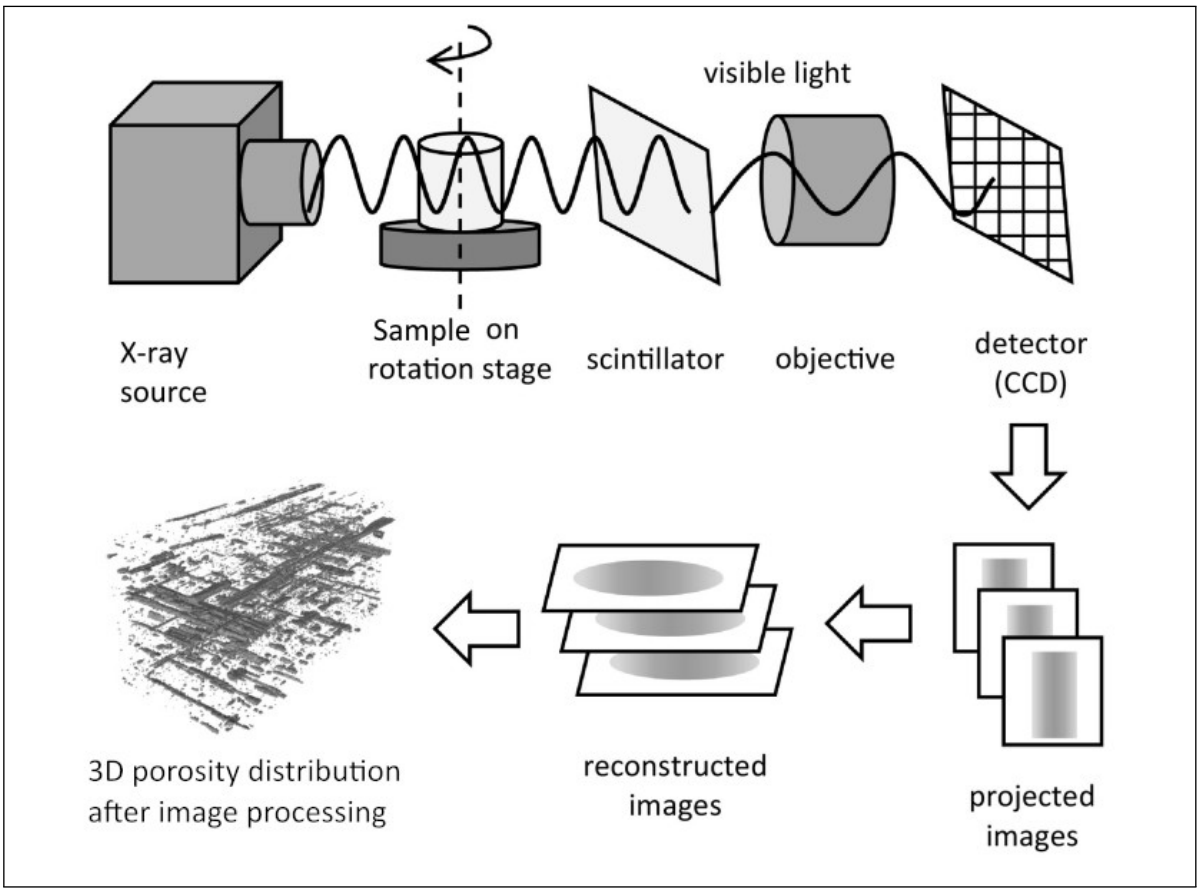

Figure 3.7: Schematic illustration of X-ray microtomography [39, 52].

3.5 Conclusion

This chapter reviews the state of knowledge regarding deconsolidation in high-performance TPCs. From this review, it appears that there are currently very few studies on deconsolidation in high-performance TPCs, despite the detrimental effect of this phenomenon on composites. In aircraft sector, a structural part having a porosity content greater or equal to 1 % is rejected. Most of the processing techniques of TPCs such as welding, thermostamping or ISC are subject to the deconsolidation issue. The necessity of a thorough understanding of deconsolidation is therefore obvious, in order to better control these processes and ensure a significant progress of TPCs towards structural applications in aerospace industry.

The understanding of the physical origin of deconsolidation is not yet established. The mechanisms of pore appearance and growth in composites are complex and raise different opinions. Some authors believe that deconsolidation is related to the presence

of *moisture* in composites. For others, it would be rather the presence of *residual stresses*. This limitation of the physical understanding of the phenomenon results in a lack of quantitative predictive model of deconsolidation during high-performance CFRTPs processing. The few quantitative models that have been experimentally validated correspond to the prediction of pore growth during the curing of thermoset matrix composites or during woven fabric composites processing. However, these models are not directly applicable to high-performance TPCs because of the differences in matrix (thermoset vs thermoplastic) and reinforcement architecture (woven fabric vs UD).

In most of the studies performed in the literature, deconsolidation was mainly characterized by post-process techniques. Unfortunately, these techniques do not allow to monitor in real-time the appearance and growth of pores during heating, which limits the phenomenon understanding. To properly model the appearance and growth of pores during high-performance TPCs processing, it is necessary to observe the phenomena involved.

The objective of this thesis is thus to provide insights into the physical mechanisms involved during deconsolidation, based on experimental studies. For this purpose, deconsolidation will be characterized by *in situ* measurement techniques in order to monitor in real-time what happens during the heating of the CFRTP laminates. Among the *in situ* characterization techniques, optical measurements by laser sensors and X-ray microtomography are the most suitable for this purpose. New experimental devices integrating these characterization techniques will thus be developed. In addition, the mechanisms of moisture transport in CF/PEKK laminates will be the subject of a specific study intended to establish a *preconditioning protocol* which allows to better decouple the effect of moisture from residual stresses and to evaluate the *moisture transport kinetics* in this material. The studied laminates will be manufactured from two consolidation processes, in order to investigate the effect of the pre-consolidation process on deconsolidation. The results of the experimental studies will provide the necessary keys for the development of a physical model of high-performance CFRTP laminates deconsolidation.

References

[1] H. Shi, "Resistance welding of thermoplastic composites: process and performance," Ph.D. dissertation, Technische Universiteit Delft, 2014 (cit. on p. 63).

[2] S. Roychowdhury, J. W. Gillespie, and S. G. Advani, "Volatile-induced void formation in amorphous thermoplastic polymeric materials: I. Modeling and parametric studies," *Journal of Composite Materials*, vol. 35, pp. 340–366, 4 2001 (cit. on pp. 64–65).

[3] C. E. Brennen, *Cavitation and bubble dynamics*. Cambridge university press, 2014 (cit. on p. 64).

[4] H.-Y. Kwak and Y. W. Kim, "Homogeneous nucleation and macroscopic growth of gas bubble in organic solutions," *International Journal of Heat and Mass Transfer*, vol. 41, no. 4-5, pp. 757–767, 1998 (cit. on p. 64).

[5] L. Grunenfelder and S. Nutt, "Void formation in composite prepregs–Effect of dissolved moisture," *Composites Science and Technology*, vol. 70, no. 16, pp. 2304–2309, 2010 (cit. on p. 65).

[6] J. Anderson and M. Altan, "Formation of voids in composite laminates: coupled effect of moisture content and processing pressure," *Polymer composites*, 2014 (cit. on p. 65).

[7] B. de Parscau du Plessix, "Analyse et modélisation du développement de porosités lors de la cuisson de pièces composites thermodurcissables hautes performances," Ph.D. dissertation, Université de Nantes, 2016 (cit. on pp. 65, 71, 79, 82).

[8] Y. Leterrier and C. G'sell, "Formation and Elimination of Voids During the Processing of Thermoplastic Matrix Composites," *Polymer Composites*, vol. 15, pp. 101–105, 2 1994 (cit. on p. 65).

[9] H. Shi, I. F. Villegas, and H. E. Bersee, "Analysis of void formation in thermoplastic composites during resistance welding," *Journal of Thermoplastic Composite Materials*, vol. 30, pp. 1654–1674, 12 2017 (cit. on p. 65).

[10] G. Dorey, S. Bishop, and P. Curtis, "On the impact performance of carbon fibre laminates with epoxy and PEEK matrices," *Composites Science and Technology*, vol. 23, no. 3, pp. 221–237, 1985 (cit. on p. 65).

[11] R. Selzer and K. Friedrich, "Mechanical properties and failure behaviour of carbon fibre-reinforced polymer composites under the influence of moisture," *Composites Part A: Applied Science and Manufacturing*, vol. 28, no. 6, pp. 595–604, 1997 (cit. on p. 65).

[12] P. Zhou, J. Tian, C. Li, and Z. Tang, "Comparative Study of Durability Behaviors of Thermoplastic Polypropylene and Thermosetting Epoxy Exposed to Elevated Temperature, Water Immersion and Sustained Bending Loading," *Polymers*, vol. 14, no. 14, p. 2953, 2022 (cit. on p. 65).

[13] T. K. Slange, L. L. Warnet, W. J. Grouve, and R. Akkerman, "Deconsolidation of C/PEEK blanks: on the role of prepreg, blank manufacturing method and conditioning," *Composites Part A: Applied Science and Manufacturing*, vol. 113, pp. 189–199, 2018 (cit. on pp. 65–67, 69–70, 79–81).

[14] J. Favre, "Residual thermal stresses in fibre reinforced composite materials, a review," vol. 1, no. 1, pp. 37–53, 1988 (cit. on p. 68).

[15] A. Trende, B. Åström, and G. Nilsson, "Modelling of residual stresses in compression moulded glass-mat reinforced thermoplastics," *Composites Part A: Applied Science and Manufacturing*, vol. 31, no. 11, pp. 1241–1254, 2000 (cit. on p. 68).

[16] M. M. Shokrieh, *Residual stresses in composite materials*. Woodhead publishing, 2014 (cit. on p. 68).

[17] L. Ye, M. Lu, and Y.-W. Mai, "Thermal de-consolidation of thermoplastic matrix composites—I. Growth of voids," *Composites Science and Technology*, vol. 62, no. 16, pp. 2121–2130, 2002 (cit. on pp. 68, 74, 76–77).

[18] T. K. Slange, "Rapid Manufacturing of Tailored Thermoplastic Composites by Automated Lay-up and Stamp Forming," Ph.D. dissertation, University of Twente, 2019 (cit. on p. 68).

[19] R. Phillips, "Consolidation and solidification behavior of thermoplastic composites," Ph.D. dissertation, École Polytechnique Fédérale de Lausanne, 1996 (cit. on p. 68).

[20] V. Donadei, F. Lionetto, M. Wielandt, A. Offringa, and A. Maffezzoli, "Effects of blank quality on press-formed PEKK/carbon composite parts," *Materials*, vol. 11, 7 2018 (cit. on pp. 68–70, 79–80).

[21] C.-C. M. Ma and S.-W. Yur, "Environmental effects on the water absorption and mechanical properties of carbon fiber reinforced PPS and PEEK composites. Part II," *Polymer Engineering & Science*, vol. 31, no. 1, pp. 34–39, 1991 (cit. on p. 70).

[22] C.-C. M. Ma, C.-L. Lee, M.-J. Chang, and N.-H. Tai, "Hygrothermal behavior of carbon fiber-reinforced poly (ether ether ketone) and poly (phenylene sulfide) composites. I," *Polymer composites*, vol. 13, no. 6, pp. 448–453, 1992 (cit. on p. 70).

[23] K.-M. Lee, S.-J. Park, T. Yu, S.-J. Park, and Y.-H. Kim, "Experimental prediction of internal defects according to defect area on NDI via water absorption behavior," *International Journal of Modern Physics B*, vol. 35, no. 14n16, p. 2 140 021, 2021 (cit. on p. 70).

[24] F. C. Campbell, A. R. Mallow, and C. E. Browning, "Porosity in carbon fiber composites an overview of causes," *Journal of advanced materials*, vol. 26, no. 4, pp. 18–33, 1995 (cit. on p. 70).

[25] J. R. Wood and M. G. Bader, "Void control for polymer-matrix composites (1): theoretical and experimental methods for determining the growth and collapse of gas bubbles," *Composites manufacturing*, vol. 5, no. 3, pp. 139–147, 1994 (cit. on pp. 71–72).

[26] J. Kardos, M. Duduković, and R. Dave, "Void growth and resin transport during processing of thermosetting—matrix composites," *Epoxy resins and composites IV*, pp. 101–123, 1986 (cit. on p. 71).

[27] Y. Ledru, G. Bernhart, R. Piquet, F. Schmidt, and L. Michel, "Coupled visco-mechanical and diffusion void growth modelling during composite curing," *Composites Science and Technology*, vol. 70, no. 15, pp. 2139–2145, 2010 (cit. on pp. 71, 73).

[28] B. de Parscau du Plessix, S. Le Corre, F. Jacquemin, P. Lefebure, and V. Sobotka, "Improved simplified approach for the prediction of porosity growth during the curing of composites parts," *Composites Part A: Applied Science and Manufacturing*, vol. 90, pp. 549–558, 2016 (cit. on pp. 73, 75).

[29] J. Wolfrath, V. Michaud, and J.-A. E. Månson, "Deconsolidation in glass mat thermoplastic composites: Analysis of the mechanisms," *Composites Part A: Applied Science and Manufacturing*, vol. 36, pp. 1608–1616, 12 2005 (cit. on pp. 74, 78, 80).

[30] F. Henninger, L. Ye, and K. Friedrich, "Deconsolidation behaviour of glass fibre-polyamide 12 composite sheet material during post-processing," *Plastics rubber and composites processing and applications*, vol. 27, no. 6, pp. 287–292, 1998 (cit. on p. 75).

[31] J. Williams, "Stress analysis of polymers, 1980," *Ellis Harwood Ltd: Chichester, UK*, pp. 291–353, (cit. on p. 78).

[32] M. Brzeski, "Experimental and analytical investigation of deconsolidation for fiber reinforced thermoplastic composites," Ph.D. dissertation, TU Kaiserslautern, 2014 (cit. on pp. 78, 81).

[33] Y. Wan and J. Takahashi, "Deconsolidation behavior of carbon fiber reinforced thermoplastics," *Journal of Reinforced Plastics and Composites*, vol. 33, no. 17, pp. 1613–1624, 2014 (cit. on p. 78).

[34] F. Lessard, M. Dubé, and L. L. Lebel, "A comprehensive model of the deconsolidation behaviour of unidirectional carbon fibre reinforced thermoplastic composites," *Composites Part A: Applied Science and Manufacturing*, vol. 163, p. 107 176, 2022 (cit. on p. 78).

[35] K. Friedrich, S. Fakirov, Z. Zhang, L. Ye, M. Lu, and H.-Y. Liu, "Deconsolidation and reconsolidation of thermoplastic composites during processing," *Polymer Composites: From Nano-to Macro-Scale*, pp. 233–254, 2005 (cit. on p. 79).

[36] M. Wakeman, P. Blanchard, and J.-A. E. Månson, "Void evolution during stamp-forming of thermoplastic composites," in *15th international conference on composite materials (ICCM-15)*, Citeseer, 2005 (cit. on p. 79).

[37] D. Zhang, A. Levy, and J. Gillespie, "On the void consolidation mechanisms of continuous fiber reinforced thermoplastic composites," *SAMPE 2012-Baltimore, MD*, p. 16, 2012 (cit. on p. 79).

[38] ASTM, "Standard test methods for void content of reinforced plastics," *ASTM designation D*, pp. 2734–94, 2009 (cit. on p. 79).

[39] J. E. Little, X. Yuan, and M. I. Jones, "Characterisation of voids in fibre reinforced composite materials," *Ndt & E International*, vol. 46, pp. 122–127, 2012 (cit. on pp. 79, 82–83).

[40] Y. Ledru, "Etude de la porosité dans les matériaux composites stratifiés aéronautiques," Ph.D. dissertation, Université de Toulouse, 2009 (cit. on pp. 79, 82).

[41] D. Saenz-Castillo, M. Martín, S. Calvo, F. Rodriguez-Lence, and A. Güemes, "Effect of processing parameters and void content on mechanical properties and NDI of thermoplastic composites," *Composites Part A: Applied Science and Manufacturing*, vol. 121, pp. 308–320, 2019 (cit. on pp. 79–80).

[42] V.-T. Hoang, B.-S. Kwon, J.-W. Sung, H.-S. Choe, S.-W. Oh, S.-M. Lee, J.-H. Kweon, and Y.-W. Nam, "Postprocessing method-induced mechanical properties of carbon fiber-reinforced thermoplastic composites," *Journal of Thermoplastic Composite Materials*, vol. 36, no. 1, pp. 432–447, 2020 (cit. on p. 79).

[43] L. Ye, Z. R. Chen, M. Lu, and M. Hou, "De-consolidation and re-consolidation in CF/PPS thermoplastic matrix composites," *Composites Part A: Applied Science and Manufacturing*, vol. 36, pp. 915–922, 7 2005 (cit. on p. 80).

[44] L. Amedewovo, A. Levy, B. de Parscau du Plessix, J. Aubril, A. Arrive, L. Orgéas, and S. Le Corre, "A methodology for online characterization of the deconsolidation of fiber-reinforced thermoplastic composite laminates," *Composites Part A: Applied Science and Manufacturing*, vol. 167, p. 107 412, 2022 (cit. on pp. 80–81).

[45] P. Irving and C. Soutis, *Polymer composites in the aerospace industry*. Woodhead Publishing, 2019 (cit. on p. 80).

[46] F. A. Reed, T. J. Batzinger, R. W. Reed, and S. Jönsson, "Porosity measurement in composites using ultrasonic attenuation methods," *Review of Progress in Quantitative Nondestructive Evaluation: Volumes 12A and 12B*, pp. 1265–1272, 1993 (cit. on p. 80).

[47] P. A. Olivier, B. Mascaro, P. Margueres, and F. Collombet, "CFRP with voids: ultrasonic characterization of localized porosity, acceptance criteria and mechanical characteristics," in *Proceedings of ICCM*, vol. 16, 2007 (cit. on p. 80).

[48] M. L. Costa, S. f. M. De Almeida, and M. C. Rezende, "The influence of porosity on the interlaminar shear strength of carbon/epoxy and carbon/bismaleimide fabric laminates," *Composites Science and Technology*, vol. 61, no. 14, pp. 2101–2108, 2001 (cit. on p. 80).

[49] L. Liu, B.-M. Zhang, D.-F. Wang, and Z.-J. Wu, "Effects of cure cycles on void content and mechanical properties of composite laminates," *Composite structures*, vol. 73, no. 3, pp. 303–309, 2006 (cit. on p. 80).

[50] J. Baruchel, J.-Y. Buffière, E. Maire, P. Merle, and G. Peix, *X-ray tomography in material science*. HERMES Science Publications, 2000 (cit. on p. 82).

[51] E. N. Landis and D. T. Keane, "X-ray microtomography," *Materials characterization*, vol. 61, no. 12, pp. 1305–1316, 2010 (cit. on p. 82).

[52] A. K. Schomberg, A. Diener, I. Wünsch, J. H. Finke, and A. Kwade, "The use of X-ray microtomography to investigate the microstructure of pharmaceutical tablets: Potentials and comparison to common physical methods," *International journal of pharmaceutics: X*, vol. 3, p. 100 090, 2021 (cit. on p. 83).

[53] P. Latil, L. Orgéas, C. Geindreau, P. J. Dumont, and S. R. Du Roscoat, "Towards the 3d in situ characterisation of deformation micro-mechanisms within a compressed bundle of fibres," *Composites Science and Technology*, vol. 71, no. 4, pp. 480–488, 2011 (cit. on p. 82).

[54] P. Galvez-Hernandez, C. Jimenez-Martin, R. Smith, M. Mavrogordato, V. Maes, T. McMahon, I. Sinclair, and J. Kratz, "In-situ CT of out-of-autoclave composites manufacturing processes," in *International conference on manufacturing of advanced composites*, 2022 (cit. on p. 82).

[55] J. Torres, M. Simmons, F. Sket, and C. González, "An analysis of void formation mechanisms in out-of-autoclave prepregs by means of x-ray computed tomography," *Composites Part A: Applied Science and Manufacturing*, vol. 117, pp. 230–242, 2019 (cit. on p. 82).

[56] T. Centea and P. Hubert, "Measuring the impregnation of an out-of-autoclave prepreg by micro-CT," *Composites Science and Technology*, vol. 71, no. 5, pp. 593–599, 2011 (cit. on p. 82).

[57] B. de Parscau du Plessix, P. Lefébure, N. Boyard, S. L. Corre, N. Lefèvre, F. Jacquemin, V. Sobotka, and S. Rolland du Roscoat, "In situ real-time 3d observation of porosity growth during composite part curing by ultra-fast synchrotron X-ray microtomography," *Journal of Composite Materials*, vol. 53, no. 28-30, pp. 4105–4116, 2019 (cit. on p. 82).

CHAPTER 4

CHARACTERIZATION OF MOISTURE TRANSPORT IN CF/PEKK LAMINATES AT HIGH TEMPERATURES

Contents

Abstract

Prior to processing, high-performance Carbon Fiber-Reinforced ThermoPlastic (CFRTP) are usually stored in ambient conditions, thus causing moisture sorption. During processing at high temperature, the stored moisture induces defects that deteriorate the mechanical properties of the produced parts. In order to understand these effects, it is necessary to study water (de)sorption phenomena in CFRTP, which was only characterized at low temperatures up to now ($<100\,^{\circ}C$). Thus, we characterized online moisture (de)sorption mechanisms at high temperatures (up to $300\,^{\circ}C$) on large and representative samples of a high-performance Carbon Fiber (CF) reinforced PolyEtherKetoneKetone (PEKK) laminates. This characterization was performed thanks to a new thermogravimetric device named Online Moisture Ingress CHAracterization (OMICHA) that we developed purposely. This new device allows to continuously measure weight variation of large composite samples under controlled and high temperature and/or humid environment. Sorption and desorption tests allowed to determine macroscopic moisture diffusion coefficient of CF/PEKK at several temperatures, highlighting a complex dual stage macroscopic diffusive behavior which is also modeled and discussed.

In Chapter 3, moisture and residual stresses were identified as main potential origins of deconsolidation. These two factors must therefore be properly decoupled to better study their effect separately. This requires a good knowledge of the moisture transport mechanisms and moisture-related properties of the composite material. The purpose of this chapter is thus to characterize the moisture diffusivity of CF/PEKK and identify its hygrothermal behavior.

4.1 Introduction

Due to their high specific mechanical properties, advanced fiber-reinforced polymer composites are increasingly used in aircraft and aerospace industries. Although thermoset polymers are currently the most widely used in composites, novel high-performance thermoplastic polymers are being introduced to manufacture fiber-reinforced ThermoPlastic Composites (TPCs). TPCs exhibit several advantages over thermoset matrix composites, *e.g.*, in terms of weldability and shelf (storage) life. In addition, high-performance polymers exhibit good mechanical properties which meet the aeronautical specifications. They also have high glass transition temperature (T_g) and high melting temperature (T_m) that allow high service temperatures (in general up to 250 °C). Finally, they have a good chemical resistance to solvents. Classical high-performance thermoplastic polymers used in TPCs are PolyEtherEtherKetone (PEEK) and PEKK. They are semi-crystalline polymers with an aromatic structure which confers them the aforementioned properties. However, the processing of high-performance CFRTPs requires high temperatures (between 330 °C and 400 °C) unlike thermoset matrix composites (between 120 °C and 175 °C). This makes their manufacturing challenging.

Several studies carried out on thermoset matrix composites have revealed that thermoset polymers uptake water when subjected to a humid environment [1–4]. The moisture sorption usually occurs during the storage of the composites before processing. During processing at high temperature, the initial moisture stored inside the composites provides pores nucleation sites which can lead to the formation of defects (delaminations, voids, *etc.*) [5–7]. Although high-performance CFRTPs generally uptake less water than high-performance thermoset matrix composites [8–10], the effect of moisture is not negligible. To avoid this detrimental effect of moisture, understanding of the moisture (de)sorption mechanisms, especially the moisture dif-

fusion kinetics in the material is required. Moisture (de)sorption in fiber-reinforced thermoset polymer composites has been widely studied in the literature [11–17]. On the contrary, there are very few studies dedicated to (de)sorption mechanisms in CFRTPs [18–23]. Most of them focused on CF/PEEK. Only five recent articles have been found on CF/PEKK [24–28]. In most of these studies (de)sorption is characterized at low and constant temperatures, either in a humid atmosphere or in water. Since high-performance CFRTPs are processed at high temperatures, a characterization of moisture desorption at high temperatures is required.

The traditional method used to characterize moisture (de)sorption is to measure the weight variation of a specimen exposed to a controlled temperature and humidity environment, through gravimetric measurements. These measurements are made at periodic time intervals, by using a weighing scale (static gravimetric method) [14, 29]. This technique is labor intensive since the samples must be taken out of the testing environment at various times and over a long period of time, for external weighing. Moreover, the handling time outside the test environment can be a significant source of error.

To overcome these limitations, another technique used in the literature is the Dynamic Vapor Sorption (DVS) method [30, 31]. DVS instruments operate by flowing precisely controlled concentrations of water vapors in dry air over a sample at a known flow rate and temperature. The sample is supported, through a sample holder, by a digital micro weighing scale which detects the sorption or desorption of water vapor through the increase or decrease of the material weight, as the relative humidity varies (dynamic gravimetric method). The benefit of this technique is to provide a continuous and automatic, *i.e.* online measurement of the weight variation which makes it widely used in fields such as the pharmaceutical, food, textile production or building materials (concrete) [32, 33]. However, this technique is limited to small sample sizes (up to 8 mm $\times$ 8 mm) and low sample weights (up to 5 g) [34]. This is detrimental for CFRTPs which require larger sample size to get representative characterization of moisture (de)sorption mechanisms. Moreover, the maximum temperature that can be reached on these devices are 200 °C which is also a drawback for CFRTPs. Standard Thermo-Gravimetric Analysis (TGA) equipment allows to largely exceed this temperature but here again, the required sample size is also too small (about 4 mm in diameter) to allow proper and representative characterization of moisture (de)sorption in CFRTPs.

For these reasons, we developed a new thermogravimetric device to perform moisture sorption and desorption tests at temperatures above 200 °C on large and representative samples of CFRTPs. This new device was used to characterize the moisture desorption mechanisms at high temperatures on an aerospace grade CF/PEKK 7002 composite laminate.

4.2 Materials

CF/PEKK prepreg plies supplied by Toray Advanced Composite were used to produce consolidated laminates. The plies have a Fiber Areal Weight (FAW) of 194 g/m^2 and a theoretical thickness of 0.185 mm. The PEKK mass content is 34 %. The glass transition temperature (T_g), melting temperature (T_m) and crystallization temperature (T_c) of PEKK 7002 are respectively 160 °C, 337 °C, and 265 °C (according to the manufacturer). In practice, the melting zone observed during Differential Scanning Calorimetry (DSC) experiments extends between 310 °C and 360 °C, with a melting point at 338 °C. In non-isothermal conditions, the crystallization zone extends between 240 °C and 283 °C, with a crystallization peak at 269 °C. This melting and crystallization range can also be found in [35–37].

From the prepreg plies, $[0]_{16}$ laminates were consolidated in a hot press. The 348 mm × 348 mm prepreg plies were stacked in a picture-frame mold (internal cavity dimensions: 350 mm × 350 mm) and consolidated on a 50 t Pinette P.E.I press according to the following cycle: heating at 10 °C/min up to 380 °C under a pressure of 0.1 MPa; the temperature was held for 20 min under a pressure of 4 MPa; cooling at 10 °C/min at the same pressure, then demolding. The final part dimensions after consolidation are 350 mm × 350 mm × 2.90 mm. This final size of the laminate is due to the high pressure and the clearance between the plies and the internal cavity of the mold which promotes PEKK resin squeeze out.

Since a significant porosity content has a significant influence on the moisture diffusion kinetics [38–40], optical micrographs of the consolidated laminates validate the negligible porosity content after the consolidation (Figure 4.1). To perform microscopic observations, the samples were encapsulated using a slow-curing epoxy resin (EpoFix, Struers). The samples were then prepared using traditional grinding and polishing techniques on an automated polishing machine (Tegrapol-21 and TegraForce-5, Struers) and observed on the digital microscope KEYENCE VHX-7000 series. The cross

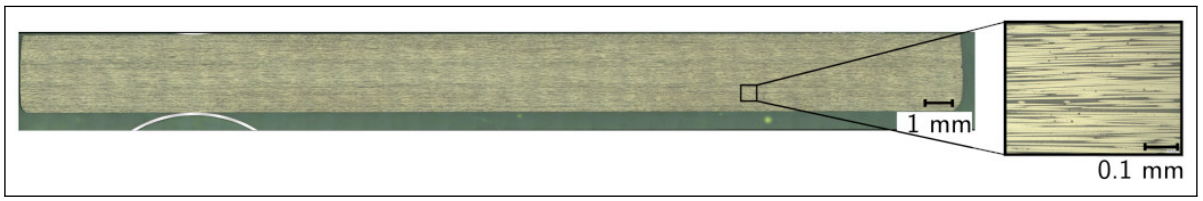

Figure 4.1: Micrograph (cross section parallel to the fibers main axis) of the consolidated samples before deconsolidation tests (objective magnification $\times 200$ and resolution 1.55^2 µm^2/pixel). The initial porosity content is not measurable.

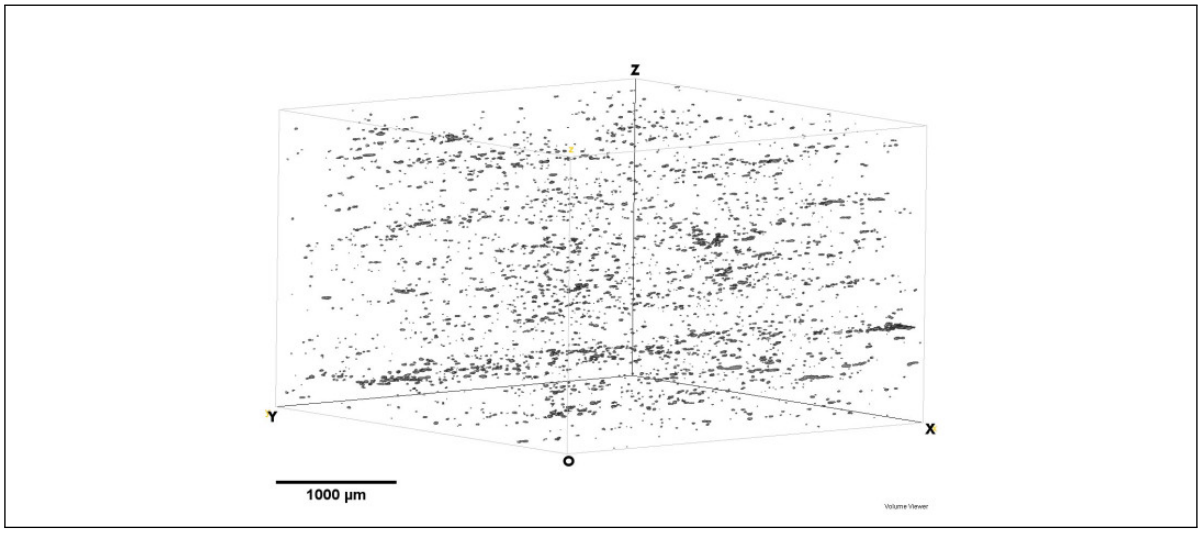

Figure 4.2: 3D image of the porosity distribution in a sample of 20 mm diameter cut from the consolidated laminate (Region Of Interest size: 3.81 mm $\times$ 3.81 mm $\times$ 2.48 mm). The porosity content is 0.02 %.

section micrographs were obtained by assembling several sections with a resolution of 2880 pixel $\times$ 2160 pixel (objective magnification $\times 200$) resulting in an image with a large area of observation and a good resolution ($\approx 1.55^2$ µm^2/pixel).

This microscopic observation was validated by a micro-CT analysis which showed an initial porosity content of 0.02 % (Figure 4.2). This value is a minor of the laminate porosity content. The 3D image of the sample (20 mm diameter) was obtained on one of the X-ray tomographs of the ID19 line at European Synchrotron Radiation Facilities (Grenoble, France). The raw 3D image was produced (i) with a voxel size of 3.81^3 µm^3 and a large observation volume (7.68 mm $\times$ 7.68 mm $\times$ 5.37 mm), (ii) by using Paganin method [41]. Additional post-treatment on a Region Of Interest

(ROI) of 3.81 mm × 3.81 mm × 2.48 mm (picked from the raw 3D image) using the trainable weka segmentation algorithm, in an image processing software (Fiji), allowed to measure the porosity content.

4.3 Online Moisture Ingress CHAracterization (OMICHA) bench

Sorption or desorption tests consist in measuring the weight gain or loss of a sample under controlled temperature and hygrometry conditions. In the case of desorption tests, the initially wet sample is dried at a given isotherm and constant relative humidity until the sample is completely dried. In the case of sorption tests, the initially dry sample is moisturized in an environment with a known constant relative humidity and temperature.

Usually, sorption tests are carried out in climatic chambers. The Relative Humidity (RH) is set either by using relative humidity generators or by saturated water solutions of properly selected salts. These salts are selected in the Greenspan table which gives the equilibrium relative humidity of Saturated Salt Solutions from 0 to 100 °C [42]. During the sorption tests, the weight changes are measured at different times on an external weighing scale in accordance with the standard ASTM D5229/D5229M (static gravimetric method). This makes this method laborious and the existing online weighing methods (DVS and standard TGA) require small samples that are not representative of composite structures. In order to overcome the limitations of these methods, a new device for the characterization of moisture diffusion kinetics has been developed.

4.3.1 Bench development

OMICHA device has been developed to measure continuously the weight of samples of a size representative of a structure scale (up to 150 mm × 150 mm), in a controlled hygrothermal environment.

4.3.1.1 Design

As shown in Figure 4.3, the device is composed of an oven (Heratherm OGH60 from Thermo Scientific), a sample holder made of aluminum and a semi-micro weighing scale (Explorer EX125M from OHAUS) with an accuracy of 0.01 mg, in accordance

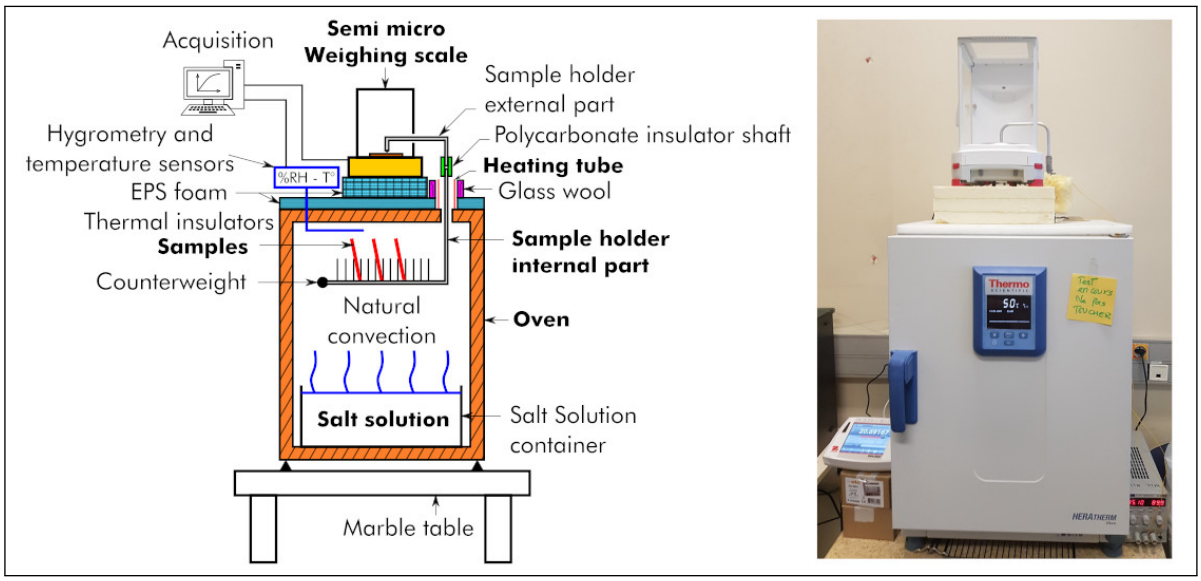

Figure 4.3: Online Moisture Ingress CHAracterization (OMICHA) bench. Schematic view (left) and setup picture (right).

with the ASTM D5229/D5229M standard. The whole device was placed on a marble table to avoid the influence of external vibrations on the weight measurements. The oven allows to heat up to 330 °C by natural convection. A suspended sample holder was specifically designed and manufactured, in order to transfer the samples weight to the semi-micro weighing scale. A metallic tip was connected to the upper extremity of the sample holder, in order to avoid force torque at the contact zone between the weighing scale and the sample holder. The stability of the sample holder was provided by a counterweight placed at its lower extremity. Due to the total weight of the sample holder and the counterweight (83.26 g), the measuring range of the weighing scale was reduced from 120 g to 36.74 g.

4.3.1.2 Heat management

To prevent high heat exchanges along the aluminum sample holder which may result in condensation and artifacts, the sample holder was made of two parts connected by a polycarbonate insulator shaft. Since polycarbonate has a low thermal conductivity ($\approx 0.04\,\mathrm{W/(m \cdot K)}$ [43]), the shaft allowed to insulate thermally the external part of the sample holder from its internal part which is in the oven. The weighing scale was also thermally insulated from the oven by means of Expanded PolyStyrene (EPS) foam.

With respect to external environment of the setup, there was no significant variation of ambient temperature (23 °C measured with a K-type thermocouple) and atmospheric pressure (0.1 MPa or 1.024 bar measured by a pressure sensor, from Keller's 35XTC series) during the experiments.

4.3.1.3 Humidity management

During sorption tests, the moisture in the oven was provided by a saturated salt solution selected from the Greenspan table. The saturated salt container was let in the oven during the whole experiment. The container volume is large enough (14×10^{-3} m^3) to avoid refilling with salt solution during a test. A heating tube surrounded by glass wool was placed at the exit of the sample holder out of the oven. This heating tube was used to heat locally the water vapor which escaped from the oven and thus prevented water condensation on the sample holder.

The OMICHA bench was used in two different configurations, *i.e.* sorption at low temperature and desorption at high ones. The saturated salt container is not used in desorption configuration, since the environment in the oven had to be dried. We did not performed sorption tests above 100 °C, as these tests would require an additional pressure: this was not possible here.

4.3.1.4 Measurements

The temperature and the relative humidity were respectively measured by K-type thermocouple and a thermohygrometer (TH 210-R from Kimo) with an accuracy of ±1.5 %RH. The weight, temperature and relative humidity measurements were synchronized and performed automatically using a single piece of software developed on LabVIEW. The weight variation Δw (%) over time was calculated from the weight measurements according to the following equation (4.1):

$$\Delta w(t) = \left(\frac{w(t) - w(0)}{w(0)} \right) \times 100 \tag{4.1}$$

where $w(t)$ and $w(0)$ are the actual and initial sample weights, respectively.

Compared to the small sample sizes (up to 8 mm × 8 mm) and low sample weight (up to 5 g) required in DVS and TGA methods, the OMICHA device sample holder can

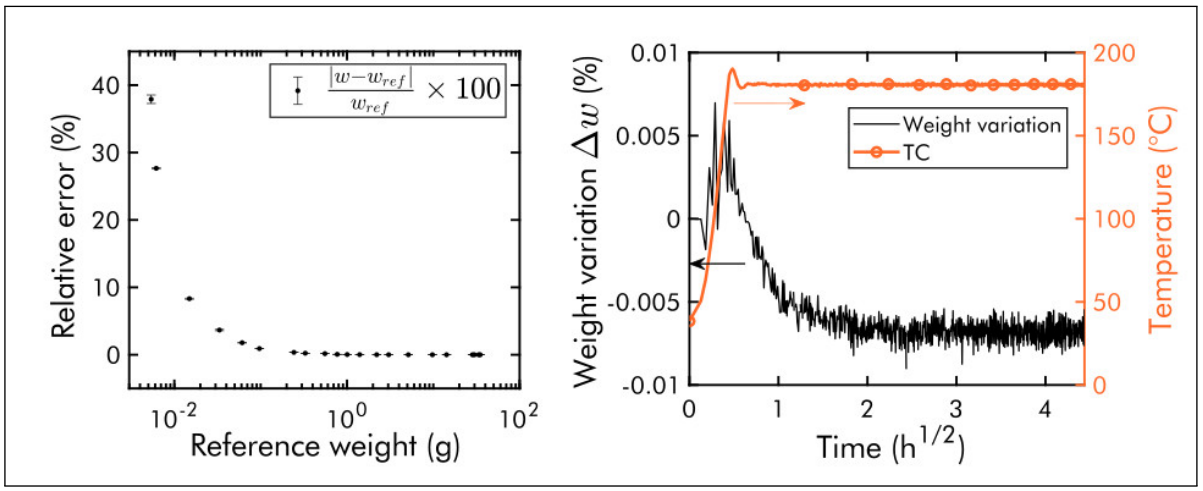

Figure 4.4: OMICHA measurements validation. Relative error (%) for different reference weights (left) and effect of the oven temperature on the weight variation Δw (right).

support large size samples up to 150 mm × 150 mm × 10 mm with a weight up to 36 g. Additionally, desorption tests on OMICHA can be performed up to 330 °C (which is in the melting zone of the studied material).

4.3.2 Validation

The weighing scale used on the OMICHA device was pre-calibrated by the supplier and has an accuracy of 0.01 mg. To evaluate the effect of the sample holder on the measurement, several objects were weighed directly on the pan of the weighing scale without the sample holder. The weight values obtained from these measurements were used as reference. The same objects were weighed by mean of the sample holder, in ambient conditions. Since there are fifteen positions available on the sample holder, the samples were placed at the middle of the sample holder. Figure 4.4 (left) shows the relative error between the measurements with the sample holder and the reference weights. All the weighing were performed three times. The error bars plotted in Figure 4.4 represent the standard deviation. The relative error related to the use of the sample holder decreases with increasing sample weight. First, for low weight samples (inferior to 0.01 g), the relative error is superior to 5 %. Second, for samples weight between 0.01 g and 1 g, the maximum relative error is 4 %. Finally, over 1 g, the

maximum relative error is 0.03 %. As discussed hereunder, such a precision enables to properly characterize moisture diffusion kinetics with the targeted composite sample size (80 mm $\times$ 80 mm) and weights ($\approx$ 30 g).

In addition, a heating test at 180 °C was performed without any sample on the sample holder. During this test, the oven was heated to 180 °C and maintained at this temperature. As shown in Figure 4.4 (right), during the ramp-up, some weight variations can be seen with a low magnitude (0.007 %). These variations are attributed to convective effect in the oven. As soon as the temperature reaches the dwell temperature, a weight loss is observed. This weight loss stabilizes after a time period and remains constant during the whole dwell. This observation under isothermal condition is probably attributed to a desorption of the aluminum sample holder. However, the weight variation stabilization shows that at isothermal temperature, the temperature inside the oven has almost no influence on the measurement of the weighing scale. It also highlighted the efficiency of the insulation system.

For these reasons, before all measurement on the OMICHA device, the system is pre-heated up to the target temperature until weight variation stability is reached, before the sample positioning. This is illustrated in Figure 4.9 (see Appendix 4.A), which shows a negligible weight variation Δw evolution ($\pm$ 0.004 %).

4.4 CF/PEKK laminate characterization procedure

Using the OMICHA device, desorption tests were carried out on 80 mm $\times$ 80 mm $\times$ 2.90 mm composite samples cut from the press consolidated laminates. All the samples were cut from the laminates after consolidation, by water jet cutting on a ProtoMAX abrasive waterjet machine. The samples were then cleaned with a cloth and stored in ambient conditions ($\approx$ 23 °C and 50 %RH) for 5 months. Before each desorption test, the oven was pre-heated to the defined temperature for the test. As mentioned earlier, the saturated salt container is removed from the oven in the desorption configuration. The defined temperatures for the desorption tests are listed in Table 4.1.

After the oven pre-heating, the desorption test was performed on a single sample placed in the middle of the sample holder. The time evolution sample weight was recorded and the corresponding weight variation Δw was determined according to

Table 4.1: Desorption and sorption tests parameters. T_g corresponds to the material glass transition temperature and T_c its lowest crystallization temperature.

Desorption		Sorption	
Range	Temperature	Relative humidity	Temperature
$T < T_g$	140 °C		
$T_g < T < T_c$	180 °C, 200 °C	65 %	40 °C
$T \geq T_c$	250 °C, 300 °C		
Sample: consolidated laminate		Sample: 7 × 1 tape	

equation (4.1). The initial weights ranged from 29 g to 30 g. All the desorption tests were performed under air atmosphere, in order to be representative of the atmosphere in which the composite is processed.

Desorption tests have been carried out to analyze the moisture desorption kinetics at high temperatures. In order to characterize the moisture sorption kinetics at a lower temperature, sorption tests were performed at 40 °C and 65 %RH. To limit the duration of the test, sorption tests were not performed on laminates but rather directly on a prepreg ply (80 mm × 80 mm × 0.2 mm).

Before sorption tests, a salt solution was prepared by mixing a Sodium Chloride salt (NaCl) with a hot distilled water at 80 °C. A fully saturated solution was obtained when the NaCl salt can no longer dissolve in the water. The resulting salt solution was then cooled down to the testing temperature (40 °C) by natural convection and placed in the pre-heated oven. When the humidity reached equilibrium in the oven, samples were positioned on the sample holder. The relative humidity at equilibrium (65 %RH) was given by the thermohygrometer placed in the oven. Since the weight of a single prepreg ply was less than the weight of a laminate, the sorption test was performed on a set of seven samples of one tape (80 mm × 80 mm × 0.2 mm) in order to obtained a mean weight variation value. The time evolution of the samples weight was recorded and the corresponding weight variation was also determined according to equation (4.1). This sorption procedure was repeated twice.

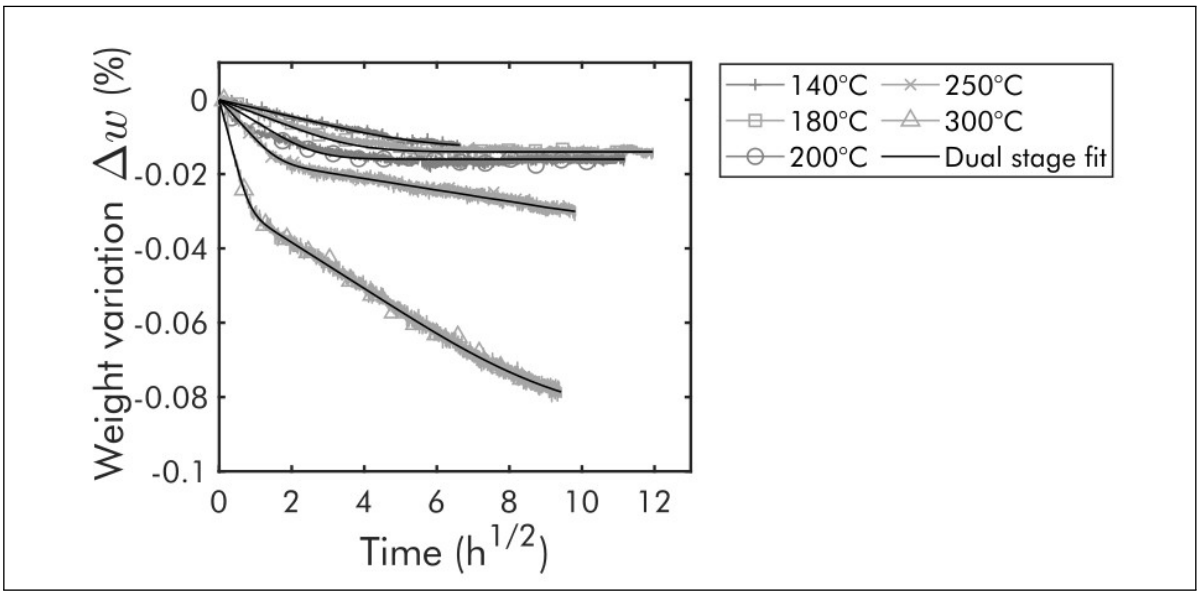

Figure 4.5: Desorption curves. Evolution of the weight variation Δw of tested samples with the square root of time $\sqrt{t}$ at different constant heating temperatures.

4.5 Results

4.5.1 Desorption tests

Figure 4.5 shows the evolution of the weight variation Δw of tested samples with the square root of time $\sqrt{t}$ obtained at different temperatures. Since the laminates used in this study were initially consolidated at 380 °C, it is assumed that there were no residual volatiles from additives such as plasticizers present in the tested samples. In fact, most additives evaporated during the initial laminate consolidation process. The observed weight losses are thus attributed to the desorption of the moisture initially stored in the polymer matrix, during the laminate consolidation and during the storage in an ambient condition.

This figure 4.5 shows that during all tests performed at temperature $T \leq$200 °C, the weight loss stabilizes after a certain time and exhibit a Fickian-like time evolution. Instead, at $T >$200 °C, a dual stage time evolution [44] is observed: a first rapid weight decrease (similar to the one observed at $T \leq$200 °C) is followed by a slower one which does not reach a stabilization for the duration of our tests.

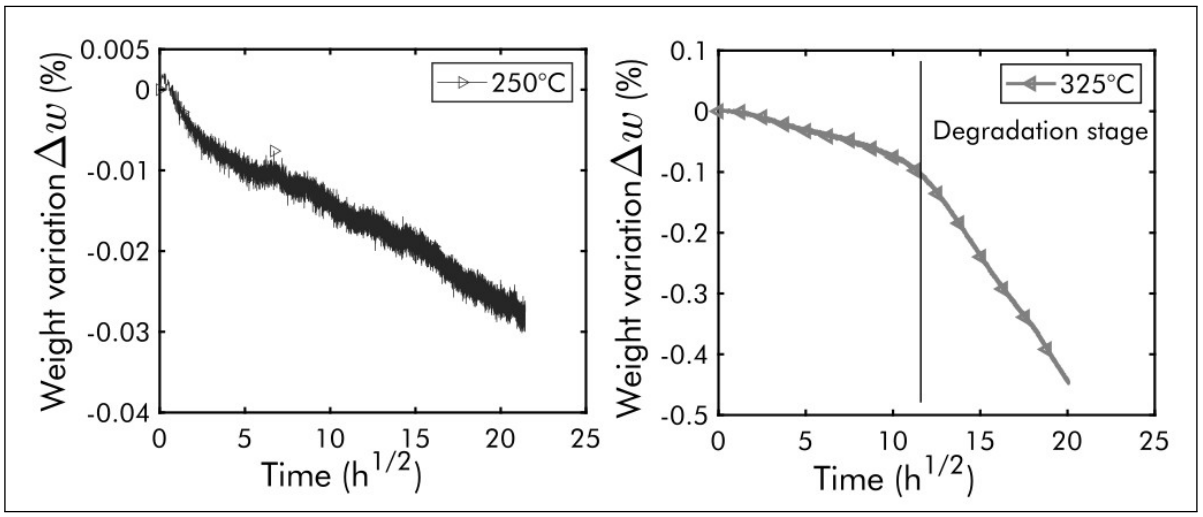

Figure 4.6: Evolution of the weight variation Δw of tested samples with the square root of time $\sqrt{t}$ for a test performed at 250 °C with a sample initially pre-dried for 72 h@180 °C (left) and at 325 °C with a sample initially pre-dried for 24 h@300 °C (right). The polymer matrix degradation occurs after long exposition at 325 °C.

4.5.2 Thermal degradation

In order to verify whether the weight variation above 200 °C can reach a stabilization, a first desorption test was performed at 250 °C on a sample already pre-dried at 180 °C for 72 h. The objective was to verify if drying at 250 °C could tend towards stabilization for longer exposure times. Figure 4.6 (left) shows that even after 16 days of exposition at 250 °C, no stabilization was reached. A second desorption test was performed at a higher temperature of 325 °C on a sample already pre-dried at 300 °C for 24 h. The objective of this test was to check if the stabilization could be reached faster at higher temperature. The initial pre-drying was done in order to reach the second stage of desorption. Figure 4.6 (right) shows that even at a temperature in the material melting zone (325 °C), the weight variation does not reach a stabilization. Conversely, the weight loss is accelerated around $t = 11^2$ h. This observation supports the fact that dual stage diffusion, in polymer composites, hardly reaches equilibrium [44]. In fact, a longer exposition of this type of material to such high temperatures (T$\geq$ 250 °C) leads to the material degradation [23, 45].

Several authors have studied the degradation phenomenon and showed that it is due to the scission of macromolecular chains of the polymer matrix which generates volatiles and radicals [46, 47]. Desorption of the volatiles produced by the chains scission

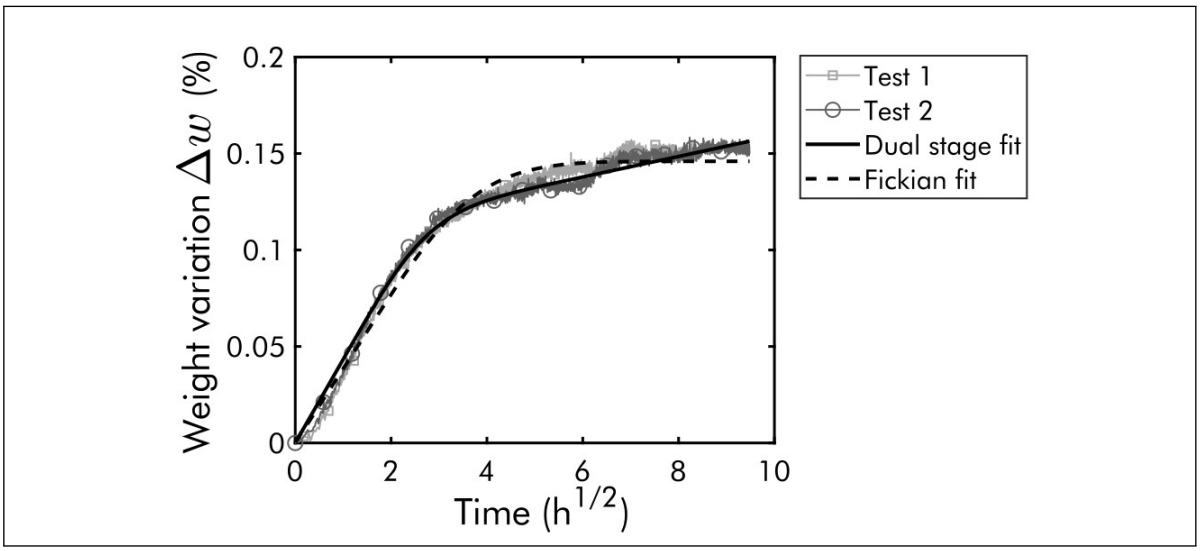

Figure 4.7: Sorption curves. Evolution of the weight variation Δw of tested samples with the square root of time $\sqrt{t}$ during two moisture sorption tests performed at 40 °C and 65 %RH on seven samples of one prepreg ply.

explains the second slope observed on the desorption curve at 325 °C (Figure 4.6 right). The authors also showed that when the material is maintained at such high temperatures (T$\geq$ 250 °C) for a long time, the radicals resulting from the chains scission can recombine together to form crosslinks. The polymer macromolecules then start branching.

4.5.3 Sorption tests

The obtained sorption curves show weight increase *vs* time (Figure 4.7). First, a good repeatability of the sorption tests is observed. The maximum absolute difference between the weight variation obtained for both tests is only 0.01 %. Second, the duration of the test is not long enough to confirm a total saturation of the samples. In addition, the reported curves can be divided into two stages. As for the desorption curves, the first stage is relatively fast (couple of hours) and is represented by the initial slope. Similar behavior has also been observed, in the literature, on CF/PEEK composite [18, 20] and on CF/PEKK composite, placed under more severe conditions (80 °C at 90 %RH [26], and water immersion at 70 °C [25]).

Additionally during the second stage of the sorption test, a sudden increase of the weight was observed around $t = 6^2$ h. This localized behavior is different from the monotonic behavior observed in the desorption tests. This behavior was also

observed in the literature by Suh *et al.* [48] on a cured CF/epoxy composite immersed in water at 70 °C. This Non-Fickian behavior suggests the presence of another physical phenomenon in sorption, but further analysis of this is not considered within the scope of this work. Only the first stage of the sorption curve was thus considered to determine the diffusion kinetics at early stages.

4.6 Moisture transport mechanisms and macroscopic modeling

The CF/PEKK material studied is an industrial complex system involving several heterogeneities such as micro-pores and fiber interfaces with undetermined sizing. Thus moisture transport mechanisms in these complex heterogeneous systems may involve adsorption, absorption, swelling or relaxation, capillary effects at small scales together with diffusion phenomena at smaller molecular scales. Nonetheless, the time evolutions of weight variations we reported in Figures 4.5 and 4.7 lead us to approach these complex possible micro-scale mechanisms by diffusive processes at the macro-scale. Thus, given the plate geometry of the tested samples, and by reasonably assuming that moisture transport only occurs along the thickness direction x of the samples, a possible diffusive transport model is the well-known Fick model, which is written for a one-dimensional (1D) case as:

$$\frac{\partial C}{\partial t} = D\frac{\partial^2 C}{\partial^2 x} \tag{4.2}$$

where C is the water concentration, D (m^2/s) the diffusion coefficient. D is assumed to be independent of the concentration C. The resolution of equation (4.2) in a plane sheet with an initial uniform water concentration C_0 and which is subjected to a constant water concentration C_1 at its upper and lower faces is given by Crank [49]:

$$\frac{C - C_0}{C_1 - C_0} = 1 - \frac{4}{\pi}\sum_{n=0}^{\infty}\frac{(-1)^n}{(2n+1)}\exp\left(-\frac{D(2n+1)^2\pi^2 t}{l^2}\right)\cos\left(\frac{(2n+1)\,\pi x}{l}\right) \tag{4.3}$$

where l the sample thickness. This solution was obtained by assuming C_0 to be initially uniform in the sample and C_1 constant because the water concentration in the sample environment is at saturation.

If M denotes the actual total amount of water absorbed or desorbed by the sample, and M_∞ the same quantity after infinite time (at saturation or equilibrium), then by

integrating equation (4.3) over the thickness l, the following equation is obtained:

$$M = M_\infty \times \left\{ 1 - \frac{8}{\pi^2} \sum_{n=0}^{\infty} \frac{1}{(2n+1)^2} \exp\left(-\frac{D(2n+1)^2 \pi^2 t}{l^2} \right) \right\} \tag{4.4}$$

or

$$M = M_\infty \times \left\{ 2 \left(\frac{Dt}{l^2} \right)^{\frac{1}{2}} \left(\pi^{-\frac{1}{2}} + 2 \sum_{n=1}^{\infty} (-1)^n \text{ierfc} \frac{nl}{(Dt)^{\frac{1}{2}}} \right) \right\} \tag{4.5}$$

with

$$\frac{M}{M_\infty} = \frac{w - w_0}{w_\infty - w_0} \tag{4.6}$$

where w_0 and w_∞ are respectively the initial sample weight and the sample weight at equilibrium.

For short times, *i.e.* when $t \ll \frac{\pi l^2}{16D}$, equation (4.5) can be simplified:

$$M = M_\infty \times \left\{ \frac{4}{\pi^{\frac{1}{2}}} \left(\frac{Dt}{l^2} \right)^{\frac{1}{2}} \right\} \tag{4.7}$$

Consequently, by plotting the weight variation as function of square root of time as in Figures 4.5 and 4.7, the diffusion coefficient can be determined from the tangent S_l at the origin of the curve recorded during (de)sorption experiments:

$$D = \pi \left(\frac{l}{4M_\infty} \right)^2 (S_l)^2 \tag{4.8}$$

The Fick model can be used to represent the diffusion mechanisms in the composite sample below 200 °C during desorption. As shown by the desorption curves above 200 °C (Figure 4.5), the weight variation does not reach a stabilization after the first linear stage. In order to take into account this behavior change at high temperatures, the Langmuir-type [50] model can be used. However, the identification of this model parameters is complex. In this study, a phenomenological model called *"dual stage"* was adopted. This model described by the equation (4.9) is based on the assumption that two decoupled Fickian diffusion operate simultaneously with two diffusion coefficients D_1 and D_2 respectively associated with two different water concentrations C_1 and C_2 [51]. The first one is introduced to moisture diffusion in the early stage and the second one for diffusive process in an second stage. This model is deduced from equation 4.2, by considering $C = C_1 + C_2$ (superposition of two Fickian diffusion). It

Table 4.2: Dual stage model parameters

Temperature (°C)	D_1 (m^2/s)	$M_{\infty,1}$ (%)	D_2 (m^2/s)	$M_{\infty,2}$ (%)	Comments
40	$0.24 \times 10^{-12} \times 10^{-12}$	0.106	-	-	Sorption test
140	14.46×10^{-12}	-0.013	0	0	Desorption test
180	32.47×10^{-12}	-0.014	0	0	Desorption test
200	63.87×10^{-12}	-0.016	0	0	Desorption test
250	174.68×10^{-12}	-0.015	1.99×10^{-12}	-0.024	Desorption test
300	660.49×10^{-12}	-0.026	4.93×10^{-12}	-0.061	Desorption test

is the most used to describe the diffusion mechanisms in epoxy matrix composites [15, 51, 52].

$$\frac{\partial C_1}{\partial t} + \frac{\partial C_2}{\partial t} = D_1 \frac{\partial^2 C_1}{\partial^2 x} + D_2 \frac{\partial^2 C_2}{\partial^2 x} \tag{4.9}$$

The solution of equation (4.9) is deduced from the analytical solution (Equation 4.4) given by Crank [49] for a purely Fickian diffusion:

$$\begin{aligned} M = M_{\infty,1} \times \left\{ 1 - \frac{8}{\pi^2} \sum_{n=0}^{\infty} \frac{1}{(2n+1)^2} \exp\left(-\frac{D_1 (2n+1)^2 \pi^2 t}{l^2} \right) \right\} \\ + M_{\infty,2} \times \left\{ 1 - \frac{8}{\pi^2} \sum_{n=0}^{\infty} \frac{1}{(2n+1)^2} \exp\left(-\frac{D_2 (2n+1)^2 \pi^2 t}{l^2} \right) \right\} \end{aligned} \tag{4.10}$$

where $M_{\infty,1}$ and $M_{\infty,2}$ represents the total amount of water absorbed or desorbed by the sample at each respective stage. At the temperature T$\leq$200 °C in desorption, the moisture diffusion becomes purely Fickian, $D_2 = 0$ and $M_{\infty,2} = 0$.

D_1, $M_{\infty,1}$, D_2, and $M_{\infty,2}$ were identified simultaneously by a standard inverse method. The residual consists of modeled and measured M differences. The residual 2-norm was minimized using the least-square method in MATLAB [53]. This generated excellent fits for all testing conditions (see Figures 4.5 and 4.7 in Section 4.5). The identified parameters are given in table 4.2.

In equation (4.10), D_1 and $M_{\infty,1}$ are interdependent. This interdependence is also valid for D_2 and $M_{\infty,2}$. During the tests, the weight variation stabilization was not reached in the second stage of diffusion. Therefore, the experimental data obtained did not allow a clear identification of D_2 and $M_{\infty,2}$. However, the adopted methodology allows to give an order of magnitude.

Firstly, the table 4.2 shows a very small variability of $M_{\infty,1}$ as a function of temperature, during desorption tests. This can be explained by the fact that the samples were initially stored in the same ambient condition before the desorption tests. Hence, when they are exposed to a dry environment, they desorbed roughly the same amount of moisture in the first stage regardless of the temperature. Such conclusion cannot be made on the temperature sensitivity in the case of $M_{\infty,2}$, since stabilization was not reached in the second stage.

Secondly, the moisture diffusion coefficients D_1 and D_2 increased with rising temperature. We fitted this temperature dependence with an Arrhenius law:

$$D_1(T) = D_{0,1}\exp\left(-\frac{E_{a,1}}{RT}\right) \tag{4.11}$$

where $D_{0,1}$ is a pre-exponential constant in m^2/s, $E_{a,1}$ the activation energy of the first stage of moisture diffusion in J/mol, R the universal (or perfect) gas constant which is equal to $8.314\,J/(mol \cdot K)$, and T the temperature in K.

We determined $D_{0,1}$ and $E_{a,1}$ (Figure 4.8) with the diffusion coefficients shown in Table 4.2 and deduced from desorption tests only (140 °C - 300 °C). In addition, the diffusion coefficient determined experimentally at 40 °C during sorption was further used to validate the Arrhenius law estimation at lower temperatures. Results are reported on Figure 4.8.

As shown in Figure 4.8, a good correlation can be observed between the diffusion coefficients obtained by other authors on CF/PEKK [25] and CF/PEEK [18] and the estimated value with the Arrhenius law (Figure 4.8). Moreover, there is a small difference between the diffusion coefficient predicted by the Arrhenius trend and the experimental value we determined during the sorption test at 40 °C. Such a symmetry sorption-desorption during transient regime is in-line with results already reported in the literature for cured carbon fiber-reinforced epoxy matrix composites [44, 54] and neat PEEK polymer [55, 56]. This implies that the diffusion coefficient can be identified, at a given temperature, by both desorption or sorption tests.

With respect to D_2, its sensitivity to temperature cannot be analyzed from the tests carried out in this study, given the stabilization that has not been reached in the second stage. However, the order of magnitude obtained from the identification allows to show that D_2 is very low compared to D_1. This means that the moisture diffusion kinetic in the first stage is much faster than the second stage.

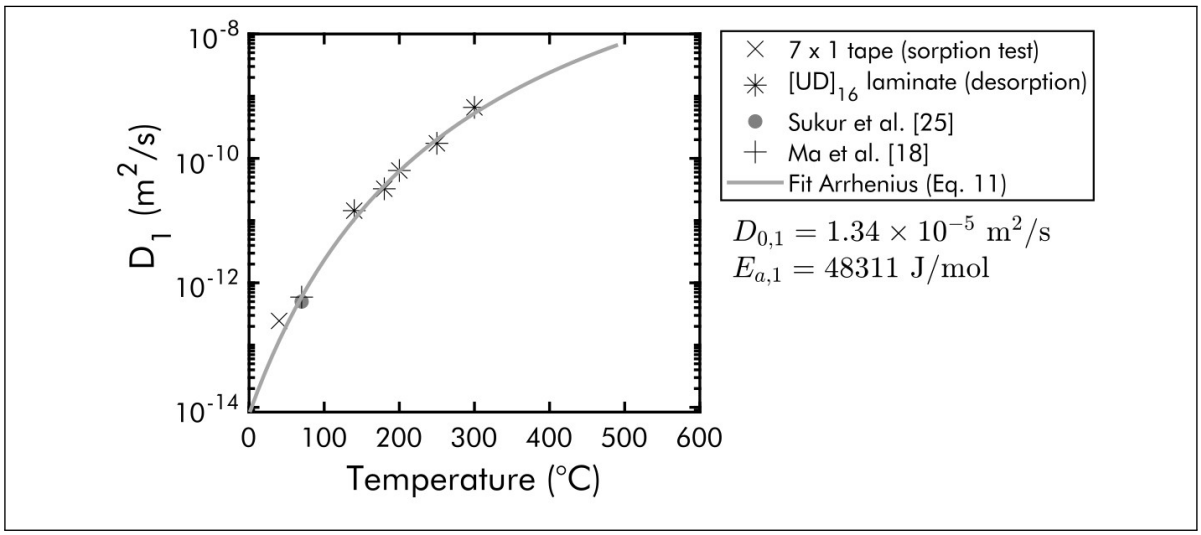

Figure 4.8: Diffusion coefficients D_1 *vs* temperature for the first stage of moisture diffusion in CF/PEKK during desorption at high temperatures (star symbols) and sorption at low temperature (cross symbol). Comparison with values obtained from the literature on CF/PEKK [25] and CF/PEEK [18] at 70 °C.

4.7 Discussion

Two different behaviors were observed during the desorption tests. The CF/PEKK samples experiment a Fickian diffusion at T≤200 °C and a Non-Fickian behavior at T>200 °C. These different behaviors can be explained by how the water molecules were initially stored in the composite samples.

Several studies have been conducted in the literature to understand how water molecules are stored in polymers. There are two main approaches. The first approach is based on the free volume theory proposed by Adamson for epoxy polymers [57]. The second approach takes into account the molecular interactions between the water molecules and the polymer molecules, by assuming that water molecules form hydrogen bonds with hydrophilic sites which are the most polar groups present in the polymer.

Several authors showed that water molecules are stored in the polymer matrix in two forms known as "free" water, diffusing in the free volumes or "bonded" water, temporarily trapped on proton receiver sites present in the molecular network of the polymer [58–60]. The first approach of free volume is based on the fact that water diffuses into the polymer, occupying essentially the free volumes present in

the polymer. Based on this approach, during moisture sorption, the water molecules can diffuse in the free volumes present in the composites or bind with the polymer matrix. The free volumes may be nano or micro-pores located in the polymer matrix or at the fiber - matrix interfaces [44]. These two mechanisms occurring throughout the sorption process lead to the dual stage behavior visible from the desorption curves. The moisture diffusion kinetic during both stages depend on temperature. The desorption of "bonded" water requires sufficient thermal energy. If the thermal energy is insufficient to break the bonds between the water molecules and the polymer, the "bonded" water remains in the material. This may explain the Fickian behavior observed at $T \leq 200\,°C$.

However, the first approach does not explain the hydrophobic character of some materials with a large free volume, such as fluoridated and silicone elastomers, or the fact that the water concentration increases when the theoretical free volume fraction decreases for some epoxy-amine polymers [61–63]. For this reason, another approach based on the interactions between the water molecules and the polar groups within the polymer is also used to explain the dual stage behavior. This approach has been validated in several works where most authors have indeed observed an increase in the water concentration in the polymer with an increase of the concentration of polar groups [64–66]. In fact, it is assumed that water molecules form two types of hydrogen bonds with the polar groups of the polymer: single bonds and double bonds [67].

The single bonds have an activation energy in desorption around 41 840 J/mol, and tend to dominate in epoxy polymers. Double bonded water molecules have a higher desorption activation energy (around 62 760 J/mol) and would be more difficult to desorb from the polymer matrix [23]. The moisture diffusion in the polymer can thus correspond to a "jump" of water molecules from one polar group to another [65]. The kinetics of water diffusion will then depend on the intensity of the hydrogen bonds between the polar groups and the polymer matrix. The stronger these bonds are, the slower the diffusion will be.

The major polar group in PEKK resin are the carbonyl (C=O) groups of the ketone function. These groups are considered moderately polar, *i.e.* they are less susceptible to form hydrogen bonds with water. In contrast, hydroxyl groups (predominant in epoxy polymers) can bond easily with water molecules and are thus classified as highly polar.

Based on this second approach, the behaviors observed on the desorption curves can be explained by the polymer-water interactions mentioned above. First, the weight loss observed at the beginning can be attributed to the breaking of single hydrogen bonds between the polymer matrix and dissolved water molecules. As it can be seen on the desorption curves, this first stage is relatively fast. Second, the weight loss stabilization occurs when the thermal energy is insufficient to break the double hydrogen bonds. As soon as the thermal energy becomes high enough, a further weight loss is observed after the first stage, corresponding to the desorption of the doubly bonded water molecules. This second stage is relatively slower compared to the first stage.

Both approaches described in the literature can explain the CF/PEKK behavior under hygrothermal conditions. Since there are generally micro-pores remaining in the composite laminates after consolidation, the free volume approach is not negligible. Perhaps the water diffusion process in CF/PEKK composite is a combination of these two approaches. To prove this, investigations at a micro scale would be necessary. The macro-scale tests performed in this study just highlight the Non-Fickian behavior of CF/PEKK at high temperatures and provide the associated diffusion kinetics.

4.8 Conclusion

The characterization of moisture diffusion kinetics at high temperatures in high-performance Carbon Fiber-Reinforced ThermoPlastic (CFRTP) has been investigated.

Moisture transport kinetics in CFRTPs can be characterized by moisture diffusion coefficient. The latter is determined after moisture sorption or desorption test. In the literature, the moisture diffusion coefficient is always determined at low temperature after sorption tests. Since high-performance CFRTPs are processed at high temperatures, it is necessary to characterize moisture diffusion at temperatures above the glass transition temperature. The existing characterization techniques (TGA, DVS) do not allow to accurately perform desorption tests at high temperatures on representative sample sizes. For this reason, a new device named OMICHA was developed and validated. This new device allowed to measure continuously the weight variation of a sample, of representative size, exposed to a controlled environment in temperature (up to 330 °C) and humidity. The Online Moisture Ingress CHAracterization (OMICHA) device was used to characterize moisture diffusion kinetics in a high-performance CFRTP (CF/PEKK) laminate samples initially stored in ambient condition for 5 months.

Thanks to the desorption tests carried out at high temperatures (from 140 °C to 300 °C), using the OMICHA device, two diffusion mechanisms have been highlighted. Depending on the desorption temperature, the diffusion is either Fickian or Non-Fickian. This dual behavior was described, with a good correlation, by a dual stage model which is based on a superposition of two simultaneous Fickian diffusion. The dual behavior supports that moisture is indeed stored in the polymer matrix in two forms: "weakly bonded water" and "strongly bonded water". A desorption test in the melting range of the material showed that it is difficult to desorb the strongly bonded water without causing material degradation.

Desorption tests also allowed the evaluation of moisture diffusion coefficients in the composite sample at high temperatures. As mentioned in other works in the literature, the diffusion is thermally activated and follows an Arrhenius type law. The characterization of the moisture diffusion kinetics at high temperatures has shown that the diffusion coefficients even at high temperatures are very low and largely lower than the thermal diffusivity (between 10^{-6} and 10^{-7} m^2/s [68]). Moisture diffusion is thus slower than heat diffusion in CF/PEKK.

These results call into question the low temperature (below 160 °C) of drying protocols often used during the processing of high-performance CFRTPs. At these low temperatures, only part of the stored water is desorbed. The other part, strongly bonded to the polymer, remains in the material. This residual water can eventually form nucleation sites for pores during the processing of the material and lead to the formation of defects (voids, delamination, *etc.*) in the final part. The drying protocols used prior to processing must take into account these slow diffusion kinetics and dual stage behavior, to achieve effective drying.

4.A Supplementary materials

Figure 4.9 (left) shows the internal part of the sample holder and the salt solution container placed in the oven. Figure 4.9 (right) shows the weight variation Δw of the sample holder at 40 °C and 65 %RH before the sample positioning. Under constant temperature and hygrothermal conditions, the sample holder does not experiment a significant weight variation.

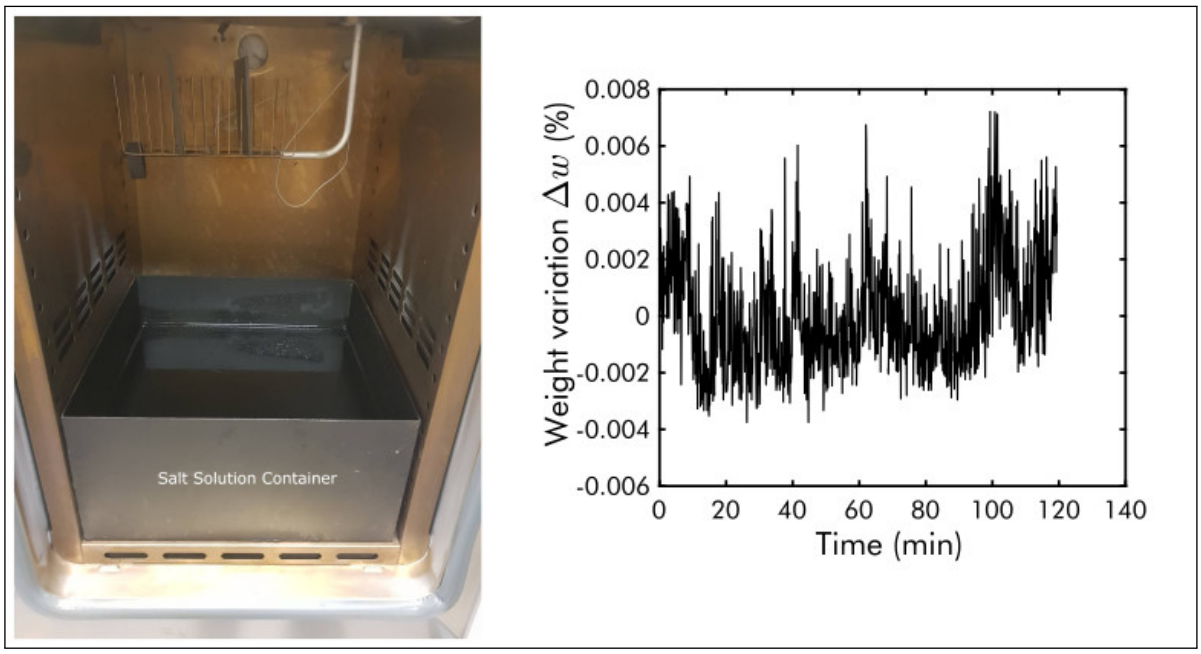

Figure 4.9: Internal picture of OMICHA bench showing the internal part of the sample holder and the salt solution container (left). Evolution of the weight variation Δw of the sample holder at 40 °C and 65 %RH before sample positioning (right).

References

[1] C. Shirrell and J. Halpin, "Moisture absorption and desorption in epoxy composite laminates," in *Composite Materials: Testing and Design (Fourth Conference)*, ASTM International, 1977 (cit. on p. 93).

[2] A. C. Loos and G. S. Springer, "Moisture absorption of graphite-epoxy composites immersed in liquids and in humid air," *Journal of composite materials*, vol. 13, no. 2, pp. 131–147, 1979 (cit. on p. 93).

[3] E. Pérez-Pacheco, J. Cauich-Cupul, A. Valadez-González, and P. Herrera-Franco, "Effect of moisture absorption on the mechanical behavior of carbon fiber/epoxy matrix composites," *Journal of materials science*, vol. 48, no. 5, pp. 1873–1882, 2013 (cit. on p. 93).

[4] J. R. Vinson, *Advanced composite materials-environmental effects*. ASTM International, 1978 (cit. on p. 93).

[5] L. Grunenfelder and S. Nutt, "Void formation in composite prepregs–Effect of dissolved moisture," *Composites Science and Technology*, vol. 70, no. 16, pp. 2304–2309, 2010 (cit. on p. 93).

[6] J. Kardos, M. Duduković, and R. Dave, "Void growth and resin transport during processing of thermosetting—matrix composites," *Epoxy resins and composites IV*, pp. 101–123, 1986 (cit. on p. 93).

[7] G. Fernlund, J. Wells, L. Fahrang, J. Kay, and A. Poursartip, "Causes and remedies for porosity in composite manufacturing," in *IOP conference series: materials science and engineering*, IOP Publishing, vol. 139, 2016, p. 012 002 (cit. on p. 93).

[8] G. Dorey, S. Bishop, and P. Curtis, "On the impact performance of carbon fibre laminates with epoxy and PEEK matrices," *Composites Science and Technology*, vol. 23, no. 3, pp. 221–237, 1985 (cit. on p. 93).

[9] R. Selzer and K. Friedrich, "Mechanical properties and failure behaviour of carbon fibre-reinforced polymer composites under the influence of moisture," *Composites Part A: Applied Science and Manufacturing*, vol. 28, no. 6, pp. 595–604, 1997 (cit. on p. 93).

[10] P. Zhou, J. Tian, C. Li, and Z. Tang, "Comparative Study of Durability Behaviors of Thermoplastic Polypropylene and Thermosetting Epoxy Exposed to Elevated Temperature, Water Immersion and Sustained Bending Loading," *Polymers*, vol. 14, no. 14, p. 2953, 2022 (cit. on p. 93).

[11] R. Delasi and J. Whiteside, *Effect of moisture on epoxy resins and composites*. ASTM International, 1978 (cit. on p. 94).

[12] A. Zafar, F. Bertocco, J. Schjødt-Thomsen, and J. Rauhe, "Investigation of the long term effects of moisture on carbon fibre and epoxy matrix composites," *Composites Science and Technology*, vol. 72, no. 6, pp. 656–666, 2012 (cit. on p. 94).

[13] M. Lai, J. Botsis, J. Cugnoni, and D. Coric, "An experimental–numerical study of moisture absorption in an epoxy," *Composites part A: applied science and manufacturing*, vol. 43, no. 7, pp. 1053–1060, 2012 (cit. on p. 94).

[14] C. Humeau, P. Davies, and F. Jacquemin, "Moisture diffusion under hydrostatic pressure in composites," *Materials & Design*, vol. 96, pp. 90–98, 2016 (cit. on p. 94).

[15] B. de Parscau du Plessix, F. Jacquemin, P. Lefébure, and S. Le Corre, "Characterization and modeling of the polymerization-dependent moisture absorption behavior of an epoxy-carbon fiber-reinforced composite material," *Journal of Composite Materials*, vol. 50, no. 18, pp. 2495–2505, 2016 (cit. on pp. 94, 108).

[16] C. Gao and C. Zhou, "Moisture absorption and cyclic absorption–desorption characters of fibre-reinforced epoxy composites," *Journal of materials science*, vol. 54, no. 11, pp. 8289–8301, 2019 (cit. on p. 94).

[17] S. Y. Park, W. J. Choi, C. H. Choi, and H. S. Choi, "An experimental study into aging unidirectional carbon fiber epoxy composite under thermal cycling and moisture absorption," *Composite Structures*, vol. 207, pp. 81–92, 2019 (cit. on p. 94).

[18] C.-C. M. Ma and S.-W. Yur, "Environmental effects on the water absorption and mechanical properties of carbon fiber reinforced PPS and PEEK composites. Part II," *Polymer Engineering & Science*, vol. 31, no. 1, pp. 34–39, 1991 (cit. on pp. 94, 105, 109–110).

[19] C.-C. M. Ma, C.-L. Lee, M.-J. Chang, and N.-H. Tai, "Hygrothermal behavior of carbon fiber-reinforced poly (ether ether ketone) and poly (phenylene sulfide) composites. I," *Polymer composites*, vol. 13, no. 6, pp. 448–453, 1992 (cit. on p. 94).

[20] L. Zhang and M. Piggott, "Water absorption and fiber-matrix interface durability in carbon-PEEK," *Journal of Thermoplastic Composite Materials*, vol. 13, no. 2, pp. 162–172, 2000 (cit. on pp. 94, 105).

[21] Y. H. Kim, S. W. Yoon, J. W. Lee, J. C. Ha, and R. I. Murakami, "Effect of moisture absorption and fiber ply orientation for artificial hip joint on the mechanical properties of carbon/PEEK composites," in *Advanced Materials Research*, Trans Tech Publ, vol. 774, 2013, pp. 1326–1335 (cit. on p. 94).

[22] T. Saoudi and M. E. A. Belouchrani, "Mechanical Properties and Diffusion Behavior of Carbon Fiber-Reinforced PEEK on exposure to heat and water," *Composites: Mechanics, Computations, Applications: An International Journal*, vol. 10, no. 4, 2019 (cit. on p. 94).

[23] E. Courvoisier, "Analyse et modélisation cinétique du vieillissement thermique des matrices PEI et PEEK et ses conséquences sur l'absorption d'eau," Ph.D. dissertation, Paris, ENSAM, 2017 (cit. on pp. 94, 104, 111).

[24] K.-M. Lee, S.-J. Park, T. Yu, S.-J. Park, and Y.-H. Kim, "Experimental prediction of internal defects according to defect area on NDI via water absorption behavior," *International Journal of Modern Physics B*, vol. 35, no. 14n16, p. 2 140 021, 2021 (cit. on p. 94).

[25] E. F. Sukur, S. Elmas, M. Seyyednourani, V. Eskizeybek, M. Yildiz, and H. S. Sas, "A rational study on the hydrothermal aging of AFP manufactured CF/polyetherketoneketone composites with in situ consolidation supported by acoustic emission inspection," *Journal of Applied Polymer Science*, e52480, 2022 (cit. on pp. 94, 105, 109–110).

[26] R. L. Mazur, P. C. Oliveira, M. C. Rezende, and E. C. Botelho, "Environmental effects on viscoelastic behavior of carbon fiber/PEKK thermoplastic composites," *Journal of Reinforced Plastics and Composites*, vol. 33, no. 8, pp. 749–757, 2014 (cit. on pp. 94, 105).

[27] R. L. Mazur, G. M. Cândido, M. C. Rezende, and E. C. Botelho, "Accelerated aging effects on carbon fiber PEKK composites manufactured by hot compression molding," *Journal of Thermoplastic Composite Materials*, vol. 29, no. 10, pp. 1429–1442, 2016 (cit. on p. 94).

[28] J. Jeong, D. Lee, H. Ju, J. Kweon, and Y. Nam, "Effect of hygrothermal condition on single-lab shear behavior of induction-welded CF/PEKK thermoplastic composites," *Advanced Composite Materials*, pp. 1–17, 2022 (cit. on p. 94).

[29] X. Colin and J. Verdu, "Humid ageing of organic matrix composites," in *Durability of composites in a marine environment*, Springer, 2014, pp. 47–114 (cit. on p. 94).

[30] J. El Yagoubi, G. Lubineau, F. Roger, and J. Verdu, "A fully coupled diffusion-reaction scheme for moisture sorption–desorption in an anhydride-cured epoxy resin," *Polymer*, vol. 53, no. 24, pp. 5582–5595, 2012 (cit. on p. 94).

[31] L. Calabrese, V. Fiore, E. Piperopoulos, D. Badagliacco, D. Palamara, A. Valenza, and E. Proverbio, "In situ monitoring of moisture uptake of flax fiber reinforced composites under humid/dry conditions," *Journal of Applied Polymer Science*, vol. 139, no. 16, p. 51 969, 2022 (cit. on p. 94).

[32] H. Garbalińska, M. Bochenek, W. Malorny, and J. von Werder, "Comparative analysis of the dynamic vapor sorption (DVS) technique and the traditional method for sorption isotherms determination — Exemplified at autoclaved aerated concrete samples of four density classes," *Cement and Concrete Research*, vol. 91, pp. 97–105, 2017, ISSN: 0008-8846 (cit. on p. 94).

[33] S. Sheokand, S. R. Modi, and A. K. Bansal, "Dynamic vapor sorption as a tool for characterization and quantification of amorphous content in predominantly crystalline materials," *Journal of pharmaceutical sciences*, vol. 103, no. 11, pp. 3364–3376, 2014 (cit. on p. 94).

[34] S. M. Systems. "Dynamic vapour sorption apparatus." (2022), [Online]. Available: `https://www.surfacemeasurementsystems.com/products/dynamic-vapor-sorption-instruments/vapor-sorption-analyzer/dvs-intrinsic/` (visited on 2022) (cit. on p. 94).

[35] H. Perez-Martin, P. Mackenzie, A. Baidak, C. M. Ó. Brádaigh, and D. Ray, "Crystallinity studies of PEKK and carbon fibre/PEKK composites: A review," *Composites Part B: Engineering*, vol. 223, p. 109 127, 2021 (cit. on p. 95).

[36] J. Avenet, "Assemblage par fusion de composites à matrice thermoplastique: caractérisation expérimentale et modélisation de la cinétique d'auto-adhésion hors équilibre," Ph.D. dissertation, Université de Nantes (UN), 2021 (cit. on p. 95).

[37] H. Pérez-Martín, P. Mackenzie, A. Baidak, C. M. Ó. Brádaigh, and D. Ray, "Crystallisation behaviour and morphological studies of PEKK and carbon fibre/PEKK composites," *Composites Part A: Applied Science and Manufacturing*, p. 106 992, 2022 (cit. on p. 95).

[38] N. C. Judd, "Absorption of water into carbon fibre composites," *British Polymer Journal*, vol. 9, no. 1, pp. 36–40, 1977 (cit. on p. 95).

[39] M. L. Costa, M. C. Rezende, and S. F. M. De Almeida, "Effect of void content on the moisture absorption in polymeric composites," *Polymer-Plastics Technology and Engineering*, vol. 45, no. 6, pp. 691–698, 2006 (cit. on p. 95).

[40] S. Y. Park, W. J. Choi, and H. S. Choi, "The effects of void contents on the long-term hygrothermal behaviors of glass/epoxy and GLARE laminates," *Composite Structures*, vol. 92, no. 1, pp. 18–24, 2010 (cit. on p. 95).

[41] D. Paganin, S. C. Mayo, T. E. Gureyev, P. R. Miller, and S. W. Wilkins, "Simultaneous phase and amplitude extraction from a single defocused image of a homogeneous object," *Journal of microscopy*, vol. 206, no. 1, pp. 33–40, 2002 (cit. on p. 96).

[42] L. Greenspan, "Humidity fixed points of binary saturated aqueous solutions," *Journal of research of the National Bureau of Standards. Section A, Physics and chemistry*, vol. 81, no. 1, p. 89, 1977 (cit. on p. 97).

[43] M. Čekon and O. Šikula, "Experimental and numerical study on the thermal performance of polycarbonate panels," *Journal of Building Engineering*, vol. 32, p. 101 715, 2020 (cit. on p. 98).

[44] Y. J. Weitsman, *Fluid effects in polymers and polymeric composites*. Springer Science & Business Media, 2011 (cit. on pp. 103–104, 109, 111).

[45] L. Feuillerat, O. De Almeida, J.-C. Fontanier, and F. Schmidt, "Effect of poly (ether ether ketone) degradation on commingled fabrics consolidation," *Composites Part A: Applied Science and Manufacturing*, vol. 149, p. 106 482, 2021 (cit. on p. 104).

[46] P. Patel, T. R. Hull, R. W. McCabe, D. Flath, J. Grasmeder, and M. Percy, "Mechanism of thermal decomposition of poly (ether ether ketone)(PEEK) from a review of decomposition studies," *Polymer degradation and stability*, vol. 95, no. 5, pp. 709–718, 2010 (cit. on p. 104).

[47] C. Croshaw, L. Hamernik, L. Ghanbari, A. Browning, and J. Wiggins, "Melt-state degradation mechanism of poly (ether ketone ketone): the role of branching on crystallization and rheological behavior," *Polymer Degradation and Stability*, vol. 200, p. 109 968, 2022 (cit. on p. 104).

[48] D.-W. Suh, M.-K. Ku, J.-D. Nam, B.-S. Kim, and S.-C. Yoon, "Equilibrium water uptake of epoxy/carbon fiber composites in hygrothermal environmental conditions," *Journal of Composite materials*, vol. 35, no. 3, pp. 264–278, 2001 (cit. on p. 106).

[49] J. Crank, *The mathematics of diffusion*. Oxford university press, 1979 (cit. on pp. 106, 108).

[50] H. G. Carter and K. G. Kibler, "Langmuir-type model for anomalous moisture diffusion in composite resins," *Journal of composite materials*, vol. 12, no. 2, pp. 118–131, 1978 (cit. on p. 107).

[51] M. D. Placette, X. Fan, J.-H. Zhao, and D. Edwards, "Dual stage modeling of moisture absorption and desorption in epoxy mold compounds," *Microelectronics Reliability*, vol. 52, no. 7, pp. 1401–1408, 2012 (cit. on pp. 107–108).

[52] H. Shirangi, J. Auersperg, M. Koyuncu, H. Walter, W. Muller, and B. Michel, "Characterization of dual-stage moisture diffusion, residual moisture content and hygroscopic swelling of epoxy molding compounds," in *EuroSimE 2008-International Conference on Thermal, Mechanical and Multi-Physics Simulation and Experiments in Microelectronics and Micro-Systems*, IEEE, 2008, pp. 1–8 (cit. on p. 108).

[53] MATLAB (R2022a), Natick, Massachusetts, 2022 (cit. on p. 108).

[54] D. A. Bond, "Moisture diffusion in a fiber-reinforced composite: part I–non-Fickian transport and the effect of fiber spatial distribution," *Journal of Composite Materials*, vol. 39, no. 23, pp. 2113–2141, 2005 (cit. on p. 109).

[55] M. A. Grayson and C. J. Wolf, "The solubility and diffusion of water in poly (aryl-ether-ether-ketone)(PEEK)," *Journal of Polymer Science Part B: Polymer Physics*, vol. 25, no. 1, pp. 31–41, 1987 (cit. on p. 109).

[56] G. Mensitieri, A. Apicella, J. Kenny, and L. Nicolais, "Water sorption kinetics in poly (aryl ether ether ketone)," *Journal of applied polymer science*, vol. 37, no. 2, pp. 381–392, 1989 (cit. on p. 109).

[57] M. J. Adamson, "Thermal expansion and swelling of cured epoxy resin used in graphite/epoxy composite materials," *Journal of materials science*, vol. 15, no. 7, pp. 1736–1745, 1980 (cit. on p. 110).

[58] S. Popineau, C. Rondeau-Mouro, C. Sulpice-Gaillet, and M. E. Shanahan, "Free/bound water absorption in an epoxy adhesive," *Polymer*, vol. 46, no. 24, pp. 10 733–10 740, 2005 (cit. on p. 110).

[59] G. Mensitieri, M. Lavorgna, P. Musto, and G. Ragosta, "Water transport in densely crosslinked networks: A comparison between epoxy systems having different interactive characters," *Polymer*, vol. 47, no. 25, pp. 8326–8336, 2006 (cit. on p. 110).

[60] H. Hatakeyama and T. Hatakeyama, "Interaction between water and hydrophilic polymers," *Thermochimica acta*, vol. 308, no. 1-2, pp. 3–22, 1998 (cit. on p. 110).

[61] V. Bellenger, J. Verdu, and E. Morel, "Structure-properties relationships for densely cross-linked epoxide-amine systems based on epoxide or amine mixtures," *Journal of materials science*, vol. 24, no. 1, pp. 63–68, 1989 (cit. on p. 111).

[62] F. Perrin, M. H. Nguyen, and J. Vernet, "Water transport in epoxy–aliphatic amine networks–Influence of curing cycles," *European Polymer Journal*, vol. 45, no. 5, pp. 1524–1534, 2009 (cit. on p. 111).

[63] G. Bouvet, N. Dang, S. Cohendoz, X. Feaugas, S. Mallarino, and S. Touzain, "Impact of polar groups concentration and free volume on water sorption in model epoxy free films and coatings," *Progress in Organic coatings*, vol. 96, pp. 32–41, 2016 (cit. on p. 111).

[64] E. Gaudichet-Maurin, F. Thominette, and J. Verdu, "Water sorption characteristics in moderately hydrophilic polymers, Part 1: Effect of polar groups concentration and temperature in water sorption in aromatic polysulfones," *Journal of applied polymer science*, vol. 109, no. 5, pp. 3279–3285, 2008 (cit. on p. 111).

[65] I. Merdas, F. Thominette, A. Tcharkhtchi, and J. Verdu, "Factors governing water absorption by composite matrices," *Composites Science and technology*, vol. 62, no. 4, pp. 487–492, 2002 (cit. on p. 111).

[66] A. Tcharkhtchi, P. Bronnec, and J. Verdu, "Water absorption characteristics of diglycidylether of butane diol–3, 5-diethyl-2, 4-diaminotoluene networks," *Polymer*, vol. 41, no. 15, pp. 5777–5785, 2000 (cit. on p. 111).

[67] J. Zhou and J. P. Lucas, "Hygrothermal effects of epoxy resin. Part I: the nature of water in epoxy," *Polymer*, vol. 40, no. 20, pp. 5505–5512, 1999 (cit. on p. 111).

[68] M. Coulson, E. Dantras, P. Olivier, N. Gleizes, and C. Lacabanne, "Thermal conductivity and diffusivity of carbon-reinforced polyetherketoneketone composites," *Journal of Applied Polymer Science*, vol. 136, no. 38, p. 47 975, 2019 (cit. on p. 113).

"This page left intentionally blank"

CHAPTER 5

DEVELOPMENT OF THERMOPLASTIC COMPOSITES DECONSOLIDATION CHARACTERIZATION BENCH

Contents

Abstract

Pre-consolidated Carbon Fiber-Reinforced ThermoPlastic (CFRTP) laminates often need a secondary manufacturing step such as welding, forming. When a low pressure is applied during the laminate heating stage, pores can appear in various forms (bubbles, delaminations, *etc.*). This is the deconsolidation phenomenon. These pores significantly deteriorate the mechanical properties of the composites. Usually, deconsolidation is characterized by analysis after processing or by ThermoMechanical Analysis (TMA). However, these techniques do not allow online investigation of deconsolidation mechanisms on representative composite laminates.

In order to overcome these limitations, a new experimental device has been developed. It allows the online characterization of fiber-reinforced thermoplastic laminate deconsolidation, by continuous measurement of deconsolidation strain of samples with large size (several centimeters in contrast to a few millimeters in TMA) under representative heating conditions. The capability of the setup is illustrated on plate samples made of a high-performance Carbon Fiber (CF) - reinforced thermoplastic (CF/PEKK laminates).

The previous Chapter 4 provided the preconditioning protocol which allow to decouple the effect of moisture from residual stresses. Now, the actual deconsolidation of CF/PEKK must be studied. The review of the deconsolidation characterization techniques carried out in Chapter 3, allowed to identify two characterization methods suitable for this study: continuous thickness measurement by laser sensors (macro scale) and X-ray microtomography (micro scale). In this chapter, a new methodology is developed based on the solution of laser sensors to characterize deconsolidation at a macroscopic scale.

5.1 Introduction

The demand for composite materials in the aeronautical sector is continuously growing, due to their high specific mechanical properties. Thermoset Carbon Fiber-Reinforced Plastics (CFRPs) which are commonly used in aeronautics, present major issues mainly related to assembly [1–3]. One of the solutions to avoid this problem is the use of thermoplastic CFRPs.

Unlike thermoset matrix CFRPs, thermoplastic matrix CFRPs can be repeatedly re-heated and then re-consolidated, re-formed as well as welded. However, when a low or no pressure is applied during re-heating, pores appear and may remain in the final part after processing: this is the deconsolidation phenomenon. It is well known that pores strongly degrade the mechanical strength of materials [4–6]. It is, therefore, crucial to avoid deconsolidation during processing. For that purpose, the mechanisms involved during deconsolidation of Carbon Fiber-Reinforced ThermoPlastic (CFRTP) composites must be properly characterized and understood.

Many studies in the literature showed that deconsolidation of thermoset composites laminates, during curing, is mainly due to volatile evaporation and/or diffusion mechanisms [7–9]. In fact, volatile substances are trapped in the material during its storage in a freezer or during its lay-up in a room environment. Under temperature and pressure effect, the volatiles cause deconsolidation through diffusion and coalescence mechanisms. Based on these results, some authors suggest that thermoplastic composite deconsolidation could also be related to the same mechanisms. To verify this hypothesis, most of the work in the literature has focused on Glass Fiber-Reinforced ThermoPlastic (GFRTP) composites [10–12]. Recently Slange *et al.* [13] carried out deconsolidation tests (in an convection oven) on dried and undried UniDirectional

(UD) $[0/90]_{4s}$ CF/PolyEtherEtherKetone (PEEK) laminate samples, pre-consolidated at 1 MPa in a press. The results showed that the thickness increase of dried samples after deconsolidation is smaller than undried ones. Slange *et al.* then concluded that moisture diffusion is the main factor responsible for deconsolidation in press consolidated UD CF/PEEK laminates samples. Consequently, the authors recommended drying the laminates at 250 °C for 3 h, in order to eliminate moisture effects before laminates processing.

Unlike thermoset composites, synthetic and oil-based ThermoPlastic Composite (TPC) usually uptake less water. For this reason, other authors showed that the deconsolidation of these hydrophobic TPC laminates is mainly caused by residual stresses stored in the laminates after their consolidation. In the literature, this hypothesis is mainly highlighted for woven and mat laminates [14–16]. To the author knowledge, in the case of high-performance UD CFRTP laminates, only Donadei *et al.* [17], showed that deconsolidation is linked to residual stresses. To do so, the authors carried out deconsolidation tests (in an infrared oven) on annealed and non-annealed UD $[-45/90/45/0]_{3S}$ CF/PolyEtherKetoneKetone (PEKK) laminates pre-consolidated at 0.6 MPa in an autoclave.

These different conclusions suggest that both moisture and residual stresses may be involved in the deconsolidation phenomenon. It also appears as difficult to decorrelate these two effects. Indeed, drying and relaxing residual stresses are usually performed altogether during preconditioning.

In most of the studies performed, deconsolidation is characterized by analysis after experiment (thickness measurement, micrographs, *etc.*) [13, 17, 18]. These characterization methods do not allow the analysis of what happens during heating and dwell. Indeed, during cooling, shrinkage and crystallization phenomena can affect the final state (thickness) of the material. It is then difficult with these techniques to characterize the real impact of the consolidation processes and the volatile substances initially stored in the material on deconsolidation.

Another solution mainly used to characterize deconsolidation during heating is ThermoMechanical Analysis (TMA) [19]. It allows the application of representative cycles to a small lab scale sample (8 mm × 8 mm). However, deconsolidation may be affected by free stress edges, if the sample size is not representative of a laminate structure. Brzeski [20] uses image correlation method to characterize deconsolida-

tion of 50 mm × 50 mm woven laminates made of glass fiber-reinforced plastics. The team measured online thickness evolution due to deconsolidation in a press, using CCD camera. Unfortunately, they did not analyse the measurements. This is probably because of the edge effect, as the thickness was measured on the lateral side of the sample. Deconsolidation, indeed, mostly occurs in the core [12, 13, 17]. Furthermore, no information was mentioned on the validation of the measurements and a thermal analysis was not performed to estimate the samples temperature field during the experiments.

The major contribution of this work is the design, fabrication and validation of a new device. It can characterize continuously and online deconsolidation of high-performance fiber-reinforced thermoplastic composite. This device will allow online observation of the phenomena involved during heating, on samples of sizes representative of a structure. This is illustrated with a aerospace grade CFRTP laminates CF/PEKK initially consolidated by Hot Press Consolidation (HPC) and deconsolidated under various conditions. These test results enabled preliminary understanding of the effect of moisture and residual stresses on subsequent CFRTP laminate deconsolidation.

5.2 CODEC bench

COmposite DEconsolidation Characterization (CODEC) bench is developed for continuous and online characterization of large TPC laminates deconsolidation under different processing conditions (pressure, temperature, heating rate, *etc.*). Deconsolidation is characterized on the device by a thickness variation measurement using optical sensors. The thickness variation measured corresponds to the macroscopic structural change in the material due to pores appearance and growth (deconsolidation).

5.2.1 Development

The device is composed of a large copper heating plate which can heat up to 450 °C with a maximal heating rate of 60 °C/min (Figure 5.1). The hot plate temperature was measured by a K-type monitoring thermocouple sensor located in the middle of the hot plate, 1 mm beneath its surface. The heating power was generated by resistive cartridge heaters and regulated according to the temperature measured by the monitoring thermocouple. The hot plate was placed in a closed thermal chamber (aluminum) with a 25 mm thick borosilicate upper glass window. In order to limit

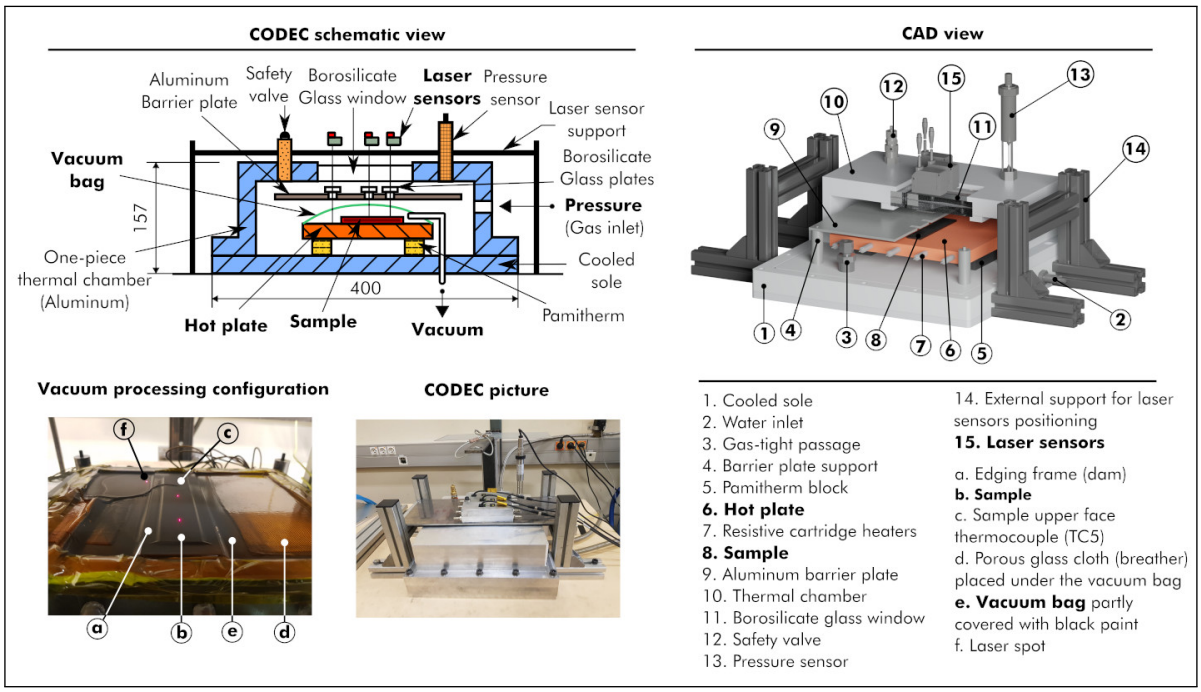

Figure 5.1: CODEC bench designed for continuous and online characterization of thermoplastic composite laminates deconsolidation under processing conditions. Laminate thickness evolution is measured in the chamber with contact-less laser sensors.

the thermal chamber expansion due to temperature variations, the chamber walls were cooled by an active water flow in the sole. Two Pamitherm thermal insulators were placed between the sole and the hot plate to reduce conductive heat transfer between the hot plate and the aluminum chamber. The chamber was equipped with a compressed gas inlet, to pressurize the chamber up to 1 MPa (10 bar). The sample can also be processed in a classical vacuum bag setup and a gas-tight passage permits the sample to be vacuumed.

During experiments on CODEC device, the sample can be let free under atmospheric pressure in the thermal chamber. This case refers to a test at No Counter Pressure (NCP). When a vacuum pressure (0.1 MPa) is required for a test, the sample is surrounded by edging frames, acting as dams, and placed under a vacuum bag (Figure 5.1). A primary vacuum ($\approx$ 0.01 MPa) is then applied under the vacuum bag through a VARIAN SD-450 serial no.241 687 vacuum pump connected to the gas-tight passage. It should be noted that only the sample is under vacuum and the thermal chamber is still at an atmospheric pressure. Finally, the sample can be processed as in an autoclave. In addition to the vacuum pressure in the bag, an inert gas (Argon) can be injected in the

thermal chamber to increase the counter pressure, up to a given absolute value. The chamber pressure was measured by a pressure sensor, from Keller's 35XTC series. The chamber is designed for a pressure of up to 1 MPa. The pressure sensor has a larger measurement range of 0 to 3 MPa and an accuracy of $\pm 0.05\,\%$ of the measurement range. The chamber is also equipped with a safety valve to evacuate the gas in case of over-pressure.

The samples thickness variation was measured using three Keyence IL-S65 laser sensors through the borosilicate window. The three distance measurement sensors have a measurement range of 55 to 75 mm and a linearity of $\pm 0.075\,\%$ of the full scale. The laser emitted by the sensors has a wavelength of 655 nm (visible light), to which the borosilicate is transparent. The maximum environmental temperature that the sensors can withstand is 50 °C. For this reason, the sensors were positioned in an aluminum box located on a structure outside the chamber. This solution was however insufficient to protect the sensors, given the radiation emitted by the hot plate which passes through the glass window.

A 3 mm thick aluminum barrier plate was thus placed between the hot plate and the glass window. The barrier plate mainly plays two roles. The first role was to avoid a significant rise of the glass window temperature, by reflecting and absorbing the heat emitted by the hot plate. The emissivity of the barrier plate was minimized by polishing its faces. This barrier also helped to avoid significant distortion of the glass window, which can lead to significant measurement errors of the laser sensors. The second role of the barrier plate was to limit gas convection movements in the chamber, which cause significant noise on the sensors measurement. The holes machined in the barrier plate for the laser rays passage were covered by 2 mm thick borosilicate glass plates.

Laser and pressure sensors, thermocouples, and power controller were connected by mean of modules to a single NI CompactDAQ acquisition system. The control was performed automatically using a single piece of software developed on LabVIEW. Thus, the temperature, pressure, distance data acquisition, and temperature control were synchronized. This provided a better control of the experiment conditions (heating rate, temperature, pressure).

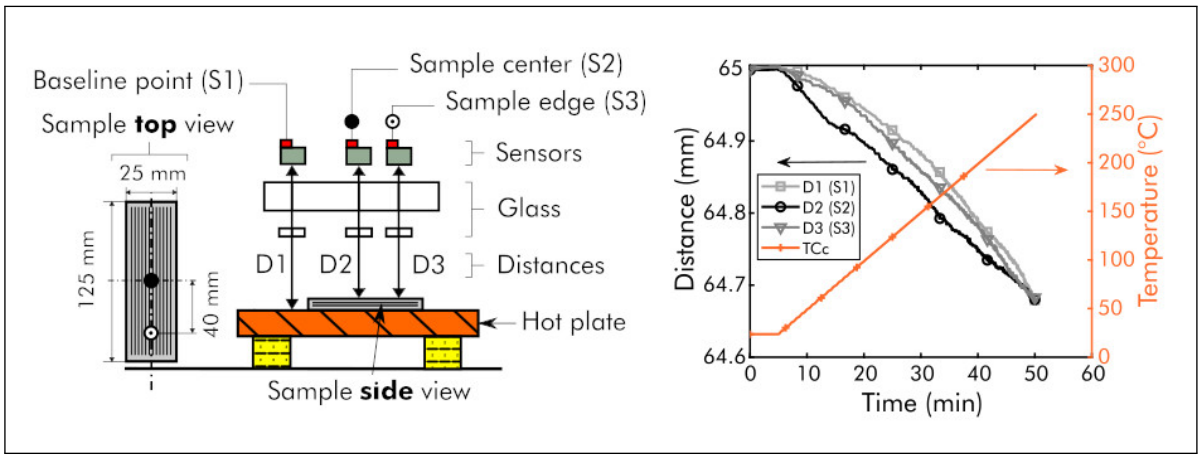

Figure 5.2: Validation of the CODEC bench using an aluminum sample. Positioning of the contact-less laser sensors (left) and example of raw distance measurement *vs* time during a ramp up of 5 °C/min up to 250 °C on an aluminum sample (right).

5.2.2 Thickness variation measurement

Among the three laser sensors placed on the CODEC device, only two sensors aim at the sample. The first sensor (S1) aims at the hot plate (Figure 5.2 left). The second sensor (S2) aims at the center of the sample and the last one (S3) aims 40 mm from the center. During a ramp-up, the distances between the sensor positions and the targets (sample and hot plate) are recorded (Figure 5.2 right). From the distance measurements, elongations (expansion or contraction of the targets) are obtained at the three measurement points, as the difference between the actual distance and the initial ones as depicted in equation (5.1). The hot plate elongation (baseline, S1) was subtracted from the total elongation calculated on the sample (5.2). This procedure allowed us to estimate the real sample elongation.

$$\Delta L_i(t) = D_i(0) - D_i(t) \quad i = \{S1; S2; S3\} \tag{5.1}$$

$$\Delta L_j(t) = \Delta L_j(t) - \Delta L_{S1}(t) \quad j = \{S2; S3\} \tag{5.2}$$

$$\varepsilon_D = \varepsilon_j(t) = \ln\left(1 + \frac{\Delta L_j(t)}{L_0}\right) \tag{5.3}$$

where $D_i(0)$ is the initial distance measured at a given measurement point, $D_i(t)$ the distance over time, $\Delta L_j(t)$ and ε_j respectively the sample elongation and strain at the two measurement points, L_0 is the sample initial thickness measured by a micrometer.

The sample deconsolidation true strain (ε_D) was then determined according to equation (5.3) at the two measurement points. This deconsolidation strain is a *global strain*.

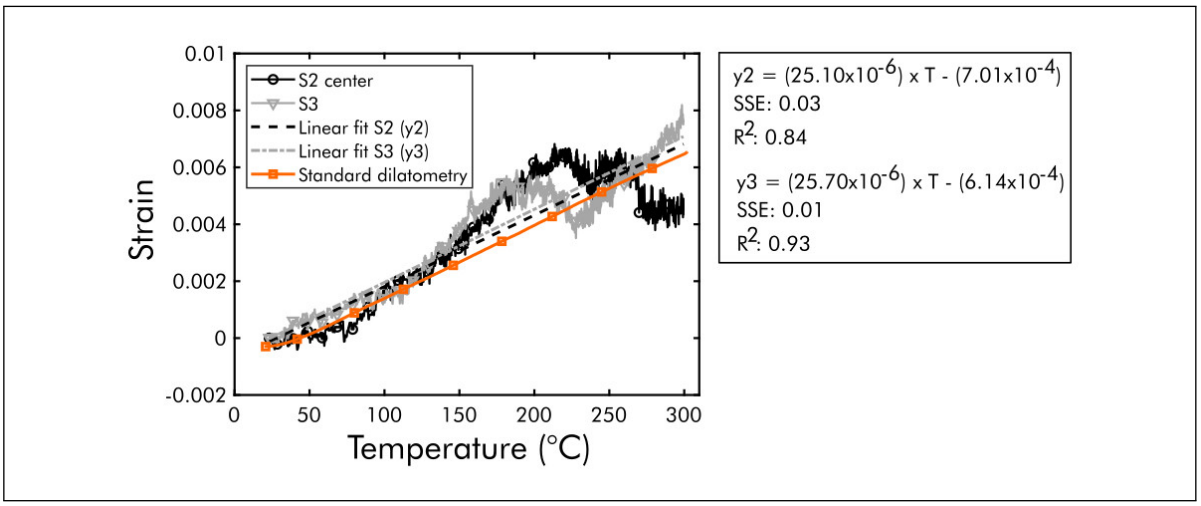

Figure 5.3: Comparison between dilatometry test results obtained by standard dilatometer and by CODEC device, on an aluminum sample. On CODEC device, vacuum pressure is applied on the sample.

Indeed, the strain is heterogeneous during UD prepreg-based TPC laminates deconsolidation. Hencky or logarithmic strain is used because of the high strains produced by deconsolidation. Distance, temperature, and pressure measurements are synchronized on CODEC device. It is thus possible to characterize the deconsolidation of large samples (up to 150 mm $\times$ 50 mm), under controlled conditions of temperature and pressure representative of industrial processes (autoclave, VBO, *etc.*).

5.2.2.1 Measurement validation

In order to estimate the accuracy of the developed CODEC bench, the setup was tested with a reference homogeneous metallic sample, *i.e.* 6061 aluminum. The metallic sample does not experience phase change or deconsolidation during heating in the tested temperature range. The expansions measured with the CODEC bench are compared with standard dilatometry measurement.

Firstly, using a Linseis L75HS500LT dilatometer, a dilatometry test was performed on a 10 mm $\times$ 10 mm $\times$ 2.98 mm sample of 6061 aluminum. The sample was heated at 2 °C/min from 20 °C to 300 °C. Strain as a function of temperature is plotted on the Figure 5.3. From this curve, the linear Coefficient of Thermal Expansion (CTE) was determined along the thickness direction (see Table 5.1 in Section 5.2.2.2).

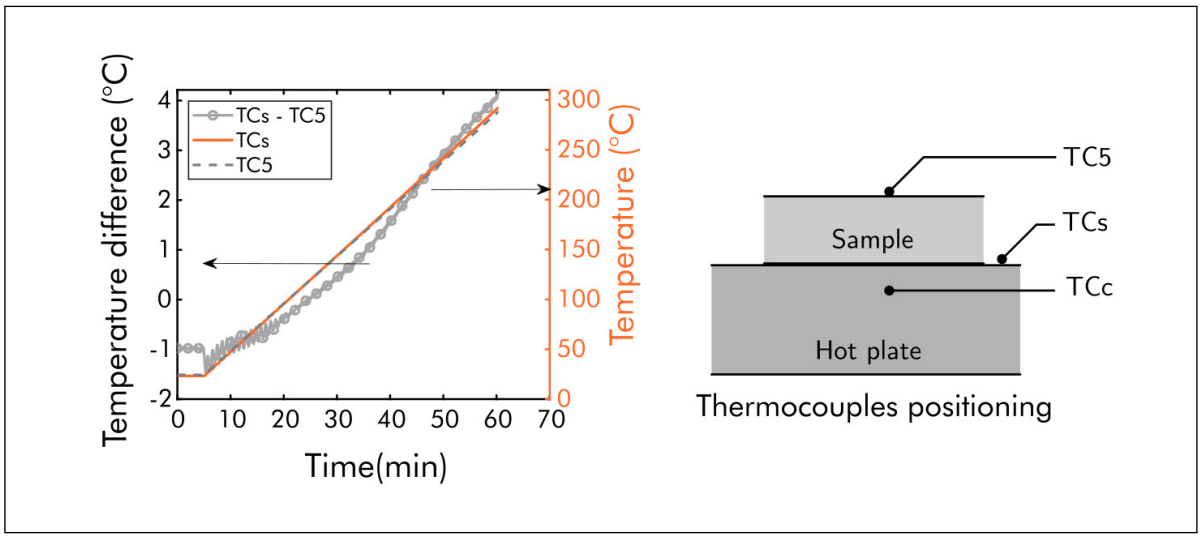

Figure 5.4: Temperature difference between the top surface temperature of the aluminum sample ($TC5$) and the top surface temperature of the hot plate (TCs).

Secondly, using the CODEC bench, another test was performed on a bigger plate (125 mm × 25 mm × 2.98 mm) of the same alloy. The size of the sample was increased in order to avoid edge effects related to air convection, according to the hot plate size and the thermal chamber volume. The sample was heated at 5 °C/min up to 300 °C under a vacuum pressure (0.1 MPa). This dilatometry test was repeated twice. Since aluminum has a high thermal conductivity ($\approx 167\,\mathrm{W/(m \cdot K)}$), the defined heating rate allowed to obtain an homogeneous temperature in the aluminum sample. During the test, one K-type thermocouple was placed on the top surface of the sample ($TC5$) and another directly taped on the copper top surface below the vacuum bag (TCs). The maximum temperature difference between the two measurements was 4 °C (Figure 5.4). $TC5$ thermocouple is pressed against the aluminum top surface by the vacuum bag. Thus, the measured temperature at this point is assumed to be the aluminum sample temperature. The vacuum pressure is applied during the experiment in order to maintain a good contact between the sample and the hot plate. The sample strain as a function of temperature is plotted on Figure 5.3.

5.2.2.2 Accuracy of the CODEC setup

The strain curve obtained with the CODEC device is rather non-linear and scattered (see Figure 5.3 in Section 5.2.1). This non-linearity is due to the macroscopic movements of the heating plate on its Pamitherm blocks (Figure 5.1) and the air convection which

Table 5.1: Comparison of CTEs obtained by standard dilatometry and with the CODEC bench.

Dilatometry ($°C^{-1}$)	25.67×10^{-6}	
CODEC setup ($°C^{-1}$)	Sensor 2	Sensor 3
Test 1	25.10×10^{-6}	25.70×10^{-6}
Test 2	25.57×10^{-6}	24.65×10^{-6}
Mean	25.34×10^{-6}	25.18×10^{-6}
Absolute error ($°C^{-1}$)	0.33×10^{-6}	0.49×10^{-6}
Relative error (%)	1.29	1.91

disturbed the laser measurement. Indeed, the distance measurement is based on laser triangulation principle. For this reason, the measurement is affected by the environment conditions (air convection and temperature) and the hot plate flatness.

Moreover, the measured strain deviates above 150 °C. It is assumed that this is probably due to an optical effect related to the aluminum sample. This deviation was not repeatable and was not observed on composite samples tests (see Section 5.4.2). Furthermore, the magnitude of this deviation is small (0.2 % strain) and negligible compared to the strains in composite samples ($\gg$ 5 %) during deconsolidation.

A comparison of the CTEs obtained, with a standard dilatometer and with the CODEC device, was performed at the measurement points (Table 5.1). These CTEs were obtained by a linear regression over a temperature range of 25 °C to 300 °C. The CTEs comparison shows that the CODEC device is able to characterize small strains with a relative error of $\pm$ 2 %. As it will be clear in the following, such a precision enables to properly observe and quantify the targeted phenomena.

5.3 Material and Procedure

In order to investigate the deconsolidation phenomenon occurring on an aerospace grade thermoplastic composite material, UD CF/PEKK composite laminates were tested with the CODEC bench.

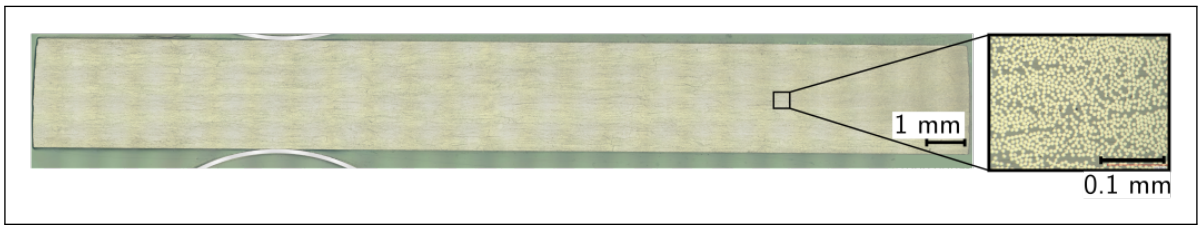

Figure 5.5: Micrograph of the consolidated samples before deconsolidation tests (objective magnification $\times 200$ and resolution 1.55^2 µm^2/pixel). The initial porosity content is not measurable.

5.3.1 CF/PEKK composite manufacturing

The CF/PEKK prepreg plies were supplied by Toray Advanced Composite. The plies have a Fiber Areal Weight (FAW) of 194 g/m^2 and a theoretical thickness of 0.185 mm. The resin mass content is 34 %. The glass transition temperature (T_g) and melting temperature (T_m) of PEKK 7002 are 160 °C and 337 °C, respectively (according to the manufacturer). In practice, the melting zone observed during Differential Scanning Calorimetry (DSC) experiments extends between 310 °C and 360 °C, with a melting point at 338 °C. This melting range can also be found in [21–23].

From the prepreg plies, $[0]_{16}$ laminates were consolidated in a hot press. The 348 mm $\times$ 348 mm prepreg plies were stacked in a picture-frame mold (internal cavity dimensions: 350 mm $\times$ 350 mm) and consolidated on a 50 t Pinette P.E.I press according to the following cycle: heating at 10 °C/min up to 380 °C under a pressure of 0.1 MPa; the temperature was held for 20 min under a pressure of 4 MPa; cooling at 10 °C/min at the same pressure, then demolding. The final part dimensions after consolidation are 350 mm $\times$ 350 mm $\times$ 2.90 mm. This final size of the laminate is due to the high pressure and the clearance between the plies and the internal cavity of the mold which promotes PEKK resin squeeze out.

Optical micrographs of the consolidated laminates validate a porosity content lower than the measurement limit after the consolidation (Figure 5.5). To perform the microscopic observations, 25 mm wide samples were encapsulated using a slow-curing epoxy resin (EpoFix, Struers). The samples were then prepared using traditional grinding and polishing techniques on an automated polishing machine (Tegrapol-21 and TegraForce-5, Struers) and observed on the digital microscope KEYENCE VHX-7000 series. The cross section micrographs were obtained by assembling several sections with a resolution of 2880 pixel $\times$ 2160 pixel (objective magnification $\times 200$) resulting in

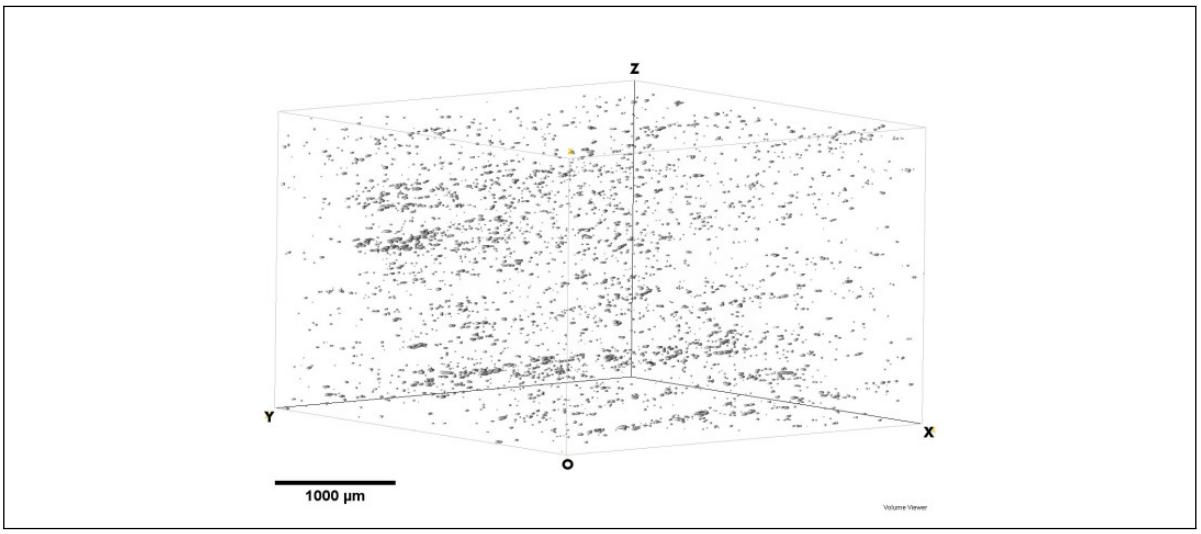

Figure 5.6: 3D image of the porosity distribution in a sample of 20 mm diameter cut from the consolidated laminate (Region Of Interest size: 3.81 mm × 3.81 mm × 2.48 mm). The porosity content is 0.02 %.

an image with a large area of observation and a good resolution ($\approx 1.55^2$ µm^2/pixel). Using the trainable weka segmentation algorithm [24] in an image processing software (Fiji), the porosity content was measured.

This microscopic observation was validated by a micro-CT analysis which showed an initial porosity content of 0.02 % (Figure 5.6). This value is a minor of the laminate porosity content. The 3D image of the sample (20 mm diameter) was obtained on one of the X-ray tomographs of the ID19 line at European Synchrotron Radiation Facilities (Grenoble, France). The raw 3D image was produced (i) with a voxel size of 3.81^3 µm^3 and a large observation volume (7.68 mm × 7.68 mm × 5.37 mm), (ii) by using Paganin method [25]. Additional post-treatment on a Region Of Interest of 3.81 mm × 3.81 mm × 2.48 mm (picked from the raw 3D image) using the trainable weka segmentation algorithm, in an image processing software (Fiji), allowed to measure the porosity content.

5.3.2 Thermal characterization

The thermal properties of the consolidated laminate are given in Table 5.2. These data were obtained, following the procedure detailed by Avenet [22]. The thermal charac-

Table 5.2: CF/PEKK $[0]_{16}$ laminate thermal properties.

	Density ρ	Specific heat capacity C_p
	kg/m^3	$J/(kg \cdot K)$
$T < T_g$	$\rho(T) = 1602.7 - 0.10 \times T[°C]$	$C_p(T) = 2.62 \times T[°C] + 769.7$
$T > T_g$	$\rho(T) = 1605.8 - 0.40 \times T[°C]$	$C_p(T) = 2.34 \times T[°C] + 850.6$
$T > 300\,°C$		$C_p(T) = 0.75 \times T[°C] + 1296$
	Transverse conductivity k_z	
	$W/(m \cdot K)$	
$T < T_g$	$k_z(T) = 8.76 \times 10^{-4} \times T[°C] + 0.73$	
$T > T_g$	$k_z(T) = 7.31 \times 10^{-4} \times T[°C] + 0.81$	

terization (DSC, guarded hot plate, hydrostatic weighing, and TMA) was performed on samples taken from hot press consolidated laminates. Note that the carbon fibers used by Avenet are different from the ones used in this study.

The material heat capacity was obtained, using a TA Instruments DSC Q200. The measurement was performed on a 53.8 mg composite laminate sample of 4 mm diameter cut by waterjet. The sample was first heated at 20 °C/min up to 400 °C in order to erase its thermal history related to the consolidation process. The heat capacity measurement was then performed during a second heating of the sample at 5 °C/min up to 400 °C. The same cycle was applied on an empty specimen holder to obtain the baseline for the heat capacity determination. The low heating rate during the experiments allowed to minimize thermal gradients in the sample during the measurements.

The material thermal conductivity was obtained by standard guarded hot plate method (according to standard ISO 8302:1991) on a sample of 15 mm × 15 mm surrounded by a guard cut from the same laminate (CF/PEKK). The thermal conductivity measurements were performed at different temperatures between 25 °C and 245 °C. The linear relation between the temperature and the thermal conductivity was obtained by a linear fit of the experimental data. Further details about the equipment used to obtained the thermal conductivity can be founded in [22, 26]. The hydrostatic weighing was performed on five composite samples of 20 mm diameter, using a METTLER TOLEDO

AG245 balance with 10 µg accuracy. The reference liquid used was ethanol. Finally, the TMA measurements were performed on a Linseis L75HS500LT dilatometer where the samples were heated at 2 °C/min up to 300 °C.

5.3.3 Preconditioning

After consolidation, the large laminates were cut into small 125 mm × 25 mm samples using a Protomax waterjet cutting machine. The samples were then separated into two groups: Dried Sample (DS) and Ambient Storage sample (AS).

The DS samples were dried at 180 °C for 72 h in order to eliminate residual moisture. This drying condition was carefully checked by continuous weight measurement during drying tests at different temperatures (140 °C, 180 °C, 250 °C), using an OHAUS Explorer EX125M balance with an accuracy of 10 µg. Drying at 180 °C for 72 h fully eliminated the effect of humidity without any thermal degradation of the material (no further significant weight change was observed at 180 °C over this duration of drying).

The AS samples were stored in the workshop for 5 months in ambient condition. After a drying test on a 80 mm × 80 mm AS sample at 180 °C, a weight measurement showed that the water content of the stored samples is 0.013 % at the end of the storage. Both groups of samples allowed us to investigate the effect of moisture and residual stresses on deconsolidation.

5.3.4 Deconsolidation Tests

Thereafter, the 125 mm × 25 mm samples were deconsolidated within the CODEC setup. The samples were heated at 60 °C/min or 10 °C/min up to 380 °C, then maintained at this temperature for 5 min, and cooled (natural convection between the sample and air). The test matrix is shown in Table 5.3. This heating cycle is representative of a typical temperature cycle for CF/PEKK during its processing. During the heating, the sample can be let free under atmospheric pressure in the thermal chamber. This is the case of the test at NCP where no vacuum and no external pressure was applied.

The last test was performed on a DS sample at 0.5 MPa. In this latter case, not only the sample is maintained under vacuum in the bag, an inert gas is injected in the thermal

Table 5.3: Deconsolidation tests.

Test #	Conditioning	Counter pressure	Heating rate	Repeat
1	AS	NCP	60 °C/min	3
2	DS	NCP	60 °C/min	3
3	AS	NCP	10 °C/min	3
4	DS	NCP	10 °C/min	3
5	DS	0.5 MPa	10 °C/min	1

chamber to increase the counter pressure up to an absolute value of 0.5 MPa. This pressure value is half of the maximum pressure that can be reached with the CODEC bench in the thermal chamber. It is representative of autoclave processing.

5.3.5 Composite sample temperature estimation

During the non-isothermal deconsolidation test, the temperature measured by the thermocouple implemented in the hot plate is not representative of the composite sample temperature. In particular, this is due to the non perfect plate/sample contact inducing thermal contact resistance. For a proper analysis of the thermomechanical conditions of the deconsolidation occurrence, the temperature inside the composite sample has to be estimated more accurately. In this section, heat transfer is modeled to estimate the temperature distribution in the composite part using an AS sample instrumented with three embedded thermocouples (Figure 5.7). One thermocouple is located at the sample center ($TC3$) and the others two plies deep (≈ 0.4 mm) underneath the sample upper ($TC4$) and lower face ($TC2$).

5.3.5.1 Modeling

Because of the aspect ratio of the samples (125 mm $\times$ 25 mm $\times$ 2.90 mm), the heat transfer in the composite plate was modeled using a one dimensional heat equation through its thickness L, *i.e.*:

$$\rho(T)C_p(T)\frac{\partial T}{\partial t} = \frac{\partial}{\partial z}\left(k_z(T)\frac{\partial T}{\partial z}\right) \quad \forall z \in [0, L] \tag{5.4}$$

where ρ is the composite density, C_p its heat capacity and k_z its through thickness or transverse conductivity. These properties are given in Table 5.2 in Section 5.3.2. Mixed boundary conditions are considered at both surfaces of the composite plate:

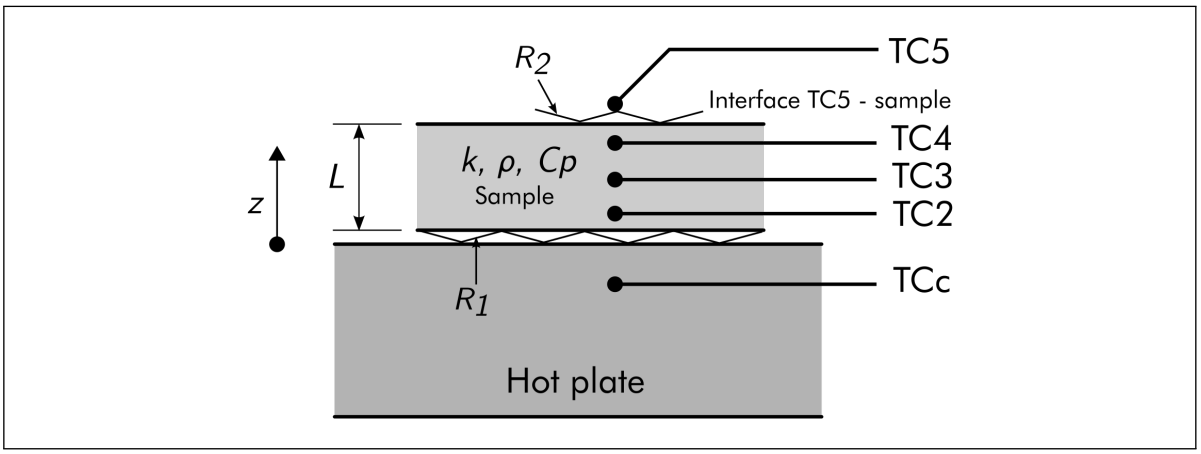

Figure 5.7: Estimation of the effective laminate temperature using a through thickness heat transfer model. The model is fitted using 5 thermocouple measurements. R_1 and R_2 represent the thermal contact resistances between (i) the copper and composite lower face and (ii) the composite upper face and taped thermocouple $TC5$.

- At the contact with the copper platen, the heat flux writes:

$$k_z \frac{\partial T}{\partial z}(z = 0, t) = -\frac{TCc - T}{R_1} \tag{5.5}$$

  where R_1 accounts for the thermal contact resistance between the sample and the copper platen and TCc is the copper platen temperature which is considered uniform and known as measured by the thermocouple (Figure 5.7).

- At the upper surface, the heat flux writes:

$$k_z \frac{\partial T}{\partial z}(z = L, t) = \frac{TC5 - T}{R_2} \tag{5.6}$$

  where R_2 is the thermal contact resistance between the taped thermocouple and the sample upper face. $TC5$ is measured with the taped upper thermocouple (Figure 5.7). The measured temperature at $TC5$ accounts for both the conducto-convective exchange with the air and the radiative exchange with the facing barrier plate.

For a given set of constant R_1 and R_2 thermal resistances, the above transient one dimensional heat transfer model was solved. Spatial integration used quadratic finite elements and time was integrated implicitly with the backward Euler method. The implementation was done in COMSOL Multiphysics [27].

5.3.5.2 Boundary conditions identification

A standard inverse method was used to identify the thermal resistance R_1 and R_2 used in equations (5.5) and (5.6). The residual consists of the modeled and measured temperature differences for each of the three embedded thermocouples (Figure 5.7) at each time step over a temperature cycle at 10 °C/min up to 250 °C, and a dwell of 20 min followed by a natural convection cooling. The residual 2-norm was minimized using the simplex method built in MATLAB [28]. It corresponds to a least squares fit.

Figure 5.8 shows the temperature measurements when no pressure is applied on the sample. A significant temperature difference can be observed between the copper and the first thermocouple $TC2$ near the composite lower surface ($TCc - TC2$). Similarly, a temperature gap is observed between the upper face temperature measured by the taped thermocouple $TC5$ and the last thermocouple $TC4$ near the composite upper face ($TC4 - TC5$). These temperature differences are due to the thermal contact resistance at the copper-composite and upper thermocouple-composite interfaces modeled with R_1 and R_2.

When a vacuum ($P = 0.1$ MPa) is applied to the composite, a decrease of these temperature differences is observed (Figure 5.9). Indeed, the application of pressure improves the contact at the composite's boundaries which leads to a decrease of the thermal resistance at the boundaries. However, when in addition to the vacuum, an overpressure is applied to the sample using pressurized gas (Argon in this case), the temperature differences at the composite boundaries are slightly higher than when only the vacuum is applied (Figure 5.9). As pressure improves the contact at the interfaces, the increase in pressure should lead to smaller temperature differences. The opposite trend observed on the CODEC device is due to the continuous pressure regulation. In fact, in order to regulate the pressure in the chamber at the set value, pressurized gas at low temperature ($\approx$ 20 °C - 30 °C) is sent continuously, even during the dwell, to compensate the fluctuations linked to the leaks and the gas thermal expansion in the chamber. The continuous cold gas injection creates a convection flow in the chamber which dissipates a part of the heat emitted by the hot plate and slightly cools the upper part of the composite. This effect was not observed when only vacuum is applied because there is no need for pressure regulation.

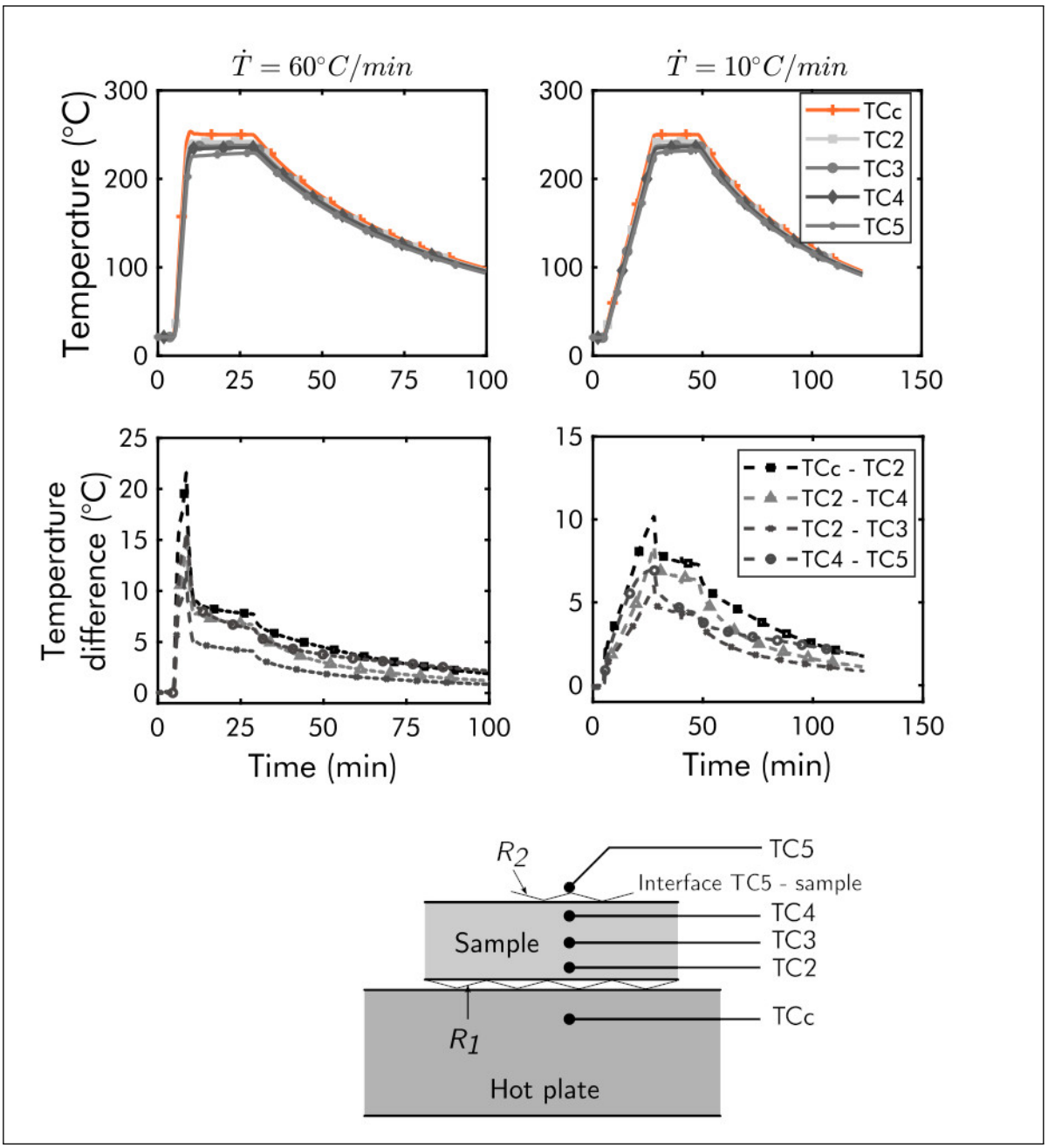

Figure 5.8: Thermocouples measurements at two different heating rates and no applied counter pressure.

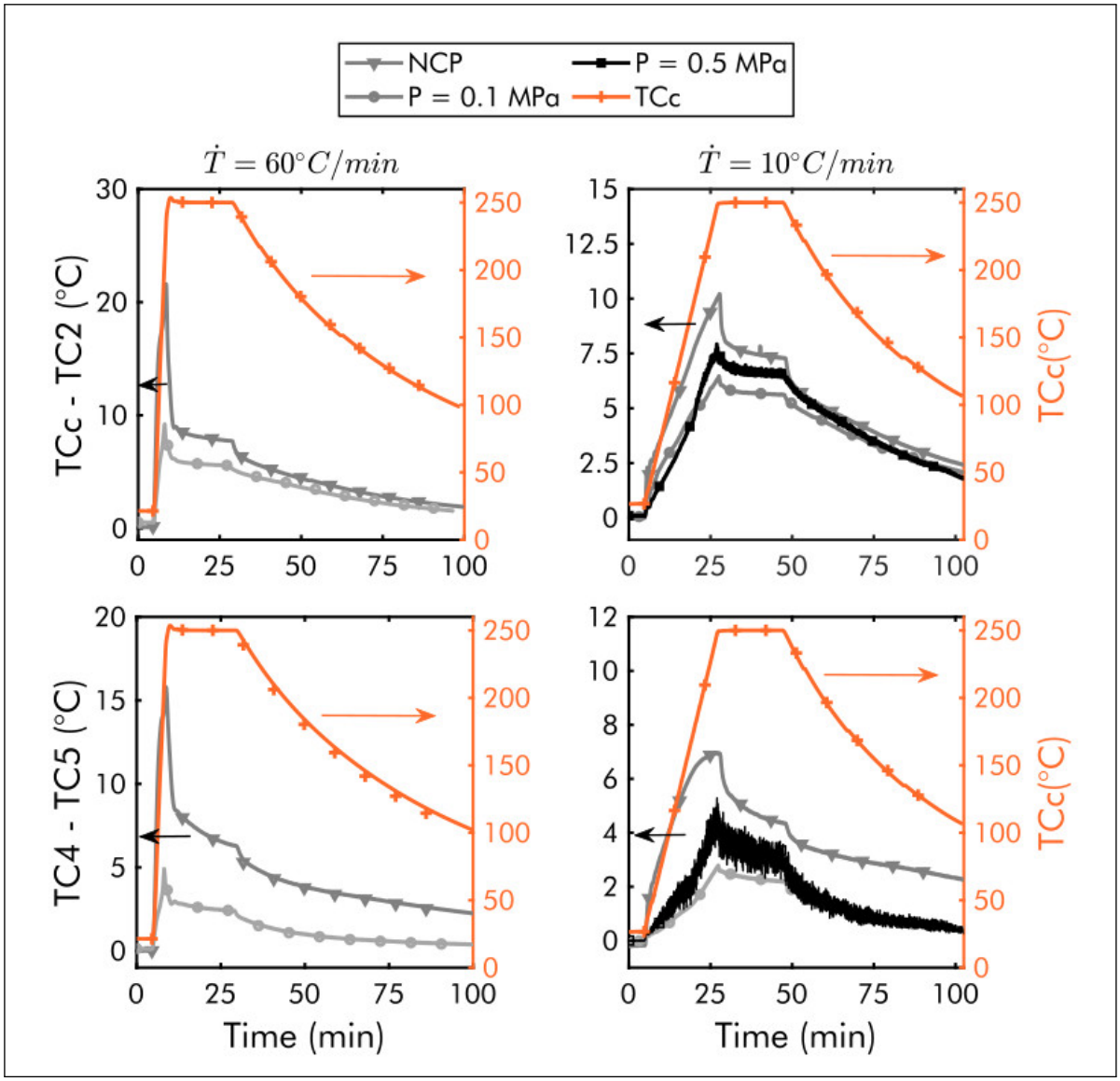

Figure 5.9: Effect of pressure on thermal boundary conditions. Temperature discontinuity across the sample lower face (top) and upper face (bottom).

Table 5.4: Thermal resistances in $(m^2 \cdot K)/W$ identified by inverse method for different counter pressures.

	NCP	P = 0.1 MPa	P = 0.5 MPa
R_1	16.04×10^{-4}	11.89×10^{-4}	14.24×10^{-4}
R_2	39.48×10^{-4}	12.04×10^{-4}	12.12×10^{-4}

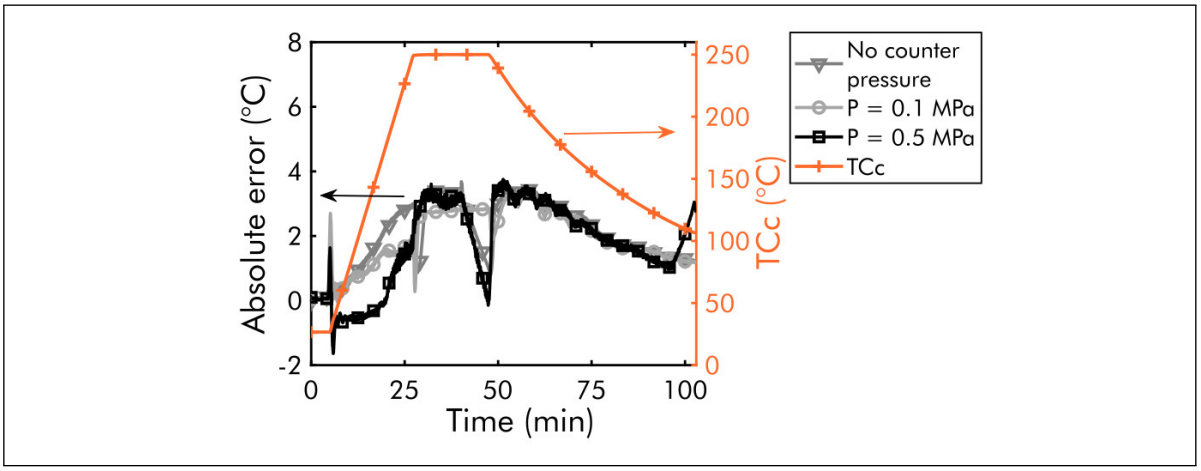

Figure 5.10: Model validation at a different pressures.

In order to reproduce the composite real thermal conditions with the thermal model, the thermal resistances were identified for three different pressures (no counter pressure, 0.1 MPa, 0.5 MPa).

5.3.5.3 Thermal model validation

The obtained values of thermal resistances are given in Table 5.4 and the temperature residuals at the sample lower face ($Tc2$) are plotted versus time in Figure 5.10. The maximum difference obtained between the experimental and the computed temperatures at the three measurement points and for the three pressures is 3 °C. The range of the error is therefore ±3 °C. The thermal model developed in this section will allow the estimation of the composite laminate temperature during the deconsolidation tests on the CODEC device.

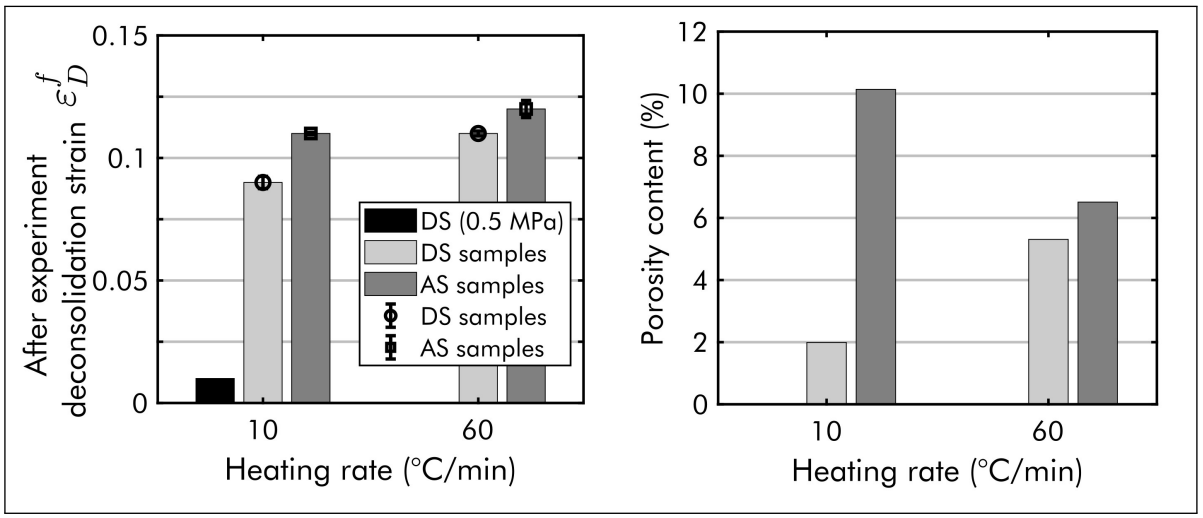

Figure 5.11: Data after experiment. Deconsolidation strain obtained for each test condition (left) and final porosity content after the experiments (right).

5.4 Results and analysis

The results of the deconsolidation tests performed on the CODEC device (listed in Table 5.3) are presented in this section.

5.4.1 After experiment analysis

At the end of the deconsolidation tests, mean deconsolidation strain was calculated by thickness measurements at five measurement points on the sample with a micrometer of 0.01 mm accuracy. One point is located on the sample center and the others are spaced 20 mm on each side of the center. In this case the deconsolidation strain ε_D^f after experiment is calculated, at each point, as (5.7).

$$\varepsilon_D^f = \ln\left(\frac{L_f}{L_0}\right) \tag{5.7}$$

where L_f is the final sample thickness after the deconsolidation test, and L_0 the sample initial thickness before the test. Figure 5.11 (left) shows the mean ε_D^f of the three repetitions performed for each test condition. The error bar indicates the standard deviation. The low ε_D^f obtained after the test under 0.5 MPa shows that there was no deconsolidation. The difference between the AS and DS samples is also small for both heating rates. From these observations, it can thus be stated that moisture has a negligible impact on deconsolidation and there is no significant effect of heating rate on deconsolidation.

In order to observe the micro-structural changes that result from deconsolidation, micrographs were performed at the end of the deconsolidation tests according to the procedure describe in section 5.3.1. The porosity content estimation were performed on three sections per sample.The sections were cut exactly at the same location on all the samples in order to performed a comparative analysis of the pores spatial distribution and morphology.

Initially, the porosity content of the samples is lower than the measurement limit (Figure 5.5). A non measurable porosity content was also observed on the sample tested at 0.5 MPa (Figure 5.12 e). The highest porosity content was obtained on the AS samples (Figure 5.12 c). The pores are also much larger and mainly located at the subsurface. In the DS samples, the pores have small sizes and are homogeneously located in the middle of the sample (Figure 5.12 b, d). Moreover, there is a huge difference (8 %) between the porosity content of AS and DS samples at 10 °C/min (Figure 5.11 right). This difference may be related to the lack of sufficient number of micrographs per sample. Nevertheless, the pore morphology and distribution clearly shows a significant effect of moisture and heating rate on deconsolidation.

However, the final measured thickness indicates a small strain difference ($\Delta\varepsilon_D^f = 0.02$) between the AS and DS sample (see Figure 5.11 left). The micrographs thus show that the differences in the samples micro-structure cannot be highlighted with only deconsolidation strains measured after experiment. In order to explain these micro-structure differences, continuous and online characterization of the deconsolidation is required. The results obtained by the online measurement are subsequently analyzed to better understand the mechanisms involved during the deconsolidation experiments.

5.4.2 Online measurements analysis

On the CODEC device, three data are obtained after each deconsolidation test (Figure 5.13 left): the hot plate temperature, the sample upper face temperature and the sample deconsolidation strain, at the two measurement points calculated from the distance measurements.

According to the unilateral heating, we can expected that deconsolidation will start at the samples lower face. In order to estimate the samples lower face temperature, the measured temperatures TCc and $TC5$ are used as boundary condition in the thermal

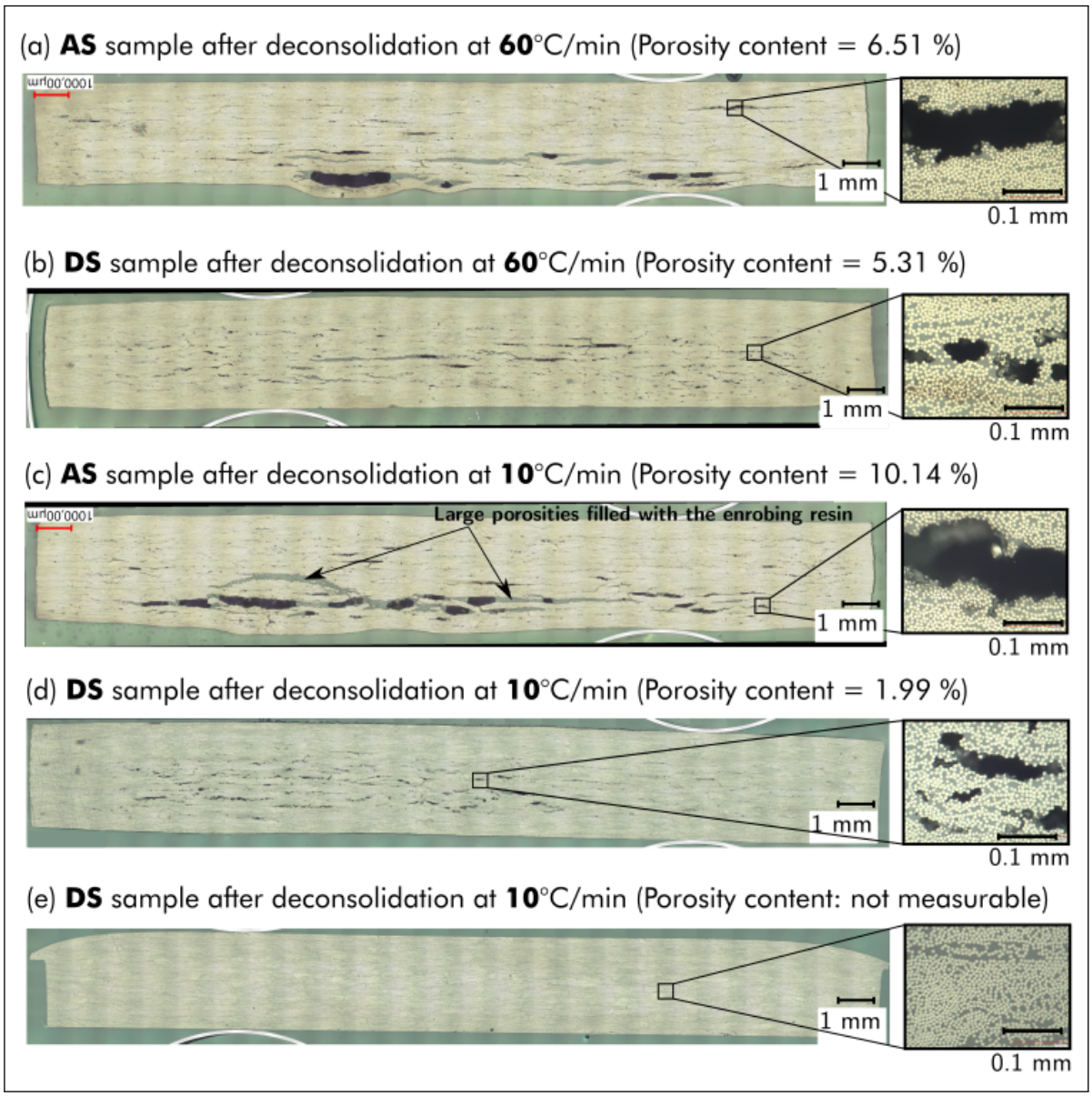

Figure 5.12: Micrographs of deconsolidated samples (objective magnification $\times 200$ and resolution 1.55^2 µm^2/pixel). After the experiment, the pores morphology and distribution are very different between AS samples and DS samples.

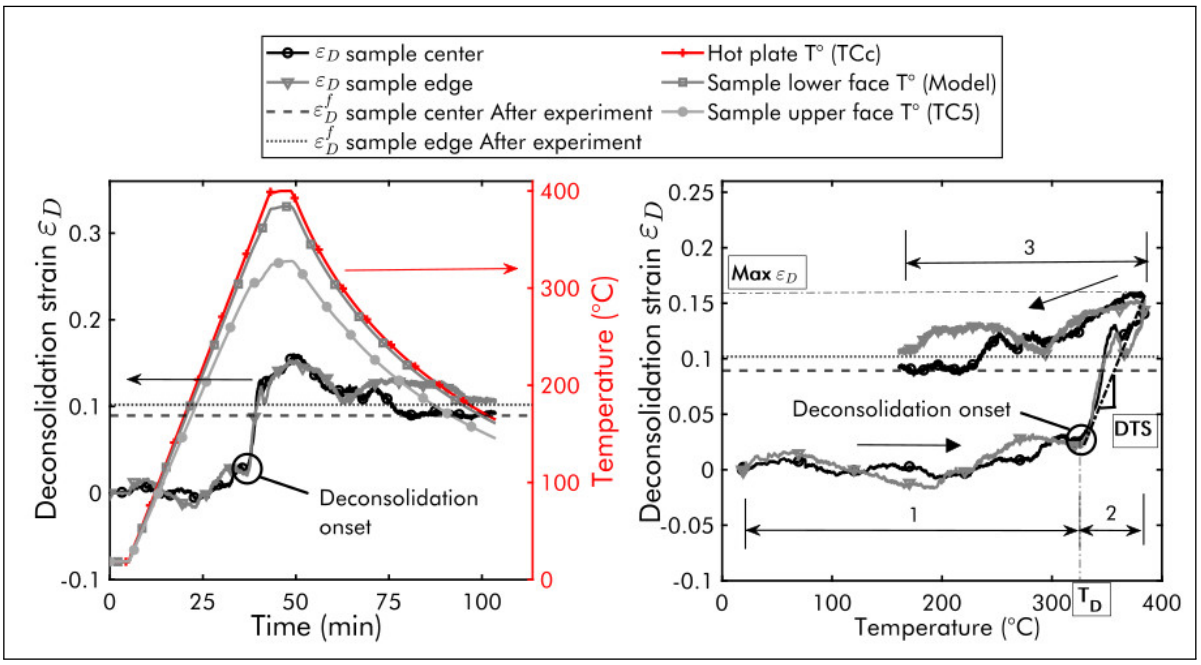

Figure 5.13: Continuous and online deconsolidation monitoring. Through thickness deconsolidation strain *vs* time (left) and deconsolidation strain *vs* the sample lower face temperature estimated with the thermal model (right) of hot press consolidated sample dried for 72 h@180 °C and heated at 10 °C/min without any applied counter pressure.

model developed in section 5.3.5. The lower face temperature is estimated as the average of the simulated temperature field over a thickness corresponding to the three first plies.

The deconsolidation strain of the samples can then be plotted versus the lower face temperature of the samples (Figure 5.13 right). As can be seen from Figure 5.13, there is a very good correlation between the final deconsolidation strain obtained with the continuous measurement and with the measurement after experiment, at both measuring points. However, in contrary to analysis after experiment, the sample behavior during heating can be observed thanks to the online and continuous measurement. As shown on Figure 5.13, the deconsolidation strain achieved by the sample during the heating is much higher than the final strain.

The sample behavior during heating can be divided in three stages visible in Figure 5.13 right.

1. During the first stage, the samples experience thermal expansion as the temperature increases until deconsolidation occurs. A significant slope change is then observed on the deconsolidation strain curve. By observing the evolution of the measured temperature on the sample upper face ($TC5$), we can also noted that the deconsolidation onset coincides with a regime change in the sample thermal behavior. This slight drop in temperature can be explained by a decrease in the thermal conductivity of the material due to the appearance of pores. The temperature measurement can therefore be a mean to detect the deconsolidation onset.

2. In the second stage, the samples experience deconsolidation which extends during the dwell. During this stage, the deconsolidation strain increases significantly (from ε_D = 0.02 to 0.15) and rapidly ($\dot{\varepsilon}_D \approx 0.64 \times 10^{-3}\,\mathrm{s}^{-1}$).

3. In the last stage, sample shrinkage occurs due to the polymer matrix crystallization and thermal shrinkage during the cooling. During this stage, an increase of the strain, which is a structural artifact related to the sample warpage, may be observed. The sample warpage is due to the non uniform temperature field in the sample induced by the unilateral cooling. The warpage effect explains the difference between the final deconsolidation strain obtained by continuous measurement in CODEC and by final thickness measurement. By comparing the curves obtained at the two measurement points, it can be seen that the edge effect is negligible. During the entire heating stage, the maximum difference between the strain obtained at the two measurement points ($\Delta\varepsilon_D$) is 0.02.

Moreover, thanks to this novel online CODEC methodology, several characteristic magnitudes related to the dynamic deconsolidation phenomenon could be quantified (for the first time). These are for instance:

- **Deconsolidation temperature** T_D **(**°C**)** characterizes the deconsolidation start. It corresponds to the temperature at which a slope change of the deconsolidation strain curve is observed. Since deconsolidation can start at one point before the other, the final value of deconsolidation temperature retained for the analysis corresponds to the minimum temperature between the two deconsolidation temperatures determined at the two measurement points.

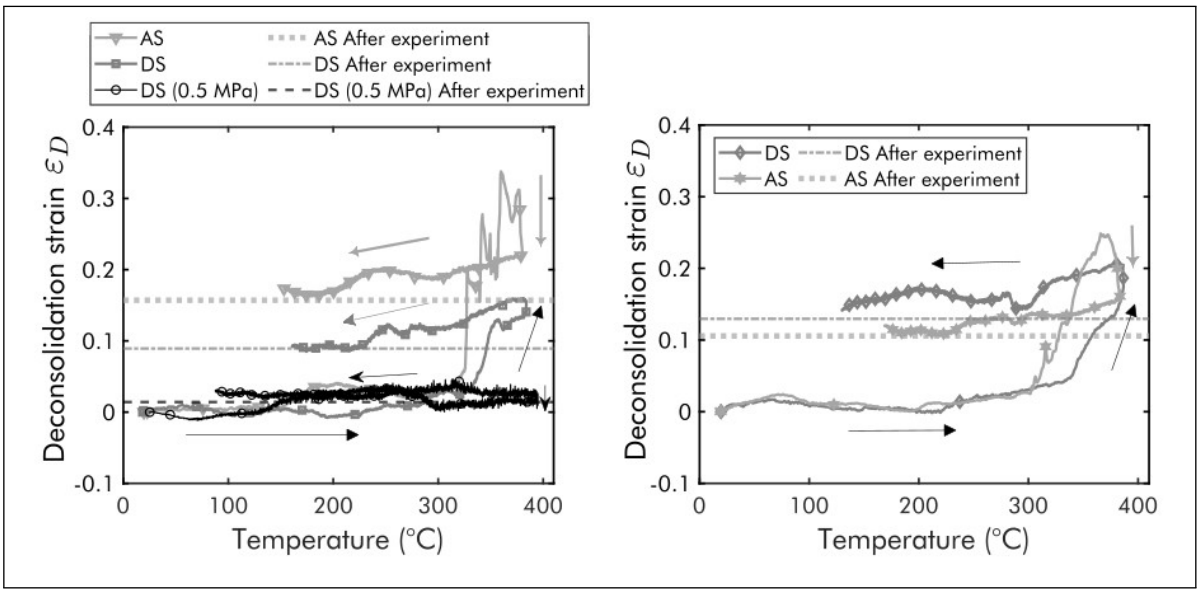

Figure 5.14: Deconsolidation graphs obtained at the sample center. Deconsolidation of Dried Sample (DS) and Ambient Storage sample (AS) samples heated at 10 °C/min (left) and at 60 °C/min (right).

- **Maximum deconsolidation strain (Max ε_D)** characterizes the maximal strain induced by deconsolidation during the heating. It corresponds to the maximum deconsolidation strain value achieved by the samples during their heating.
- **Deconsolidation's Thermal Sensitivity (DTS) (°C^{-1})** characterizes the sample deconsolidation strain variation with increasing temperature. It is calculated by plotting the sample strain versus the sample lower face temperature (Figure 5.13 right). The sample strain values during the deconsolidation stage are then fitted with a linear curve using the least squares method. The DTS corresponds to the linear curve slope value. The maximum DTS, between the two measurement points, was retained for the analysis.
- **Deconsolidation rate (s^{-1})**. Similarly in the deconsolidation versus time plot (Figure 5.13 left), a deconsolidation rate can be identified by fitting the strain values during the deconsolidation stage with a linear curve.

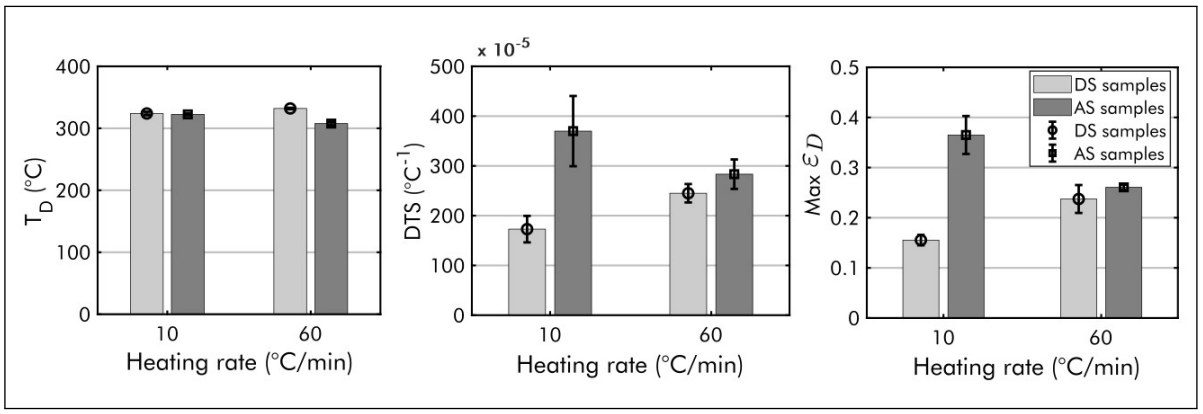

Figure 5.15: Effect of moisture and residual stresses on deconsolidation temperature (left) DTS (middle) and maximum deconsolidation strain (right).

5.4.3 Deconsolidation test results

Figure 5.14 shows the measured strains obtained at both heating rates for AS samples and DS samples. First, all the samples experience roughly the same thermal expansion during ramp-up and the same shrinkage during cool down. Second, regardless of the heating rate, two different deconsolidation dynamics are observed. When the samples are initially dried (DS samples), the strain increases smoothly during the ramp-up and even during the dwell. On the opposite, AS samples show a brutal increase of the deconsolidation strain and rather a decrease of the strain during the dwell.

These dynamic structural effects could not have been observed with classical testing after experiment or with standard TMA. Moreover, the maximum deconsolidation strain achieved by AS samples are much higher than DS samples. Finally, no deconsolidation was observed during the test under 0.5 MPa. This pressure is thus high enough to avoid deconsolidation.

From these deconsolidation graphs (Figure 5.14), characteristic quantities of deconsolidation were determined (Figure 5.15). Under atmospheric pressure (NCP test), deconsolidation appears in the melting zone, but before the material melting point (338 °C) for both groups of samples at 10 °C/min (Figure 5.15 left). At 60 °C/min, the deconsolidation occurs as soon as the temperature reaches the melting zone (310 °C) for AS samples and the melting point for DS samples. During the deconsolidation stage, independently of the heating rate, the DTS (Figure 5.15 middle) and maximum deconsolidation strain (Figure 5.15 right) of AS samples are all higher than DS samples.

However, in the case of AS samples, the DTS and maximum deconsolidation strain increase with decreasing heating rate while the opposite is observed for DS samples. These observations mean that when the sample is initially dried (DS), a higher heating rate leads to a higher sensitivity of the strain to temperature change (DTS). When moisture is initially present in the sample (AS), a higher heating rate rather leads to a lower sensitivity (DTS). Deconsolidation is thus heating-rate dependent and this dependency is affected by the preconditioning.

Thanks to the online and continuous measurement on CODEC, the large pores observed in the AS samples can now be explained by the fast and high increase of the pores size visible on the deconsolidation graphs (Figure 5.14). The low porosity content observed in the DS samples is related to the slow growth of the pores during the heating, also visible in the deconsolidation graphs. Hence, the sample behavior during heating described by the online measurements correlates with the sample final microstructure. This correlation shows that the pore final morphologies and distribution are highly affected by the dynamic mechanisms during the sample heating. Therefore, the online measurements on the CODEC device provide a better understanding of the mechanisms involved during deconsolidation.

5.4.4 Discussion

There was initially no moisture in DS samples. It is assumed that there are also no residual volatiles from additives such as plasticizers. Indeed, the additives used in TPC prepreg manufacturing, often have a higher boiling point ($\gg 100\,^{\circ}C$) compared to water. However, their boiling point are lower than the melting temperature of the high-performance polymer matrix. In our case where the laminates have been pre-consolidated, most additives evaporated during the initial laminate pre-consolidation process. For example, after consolidation in press of CF/PEEK laminates, Slange *et al.* [13] did not detect any residual volatiles (from additives) other than water with Residual Gas Analysis (RGA). The DS sample deconsolidations are thus attributed to the residual stresses effect.

During consolidation, residual stresses are trapped in the laminates during cooling. For Hot Press Consolidation, the cooling was done at $10\,^{\circ}C/min$ under a pressure of 4 MPa. Therefore, in addition to fiber bed compaction stresses, stresses due to thermal and crystallization shrinkage, and eventually the skin-core thermal gradient [29, 30], are not fully relaxed before the material solidification. This may result in *a complex*

three-dimensional residual stress state within the laminate [31]. During deconsolidation tests, when the temperature reaches T_m, the residual stresses trapped in the matrix and the fibrous network may induce strains in the composite. This causes the formation of pores in the matrix and at the fiber-matrix interfaces through complex local strain phenomena. When the applied counter pressure is greater than the internal stresses, deconsolidation does not occur. This is the case for the test with a high counter pressure. Thus, the application of a counter pressure of 0.5 MPa is sufficient to limit the amplitude of deconsolidation, hence the decrease of the DTS and the maximum deconsolidation strain.

Varying the heating rate gives insight on the effect of moisture or residual stresses. In the case of DS samples, an increase in heating rate leads to an increase in deconsolidation strain (see Figure 5.15). We assume that in addition to the higher thermal gradient through thickness, the composite material does not have enough time to relax residual stresses before melting. On the contrary, in the case of AS samples, an increase in heating rate results in a decrease in deconsolidation. This cannot be attributed to residual stress effects. We assume that this is rather dissolved moisture which cannot diffuse and coalesce at high heating rate. Thus, the presence of moisture is also involved in deconsolidation.

This is also supported by the micrographs. The pores in AS samples are mainly located at the samples subsurface (see Figure 5.12 a, c). We believe these pores are the consequence of moisture. The initial pores nucleate in the vicinity of the hot plate. Once formed, the remaining moisture from the laminate may diffuse in these pores. In the case of DS samples (see Figure 5.12 b, d), there is smaller pores located in the center. It suggests that the drying has not been effective down to the core of the laminate.

These are, to the author knowledge, the first deconsolidation experiments using online measurements in representative conditions of high-performance CFRTP laminates processing. Residual stresses and moisture trapped in the pre-consolidated laminates are driving deconsolidation. These conclusions could not have been reached with an after experiment measurement only.

5.5 Conclusion

The phenomenon of deconsolidation is a major problem that limits the application of thermoplastic composites in aeronautics structures. In spite of the research carried out

on this subject in the literature, several questions on the causes of deconsolidation are still unanswered. The generally used means of deconsolidation characterization do not allow investigation into what happens during deconsolidation under representative process conditions.

For this reason, a new TMA device called CODEC has been developed in this study. The device allows to characterize the deconsolidation continuously and online, on large samples (up to 150 mm $\times$ 50 mm), under industrial conditions. The deconsolidation characterization on CODEC is performed by contact-less thickness variation measurement with a relative error of $\pm$ 2 %. This novel bench allows for a temperature and pressure control reproducing industrial manufacturing conditions. Hence, CODEC allows tracking of the deconsolidation kinetics during processing.

The CODEC device was used to investigate the effect of residual stresses, moisture, and heating rate, during the re-heating stage of a pre-consolidated laminate. The deconsolidation tests were performed on UD laminate samples consolidated in a hot press. Some samples were thoroughly dried to eliminate possible effects of moisture content and others were stored in ambient condition.

Thanks to the online and continuous measurement on CODEC device, the effect of moisture and residual stresses were highlighted. Contrary to what is mainly found in the literature, the effect of residual stresses is not negligible. The measurements on CODEC also showed an effect of the heating rate on the deconsolidation phenomenon. From the different behavior obtained at the different heating rates, two main mechanisms appear to be involved in deconsolidation: residual stresses loading and moisture evaporation and/or diffusion. Finally, the deconsolidation kinetics measured correlates with the final porosity contents and morphologies observed on micrographs after experiment.

Nevertheless, it should be noted that these results do not allow to rule on the driving mechanism of deconsolidation. Do pores grow mainly by moisture evaporation and/or diffusion or by residual stresses? What is the contribution of moisture or residual stresses during deconsolidation? Furthermore, all the tests performed in this study were carried out on UD laminates. Do these observations remain valid for other ply stacking sequences? In order to answer these questions, further investigations

are needed to have a better understanding of deconsolidation which is now made possible thanks to the CODEC device. These questions will be the subject of further investigations.

References

[1] C. Sarr, S. Chataigner, L. Gaillet, and N. Godin, "Auscultation des assemblages collés par acousto-ultrasons : Application à des assemblages acier-composite du génie civil," *Journées Nationales sur les Composites*, 2019 (cit. on p. 125).

[2] J. B. Robles, R. Cole, and J. M. Sands, "Development of controlled adhesive bond strength for assessment by advanced non-destructive inspection techniques," *Society for the Advancement of Material and Process Engineering*, 2010 (cit. on p. 125).

[3] R. L. Crane and G. Dillingham, "Composite bond inspection," *Journal of Materials Science*, vol. 43, pp. 6682–6694, 20 2008 (cit. on p. 125).

[4] H. Shi, I. F. Villegas, and H. E. Bersee, "Strength and failure modes in resistance welded thermoplastic composite joints: Effect of fibre-matrix adhesion and fibre orientation," *Composites Part A: Applied Science and Manufacturing*, vol. 55, pp. 1–10, 2013 (cit. on p. 125).

[5] P. O. Hagstrand, F. Bonjour, and J. A. Månson, "The influence of void content on the structural flexural performance of unidirectional glass fibre reinforced polypropylene composites," *Composites Part A: Applied Science and Manufacturing*, vol. 36, pp. 705–714, 5 2005 (cit. on p. 125).

[6] X. Liu and F. Chen, "A Review of Void Formation and its Effects on the Mechanical Performance of Carbon Fiber Reinforced Plastic," *Engineering Transactions*, vol. 64, pp. 33–51, 2016 (cit. on p. 125).

[7] L. Grunenfelder and S. Nutt, "Void formation in composite prepregs–Effect of dissolved moisture," *Composites Science and Technology*, vol. 70, no. 16, pp. 2304–2309, 2010 (cit. on p. 125).

[8] J. Anderson and M. Altan, "Formation of voids in composite laminates: coupled effect of moisture content and processing pressure," *Polymer composites*, 2014 (cit. on p. 125).

[9] B. de Parscau du Plessix, "Analyse et modélisation du développement de porosités lors de la cuisson de pièces composites thermodurcissables hautes performances," Ph.D. dissertation, Université de Nantes, 2016 (cit. on p. 125).

[10] Y. Leterrier and C. G'sell, "Formation and Elimination of Voids During the Processing of Thermoplastic Matrix Composites," *Polymer Composites*, vol. 15, pp. 101–105, 2 1994 (cit. on p. 125).

[11] S. Roychowdhury, J. W. Gillespie, and S. G. Advani, "Volatile-induced void formation in amorphous thermoplastic polymeric materials: I. Modeling and parametric studies," *Journal of Composite Materials*, vol. 35, pp. 340–366, 4 2001 (cit. on p. 125).

[12] H. Shi, I. F. Villegas, and H. E. Bersee, "Analysis of void formation in thermoplastic composites during resistance welding," *Journal of Thermoplastic Composite Materials*, vol. 30, pp. 1654–1674, 12 2017 (cit. on pp. 125, 127).

[13] T. K. Slange, L. L. Warnet, W. J. Grouve, and R. Akkerman, "Deconsolidation of C/PEEK blanks: on the role of prepreg, blank manufacturing method and conditioning," *Composites Part A: Applied Science and Manufacturing*, vol. 113, pp. 189–199, 2018 (cit. on pp. 125–127, 151).

[14] M. Lu, L. Ye, and Y. W. Mai, "Thermal de-consolidation of thermoplastic matrix composites-II. "Migration" of voids and "re-consolidation"," *Composites Science and Technology*, vol. 64, pp. 191–202, 2 2004 (cit. on p. 126).

[15] L. Ye, Z. R. Chen, M. Lu, and M. Hou, "De-consolidation and re-consolidation in CF/PPS thermoplastic matrix composites," *Composites Part A: Applied Science and Manufacturing*, vol. 36, pp. 915–922, 7 2005 (cit. on p. 126).

[16] J. Wolfrath, V. Michaud, and J.-A. E. Månson, "Deconsolidation in glass mat thermoplastic composites: Analysis of the mechanisms," *Composites Part A: Applied Science and Manufacturing*, vol. 36, pp. 1608–1616, 12 2005 (cit. on p. 126).

[17] V. Donadei, F. Lionetto, M. Wielandt, A. Offringa, and A. Maffezzoli, "Effects of blank quality on press-formed PEKK/carbon composite parts," *Materials*, vol. 11, 7 2018 (cit. on pp. 126–127).

[18] M. Brzeski and P. Mitschang, "Deconsolidation and its Interdependent Mechanisms of Fibre Reinforced Polypropylene," *Polymers & Polymer Composites*, vol. 23, pp. 515–524, 8 2015 (cit. on p. 126).

[19] T. K. Slange, "Rapid Manufacturing of Tailored Thermoplastic Composites by Automated Lay-up and Stamp Forming," Ph.D. dissertation, University of Twente, 2019 (cit. on p. 126).

[20] M. Brzeski, "Experimental and analytical investigation of deconsolidation for fiber reinforced thermoplastic composites," Ph.D. dissertation, TU Kaiserslautern, 2014 (cit. on p. 126).

[21] H. Perez-Martin, P. Mackenzie, A. Baidak, C. M. Ó. Brádaigh, and D. Ray, "Crystallinity studies of PEKK and carbon fibre/PEKK composites: A review," *Composites Part B: Engineering*, vol. 223, p. 109 127, 2021 (cit. on p. 134).

[22] J. Avenet, "Assemblage par fusion de composites à matrice thermoplastique: caractérisation expérimentale et modélisation de la cinétique d'auto-adhésion hors équilibre," Ph.D. dissertation, Université de Nantes (UN), 2021 (cit. on pp. 134–136).

[23] H. Pérez-Martín, P. Mackenzie, A. Baidak, C. M. Ó. Brádaigh, and D. Ray, "Crystallisation behaviour and morphological studies of PEKK and carbon fibre/PEKK composites," *Composites Part A: Applied Science and Manufacturing*, p. 106 992, 2022 (cit. on p. 134).

[24] I. Arganda-Carreras, V. Kaynig, C. Rueden, K. W. Eliceiri, J. Schindelin, A. Cardona, and H. S. Seung, "Trainable Weka Segmentation: a machine learning tool for microscopy pixel classification," *Bioinformatics*, vol. 33, pp. 2424–2426, 15 2017 (cit. on p. 135).

[25] D. Paganin, S. C. Mayo, T. E. Gureyev, P. R. Miller, and S. W. Wilkins, "Simultaneous phase and amplitude extraction from a single defocused image of a homogeneous object," *Journal of microscopy*, vol. 206, no. 1, pp. 33–40, 2002 (cit. on p. 135).

[26] A. Lepoivre, "Étude des transferts thermiques et de l'adhésion à l'échelle du cordon dans le procédé de fabrication additive FFF (extrusion de filament fondu)," Ph.D. dissertation, Université de Nantes (UN), 2021 (cit. on p. 136).

[27] COMSOL Multiphysics ® v.6.0., COMSOL AB, Stockholm, Sweden, 2022. [Online]. Available: `https://www.comsol.com` (cit. on p. 139).

[28] MATLAB (R2022a), Natick, Massachusetts, 2022 (cit. on p. 140).

[29] J. Favre, "Residual thermal stresses in fibre reinforced composite materials, a review," vol. 1, no. 1, pp. 37–53, 1988 (cit. on p. 151).

[30] P. P. Parlevliet, H. E. Bersee, and A. Beukers, "Residual stresses in thermoplastic composites—A study of the literature—Part I: Formation of residual stresses," *Composites Part A: Applied Science and Manufacturing*, vol. 37, no. 11, pp. 1847–1857, 2006 (cit. on p. 151).

[31] M. M. Shokrieh, *Residual stresses in composite materials*. Woodhead publishing, 2014 (cit. on p. 152).

"This page left intentionally blank"

CHAPTER 6

REAL-TIME SYNCHROTRON X-RAY MICROTOMOGRAPHY OF CF/PEKK LAMINATES DECONSOLIDATION

Contents

Abstract

High-performance carbon fiber-reinforced thermoplastic composites have attracted a considerable interest in the aircraft and aerospace industry in the past decades. A major issue that restrains their industrial development is, however, the deconsolidation phenomenon which often occurs while pre-heating these materials during their forming process: detrimental pores nucleate, grow and conduct to a significant degradation of the mechanical properties of the produced composite parts. Such deconsolidation mechanisms are complex and, for the moment, mainly characterized with *post-process* analyses which do not provide insight of their *in situ* evolutions. They are thus still poorly understood and raise different opinions in the literature. Here, a new experimental device was developed and installed inside a synchrotron beamline (dedicated to fast X-ray microtomography) allowing unique 3D real-time and *in situ* observations of pore nucleation and growth while heating laminate samples made of a PolyEtherKetoneKetone (PEKK) matrix reinforced with aligned carbon fiber. Combined with image analysis procedures, we could assess the time evolution of the sample deconsolidation strain, porosity content, as well as the number, the size and the morphology of pores. Results clearly highlight the roles of the initial moisture content and fiber orientation, as well as those of the confining compression stress and the heating conditions on the kinetics of deconsolidation. The provided data can also be used as input data for modeling purpose or for validation of existing models.

In the previous Chapter 5, a new device was developed to characterize deconsolidation at the sample scale. The characterization technique used is based on a continuous and online measurement of the samples global strain during a given heating and pressure cycle. However, there is no way to know if the measured strain is actually correlated to the pores growth in the composite. Moreover, this technique do not allow to highlight the micro-structural changes occurring in the composite during deconsolidation. The purpose of this chapter is thus to study the evolution of the composite micro-structure during deconsolidation, in order to validate the reliability of the strain measurement on the one hand, and to highlight the involved mechanisms during deconsolidation at the fibers scale on the other.

6.1 Introduction

High-performance ThermoPlastic Composites (TPCs) are promising materials for the aerospace industry given their many advantages such as weldability, unlimited shelf (storage) life, good mechanical properties and chemical resistance. While manufacturing and assembling, these materials may be subjected to deconsolidation, *i.e.* the nucleation and growth of pores during the heat-assisted forming processes of pre-consolidated TPC laminates. Deconsolidation usually occurs when laminates are subjected to sufficiently low confining pressure during their heating stage and lead to a final composite part with, sometimes, substantial and detrimental porosity content. Several works have already shown a significant degradation of mechanical properties when the composite porosity content overcomes critical volume content [1–3]. In order to avoid such a porosity content, a good understanding of deconsolidation phenomenon is necessary.

The mechanisms of pore nucleation and growth in high-performance TPC laminates are complex and raise different opinions in the literature. The first approach suggests that deconsolidation is related to the initial moisture and volatile contents in the laminates. This approach was inspired from the findings made during the forming of thermoset composites, which showed that moisture was one of the main causes of deconsolidation [4–6]: the increase of temperature up the sample heating stages leads to an increase of water vapor pressure which exceeds the confining pressure the composite may be subjected to, and causes the pores nucleation and growth through moisture diffusion. Considering that high-performance thermoplastic polymers also

uptake moisture when exposed to a humid environment, this hypothesis was mainly used to explain the deconsolidation observed with some Glass Fiber (GF) reinforced TPCs (GF/PolyPropylene, GF/PolyEtherImide) [7–9]. In the case of high-performance TPCs, this hypothesis was supported by Slange *et al.* [10] after carrying out deconsolidation experiments on dried and undried UniDirectional (UD) layered $[0/90]_{4s}$ Carbon Fiber (CF) reinforced PolyEtherEtherKetone (PEEK) laminates, consolidated with a 1 MPa confining pressure. The authors showed that the thickness increase induced by the deconsolidation of the dried samples was significantly lower than that of the undried ones. Consequently, the authors recommended to dry the laminates at 250 °C for 3 hours prior to processing.

The second possible origin of deconsolidation was inspired from the findings on the pores growth in woven and mat TPC laminates. Related works showed that residual stresses stored in the laminates during their fabrication, *e.g.* the elastic energy of the fibrous networks stored after their pre-compaction and cooling down, could also be another important driving force of deconsolidation [11–13]. Indeed, during re-heating of the aforementioned consolidated laminates, the polymer melting allows such residual stresses to be released, thus enhancing pores growth [14]. In the case of high-performance TPCs, this hypothesis was supported by Donadei *et al.* [15] after carrying out deconsolidation experiments on annealed and non annealed layered UD $[-45/90/45/0]_{3S}$ CF/PolyEtherKetoneKetone (PEKK) laminates consolidated at 0.6 MPa in an autoclave: a drying at 240 °C for 3 hours was not sufficient to prevent deconsolidation. The authors showed that annealing at 240 °C fo 20 hours was required to relax residual stresses, in order to avoid deconsolidation.

These different conclusions suggest that both the initial moisture content and residual stresses, both stored in the consolidated laminates, may be involved in high-performance TPCs deconsolidation mechanisms. Since drying and internal stress release are prone to occur altogether, it appears as difficult to decorrelate these two effects. Moreover, the post-process techniques (thickness measurement, micrographs, *etc.*) used to characterize deconsolidation in these studies [10, 15] do not allow a proper analysis of what happens during heating and dwell [16]. Another interesting technique used to characterize porosity in composites is *ex situ* X-ray microtomography [17]. In contrast with 2D micrographs, this technique allows 3D characterization of pores,

including their volume content, shape and spatial distribution. However, scanning times of laboratory microtomographs are too long to provide relevant real-time and *in situ* monitoring of the micro-structure changes during the composite processing [18].

The development of synchrotron X-Ray tomographs has made possible the real-time and *in situ* monitoring of micro-structure evolution [19–21] during the forming processes of composite materials without the need to interrupt the processing cycle [22]. Another interesting study is the work carried out by de Parscau *et al.* [23] in order to study pore nucleation and growth during the heating of fiber-reinforced thermoset composite. Their work demonstrated the ability of synchrotron X-ray microtomography to characterize in real-time via fast scans important 3D structural parameters (such as pore shape, size and spatial distribution) that are difficult to measure with other experimental techniques. Thanks to those unique advantages, this technique has been used several times in the literature to study curing issues in thermoset composites [24–27]. However, to the author's knowledge, there is no available study of deconsolidation of high-performance thermoplastic processing using fast *in situ* X-ray tomography. This could be due to the processing conditions of high-performance TPCs which are more severe than those of thermoset composites, *i.e.* requiring high temperatures (330 °C - 400 °C).

Thus, within this context, we developed a new experimental device named *In situ* COmposite DEconsolidation Tomography Observation (InCODETO) to perform deconsolidation experiments under representative conditions of high-performance TPC processing while allowing 3D real-time and *in situ* images by using fast X-ray synchrotron microtomography. We could thus observe and quantify the nucleation and the growth of pores during the representative heating of high-performance TPC laminates CF/PEKK.

6.2 Materials and methods

6.2.1 CF/PEKK composite manufacturing

The laminates used in this study were produced using unidirectional CF/PEKK 7002 prepreg plies supplied by Toray Advanced Composites. The plies have a fiber areal weight of 194 g/m^2 and a theoretical thickness of 0.185 mm. The PEKK mass content is 34 %. According to the manufacturer, its glass transition temperature (T_g), melting temperature (T_m) and crystallization temperature (T_c) are 160 °C, 337 °C, and 265 °C,

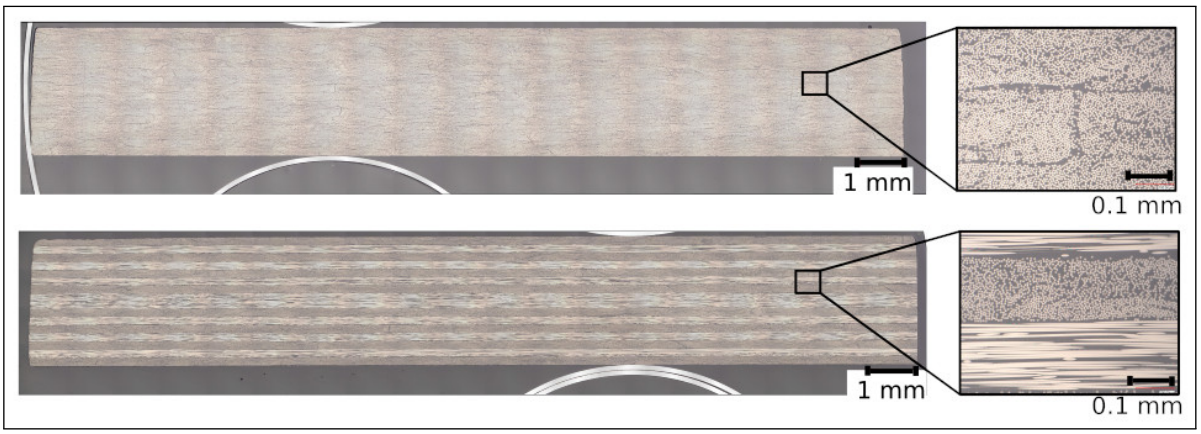

Figure 6.1: Micrograph of the consolidated unidirectional (top) and cross-ply (bottom) samples before deconsolidation tests (objective magnification $\times 200$ and resolution 1.55^2 µm^2/pixel). The initial porosity content is not measurable.

respectively. In practice, the melting zone, observed during Differential Scanning Calorimetry (DSC) experiments, ranges between 310 °C and 360 °C, with a melting point at 338 °C [28–30]. Besides, during cooling, the crystallization zone extends between 240 °C and 283 °C, with a crystallization peak at 269 °C, for the matrix alone and assuming no transcrystallization [28–30].

Using the prepreg plies, UniDirectional (UD) $[0]_{16}$ and Cross-Ply (CP) $[0/90]_{4S}$ laminates of 350 mm $\times$ 350 mm $\times$ 2.90 mm containing 16 plies were manufactured by hot press consolidation. The consolidation was carried out in a 50 t Pinette P.E.I press by using a picture-frame mold and according to the following cycle: heating at 10 °C/min up to 380 °C under a confining pressure of 0.1 MPa; isothermal holding for 20 min under a confining pressure of 4 MPa; cooling at 10 °C/min at the same pressure, then demolding.

Optical micrographs of the consolidated laminates validate a porosity content lower than the measurement limit after consolidation step (Figure 6.1). The micrographs were obtained with a digital microscope KEYENCE VHX-7000 series. The 20 mm wide samples were first encapsulated using a slow-curing epoxy resin (EpoFix, Struers). The surface was then prepared using traditional grinding and polishing techniques on an automated polishing machine (Tegrapol-21 and TegraForce-5, Struers). Finally, the cross section micrographs were obtained by assembling several sections of the

observation surface with a resolution of 2880 pixel × 2160 pixel (objective magnification ×200) resulting in an image with a large area of observation and a good resolution ($\approx 1.55^2$ µm^2/pixel).

6.2.2 Preconditioning

In order to investigate the role of moisture during deconsolidation, 20 mm diameter cylinders were cut out from the consolidated laminates using a Protomax waterjet cutting machine and separated into two groups: Dried Sample (DS) and Water Immersed (WI) samples. DS samples were dried at 180 °C for 72 hours in order to restrain moisture. A continuous weight measurement during drying experiments at different temperatures proved that this drying condition fully eliminated the effect of moisture without any thermal degradation of the material: no further significant weight change was observed at 180 °C after this duration [31]. WI samples were immersed in distilled water at room temperature (≈23 °C) for 3 months before the experiments. A weight measurement of the samples before and after the immersion showed that the relative moisture weight content of the immersed samples was 0.1 % at the end of the immersion.

6.2.3 Experimental setup

In order to observe the micro-structural changes in the laminates during the deconsolidation experiments, we developped a specific device named *In situ* COmposite DEconsolidation Tomography Observation (InCODETO). The setup functions are twofold: to subject samples to temperature and pressure cycles which are representative of TPC laminates processing conditions, while allowing 3D real-time *in situ* observations of the sample microstuctures with synchrotron X-ray microtomography. For that purpose, the setup was designed to be mounted onto the rotation stage of the ID19 beamlime microtomograph (ESRF, France).

As illustrated in Figure 6.2, the device was composed of two cylindrical copper hot platens which can heat up to 450 °C with a maximal heating rate of 2 °C/s. The temperature of the hot platens was measured by K-type thermocouples located in the middle of each hot platen, 1 mm beneath their surfaces. The platen heating was achieved with one resistive cartridge of 200 W placed in each hot platen, and regulated by two 3508 Eurotherm PID temperature controller. 30 mm thick calcium silicate thermal insulators were placed between the hot platens and the other components, in

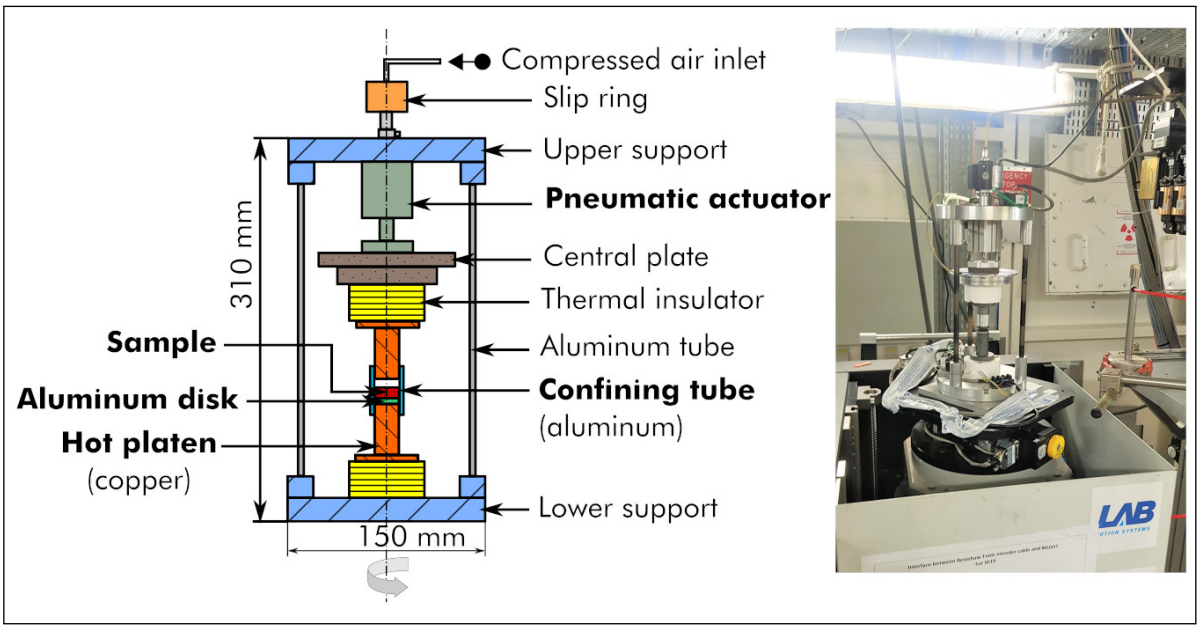

Figure 6.2: *In situ* COmposite DEconsolidation Tomography Observation (InCODETO) setup. Schematic view (left) and picture of the device installed onto the rotation stage of the ID19 beamline X-Ray microtomograph (right).

order to restrain the thermal expansion of the whole setup during the experiments. In order to limit convective heat losses, samples were also confined by a thin (0.5 mm thickness) aluminum tube, with a rather low X-ray absorption. In order to improve the image contrast at the sample boundaries, an aluminum disk was placed between the sample and the lower hot platen.

A pneumatic actuator (CDQMB25-25 from SMC) was placed on top of the upper hot platen in order to subject tested samples to a confining pressure up to 1.2 MPa. A central plate was placed between the actuator and the hot platen to enhance the transmission of the piston load to the hot platen. Since the device must be in rotation during the tests in the synchrotron, all power cables and thermocouple wires were connected to a SVTS C 3 slip ring connector provide by Servotecnica, to allow rotation of the microtomograph platform. The slip ring allowed the compressed air supply during the rotation too. The upper part of the device was supported by three aluminum tubes (0.5 mm thickness) connected to the lower support.

Lastly, during the experiments, the pressure was regulated by a pressure controller supplied by Festo (vppm-6l-l-1-g18-0l6h-v1p-s1c1). The temperature data acquisition

Table 6.1: Testing conditions used for deconsolidation experiments.

Test #	Laminate	Conditioning	Pressure	Dwell time	Heating type	Label
1	UD	WI	NAP	10 min	two-sided	UD-WI-2SH
2	UD	DS	NAP	10 min	two-sided	UD-DS-2SH
3	CP	WI	NAP + P_R=0.1 MPa	10 min + 10 min	two-sided	CP-WI-2SH
4	UD	WI	NAP + P_R=0.05 MPa	10 min + 5 min	one-sided	UD-WI-1SH

and control were performed automatically using a KEYSIGHT 34972A data acquisition unit provide by Agilent and the Eurotherm itools software. This provided a full control of the experiment conditions (heating rate, temperature, and pressure).

6.2.4 Deconsolidation experiments

The deconsolidation tests consisted in heating samples at 60 °C/min up to a first dwell at 120 °C for 5 min followed by a heating at 10 °C/min up to a second dwell at 380 °C for 10 min. The first dwell allowed to have the same reference temperature for the scans start-up. To check the effect of thermal gradients on deconsolidation, samples were heated either by one hot platen only (one-Sided Heating, 1SH) or by both hot platens simultaneously (two-Sided Heating, 2SH). Also, sample were either let free, *i.e.* with No Applied Pressure (NAP), or subjected to a given constant confining pressure. More precisely, to observe pressure effects on the reduction of porosity content after free deconsolidation, a re-consolidation pressure (P_R) was applied during the second dwell at 380 °C (NAP + P_R). In this case, the dwell time was extended from 10 min to 15 min or 20 min so that the re-consolidation pressure was maintained for 5 min or 10 min. The whole investigated testing conditions are summarized in Table 6.1.

6.2.5 Estimation of the sample temperatures

During the deconsolidation tests, the temperature measured by the thermocouples inserted in the hot platens are not representative of the sample temperatures. On the one hand, this is due to the gap of 2 mm left between the upper hot platen and the sample. On the other hand, the aluminum disk placed between the sample and the lower hot platen also induces a thermal contact resistance. For a proper analysis of the thermomechanical conditions of deconsolidation, the temperature inside the

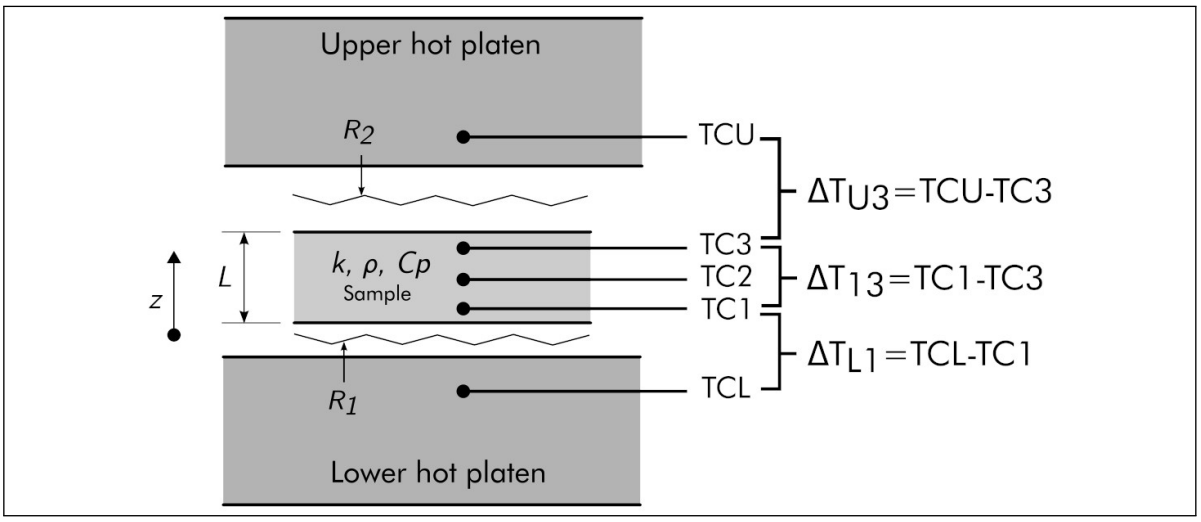

Figure 6.3: Estimation of the effective laminate temperature using a through thickness 1D heat transfer model. The model is fitted using 5 thermocouples measurements. R_1 and R_2 represent the thermal resistances between (i) the lower hot platen and composite lower face and (ii) the composite upper face and the upper hot platen.

composite sample has to be estimated more accurately. A conductive heat transfer model was thus developed and calibrated to estimate the temperature distribution in the samples using one specimen instrumented with three embedded K-type thermocouples (Figure 6.3). One thermocouple was located at the sample center ($TC2$) and the others two plies deep ($\approx 0.4\,mm$) underneath the sample upper ($TC3$) and lower face ($TC1$). The temperature measurements during the heating cycle of the deconsolidation experiments (described in Section 6.2.4) are shown in Figure 6.4.

First, a significant temperature difference ΔT can be observed between the hot platens and the center of the composite sample, during the heating for both configuration. The temperature difference ΔT_{L1} between the lower hot platen (TCL) and the sample lower face ($TC1$) as well as the temperature difference ΔT_{U3} between the upper hot platen (TCU) and the sample upper face ($TC3$), are largely higher than $10\,°C$ during the heating stage. This temperature difference is due to the thermal contact resistances mentioned earlier and the non-isothermal heating during the one-sided heating.

Secondly, the application of pressure during the dwell causes a decrease in the temperature difference between the hot platens and the sample. In fact, pressure improves the contact at the interfaces and thus promotes a better heat transfer. However, in the

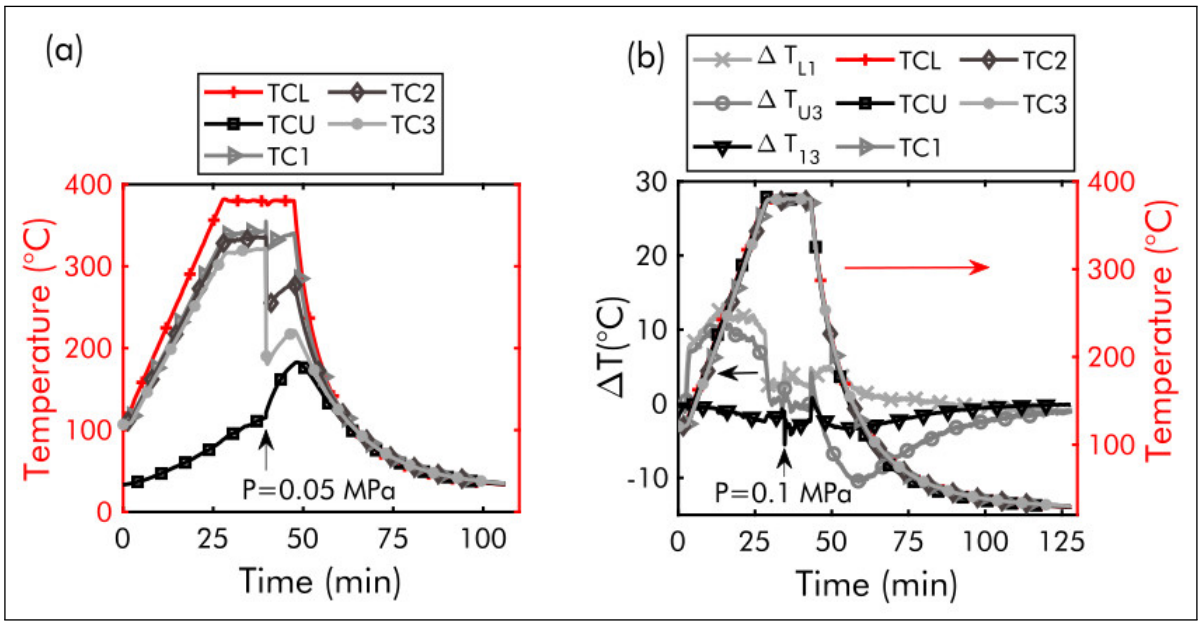

Figure 6.4: Thermocouple measurements during one-sided heating with natural cooling (a) and two-sided heating with enforced cooling (b) cycle of deconsolidation experiments.

case of one-Sided Heating (1SH), the application of pressure also leads to an increase in the temperature gradient in the sample (Figure 6.4 a). This is due to the fact that the upper hot platen is initially cold.

Finally, the temperature difference ΔT is much smaller during cooling in the case of one-sided heating (Figure 6.4 a) compared to the case of two-sided heating (Figure 6.4 b). This difference is related to the fact that for the one-sided heating case, the sample was cooled by natural convection with the ambient air. For the two-sided heating case, the sample was rather cooled by forced convection by blowing a cold air ($\approx 20\,^{\circ}\mathrm{C}$) on the hot platens edges. Forced convection results in a greater temperature difference by causing a rapid cooling of the copper hot platens.

The temperature cycles presented here correspond to the thermal cycle experienced by the samples during the deconsolidation tests at ESRF. The experimental temperature measurements were used to validate the thermal model.

6.2.5.1 Thermal model

The heat transfer was modeled by a 1D transient heat equation (6.1) following the procedure described in Amedewovo *et al.* [16].

$$\rho C_p \frac{\partial T}{\partial t} = \frac{\partial}{\partial z}\left(k_z \frac{\partial T}{\partial z}\right) \quad \forall z \in [0, l] \tag{6.1}$$

where ρ is the composite density, C_p its heat capacity, k_z its thickness or transverse conductivity and l its thickness. The physical properties of the CF/PEKK used are also available in Amedewovo *et al.* [16]. The 1D model was used given the plate-like geometry of the samples and also because the samples were confined during heating, thus limiting convection losses around the samples. Though the 1D model is not suited to account for the forced convection occurring during cooling stage, it was used and implemented as a slab (representing the composite sample) subjected to two heat flux at its boundaries.

Mixed boundary conditions were considered at both surfaces of the composite plate:

- At the contact with the lower hot platen, the heat flux writes:
$$k_z \frac{\partial T}{\partial z}(z = 0, t) = -\frac{TCL - T}{R_1} \tag{6.2}$$
where R_1 accounts for the thermal contact resistance between the sample and the lower hot platen, and TCL is the lower hot platen temperature which is considered uniform and known as measured by a monitoring thermocouple (Figure 6.3).

- At the upper surface, the heat flux writes:
$$k_z \frac{\partial T}{\partial z}(z = l, t) = \frac{TCU - T}{R_2} \tag{6.3}$$
where R_2 is the thermal contact resistance between the upper hot platen and the sample upper face. TCU is the upper hot platen temperature also measured by a monitoring thermocouple (Figure 6.3). R_2 accounts for both the conducto-convective exchange with the air and the radiative exchange with the facing upper hot platen.

For a given set of constant R_1 and R_2 thermal resistances, the above set of equations was solved with the FE code COMSOL Multiphysics [32]. Spatial integration used quadratic finite elements and time was integrated implicitly with the backward Euler method [16].

Table 6.2: Thermal resistances in $(m^2 \cdot K)/W$ identified by inverse method for different pressures.

	one-Sided Heating (1SH)		two-Sided Heating (2SH)	
	NAP	P = 0.05 MPa	NAP	P = 0.1 MPa
R_1	0.50×10^{-2}	0.67×10^{-5}	0.21×10^{-1}	0.68×10^{-2}
R_2	0.33×10^{-1}	0.68×10^{-5}	0.11×10^{-1}	0.59×10^{-2}

6.2.5.2 Boundary conditions identification

A standard inverse method was used to identify the thermal resistances R_1 and R_2 used in equations (6.2) and (6.3). The residual consists of the differences between the modeled and measured temperature for each of the three embedded thermocouples (Figure 6.3) at each time step over the temperature cycles. The residual 2-norm was minimized using the simplex method built in MATLAB [33].

The obtained values of thermal resistances are given in Table 6.2. For each heating configuration, the thermal resistances before (No Applied Pressure) and after pressure application are provided.

6.2.5.3 Thermal model validation

The temperature residuals at the sample middle ($TC2$), lower ($TC1$) and upper face ($TC3$) are plotted versus time in Figure 6.5. The range of the error is $\pm 5\,^{\circ}C$ for the one-Sided Heating (1SH) (Figure 6.5 a) and $\pm 3\,^{\circ}C$ for the two-Sided Heating (2SH) (Figure 6.5 b). The high peaks observed during the dwells are related to the moment when the pressure was applied. The second high peak observed at the cooling beginning is due to the forced convection which is not take into account in the 1D model (Figure 6.5 b). Moreover, the inverse method identification were performed using temperature measurements up to $380\,^{\circ}C$. At this temperature, the sample deconsolidation may occur resulting in changes of the composite thermal properties. A thorough estimation of the sample temperature field would require a more in-depth study taking into account the appearance of pores during heating.

The thermal model developed in this section allowed to estimate the composite laminate temperature during the deconsolidation experiments at ESRF. The hot platens temperatures recorded during the experiments were used as boundary condition of the thermal model. In the case of two-sided heating, the sample temperature was esti-

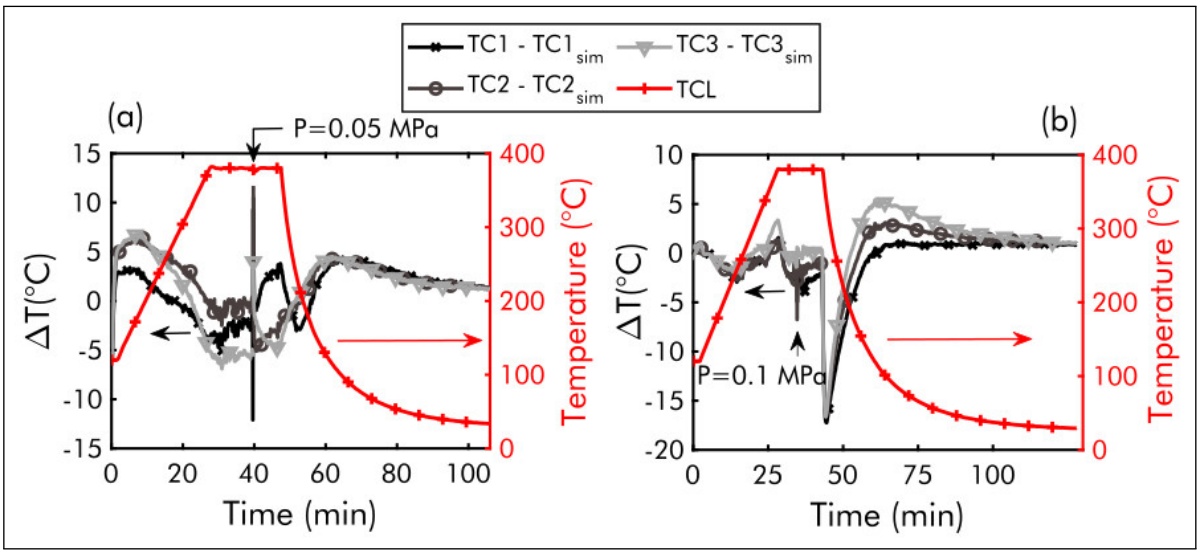

Figure 6.5: Thermal model validation for the two heating at a different pressures: one-sided heating with NAP + P=0.05 MPa (a) and two-sided heating with NAP + P=0.1 MPa (b).

mated as the average of the simulated temperature field over the sample thickness. In the case of one-sided heating, deconsolidation can be expected to start at the samples lower face. The sample lower face temperature is thus estimated as the average of the simulated temperature field over a thickness corresponding to the three first bottom plies.

6.2.6 3D real-time *in situ* imaging

During the deconsolidation experiments, tomographic scans were performed. For that purpose, fast scans of 1 s were carried out each 1 min. These scans consisted in 2016 X-Ray 2D projections obtained by an incremental rotation along the vertical axis of the rotation stage with a beam energy of 66 keV. The resulting 3D grey scale images were reconstructed from the 2D X-Ray projections using standard reconstruction algorithms combined with the Paganin method [34] to enhance the contrast between imaged phases. The reconstructed 3D grey level images represent volumes of 7.68 mm $\times$ 7.68 mm $\times$ 5.37 mm with a voxel size of 3.81^3 µm^3.

To extract quantitative micro-structural descriptors from the 3D images, we used the freeware Fiji [35], the Python SimpleITK and panda libraries [36] (Python). Hence, at the macroscale and from the greys scale vertical slices of the 3D images (see Figure 6.6 a, b), we used the "Multi-point" tool of Fiji to measure manually at 10 various

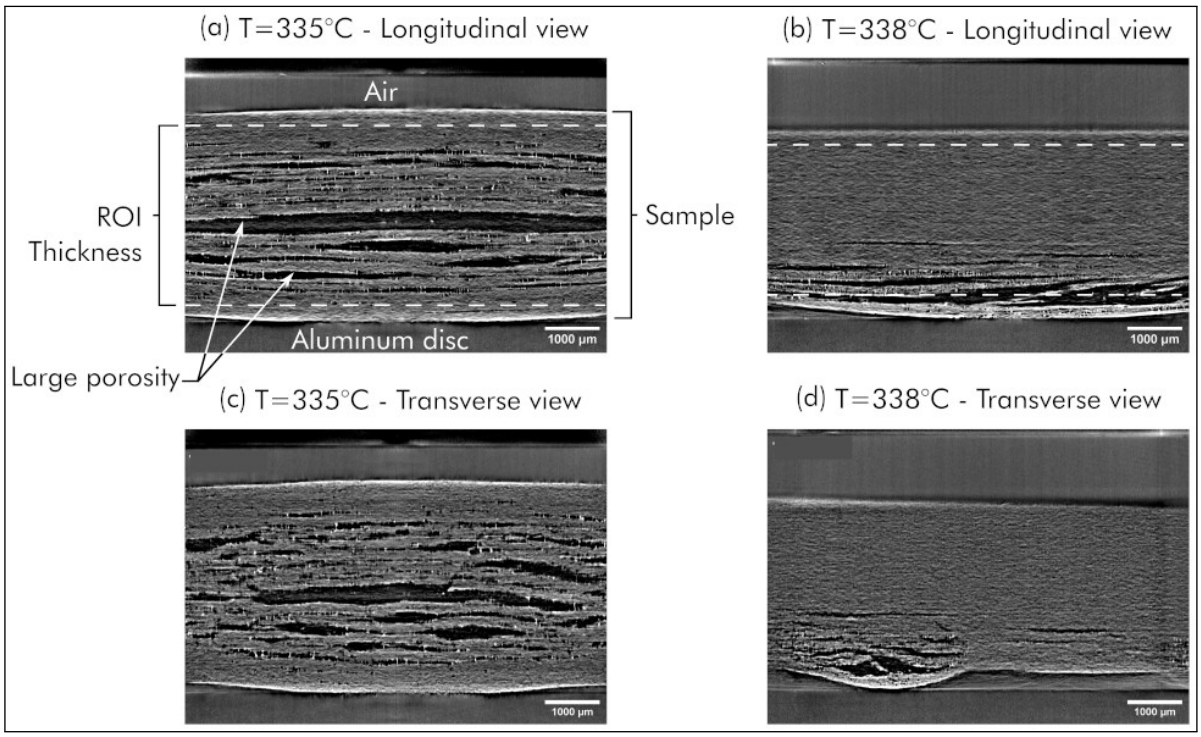

Figure 6.6: 2D grey scale slices through the thickness of a deconsolidated UD laminate showing the ROI thickness and pore during two-sided heating (a, c) and one-sided heating (b, d). The slices are parallel to the fibers orientation in (a, b) and transverse to the fibers in (c, d).

locations the sample thicknesses. These data were then averaged to estimate the mean sample thickness and a macroscopic deconsolidation strain $\varepsilon_D = \ln(l/l_0)$, where l_0 and l correspond to the initial and current mean sample thicknesses, respectively. At the microscale, additional analyses were performed with Region Of Interests (ROIs) of horizontal surface 3.81 mm $\times$ 3.81 mm picked from the 3D images. Since the thickness of the samples varied with increasing temperature, the thicknesses of the ROIs were also variable (Eulerian tracking). The ROI thicknesses were thus obtained by cropping the sample cores. The limits of the cropping frame were located one ply deep ($\approx$ 0.2 mm) underneath the sample upper and lower boundary (Figure 6.6 a, b). The as-cropped ROIs were then segmented using the trainable Weka segmentation algorithm [37] implemented in Fiji (Figure 6.7) in order to extract the pores from the solid phases (polymer matrix+carbon fibers).

Therewith, the porosity ϕ (resp. ϕ_z) of the ROIs (resp. along the thickness of the ROIs) could be estimated as the ratios of the number of the pore voxels in the ROIs (resp. in

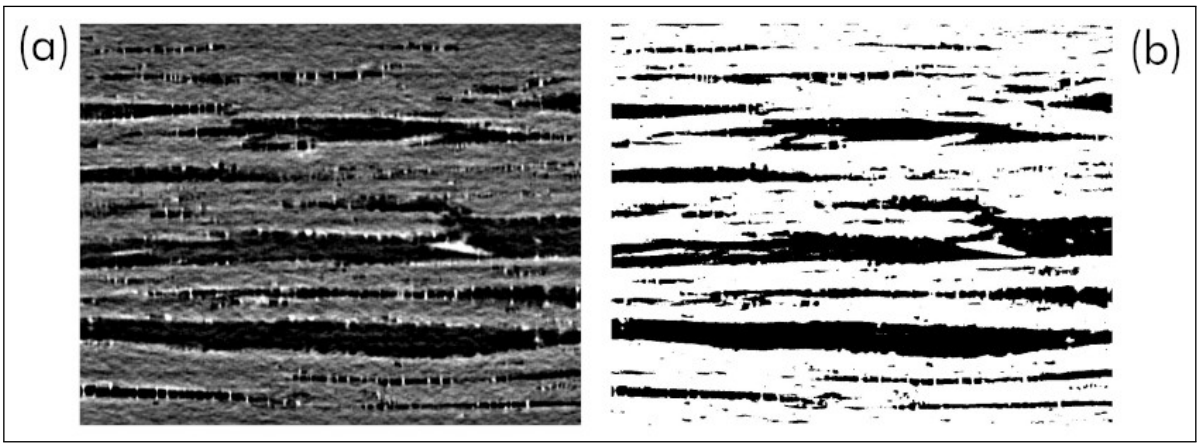

Figure 6.7: Comparison between a grey scale (a) and segmented (b) slice parallel to the fibers orientation, through the thickness of a deconsolidated laminate. The black zones represent the pores.

the stack located at a given height z) over the number of the voxels of the ROIs (resp. of the considered stack). In addition, based on the Euclidean distance map and the ConnectedComponentImageFilter function of the SimpleITK library, we could also label the pores and thus estimate their number $\mathcal{N}_p$. By using the same library, each labeled pore was also fitted with an Oriented Bounding Box (OBB) of dimensions a (length), b (width), and c (height) ($a > b > c$) from which two geometrical aspect ratios were estimated, namely the OBBs elongation el (b/a) and flatness fl (c/b) [38]. The pore morphologies were then classified in four classes: sphere-like if $el > 0.7$ and $fl > 0.7$; blade-like (or ellipsoidal) if $el < 0.7$ and $fl < 0.7$; disk-like (or oblate) if $el > 0.7$ and $fl < 0.7$; and rod-like (or prolate) if $el < 0.7$ and $fl > 0.7$ [39] (Figure 6.8).

6.3 Results

6.3.1 Qualitative analysis

Thanks to the *in situ* tomographic observations during the deconsolidation tests, it was possible to observe the evolution of the samples micro-structure over the temperature and pressure cycles. The vertical grey level slices displayed in Figure 6.9 show the time evolution of the dried UD sample (DS) structure during the two-Sided Heating

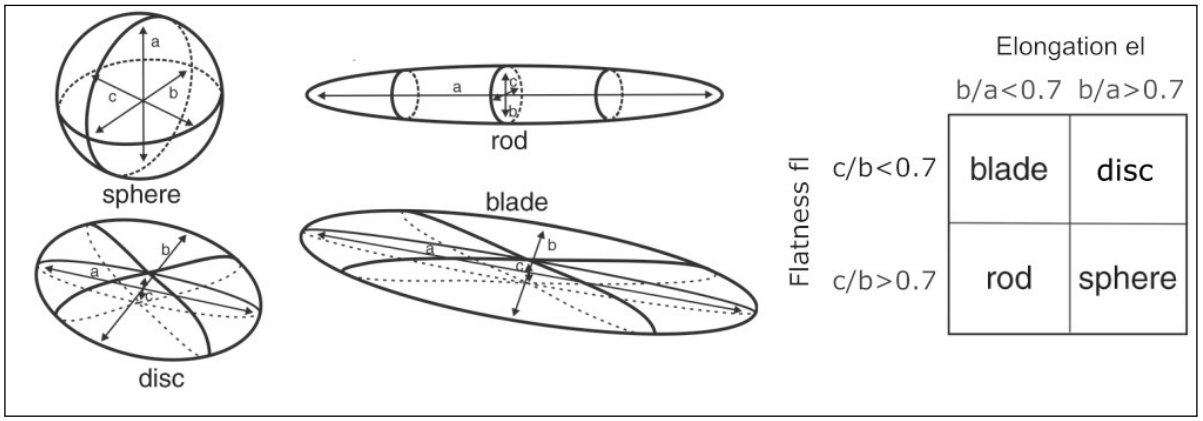

Figure 6.8: Shape classification system of Zingg [40].

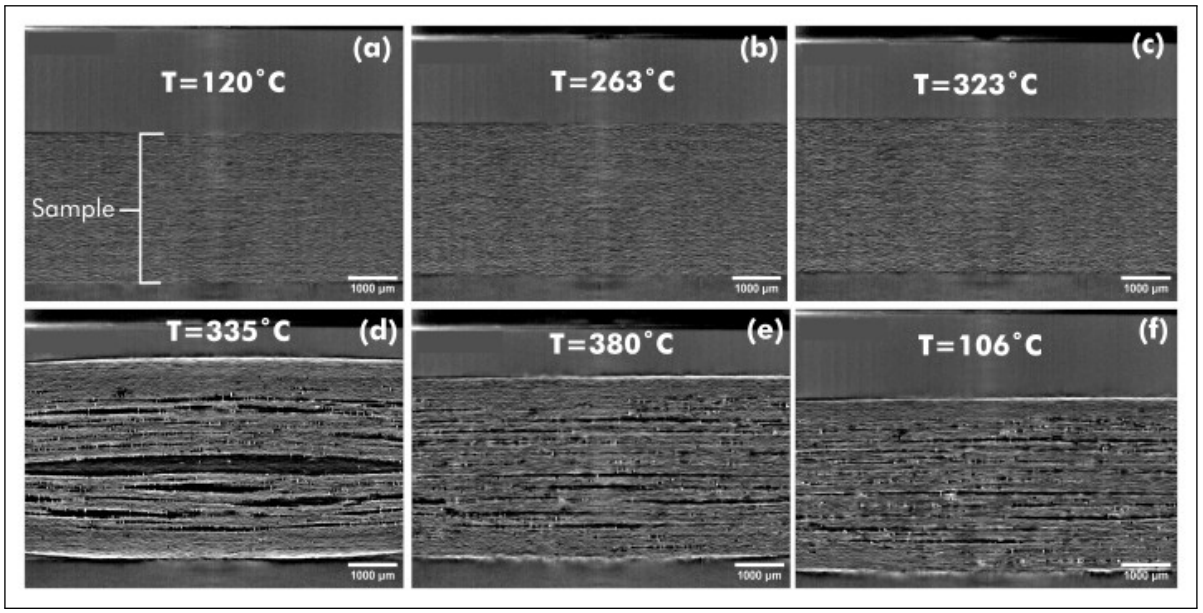

Figure 6.9: Tomographic cross section (parallel to fibers' axis)) evolution over a temperature cycle of an initially dried $[UD]_{16}$ composite sample for 72h@180°C (UD-DS-2SH). The black spots represent the porosities.

(2SH) and cooling. A first phase is observed below 323 °C, with a small increase in the sample thickness without marked occurrence of pores. This is presumably related to the sample thermal expansion (Figure 6.9 a-c).

A second phase of deconsolidation can be observed above 323 °C. It is characterized by a marked and rapid increase in the sample thickness (Figure 6.9 d). During this phase, large pores appear and lead to a visible decohesion between the plies of the composite laminate. These pore growth is systematically associated with the tension and the rupture of thin PEKK filaments which are also well-observable in the slice (d) (in white), these two features being also visible in Figures 6.6 and 6.7. It is also worth noting that the external surface exhibit non-zero valued curvature. During the dwell at 380 °C, Figure 6.9 (e) shows that the large pores subsequently tend to collapse, leading to noticeable decreases of both the sample thickness and the curvatures of its external surfaces. Finally, upon cooling, a slight decrease in the sample thickness is also observed and probably ascribed to thermal and crystallization shrinkages (Figure 6.9 f). The complete evolution of the slice related to this test as well as those of the three other tests are provided as Graphics Interchange Format (GIF) files in the supplementary materials available in [41].

The raw images allowed to compute (at the sample scale) the sample deconsolidation strain ε_D (defined in Section 6.2.6) as a function of temperature for all the tests mentioned in Table 6.1 (see Section 6.2.4). However, the first test on the UD-WI-2SH sample was discarded as the sample went out of the observation field. This was due to a first setting of the tomograph which was not appropriate.

Typical evolution of the amount, size and distribution of pores during deconsolidation are illustrated with the 3D segemented images shown in Figure 6.10 in the case of the DS sample. Firstly, it is interesting to note a small but clearly visible amount of micropores (initially) entrapped in the composite at T =120 °C (Figure 6.10 a). This porosity content was not measurable with the 2D optical micrographs reported in [16] and performed with similar spatial resolution (see Figure 6.1): this could be presumably induced by some possible artifacts induced during the the polishing used to obtain the 2D micrographs.

In addition, as the temperature increases up to 323 °C, the porosity content increases, with (i) more and more small pores and (ii) the occurrence of medium-sized pores (Figure 6.10 b-c). Between 323 °C and 335 °C, a very fast and drastic increase of the

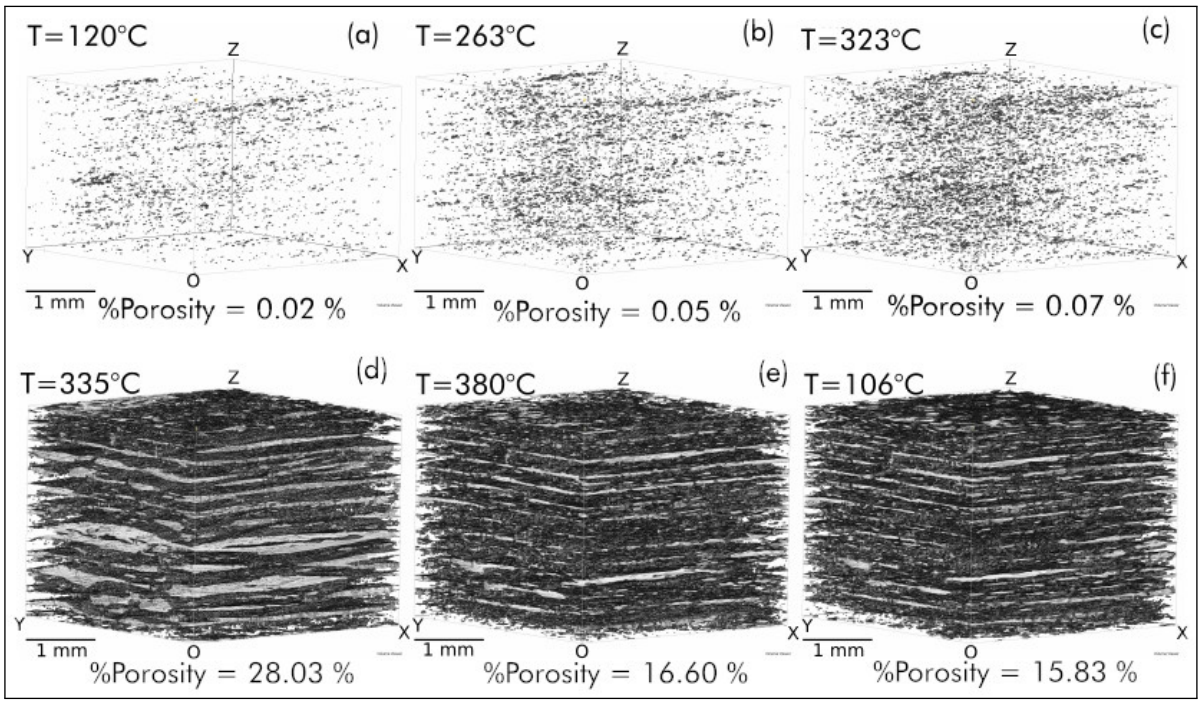

Figure 6.10: Time evolution of the porosity in a ROI of 3.81 mm × 3.81 mm × Z during deconsolidation of an initially dried $[UD]_{16}$ composite sample for 72h@180°C. The axis (OX) and (OY) are respectively parallel and transverse to the fibers main axis. The black spots represent the pores.

porosity is recorded with, in particular many large-sized pores which are the signature of interply decohesion (Figure 6.10 d). As evidenced before, during the dwell, the large-sized pores collapse and probably split into smaller pores (Figure 6.10 e). No significant change in the micro-structure is observed during cooling (Figure 6.10 f). The complete porosity evolution during the other tests is also provided as GIF files in the supplementary materials available in [41].

We have also reported a similar example in Figure 6.11 on the Cross-Ply (CP) laminate case, initially stored in distilled water (WI). The same phenomena can be observed at first glance. The focus is made here on the application of a 0.1 MPa pressure during the isothermal dwell (Figure 6.11 d-f). A very fast re-consolidation, almost instantaneous when the pressure is applied, can be observed. The porosity is drastically reduced. However, residual porosity with small or medium-sized pores remains at the end of the cooling process (Figure 6.11 f), with a progressive and slow decrease of the porosity related to a consolidation process.

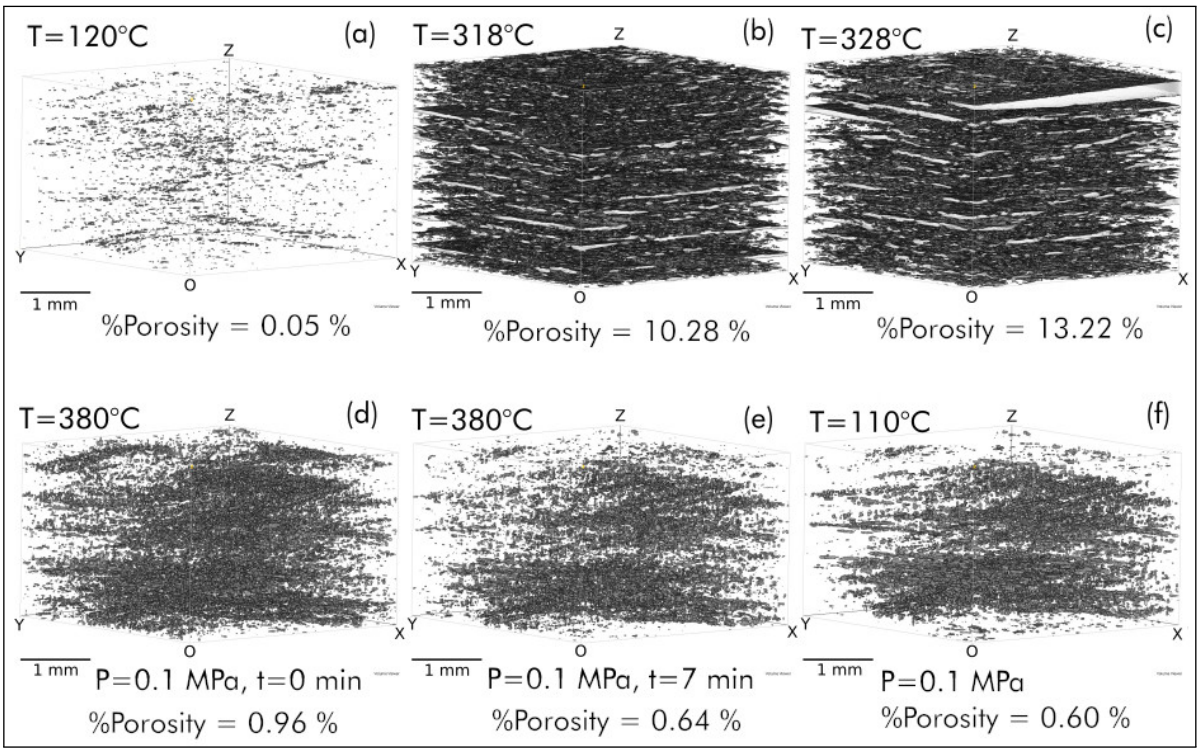

Figure 6.11: Time evolution of the porosity in a ROI of 3.81 mm $\times$ 3.81 mm $\times$ Z during deconsolidation of an $[0/90]_{4S}$ cross-ply laminate sample initially stored in distilled water. The black spots represent the porosities.

6.3.2 Quantitative analysis at the sample scale

The temperature evolution of the sample deconsolidation strain ε_D and the porosity content ϕ inside the ROIs are reported in Figure 6.12, from which three stages can be distinguished:

- For all tests, stage 1 is observed at low temperatures. Herein, the deconsolidation strain ε_D slightly increases (practically linearly) and where the porosity content ϕ does not significantly increase. As assumed previously, this stage could *a priori* be related to the thermal expansion of the samples. For the tests carried out in dried (DS) or wet (WI) conditions with two-side heating (2SH), we roughly estimated from the $\varepsilon_D(T)$ curves of Figure 6.12 (a-b) respective apparent out-of-plane thermal expansions (above $T_g \approx 160\,^{\circ}\mathrm{C}$) of $100.3 \times 10^{-6}\,^{\circ}\mathrm{C}^{-1}$ and $179.1 \times 10^{-6}\,^{\circ}\mathrm{C}^{-1}$, *i.e.* two values which are in-line to that measured from standard dilatometry with a sample stored in ambient conditions, *i.e.* $139.4 \times 10^{-6}\,^{\circ}\mathrm{C}^{-1}$ [16] and suggesting that the higher the initial moisture content, the higher the apparent thermal

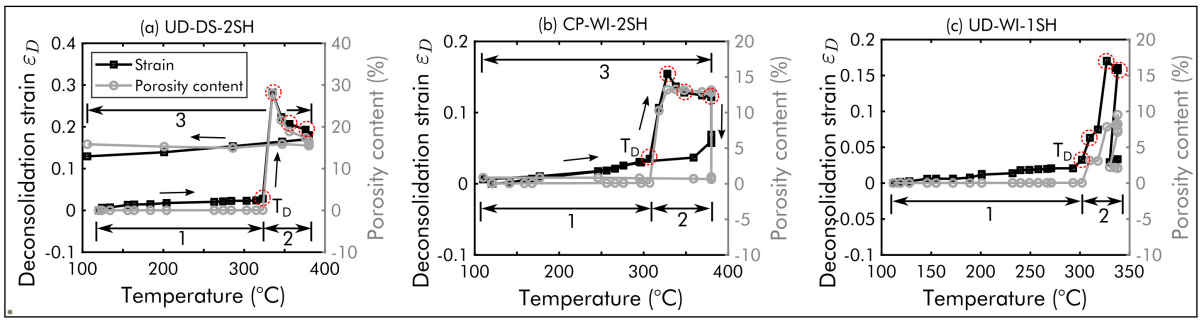

Figure 6.12: Deconsolidation strain ε_D and porosity content ϕ of the samples *vs* sample temperature estimated with the thermal model during the deconsolidation tests: test 2 on UD-DS-2SH (a), test 3 on CP-WI-2SH (b) and test 4 on UD-WI-1SH (c). The dashed circles indicate characteristic temperatures used later for micro-structural analysis during deconsolidation.

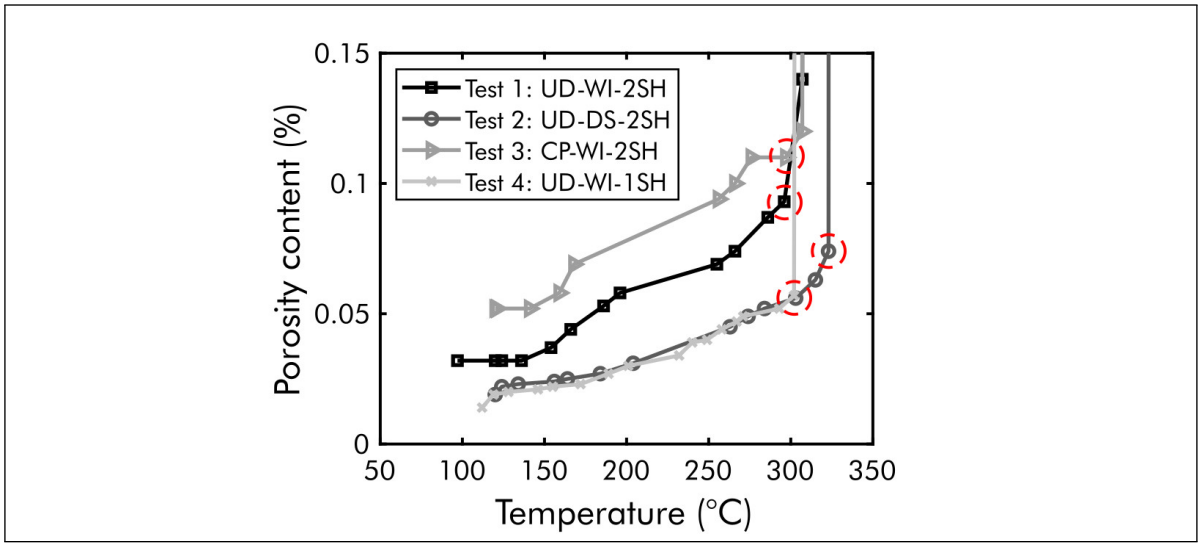

Figure 6.13: Zoom of the previous figures showing the porosity content ϕ in the samples as function of temperature estimated with the thermal model during the deconsolidation tests. The dashed circles indicate the onset temperature of deconsolidation.

expansion. The trend could be explained by a closer look at the temperature evolution of the sample porosity content ϕ during this stage for the considered samples as emphasized in the zoom carried out in Figure 6.13, which brings up the following comments.

Firstly, this figure proves that the initial porosity content ϕ in the samples is very low ($< 0.06\,\%$). No significant difference is observed between the UD

samples, albeit a slightly higher porosity content is seen for the WI sample, and the initial Cross-Ply (CP) sample porosity content is higher than those of UD samples. Secondly, above T_g, the increase of the porosity content ϕ in the UD-WI-2SH sample becomes roughly twice that of the UD-DS-2SH sample (note that the same behavior is not observed in the UD-WI-1SH because of its non-isothermal heating). This suggests that the presence of moisture should induce the enhancement of nucleation/growth of pores, so that the assessed apparent thermal expansion coefficients could be due both to intrinsic thermal expansion mechanisms but also to moisture induced pore nucleation/growth.

- It is also very interesting from figure 6.13 to note that the onset of stage 2, which corresponds to the drastic increase of deconsolidation, occurs about 20 °C earlier in the case of wet samples WI: the onset temperature is around 300 °C for them whereas it is around 320 °C for the dried ones (DS). In addition, the deconsolidation in stage 2 is characterized by sharp shifts in the sample strain and porosity content (Figures 6.12 and 6.13).

  The dried UD-DS-2SH sample exhibits a higher maximum deconsolidation strain and porosity content (close to 0.3) than the values reported for the water immersed cross-ply CP-WI-2SH (both close to 0.15). This is *a priori* unexpected and could be caused by a difference of architectures of the considered fibrous reinforcement, or by the acquisition frequency of the tomographic scans (1 min): the maximum strain of the wet CP-WI-2SH sample may be reached between 318 °C and 328 °C or between 328 °C and 338 °C (Figure 6.12 b).

  After the peaks of strain and porosity content, it is worth noticing that the deconsolidation strain as well as the porosity content decrease while heating the samples up to the dwell. This is directly correlated with the qualitative observations stated in the previous subsection: fibers, which bent during the drastic increase of the porosity, progressively debend, thus yielding in pore closing and decrease of deconsolidation strain.

- During cooling (stage 3) without subjecting samples a confining pressure (Figure 6.12 a), the strain ε_D decreases linearly while the porosity content ϕ remains almost constant. This means that the thermal and crystallization shrinkage should have almost no impact on the porosity induced upon sample heating. When a confining pressure is applied at the end of the dwell, however, fast de-

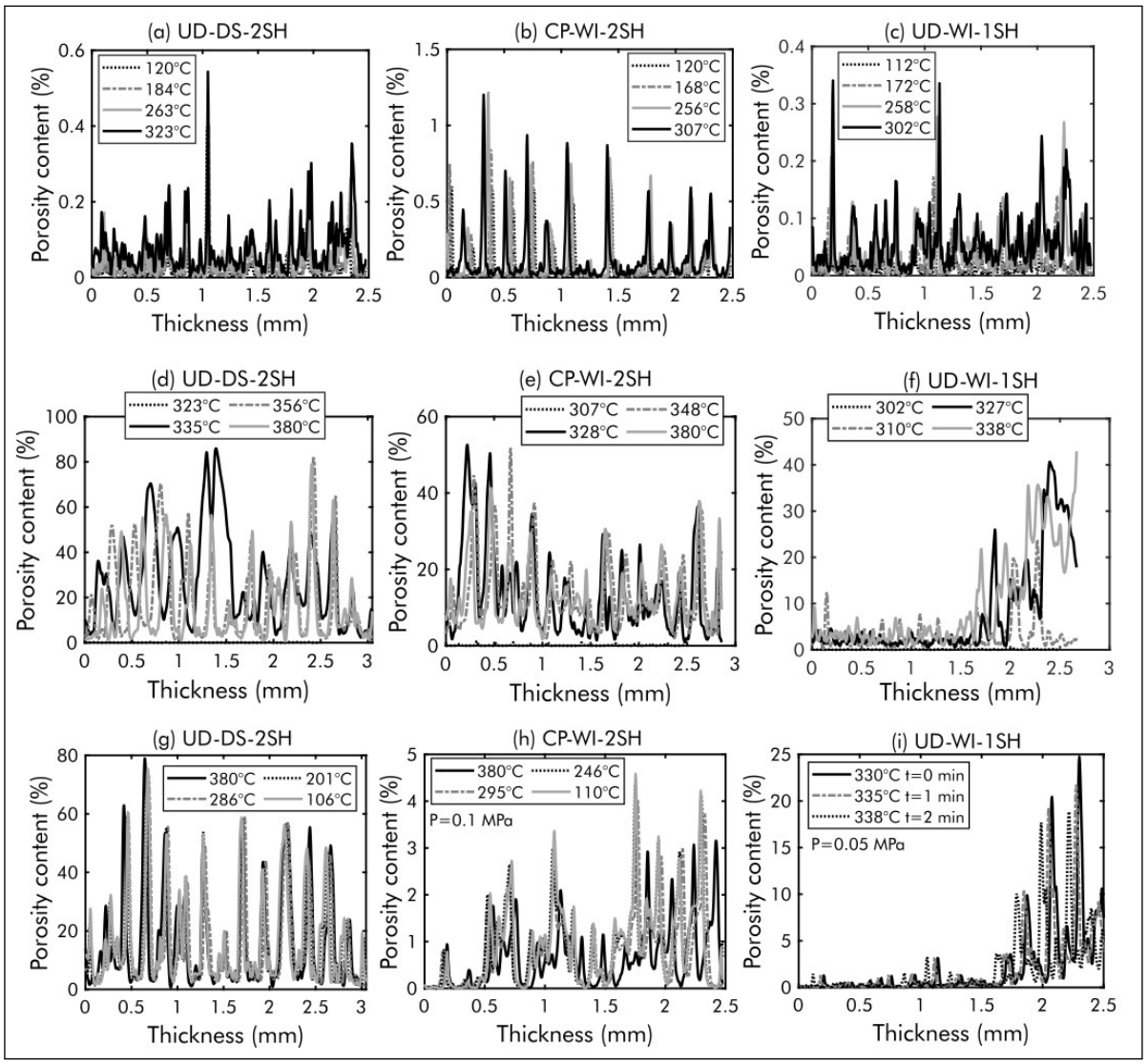

Figure 6.14: Evolution of the spatial distribution through the sample thickness porosity content ϕ_z during stage 1 (a-c), stage 2 (d-f) and stage 3 (g-i) of the deconsolidation experiments UD-DS-2SH (a,d,g), CP-WI-2SH (b,e,h) and UD-WI-1SH (c,f,i).

creases of both ε_D and porosity content ϕ are first recorded, leading to a marked sample re-consolidation (Figure 6.12 b-c). Pursuing the cooling still yields to a quasi-linear decrease of ε_D, without noticeable change in ϕ.

6.3.3 Quantitative analysis at the fiber scale

Pore distribution The evolution of the spatial distribution of the porosity content along the sample thickness ϕ_z is reported in Figure 6.14. One clearly sees from

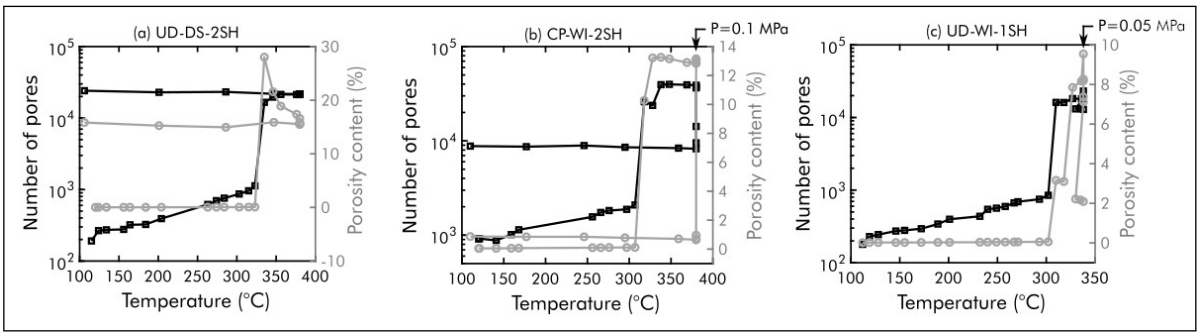

Figure 6.15: Evolution of the number of pores $\mathcal{N}_p$ and the porosity content ϕ with the temperature during deconsolidation experiments: UD-DS-2SH (a), CP-WI-2SH (b) and UD-WI-1SH (c).

graphs (a-c) that ϕ_z are mainly located at the interplies. For the Cross-Ply (CP) sample (graph b), consecutive peaks are spaced with a distance of $\approx$0.2 mm, which corresponds to the thickness of a single ply (Figure 6.14 b). For the UD samples, the interplies are less obvious but again, most of the peaks are located around the interply region (Figure 6.14 a, c). Increasing the temperature during stage 1 leads to a preferential increase of ϕ_z at interplies too; this is especially highlighted in Figure 6.14 b. During stage 2, Figure 6.14 (d-e) shows that the porosities grow mainly at the vicinities of interplies, since the ϕ_z-peaks are still and mostly located around the interply regions. As revealed by these graphs, this feature seem to be unaffected while changing the sample moisture content. Conversely, the effect of the through the thickness temperature distribution is important and clearly emphasized by comparing graph (d) and (f): the one-sided heating localizes the porosity increase only on the bottom of the sample thus affecting the overall deconsolidation dynamics, whereas, the two-sided heating allows the deconsolidation to be induced more homogeneously in the samples. Lastly, during stage 3, there is no significant change of spatial distribution during cooling (Figure 6.14 h-i).

Pore number Figure 6.15 shows the temperature-evolution of the number of pores and the porosity content recorded during the deconsolidation experiments. During stage 1, a noticeable regular increase of $\mathcal{N}_p$ while increasing temperature is observed while in the same time the increase of ϕ is limited. This can be due to the nucleation of novel pores. Moreover, apart from the single point at 120 °C with the UD-DS-2SH sample (Figure 6.15), the rate of the pore number change $\partial\mathcal{N}_p/\partial T$ for symmetric (and thus more homogeneous, see last paragraph) heating conditions seems to increase

significantly above the glass transition temperature 160 °C. In this zone, $\partial \mathcal{N}_p / \partial T$ is roughly estimated to 4.1 $°C^{-1} \cdot mm^{-3}$ for the DS sample and to 11.7 $°C^{-1} \cdot mm^{-3}$ for the WI one, thus suggesting that moisture should speed up pore nucleation. During stage 2, $\mathcal{N}_p$ together with ϕ first increase drastically. After the deconsolidation peak, there is still a slight increase of the number of pores $\mathcal{N}_p$ (albeit lower than that observed in stage 1) while the porosity ϕ decreases (Figure 6.15 a, c). This can be explained by (i) the nucleation of novel pores (ii) the fact that large pores formed up to the deconsolidation peak probably split into smaller ones (due to the relaxation of internal stresses, see below). During stage 3, it is worth mentioning that $\mathcal{N}_p$ significantly decreases with the application of a confining pressure (Figure 6.15 b, c) whereas it is almost constant during cooling whatever the pressure value (Figure 6.15 a, b). The last observation suggests again that thermal and crystallization shrinkage has a negligible impact on the porosity and pore kinetics. It also suggests that pore nucleation is limited at this stage of the experiments.

Pore size Figure 6.16 (a-c) shows the distribution of the major pore lengths a (defined in Section 6.2.6) during stage 1. The majority of pores are initially smaller than 100 µm (small-sized pores) with peak distributions between 10 µm and 20 µm. By zooming on higher pore lengths, one can notice the appearance of medium-sized pores the length of which lies between 100 µm and 1000 µm after the glass transition temperature ($T_g \approx 160$ °C), thus proving a pore growth during this stage. However, as emphasized in Figure 6.17 (a-c), the volume fraction of medium-sized pores is much lower in this stage than that measured for the small-sized pores. Combined with results gained for $\mathcal{N}_p$ (previous paragraph), this observation reinforces the scenario of (small) pore nucleation during stage 1 above T_g.

During stage 2, Figure 6.16 d-f shows that the number of small-sized pores increases drastically up to the consolidation peak, thus showing that pore nucleation should be still important during this sequence. Albeit less marked, the increase of the number of medium-sized pores but also large-sized pores ($\geq$1000 µm) are also noticeable, proving that in the same time important pore growth occurs in the samples. In addition, after the deconsolidation peak, the number of small and medium-sized pores slightly increase. Meanwhile, the volume fraction of large-sized pores decrease whereas that of small and medium-sized pores increase: this is in-line with the qualitative and

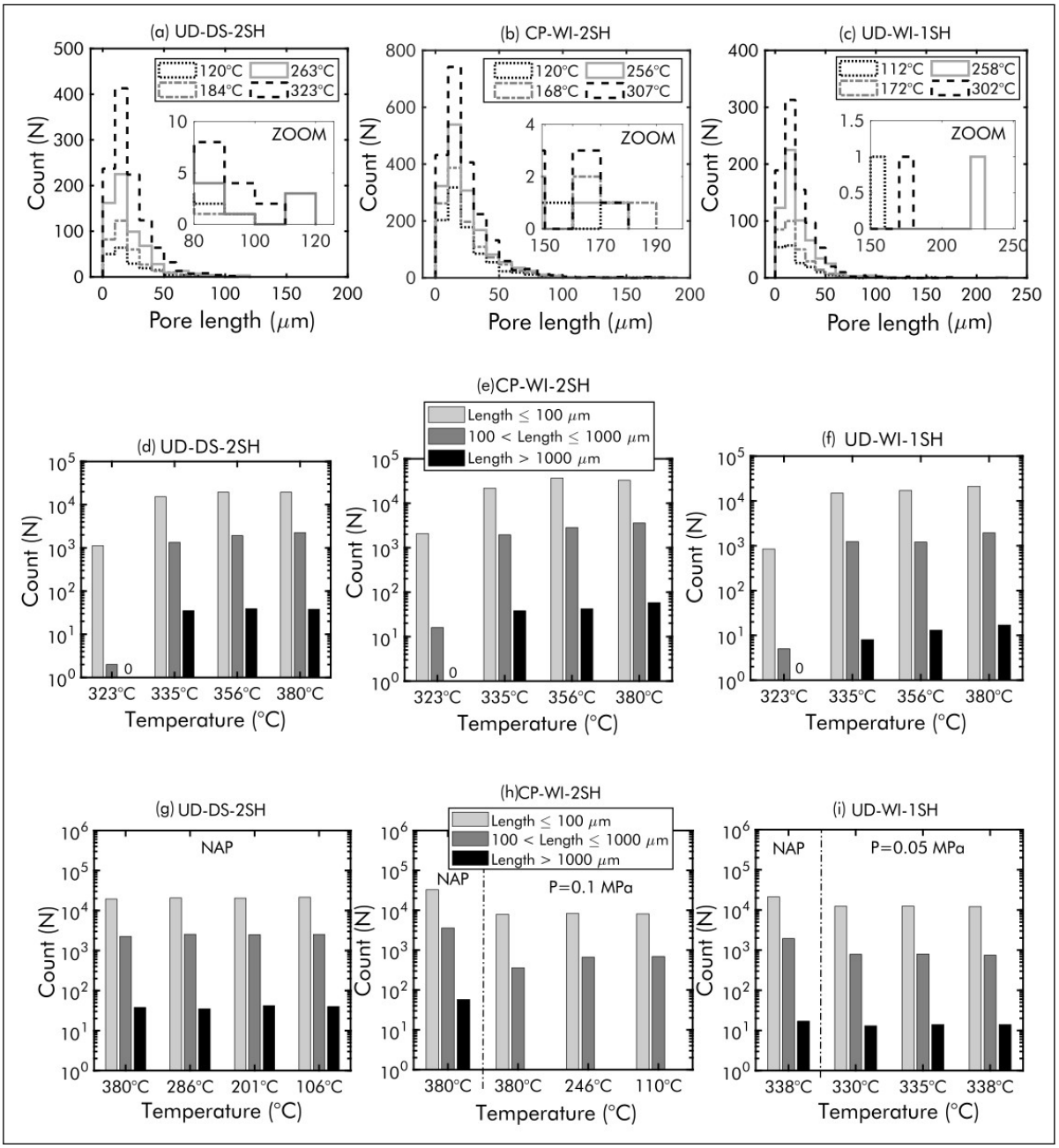

Figure 6.16: Distribution of the major pore length a during stage 1 (a-c), stage 2 (d-f) and stage 3 (g-i): UD-DS-2SH (a,d,g), CP-WI-2SH (b,e,h) and UD-WI-1SH (c,f,i) samples.

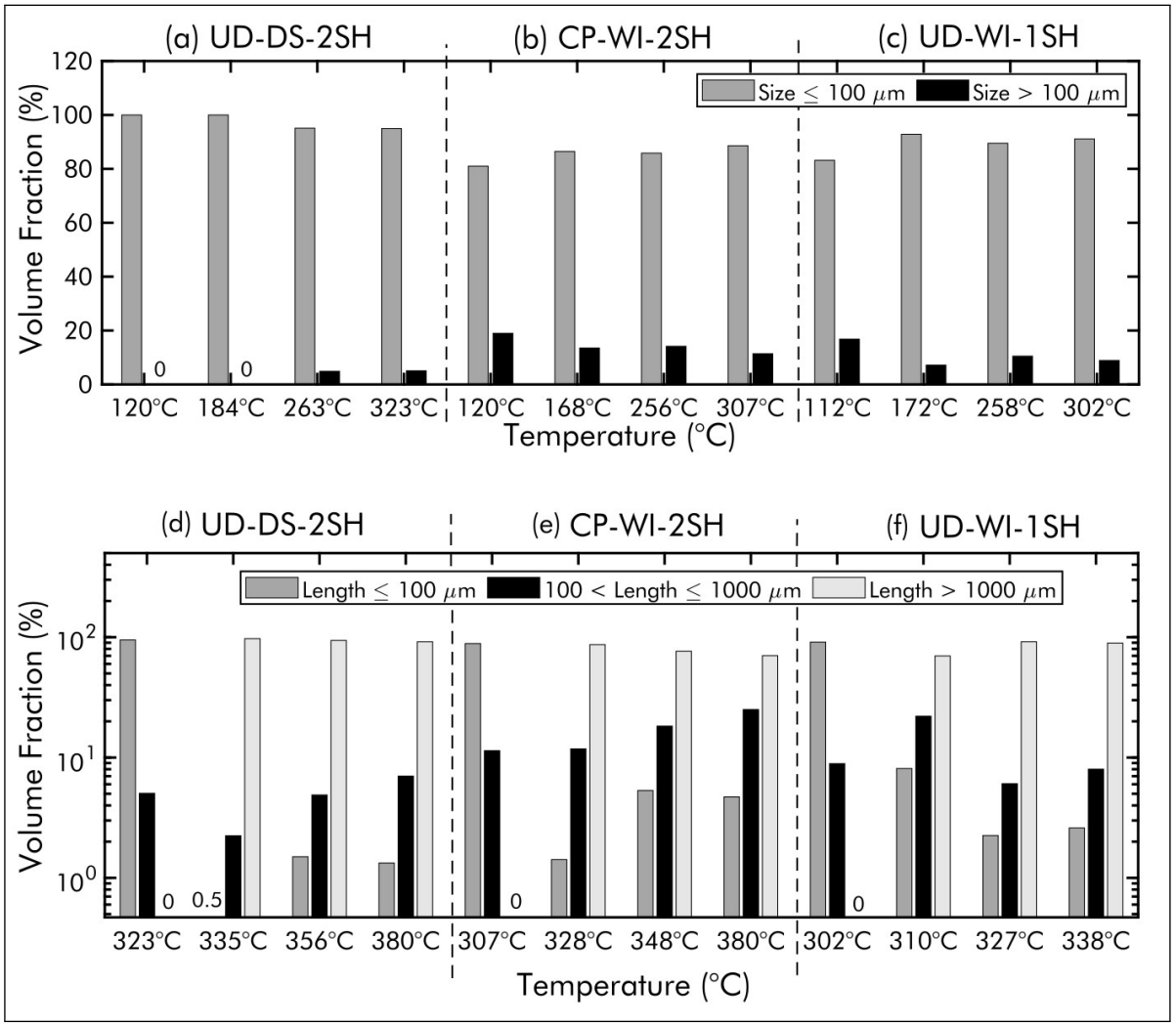

Figure 6.17: Volume fraction of the small pores compared to the medium and large pores during stage 1 (a-c) and stage 2 (d-f): UD-DS-2SH (a,d), CP-WI-2SH (b,e) and UD-WI-1SH (c,f) samples.

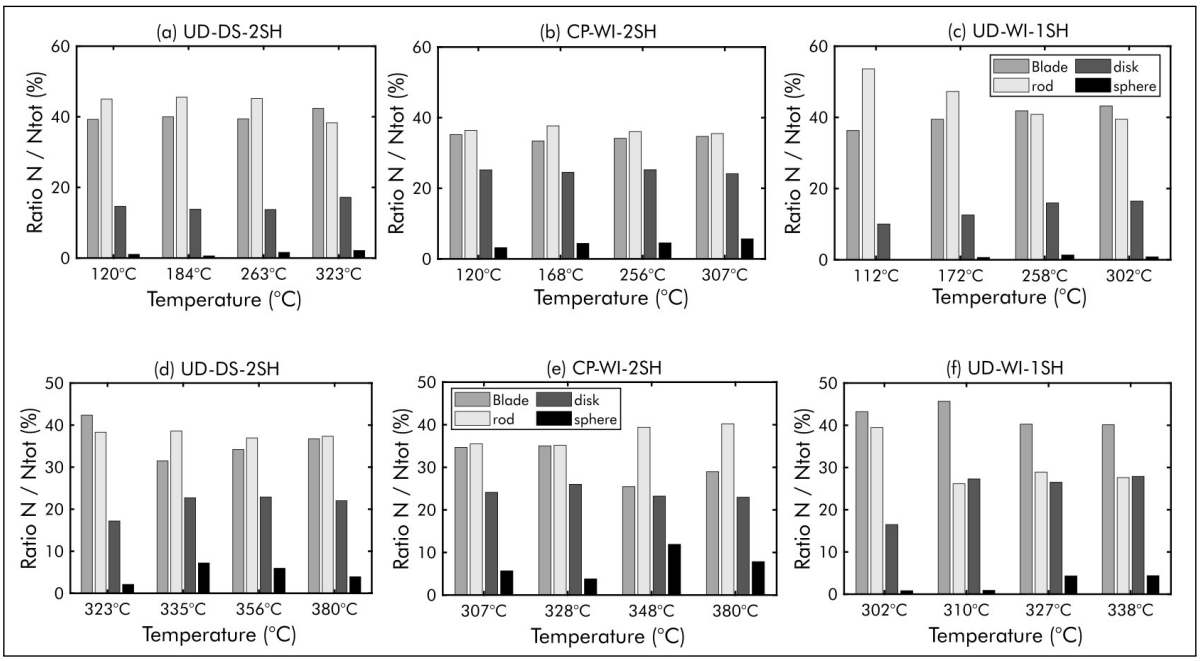

Figure 6.18: Distribution of the pore shape during stage 1 (a-c) and stage 2 (d-f): UD-DS-2SH (a,d), CP-WI-2SH (b,e) and UD-WI-1SH (c,f) samples.

quantitative observations respectively made the two previous subsections, *i.e.* the closing of bigger pores, the decrease of the deconsolidation strain and sample porosity. The closing of larger pores would also be a cause of the slight increase of smaller pores.

Lastly, during stage 3, applying a confining pressure leads to a reduction of the numbers of pores, in particular the bigger ones. In addition, whatever the applied confining pressure, the type of fibrous architecture and heating type, it is interesting to notice that upon cooling, the number of small, medium and large-sized pores practically remained constant. This suggests that either pore nucleation and pore growth/splitting/closure should be limited upon cooling.

Pore morphology Figure 6.18 shows the distribution of the pore shapes (defined in Section 6.2.6) during stages 1 and 2. This figure shows that initially, the majority of pore shapes are mainly rode-like (prolate) and blade-like (ellipsoidal) mainly oriented along the fiber axes. Pores also exhibit disk-like shapes and rare sphere-like shapes (especially in the case of unidirectional samples). Increasing the temperature in stage 1 does not

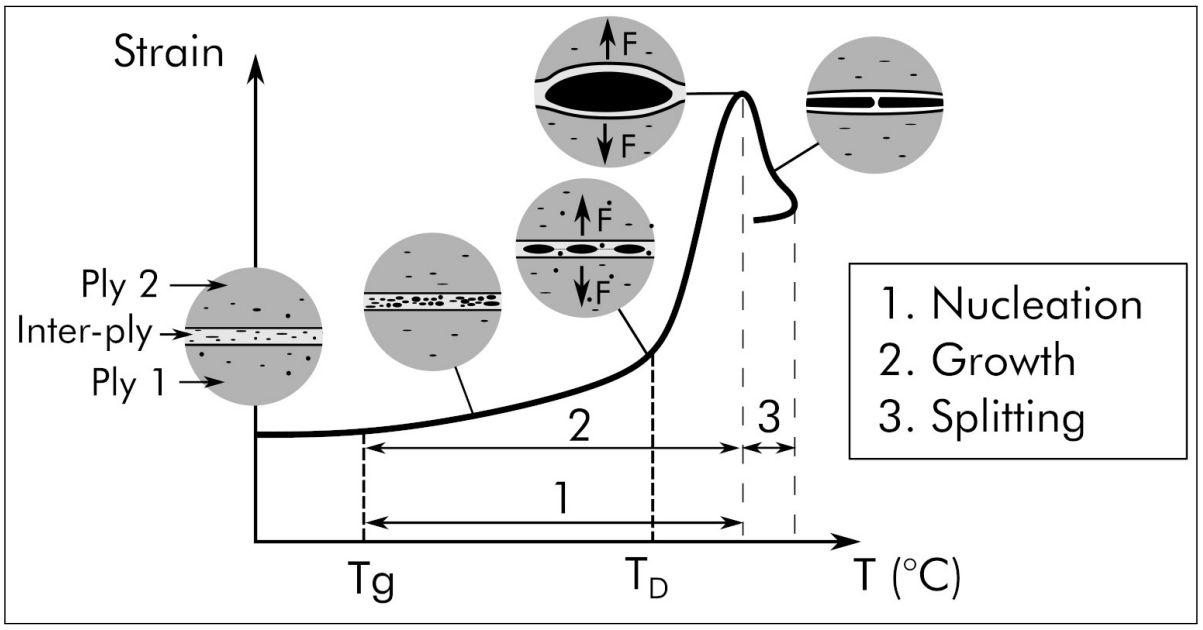

Figure 6.19: Schematic representation of deconsolidation process in unidirectional prepreg-based TPC laminates.

lead to a significant change in the shape distributions, as shown in Figure 6.18(a-c). The same remark is valid during stage 2 (Figure 6.18(d-f)), except the increase of about 5 % in the proportion of disk and sphere-like shapes.

6.4 Discussion

Thanks to the unique 3D real-time and *in situ* images provided by synchrotron X-Ray microtomography, the micro-structures and the deconsolidation mechanisms occurring during the heating and cooling of high performances TPCs could be finely characterized. We could thus emphasize three main processes illustrated in the scheme of Figure 6.19 and discussed hereafter.

6.4.1 Pore nucleation

The first process is pore nucleation. We could detect it from the glass transition temperature (T_g) at least up to the deconsolidation peak. Within this temperature range, pore nucleation is characterized by the noticeable increase of the number of pores $\mathcal{N}_p$ which, according to the graph shown in Figure 6.16, is mainly related to the number of small-sized pores. The induced small-sized pores exhibit mainly rod, blade and

disk-like shapes, they are mainly located around the laminates interplies (Figure 6.14). Our results also clearly reveal that this process is also enhanced/driven by the water content inside the tested samples: the higher the water content, the higher the pore nucleation rate $\partial \mathcal{N}_p / \partial T$. Thus, pore nucleation above T_g may be attributed several coupled effects related to moisture content and temperature (since the tested prepregs were already subjected to a heating above melting during the initial consolidation of the laminates, it is assumed that there is no other residual volatile substances from additives used in TPC prepreg manufacturing).

Above T_g, the mechanical properties of the polymer matrix and the matrix-fiber interfaces may be soft enough to allow pore nucleation, this softening being enhanced by the water content which acts as a solvent. In addition, an increase of the free volumes in the polymer matrix may allow porosity nucleation through fine scale moisture evaporation and/or diffusion. Since the polymer is not hygrophobic, moisture may also agglomerates and forms porosity nucleation sites in polymer-rich areas. This could be supported by our observations: the high porosity content at the laminates interplies (Figure 6.14) which are the most polymer-rich locations. This process may be enhanced by temperature which promotes moisture transport in the composites [31].

Our results also proved that an initial drying of the sample at 180 °C for 72 hours does not prevent pore nucleation. We previously assumed that moisture may be stored in the composite in two forms namely "weakly bonded water" and "strongly bonded water" [31]. Drying at 180 °C for 72 hours should effectively remove the "weakly bonded" water but "strongly bonded" water should remain in the composite due to the high thermal energy required to desorb it. The residual moisture strongly bonded to the composite may thus be involved in the nucleation process observed in the dried samples.

At last, at the beginning of stage 2, the mechanical properties of the polymer matrix and the fiber-matrix interfaces are soft enough to allow a rapid and sharp increase of deconsolidation. Deconsolidation is then characterized by a sharp increase of the deconsolidation strain and, in particular, the bending of the fibers which relax a part of their internal stresses which come from the consolidation process. During the Hot Press consolidation under 4 MPa, stresses due to fiber bed compaction, shrinkage mechanisms, and eventually skin-core thermal gradient may not fully relaxed before the material solidification.

Internal stresses are produced at three different scales [42, 43] (fiber, ply and laminate scale) resulting in a complex three-dimensional stress state within the composite laminate [44]. Hence, while load by their consolidation-induced internal stresses, fibers should also act as driving "tensile" forces in the polymer matrix or the fiber-matrix interfaces to enhance the nucleation of small-sized pores [14, 45, 46]. At last, above that point of the deconsolidation process, fibers keep on deforming with debending, we suspect then that nucleation is limited, the increase of being related to pore splitting/closing (see below) and freezed upon cooling.

6.4.2 Pore growth

The second important deconsolidation mechanism is pore growth. As emphasized with our results, pore growth is limited during stage 1, does not take place during stage 3, and mainly occurs during the early times of stage 2, *i.e.* above T_D. Indeed, above this temperature, medium and large-sized pores are induced in the samples, leading to significant increase of both the sample deconsolidation strain and porosity. The onset pore growth temperature T_D mainly occurs around the melting onset (between 300 °C and 310 °C) in the case of Water Immersed (WI) samples and in the melting zone ($\geq$310 °C) in the case of Dried Sample (DS). The lower T_D value recorded for wet samples may be attributed to their higher porosity content (Figure 6.13) which can weaken the laminates interfaces, and to moisture-induced softening of the sample viscoelastic properties [47]. The substantial pore growth observed in the early times of stage 2 are also attributed to the loading of residual stresses induced during the consolidation process, in particular the observed fiber bending which is in turn enhanced by the moisture and temperature-induced softening of the polymer matrix. Hence, residual stresses loading combined with the softening of the polymer matrix and the interfaces are suspected to be the main mechanisms of pore growth. Local tensile forces induced by the bending of fibers should enhance the creep of the polymer matrix (as revealed by the 3D images) as well as the decohesion of the interfaces, and thus the pore growth by crack propagation and/or pore coalescence. Additional 3D real-time images at finer scale would be required to (un)validate these hypotheses.

6.4.3 Pore closure or splitting

The third deconsolidation mechanisms which occur during the end of stage 2 and the beginning of stage 3 are pore closure and/or splitting: during these sequences, our results reveal that pores collapse and/or split into smaller ones, leading to a decrease

of the sample strain and porosity. During stage 2, here again, internal stresses loading is suspected to be the main cause of these pore scale mechanisms. Indeed, after a first loading mode which conducts to fiber bending (see last point), the polymer matrix creep allows bent fibers to recover their initial and unconstrained straight shapes, as emphasized from the 3D images (see Figure 6.9 d, e in Section 6.3.1). Combined with gravity forces, this mechanisms would induce the observed decreases of the deconsolidation strain, porosity and pore size. In addition, as also revealed by our experimental results, subjecting the samples to an additional confining pressure, as in the beginning of stage 3, enhance drastically these pore closure/splitting mechanisms. For example a low pressure of 0.1 MPa was sufficient to close/split all the large-sized pores but there are still small-sized and medium-sized residual pores (Figure 6.16 h, Figure 6.12 b). This stage practically determines the final pore content, distribution, size and shape in the composite samples as thermal or crystallization shrinkage involved during cooling do not lead to a significant change in these descriptors.

6.5 Conclusion

In this study, we investigated the mechanisms of pores nucleation, growth and closure occurring during the heating of a high-performance thermoplastic composite (TPC) CF/PEKK. For that purpose, we carried out representative deconsolidation experiments with a novel consolidation device named InCODETO for *In situ* COmposite DEconsolidation Tomography Observation, which allows, when mounted in a synchrotron X-Ray tomograph, unique 3D real-time and *in situ* observations of the TPC sample micro-structure during heating at high temperature with/without confining pressure to be acquired. Doing so, the deconsolidation of press-consolidated unidirectional and cross-ply $[0/90]_{4S}$ laminates with different preconditioning conditions was studied. One group of samples was stored in distilled water at room temperature ($\approx$ 23°C) for 3 months and the other was dried at 180°C for 72 h.

Results showed that regardless of the sample moisture preconditioning (DS or WI), heating type (1SH or 2SH) or stacking sequence (UD or CP), the deconsolidation process was systematically decomposed in three stages during which three main mechanisms were identified: pore nucleation, growth and closure/splitting. Pore nucleation mainly starts after the glass transition temperature (T_g) of CF/PEKK and extends during deconsolidation (heating and dwell), *i.e.* during stages 1 and 2. Pore nucleation is mainly driven by moisture (in stages 1 and 2) and enhanced during the

internal stresses loading (mainly occurring above the melting temperature during stage 2). An initial drying of the composite at 180 °C for 72 hours limited the nucleation process but did not prevent it, due to the residual moisture bonded to the polymer matrix which remains in the composite after drying. Pore growth was mainly observed above the melting temperature and was ascribed to the (moisture and temperature dependent) softening of the polymer matrix and fiber-matrix interfaces, allowing internal stresses to cause a first noticeable fiber deformation mode, namely bending. Fiber bending thus acts as an additional driving force enhancing the creep of the polymer, the decohesion of interfaces and thus the pore growth by widening and/or coalescence. Pore closure/splitting occurs during the end of stage 2 or the beginning of stage 3. This mechanism is still ascribed to internal stresses which conduct in a second noticeable fiber deformation mode, namely debending. Combined with gravity forces or confining pressure, this fiber debending allows large pores to be closed or split. Upon sample cooling, no more structural observation was recorded suggesting that re-crystallization or thermal shrinkage have limited effected on the measured descriptors.

Furthermore, the morphological analysis of the pore evolution during deconsolidation revealed that pores are predominantly rod-like, blade-like or disk-like oriented parallel to the fiber's principal axis, which is far from the classical spherical shapes used in the predicting models. Finally, analysis of the pore spatial distribution showed that the deconsolidation phenomenon occurs mainly at the laminates interplies. Such results provide useful information for theoretical and numerical models for the prediction of deconsolidation.

References

[1] P. O. Hagstrand, F. Bonjour, and J. A. Månson, "The influence of void content on the structural flexural performance of unidirectional glass fibre reinforced polypropylene composites," *Composites Part A: Applied Science and Manufacturing*, vol. 36, pp. 705–714, 5 2005 (cit. on p. 162).

[2] H. Shi, I. F. Villegas, and H. E. Bersee, "Strength and failure modes in resistance welded thermoplastic composite joints: Effect of fibre-matrix adhesion and fibre orientation," *Composites Part A: Applied Science and Manufacturing*, vol. 55, pp. 1–10, 2013 (cit. on p. 162).

[3] X. Liu and F. Chen, "A Review of Void Formation and its Effects on the Mechanical Performance of Carbon Fiber Reinforced Plastic," *Engineering Transactions*, vol. 64, pp. 33–51, 2016 (cit. on p. 162).

[4] L. Grunenfelder and S. Nutt, "Void formation in composite prepregs–Effect of dissolved moisture," *Composites Science and Technology*, vol. 70, no. 16, pp. 2304–2309, 2010 (cit. on p. 162).

[5] J. Anderson and M. Altan, "Formation of voids in composite laminates: coupled effect of moisture content and processing pressure," *Polymer composites*, 2014 (cit. on p. 162).

[6] B. de Parscau du Plessix, "Analyse et modélisation du développement de porosités lors de la cuisson de pièces composites thermodurcissables hautes performances," Ph.D. dissertation, Université de Nantes, 2016 (cit. on p. 162).

[7] Y. Leterrier and C. G'sell, "Formation and Elimination of Voids During the Processing of Thermoplastic Matrix Composites," *Polymer Composites*, vol. 15, pp. 101–105, 2 1994 (cit. on p. 163).

[8] S. Roychowdhury, J. W. Gillespie, and S. G. Advani, "Volatile-induced void formation in amorphous thermoplastic polymeric materials: I. Modeling and parametric studies," *Journal of Composite Materials*, vol. 35, pp. 340–366, 4 2001 (cit. on p. 163).

[9] H. Shi, I. F. Villegas, and H. E. Bersee, "Analysis of void formation in thermoplastic composites during resistance welding," *Journal of Thermoplastic Composite Materials*, vol. 30, pp. 1654–1674, 12 2017 (cit. on p. 163).

[10] T. K. Slange, L. L. Warnet, W. J. Grouve, and R. Akkerman, "Deconsolidation of C/PEEK blanks: on the role of prepreg, blank manufacturing method and conditioning," *Composites Part A: Applied Science and Manufacturing*, vol. 113, pp. 189–199, 2018 (cit. on p. 163).

[11] M. Lu, L. Ye, and Y. W. Mai, "Thermal de-consolidation of thermoplastic matrix composites-II. "Migration" of voids and "re-consolidation"," *Composites Science and Technology*, vol. 64, pp. 191–202, 2 2004 (cit. on p. 163).

[12] L. Ye, Z. R. Chen, M. Lu, and M. Hou, "De-consolidation and re-consolidation in CF/PPS thermoplastic matrix composites," *Composites Part A: Applied Science and Manufacturing*, vol. 36, pp. 915–922, 7 2005 (cit. on p. 163).

[13] J. Wolfrath, V. Michaud, and J.-A. E. Månson, "Deconsolidation in glass mat thermoplastic composites: Analysis of the mechanisms," *Composites Part A: Applied Science and Manufacturing*, vol. 36, pp. 1608–1616, 12 2005 (cit. on p. 163).

[14] L. Ye, M. Lu, and Y.-W. Mai, "Thermal de-consolidation of thermoplastic matrix composites—I. Growth of voids," *Composites Science and Technology*, vol. 62, no. 16, pp. 2121–2130, 2002 (cit. on pp. 163, 190).

[15] V. Donadei, F. Lionetto, M. Wielandt, A. Offringa, and A. Maffezzoli, "Effects of blank quality on press-formed PEKK/carbon composite parts," *Materials*, vol. 11, 7 2018 (cit. on p. 163).

[16] L. Amedewovo, A. Levy, B. de Parscau du Plessix, J. Aubril, A. Arrive, L. Orgéas, and S. Le Corre, "A methodology for online characterization of the deconsolidation of fiber-reinforced thermoplastic composite laminates," *Composites Part A: Applied Science and Manufacturing*, vol. 167, p. 107 412, 2022 (cit. on pp. 163, 171, 177, 179).

[17] G. P. Martel, A. Levy, and P. Hubert, "Squeeze flow of randomly-oriented strands thermoplastic composites," in *Proceedings of the 19th international Conference on Composite Materials, Montreal, Canada*, 2013, pp. 1864–1872 (cit. on p. 163).

[18] P. Galvez-Hernandez, C. Jimenez-Martin, R. Smith, M. Mavrogordato, V. Maes, T. McMahon, I. Sinclair, and J. Kratz, "In-situ CT of out-of-autoclave composites manufacturing processes," in *International conference on manufacturing of advanced composites*, 2022 (cit. on p. 164).

[19] D. F. Sentis, L. Orgéas, P. J. Dumont, S. R. Du Roscoat, M. Sager, and P. Latil, "3d in situ observations of the compressibility and pore transport in sheet moulding compounds during the early stages of compression moulding," *Composites Part A: Applied Science and Manufacturing*, vol. 92, pp. 51–61, 2017 (cit. on p. 164).

[20] T. Laurencin, P. J. Dumont, L. Orgéas, S. Le Corre, F. Martoia, S. R. du Roscoat, and P. Laure, "3d real time and in situ observation of the fibre orientation during the plane strain flow of concentrated fibre suspensions," *Journal of Non-Newtonian Fluid Mechanics*, p. 104 978, 2022 (cit. on p. 164).

[21] P. Latil, L. Orgéas, C. Geindreau, P. J. Dumont, and S. R. Du Roscoat, "Towards the 3d in situ characterisation of deformation micro-mechanisms within a compressed bundle of fibres," *Composites Science and Technology*, vol. 71, no. 4, pp. 480–488, 2011 (cit. on p. 164).

[22] J. Vilà, F. Sket, F. Wilde, G. Requena, C. González, and J. LLorca, "An in situ investigation of microscopic infusion and void transport during vacuum-assisted infiltration by means of X-ray computed tomography," *Composites science and technology*, vol. 119, pp. 12–19, 2015 (cit. on p. 164).

[23] B. de Parscau du Plessix, P. Lefébure, N. Boyard, S. L. Corre, N. Lefèvre, F. Jacquemin, V. Sobotka, and S. Rolland du Roscoat, "In situ real-time 3d observation of porosity growth during composite part curing by ultra-fast synchrotron X-ray microtomography," *Journal of Composite Materials*, vol. 53, no. 28-30, pp. 4105–4116, 2019 (cit. on p. 164).

[24] S. Hernández, F. Sket, J. Molina-Aldareguı, C. González, J. LLorca, *et al.*, "Effect of curing cycle on void distribution and interlaminar shear strength in polymer-matrix composites," *Composites science and technology*, vol. 71, no. 10, pp. 1331–1341, 2011 (cit. on p. 164).

[25] T. Centea and P. Hubert, "Measuring the impregnation of an out-of-autoclave prepreg by micro-CT," *Composites Science and Technology*, vol. 71, no. 5, pp. 593–599, 2011 (cit. on p. 164).

[26] N. M. Larson, C. Cuellar, and F. W. Zok, "X-ray computed tomography of microstructure evolution during matrix impregnation and curing in unidirectional fiber beds," *Composites Part A: Applied Science and Manufacturing*, vol. 117, pp. 243–259, 2019 (cit. on p. 164).

[27] J. Torres, M. Simmons, F. Sket, and C. González, "An analysis of void formation mechanisms in out-of-autoclave prepregs by means of x-ray computed tomography," *Composites Part A: Applied Science and Manufacturing*, vol. 117, pp. 230–242, 2019 (cit. on p. 164).

[28] H. Perez-Martin, P. Mackenzie, A. Baidak, C. M. Ó. Brádaigh, and D. Ray, "Crystallinity studies of PEKK and carbon fibre/PEKK composites: A review," *Composites Part B: Engineering*, vol. 223, p. 109 127, 2021 (cit. on p. 165).

[29] J. Avenet, "Assemblage par fusion de composites à matrice thermoplastique: caractérisation expérimentale et modélisation de la cinétique d'auto-adhésion hors équilibre," Ph.D. dissertation, Université de Nantes (UN), 2021 (cit. on p. 165).

[30] H. Pérez-Martín, P. Mackenzie, A. Baidak, C. M. Ó. Brádaigh, and D. Ray, "Crystallisation behaviour and morphological studies of PEKK and carbon fibre/PEKK composites," *Composites Part A: Applied Science and Manufacturing*, p. 106 992, 2022 (cit. on p. 165).

[31] L. Amedewovo, A. Levy, B. de Parscau du Plessix, L. Orgéas, and S. Le Corre, "Online characterization of moisture transport in a high-performance carbon fiber-reinforced thermoplastic composite at high temperatures: Identification of diffusion kinetics," *Composites Part B: Engineering*, vol. 256, p. 110 629, 2023 (cit. on pp. 166, 189).

[32] COMSOL Multiphysics ® v.6.0., COMSOL AB, Stockholm, Sweden, 2022. [Online]. Available: `https://www.comsol.com` (cit. on p. 171).

[33] MATLAB (R2022a), Natick, Massachusetts, 2022 (cit. on p. 172).

[34] D. Paganin, S. C. Mayo, T. E. Gureyev, P. R. Miller, and S. W. Wilkins, "Simultaneous phase and amplitude extraction from a single defocused image of a homogeneous object," *Journal of microscopy*, vol. 206, no. 1, pp. 33–40, 2002 (cit. on p. 173).

[35] J. Schindelin *et al.*, "Fiji: an open-source platform for biological-image analysis," *Nature methods*, vol. 9, no. 7, pp. 676–682, 2012 (cit. on p. 173).

[36] Z. Yaniv, B. C. Lowekamp, H. J. Johnson, and R. Beare, "SimpleITK image-analysis notebooks: a collaborative environment for education and reproducible research," *Journal of digital imaging*, vol. 31, no. 3, pp. 290–303, 2018 (cit. on p. 173).

[37] I. Arganda-Carreras, V. Kaynig, C. Rueden, K. W. Eliceiri, J. Schindelin, A. Cardona, and H. S. Seung, "Trainable Weka Segmentation: a machine learning tool for microscopy pixel classification," *Bioinformatics*, vol. 33, pp. 2424–2426, 15 2017 (cit. on p. 174).

[38] T. Zingg, "Beitrag zur schotteranalyse," Ph.D. dissertation, ETH Zurich, 1935 (cit. on p. 175).

[39] V. Angelidakis, S. Nadimi, and S. Utili, "Elongation, flatness and compactness indices to characterise particle form," *Powder Technology*, vol. 396, pp. 689–695, 2022 (cit. on p. 175).

[40] B. L. Rhoads, "Characterization of fluvial sediment," in *River Dynamics: Geomorphology to Support Management*. Cambridge University Press, 2020, pp. 406–410 (cit. on p. 176).

[41] L. Amedewovo. "Supplementary materials associated to deconsolidation experiments performed at ESRF." (2023), [Online]. Available: `https://unclo ud.univ-nantes.fr/index.php/s/Eo54A7yPgW2Fa7x` (visited on 2023) (cit. on pp. 177–178).

[42] J. Favre, "Residual thermal stresses in fibre reinforced composite materials, a review," vol. 1, no. 1, pp. 37–53, 1988 (cit. on p. 190).

[43] P. P. Parlevliet, H. E. Bersee, and A. Beukers, "Residual stresses in thermoplastic composites—A study of the literature—Part I: Formation of residual stresses," *Composites Part A: Applied Science and Manufacturing*, vol. 37, no. 11, pp. 1847–1857, 2006 (cit. on p. 190).

[44] M. M. Shokrieh, *Residual stresses in composite materials*. Woodhead publishing, 2014 (cit. on p. 190).

[45] A. Gent, "Cavitation in rubber: a cautionary tale," *Rubber Chemistry and Technology*, vol. 63, no. 3, pp. 49–53, 1990 (cit. on p. 190).

[46] C. O. Horgan and D. A. Polignone, "Cavitation in Nonlinearly Elastic Solids: A Review," *Applied Mechanics Reviews*, vol. 48, no. 8, pp. 471–485, 1995 (cit. on p. 190).

[47] M. Coulson, L. Quiroga Cortés, E. Dantras, A. Lonjon, and C. Lacabanne, "Dynamic rheological behavior of poly (ether ketone ketone) from solid state to melt state," *Journal of Applied Polymer Science*, vol. 135, no. 27, p. 46 456, 2018 (cit. on p. 190).

"This page left intentionally blank"

CHAPTER 7

A PARAMETRIC STUDY OF THE DRIVING MECHANISMS OF CF/PEKK LAMINATES DECONSOLIDATION

Contents

Abstract

Although high-performance Carbon Fiber-Reinforced ThermoPlastics (CFRTPs) are promising material for aircraft applications, their processing techniques are not always as well established as those developed for thermoset matrix composites. The basic processing steps of prepreg-based CFRTPs includes heating, consolidation and cooling to produce blank laminates. The pre-consolidated laminates often require subsequent manufacturing steps such as welding or post-forming during which they are subjected to a re-heating/cooling cycle. When a low or no pressure is applied during the re-heating stage, pores may appear and grow in the composite leading to deconsolidation. Although the detrimental effect of deconsolidation on the composites mechanical properties is widely reported, the understanding and control of the phenomenon is still under investigations. This experimental work investigates the driving mechanisms of deconsolidation in CF/PEKK laminates produced by Hot Press and Vacuum Bag Only consolidation. Several potential influencing factors such as moisture, residual stresses and processing conditions (heating rate, pressure, plies orientation) are investigated through post-process measurements (thickness and micrographs) and *in situ* measurements, during deconsolidation experiments on a specially developed COmposite DEconsolidation Characterization (CODEC) device. The experimental results revealed that residual stresses loading is the driving mechanism of CF/PEKK laminates deconsolidation.

Although the previous study (Chapter 6) at the fibers and sample scale allowed to identify the involved mechanisms that occur in the composite during processing, it does not clearly highlight the driving force of deconsolidation. In this chapter, the driving mechanisms of CF/PEKK deconsolidation are investigated through a parametric study. This chapter not only investigates the effect of moisture and residual stresses but also the influence of the pre-consolidation process of the laminates and the post-processing conditions such as heating rate, dwell time, plies orientation and pressure. The conditions of deconsolidation occurrence are finely characterized using the CODEC device.

7.1 Introduction

There is a growing interest in the aerospace industry to use high-performance Thermo-Plastic Composites (TPCs) for structural applications. TPCs have several benefits such as the unlimited shelf (storage) life in ambient conditions, their ability to be re-melt and re-processed, their good mechanical properties and chemical resistance which meet the aeronautical specifications. Several research and development projects are therefore devoted to developing rapid and reliable out of autoclave consolidation of TPCs and welding technologies for large aircraft structures.

During manufacturing and assembly, TPCs may experience deconsolidation. Deconsolidation is the appearance and growth of pores during processing of pre-consolidated TPC laminates. It occurs when a low or no external pressure is applied during the heating stage of the laminates and results in a final composite part with a non negligible porosity content. Several works have already shown a significant degradation of mechanical properties when the porosity content in the composite is over a critical volume content [1–3]. In order to avoid this detrimental effect of pores, deconsolidation should be prevented during TPC laminates processing. This requires an improved understanding and subsequent quantification of the physical mechanisms governing deconsolidation.

There are two main hypothesis in the literature to explain TPC laminates deconsolidation. According to the first assumption, deconsolidation is due to volatile substances such as moisture evaporation and/or diffusion during heating. This hypothesis was mainly highlighted in engineering TPCs such as Carbon Fiber (CF)/PolyAmide6 (PA6), Glass Fiber (GF)/PolyPropylene (PP), GF/PolyEtherImide

(PEI) [4–6] which are known for their high moisture uptake. Although the low moisture uptake in most advanced TPCs such as CF/PolyEtherEtherKetone (PEEK) or CF/PolyEtherKetoneKetone (PEKK), moisture has also been highlighted by Slange *et al.* [7] as the driving mechanism of deconsolidation for UniDirectional (UD) CF/PEEK laminates. The authors subsequently recommended to dry the CF/PEEK laminates at 250 °C for 3 hours prior to processing in order to desorb any residual moisture.

The second hypothesis assumed that TPC laminates deconsolidation is due to the residual stresses initially trapped in the laminates after their consolidation. This hypothesis was mainly highlighted in woven and mat TPCs (CF/PolyPhenylene Sulfide, GF/PolyEthylene Glycol) [8–10] which are known for their ability to store elastic energy due to the fiber bed compressibility and undulating fiber bundles (woven fabrics). Although less elastic energy is stored in the fiber bed of unidirectional prepreg-based laminates, compared to woven fabrics, residual stresses as the driving factor of deconsolidation has been highlighted by Donadei *et al.* [11] for UD CF/PEKK laminates. Here, the authors recommended to anneal the CF/PEKK laminates at 240 °C for 20 hours prior to processing in order to relax residual stresses.

It is surprising that deconsolidation has a different origin in CF/PEKK and CF/PEEK, since both material systems have similar moisture-related properties (moisture diffusivity and moisture uptake) [12–15] and can be processed in similar conditions (heating rate, temperature and pressure). In the work of Slange *et al.* [7], the Cross-Ply (CP) $[0/90]_{4s}$ laminates were consolidated at 386 °C under 1 MPa and cooled at 2.5 °C/min in a Hot Press, then tested in an convection oven. The Quasi Isotropic (QI) $[-45/90/45/0]_{3S}$ laminates used in Donadei *et al.* work [11], were rather consolidated at 375 °C under 0.6 MPa in an autoclave, then tested in an infrared oven.

The different conclusions obtained in the literature suggest that both moisture and residual stresses may be involved in the deconsolidation phenomenon. However, the post-process techniques (thickness measurement, micrographs, *etc.*) mainly used to characterize deconsolidation in these studies [7, 11] do not allow *in situ* analysis of involved mechanisms during heating and dwell [16]. Shrinkage and crystallization phenomena that occur during cooling, may affect the final thickness of the material. The ThermoMechanical Analysis (TMA) used in Slange *et al.* [17] allows online measurements under representative heating cycles applied to a small lab scale sample

(8 mm × 8 mm). However, deconsolidation may be affected by free stress edges, if the sample size is not representative of a laminate structure [16]. An online characterization of deconsolidation in representative conditions is thus required to have a deeper insight about the mechanisms involved during deconsolidation of high-performance TPCs.

The CODEC bench developed and validated in a previous work [16], enables continuous and online characterization of deconsolidation in samples of sizes representative of a structure and under representative processing conditions. In this work, the CODEC device is used to characterize experimentally the deconsolidation of high-performance CF/PEKK laminates. UniDirectional (UD), Cross-Ply (CP) and Quasi Isotropic (QI) laminates produced by both Hot Press (HP) and Vacuum Bag Only (VBO) consolidation are considered in order to investigate the effect of pre-consolidation process and plies orientation on deconsolidation.

As moisture and residual stresses have been identified as the most likely deconsolidation mechanisms, the laminates were subjected to different preconditioning treatment to decouple these two effects. Deconsolidation is quantified by post-process analysis (thickness measurements and micrographs) and online measurements provided by CODEC. The test results give insights about the physical mechanisms governing deconsolidation.

7.2 Material and Methods

7.2.1 CF/PEKK laminates pre-consolidation

Unidirectional laminates were consolidated from CF/PEKK 7002 prepregs plies supplied by Toray Advanced Composite. The plies have a Fiber Areal Weight (FAW) of 194 g/m^2 and a theoretical thickness of 0.185 mm. The resin mass content is 34 %. The glass transition temperature (T_g), melting temperature (T_m) and crystallization temperature (T_c) of PEKK 7002 are respectively 160 °C, 337 °C, and 265 °C (according to the manufacturer). In practice, the melting zone, observed during Differential Scanning Calorimetry (DSC) experiments, extends between 310 °C and 360 °C, with a melting point at 338 °C. In anisothermal conditions (cooling rate: 10 °C/min), the crystallization zone extends between 240 °C and 283 °C with a crystallization peak at 269 °C (assuming no transcrystallization phenomena). This melting and crystallization range can be found in [18–20].

From the prepreg plies, the laminates were manufactured by Hot Press (HP), and Vacuum Bag Only (VBO) consolidation, according to the procedure listed below:

- **Hot Press (HP) consolidation**. 348 mm × 348 mm prepreg plies were stacked in a picture-frame mold (internal cavity dimensions: 350 mm × 350 mm) and consolidated in a 50 t Pinette P.E.I press according to the following cycle: heating at 10 °C/min up to 380 °C under a pressure of 0.1 MPa; isothermal holding for 20 min under a pressure of 4 MPa; cooling at 10 °C/min at the same pressure, then demolding. The final part dimensions after consolidation are 350 mm × 350 mm × 2.90 mm. This final size of the laminate is due to the high pressure and the clearance between the plies and the internal cavity of the mold.
- **Vacuum Bag Only (VBO) consolidation**. 350 mm × 350 mm prepreg plies were stacked on a thick steel tool. The lay-up was covered by high-temperature thermalimide release films (Kapton) then a breather (porous glass cloth). The stacking (films and breather) was covered by a high-temperature thermalimide vacuum bag which is sealed to the periphery of the tool with a ultra-high temperature (up to 426 °C) silicone rubber sealant. The vacuum bag provides the membrane pressure (0.1 MPa) to the laminate during consolidation. The whole setup was placed in an oven for the consolidation process. The oven ensures a homogeneous temperature and therefore limits thermal gradients within the laminate during the consolidation. The laminate was heated, by convection at 2 °C/min up to 380 °C and held at this temperature for 30 min. It was then cooled by convection at roughly 2 °C/min to 80 °C at the same pressure, before demolding. Full vacuum was maintained during the whole cycle. The final part dimensions after consolidation are 350 mm × 350 mm × 2.95 mm. The difference in thickness of 0.05 mm between the VBO and the HP consolidation is due to a few resin squeeze out during HP consolidation.

The stacking sequence of the consolidated laminates are listed in Table 7.1. Optical micrographs of the consolidated laminates validate a porosity content lower than the measurement limit after the consolidation (Figure 7.1). However, a micro-CT analysis of the UD-HP and CP-HP laminates indicated a minor value of the porosity content around 0.02 % [21].

To perform the microscopic observations, 25 mm wide samples were cut from the consolidated laminates. The samples were then encapsulated using a slow-curing

Table 7.1: Stacking sequence of the consolidated laminates.

Consolidation process	Stacking sequence	Label
HP	UD $[0]_{16}$	UD-HP
	Cross-Ply $[0/90]_{4S}$	CP-HP
	Quasi Isotropic $[0/90/+45/-45]_{2S}$	QI-HP
VBO	UD $[0]_{16}$	UD-VBO
	Cross Ply $[0/90]_{4S}$	CP-VBO

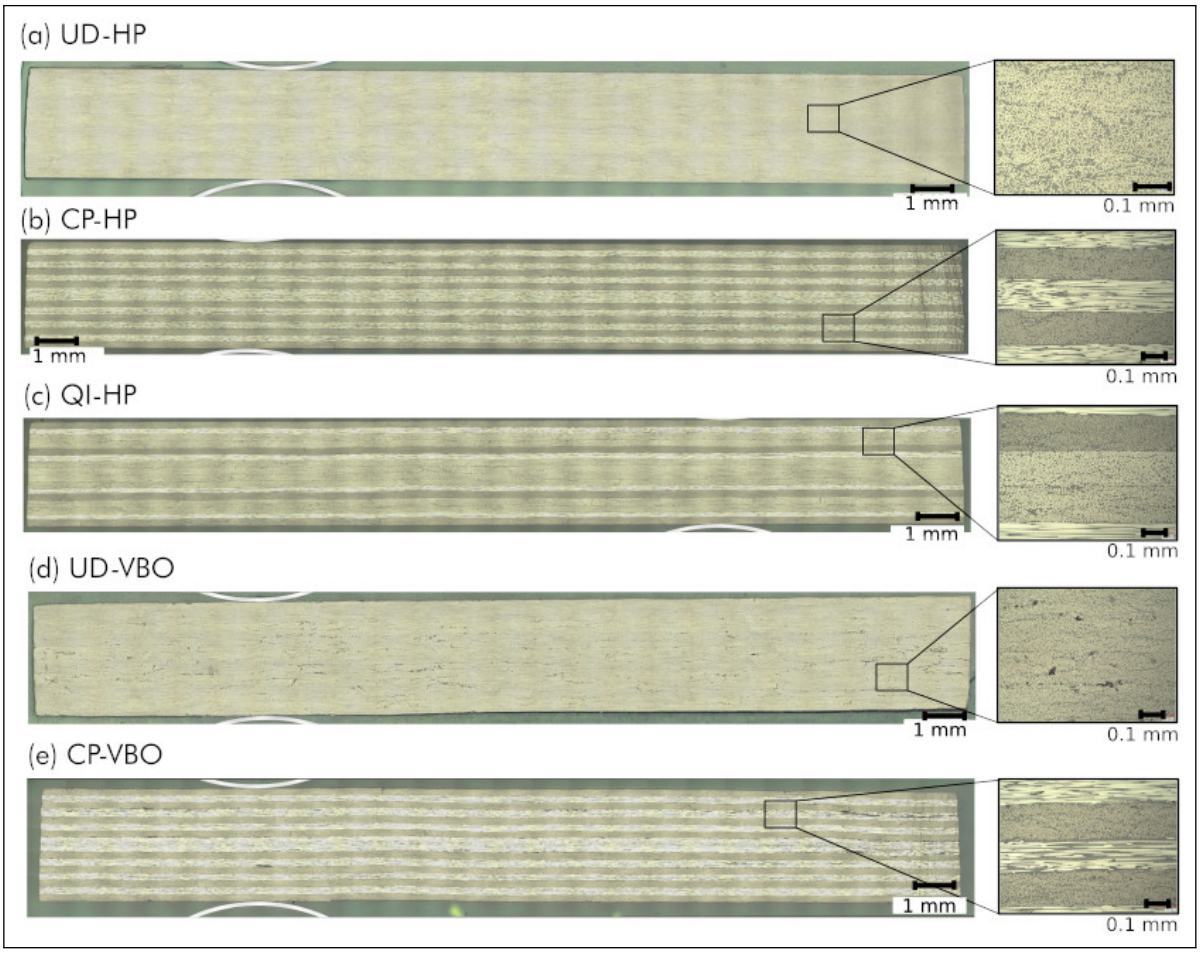

Figure 7.1: Micrographs of the consolidated samples before deconsolidation tests (objective magnification $\times 200$ and resolution 1.55^2 μm^2/pixel). The initial porosity content in the laminates is not measurable.

Table 7.2: Samples preconditioning conditions before deconsolidation tests.

#	Method	Conditions	Duration	Moisture content (Standard deviation)	Label
1	Ambient storage	workshop conditions	5 months	0.01 % (Std: 0.002 %)	AS
2	Water immersion	23 °C / 100 %RH	1 year	0.2 % (Std: 0.08 %)	WI
3	Drying	180 °C	72 hours	-	DS-72H@180C
4	Drying	180 °C	1 week	-	DS-1W@180C
5	Annealing	250 °C	3 hours	-	AN-3H@250C
6	Annealing	250 °C	48 hours	-	AN-48H@250C
7	Annealing	250 °C	5 days	-	AN-5D@250C
8	Annealing + Water immersion	250 °C + 23 °C / 100 %RH	48 hours 1 week	- 0.04 %	AN-48H@250C+WI

epoxy resin (EpoFix, Struers). The sample's surfaces were prepared using traditional grinding and polishing techniques on an automated polishing machine (Tegrapol-21 and TegraForce-5, Struers) and observed on the digital microscope KEYENCE VHX-7000 series. The cross section micrographs were obtained by assembling several sections with a resolution of 2880 pixel × 2160 pixel (objective magnification ×200) resulting in an image with a large area of observation and a good resolution ($\approx 1.55^2$ µm^2/pixel) [16].

7.2.2 Preconditioning

After consolidation, the large laminates were cut into small 125 mm × 25 mm samples using a Protomax waterjet cutting machine. The samples were then subjected to several pretreatments (Table 7.2).

7.2.2.1 Humid environment storage

In order to investigate moisture effect on deconsolidation, one group of samples was conditioned in a wet environment namely ambient environment and immersion in liquid water. The storage in ambient conditions (AS samples) allowed to simulate a long storage time between laminates consolidation and shaping (thermostamping) or assembly (welding) operations. Aging in water immersion (WI samples) allowed to obtain a higher relative moisture content in the samples. The relative moisture content

M_w (%) was estimated from the relative weight gain w (%) after storage:

$$M_w = w = \frac{w_i - w_f}{w_i} \times 100 \tag{7.1}$$

where w_i and w_f are respectively the samples weight after pre-consolidation and after conditioning. Each specimen was weighed before and after conditioning, using a semi-micro weighing scale (Mettler Toledo AG245) with an accuracy of 0.01 mg. The relative moisture content mentioned in Table 7.2 is the average value over 25 samples composed of 5 samples from each laminate group (see Table 7.1 in Section 7.2.1). The 0.01 % and 0.2 % moisture content correspond respectively to a weight gain of roughly 2 mg and 28 mg.

7.2.2.2 Drying

In order to decorrelate moisture effect from residual stresses effect, another group of samples was dried. To define the drying temperature that removes the stored moisture in the samples after consolidation, thermogravimetric tests were performed at different temperatures (140 °C, 180 °C, 200 °C, 250 °C, 300 °C). These tests were performed on the Online Moisture Ingress CHAracterization (OMICHA) bench developed purposely [15]. OMICHA allows to measure online and continuously the weight loss or gain of samples of a size representative of the scale of a structure (up to 150 mm × 150 mm), in a controlled environment. The thermogravimetric tests were performed on samples of 80 mm × 80 mm cut from UD-HP laminates. Before the tests, the samples were stored in ambient conditions for 5 months (as the AS samples). The thermogravimetric tests results showed that drying at 180 °C for 72 hours fully eliminated the moisture stored in the composite [15]. No further significant weight loss was observed at 180 °C over this duration of drying.

Since the drying was performed at a higher temperature than the material's glass transition temperature (T_g ≈160 °C), some residual stress relaxation may occur. A longer drying for 1 week (7 days) was, thus, performed to highlight this effect of residual stresses relaxation at such temperatures.

7.2.2.3 Annealing

In order to further investigate the effect of residual stresses, the last group of sample was annealed at 250 °C for different duration in order to relax the residual stresses (Table 7.2). At this temperature, additional cold crystallization may occur.

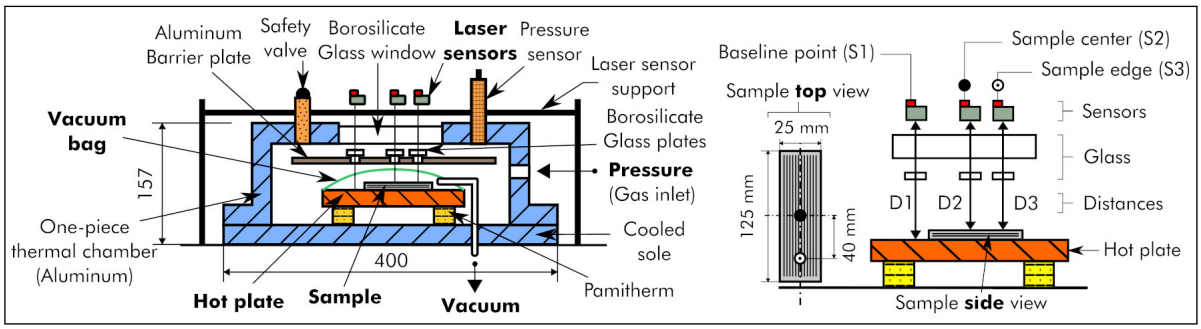

Figure 7.2: CODEC bench designed for continuous and online characterization of thermoplastic composite laminates deconsolidation under processing conditions. Laminate thickness evolution is measured in the chamber with contactless laser sensors. CODEC schematic view (left) and positioning of the contact-less laser sensors (right) [16].

7.2.2.4 Annealing and re-humidifying

After annealing at 250 °C for 48 hours, some samples were re-humidified by storing them in distilled water at room temperature for 1 week (7 days). This preconditioning treatment allowed to highlight the effect of re-humidifying an annealed specimen on deconsolidation. This would reflect the contribution of residual stresses during deconsolidation.

7.2.3 Deconsolidation test

7.2.3.1 CODEC bench

After conditioning, samples were deconsolidated in the COmposite DEconsolidation Characterization (CODEC) bench. This device was developed for continuous and online characterization of large TPC laminates (up to 150 mm × 50 mm) deconsolidation under different processing conditions (pressure, temperature, heating rate, *etc.*) [16]. The CODEC device is composed of a large copper heating plate which can heat up to 450 °C with a maximal heating rate of 60 °C/min. The hot plate is placed in a thermal chamber which can be pressurized up to an absolute pressure of 0.1 MPa (Figure 7.2 left). CODEC is a (deconsolidation) bench that permits continuous thickness measurement (Figure 7.2 right) of a laminate subjected to a thermal cycle under vacuum bag (and potentially counter pressure).

The development and validation of CODEC device was already presented in a previous article [16] where additional details about the methodology for deconsolidation characterization with CODEC are given. The advantage of CODEC device is that

it allows the study of deconsolidation under controlled conditions which are representative of TPC laminates processing. In this study, CODEC was used to perform a parametric study on the mechanisms involved during deconsolidation.

7.2.3.2 Tests conditions

During the deconsolidation experiments, the 125 mm × 25 mm samples were heated at either 60 °C/min, 10 °C/min or 5 °C/min up to 380 °C, then maintained at this temperature for 5 min, and cooled down (natural convection between the sample and air). The first series of deconsolidation tests were performed without any counter pressure. This means that samples were let free under atmospheric pressure in the thermal chamber (no vacuum or external pressure was applied). The test conditions corresponding to the experiments at No Counter Pressure (NCP) are shown in Table 7.3. Only UD-HP laminates were subjected to all the preconditioning treatments. Based on the results obtained with these laminates, the other laminates were only subjected to four preconditioning treatments. Furthermore, the tests with three different heating rate were carried out only on some samples (UD-HP and UD-VBO) with two preconditioning (AS and DS-72H@180C). The objective was to check whether the observations made at 60 °C/min and 10 °C/min are extendable to other heating rates (5 °C/min).

In order to study the effect of pressure on deconsolidation, some deconsolidation tests were performed at 10 °C/min but under different counter pressure. First, samples were processed under vacuum bag only (see Figure 7.2 in Section 7.2.3).

Second, other samples were processed under autoclave conditions. In this case, the samples were maintained under vacuum in the bag and an inert gas (Argon) was injected in the thermal chamber to increase the counter pressure up to an absolute value (0.2, 0.3, and 0.5 MPa). During these experiments, the counter pressure was maintained during the whole heating cycle. The tests conditions for these experiments under counter pressure are reported in Table 7.4. Pressure effect was investigated only on UD laminates.

7.2.3.3 Post-process thickness measurement

After completion of the deconsolidation experiments, an average deconsolidation strain was calculated by thickness measurements at five measurement points on the specimens with a micrometer of 0.01 mm accuracy. One point was located on the

Table 7.3: Deconsolidation tests conditions with No Counter Pressure (NCP).

Stacking	Conditioning	Sample	Heating rate (°C/min)
UD	WI	UD-HP, UD-VBO	10, 60
	AS	UD-HP, UD-VBO	5, 10, 60
	DS-72H@180C	UD-HP, UD-VBO	5, 10, 60
	DS-1W@180C	UD-HP	10
	AN-3H@250C	UD-HP, UD-VBO	10
	AN-48H@250C	UD-HP	10
	AN-5D@250C	UD-HP	10
	AN-48H@250C+WI	UD-HP	10
CP	WI	CP-HP, CP-VBO	10, 60
	AS	CP-HP, CP-VBO	10, 60
	DS-72H@180C	CP-HP, CP-VBO	10, 60
	AN-3H@250C	CP-HP, CP-VBO	10, 60
QI	WI	QI-HP	10, 60
	AS	QI-HP	10, 60
	DS-72H@180C	QI-HP	10, 60
	AN-3H@250C	QI-HP	10, 60

Table 7.4: Deconsolidation tests conditions for the study of pressure effect.

Sample	Conditioning	Counter pressure (MPa)	Heating rate
UD-HP	WI	vacuum bag + 0.5	10 °C/min
UD-HP	AS	vacuum bag + 0.2, 0.3, 0.5	10 °C/min
UD-HP	DS-72H@180C	0.1, vacuum bag + 0.5	10 °C/min
UD-VBO	WI	0.1	10 °C/min
UD-VBO	DS-72H@180C	0.1	10 °C/min

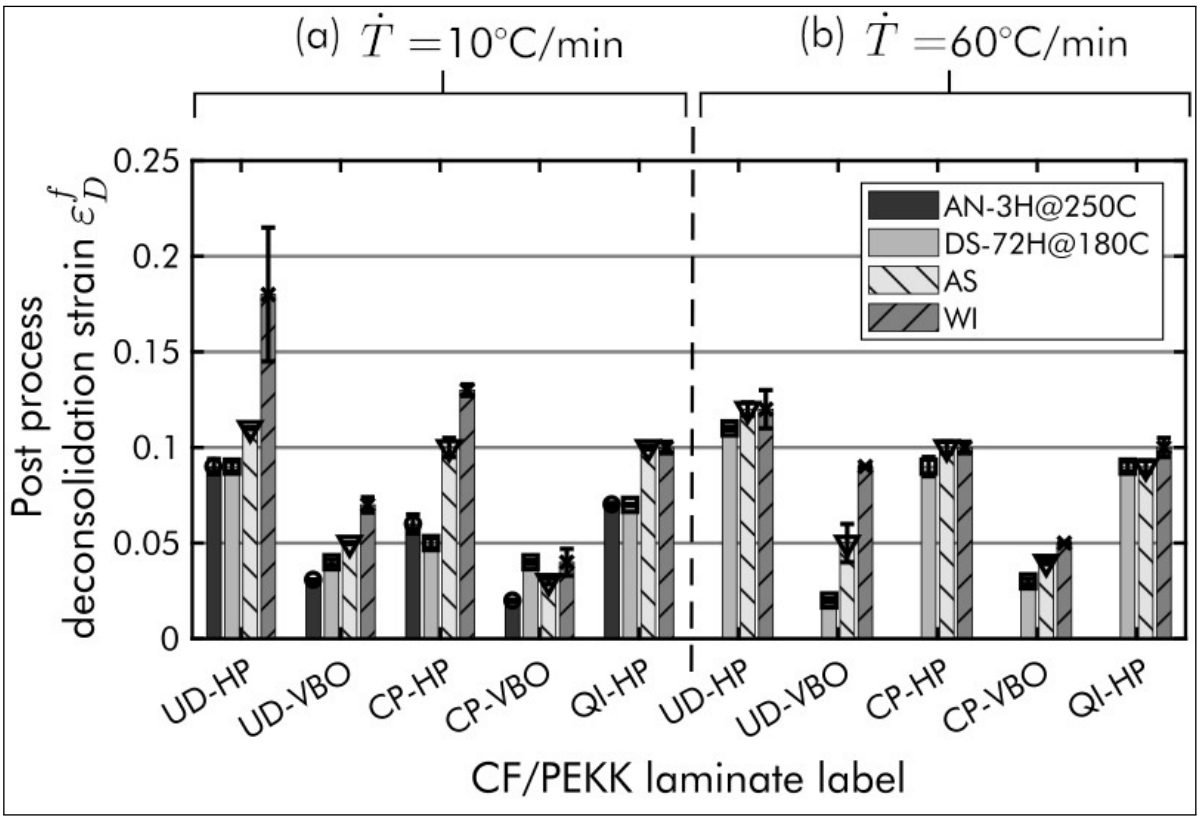

Figure 7.3: Post-process deconsolidation strain ε_D^f of the deconsolidated samples at 10 °C/min (a) and 60 °C/min (b) under No Counter Pressure (NCP).

sample center and the others were spaced 20 mm on each side of the center. In this case, the post-process deconsolidation strain ε_D^f was estimated at each point [16] as:

$$\varepsilon_D^f = \ln\left(\frac{L_f}{L_0}\right) \tag{7.2}$$

where L_f is the final sample thickness after the deconsolidation experiment, and L_0 the sample initial thickness before the test.

7.3 Results and analysis

7.3.1 Post-process analysis

7.3.1.1 Thickness measurement

Figure 7.3 shows the average ε_D^f of the three repetitions performed for each test condition. The error bar indicates the standard deviation. On Figure 7.3, ε_D^f is only estimated for annealed (AN-3H@250C), dried (DS-72H@180C) and wet (AS and WI)

samples at two different heating rates (10 °C/min and 60 °C/min). The objective is to assess if the analysis by thickness measurement can allow to highlighted the driving mechanisms of deconsolidation. For this purpose, the different factors investigated in this study namely moisture, plies orientation, pre-consolidation process, annealing and pressure are examined one by one.

Effect of moisture First, with respect to the samples initially consolidated in Hot Press (HP), it appears in the case of UD-HP and CP-HP samples that the increase in moisture content leads to an increase of ε_D^f at 10 °C/min (Figure 7.3 a). Only QI-HP samples did not show any sensitivity to increasing moisture content. Based on these results obtained at 10 °C/min solely, it appears that moisture is the predominant factor of UD-HP and CP-HP laminates deconsolidation while in the case of QI-HP laminates, deconsolidation may be attributed to another factor.

However, when the heating rate is higher (60 °C/min), there are no significant differences between the ε_D^f of dried (DS-72H@180C) and wet (AS and WI) samples (Figure 7.3 b). In fact, the strain difference $\Delta\varepsilon_D^f$ between the DS-72H@180C and WI samples drops from 0.09 m/m at 10 °C/min to 0.01 m/m at 60 °C/min for UD-HP samples. The same trend is observed for CP-HP and QI-HP samples. This shows, first, that deconsolidation of HP laminates is heating-rate dependent. Secondly, moisture has a non negligible effect only at a low heating rate (10 °C/min) and only in UD and CP laminates.

Second, contrary to UD-HP and CP-HP samples, the increase of moisture content in UD-VBO and CP-VBO samples does not lead to a significant increase of the deconsolidation strain ε_D^f at 10 °C/min (Figure 7.3 a) as in QI-HP samples. The strain difference $\Delta\varepsilon_D^f$ between DS-72H@180C and WI samples is only 0.03 m/m in average. This means that contrary to HP samples, moisture has a limited effect at a rather low heating rates in VBO samples. This behavior is strange on a physical point of view.

Furthermore, at 60 °C/min, the difference $\Delta\varepsilon_D^f$ between dried and wet samples did not decrease but rather increased (Figure 7.3 b). This time, the difference $\Delta\varepsilon_D^f$ between the DS-72H@180C and WI samples rises from 0.03 strain at 10 °C/min to 0.07 m/m at 60 °C/min for UD-VBO samples. These observations on UD-VBO and CP-VBO samples also suggest that deconsolidation is heating rate dependent but now moisture has a non negligible effect only at high heating rates and only in UD laminates.

At this stage, the analysis by thickness measurement shows two opposite results regarding the effect of moisture in the HP and VBO samples.

Effect of plies orientation Another factor investigated in this study is the effect of plies orientation in the laminates on the composite deconsolidation. At 10 °C/min, the post-process deconsolidation strain ε_D^f of the HP samples preconditioned in water (WI) decreases when all the plies of the laminate are not oriented in the same direction (Figure 7.3 a). In fact there is a difference $\Delta\varepsilon_D^f$ of 0.05 m/m and 0.08 m/m between WI UD-HP and respectively WI CP-HP and WI QI-HP. The same behavior is observed with WI VBO samples but at 60 °C/min (Figure 7.3 b). With respect to DS and AS samples, a negligible effect of plies orientation is noticed at both heating rates.

These results thus suggest that plies orientation has an effect on deconsolidation only when the samples have a high initial moisture content (0.2 wt.%).

Effect of pre-consolidation process Before the deconsolidation experiments, the laminates were consolidated by two different consolidation process namely Hot Press (HP) consolidation and Vacuum Bag Only (VBO) consolidation. With the same stacking sequence, the HP samples have a higher ε_D^f than VBO samples regardless of the heating rate. The pre-consolidation process thus seems to be of prominent importance.

Effect of annealing In order to highlight the effect of residual stresses on deconsolidation, some groups of samples were subjected to annealing treatments (see Table 7.2 in Section 7.2.2). In all the experimental conditions, there is not a significant difference ($\Delta\varepsilon_D^f = 0.01$ strain) between the ε_D^f of AN-3H@250C samples and DS-72H@180C (Figure 7.3 a). Nevertheless, ε_D^f decreases significantly ($\Delta\varepsilon_D^f = 0.06$ m/m) when the drying (DS-1W@180C) or annealing (AN-48H@250C, AN-5D@250C) time is longer (Figure 7.4 a). This means that the annealing at 250 °C for 3 hours was not effective to relax the residual stresses. In addition, the decrease of ε_D^f after drying at 180 °C for one week (DS-1W@180C) suggests that there may be significant stress relaxation after a long drying at such temperature.

Although ε_D^f is very small (< 0.05 m/m) after these long duration annealing or drying pretreatments, there is no indication at this stage that pores are absent in these samples. Nevertheless, this result suggests a significant impact of residual stresses and relaxation phenomenon on deconsolidation.

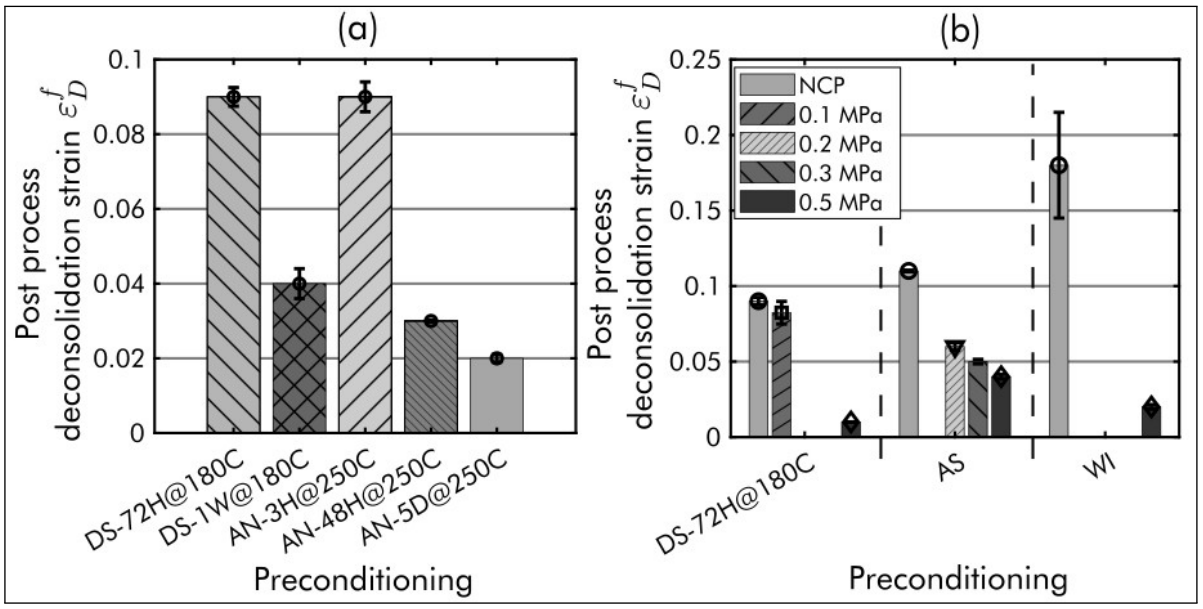

Figure 7.4: Post-process deconsolidation strain ε_D^f obtained for different preconditioning treatments under No Counter Pressure (a) and under different counter pressure (b) for UD-HP laminates tested at 10 °C/min.

Effect of pressure Up to this stage, the analysis concerned the tests performed without counter pressure. In order to investigate the effect of pressure on deconsolidation, some groups of UD-HP laminates were subjected to different counter pressure during the deconsolidation experiments at 10 °C/min. The results of these experiments showed a decrease of the post-process deconsolidation ε_D^f with increasing pressure (Figure 7.4 b). This confirms the mitigating effect of pressure on TPCs deconsolidation.

Finally, the post-process analysis performed by thickness measurements on HP and VBO laminates shows that the mechanisms involved in deconsolidation are heating-rate dependent. The results of these analysis suggest that the mechanisms involved are highly coupled and depend not only on the pre-consolidation process but also on the laminate in-plane strength and stiffness (which depend on the UD plies orientation). However, these analysis do not clearly show the driving mechanism. By considering the opposite results obtained between the HP and VBO samples regarding moisture effect, it is not possible at this stage to know whether deconsolidation is mainly driven by moisture evaporation and/or diffusion or by residual stresses.

In addition, the post-process thickness measurements are severely affected by thermal and crystallization shrinkage which determine the final thickness of samples. Therefore, the driving mechanism of deconsolidation cannot be understood by such a post-process analysis.

7.3.1.2 Micrographs

Micrographs were also performed at the end of the deconsolidation experiments, in order to analyze the micro-structural changes generated by the deconsolidation. The micrographs were carried out according to the procedure describe in Section 7.2.1. The porosity contents were estimated, using the trainable weka segmentation algorithm [22] in an image processing software (Fiji). The porosity content estimation were performed on three sections per sample. The sections were cut exactly at the same location on all the samples in order to performed a comparative analysis of the pores spatial distribution and morphology [16].

As shown on Figure 7.1 in section 7.2.1, the initial porosity content before deconsolidation tests is lower than the measurement limit. This means that the initial porosity content of the sample before deconsolidation is very low ($< 0.1\,\%$) [21]. Figure 7.5 shows the porosity content of some samples after deconsolidation. Again, the effect of the different factors studied (moisture, plies orientaion, *etc.*) on the final porosity content are analyzed hereunder.

Effect of moisture First, contrary to the results provided by the analysis from the thickness measurement, there is no significant difference ($\Delta\%\text{Porosity} \leq 1\,\%$) between the final porosity content of the UD-HP samples stored in ambient conditions (AS) and stored in distilled water (WI) at $10\,^{\circ}\text{C/min}$ (Figure 7.5 a). The same behavior is observed for UD-VBO samples. The micrographs thus show that regardless of the heating rate, an increase in moisture content does not lead to an increase in the post-process porosity content for both HP and VBO samples. Consequently, the significant difference of porosity content ($\Delta\%\text{Porosity} = 7\,\%$) between dried (DS-72H@180C) and wet samples (AS and WI) at $10\,^{\circ}\text{C/min}$ may not be due to moisture effect (Figure 7.5 a).

Second, the micrographs also reveal the heating-rate dependence of TPCs deconsolidation. In fact, the difference in porosity content $\Delta\%\text{Porosity}$ between the DS-72H@180C and WI samples decreases from $7\,\%$ at $10\,^{\circ}\text{C/min}$ to $2\,\%$ at $60\,^{\circ}\text{C/min}$ for HP samples. This difference rather increases from $1\,\%$ at $10\,^{\circ}\text{C/min}$ to $4\,\%$ at $60\,^{\circ}\text{C/min}$ in the case

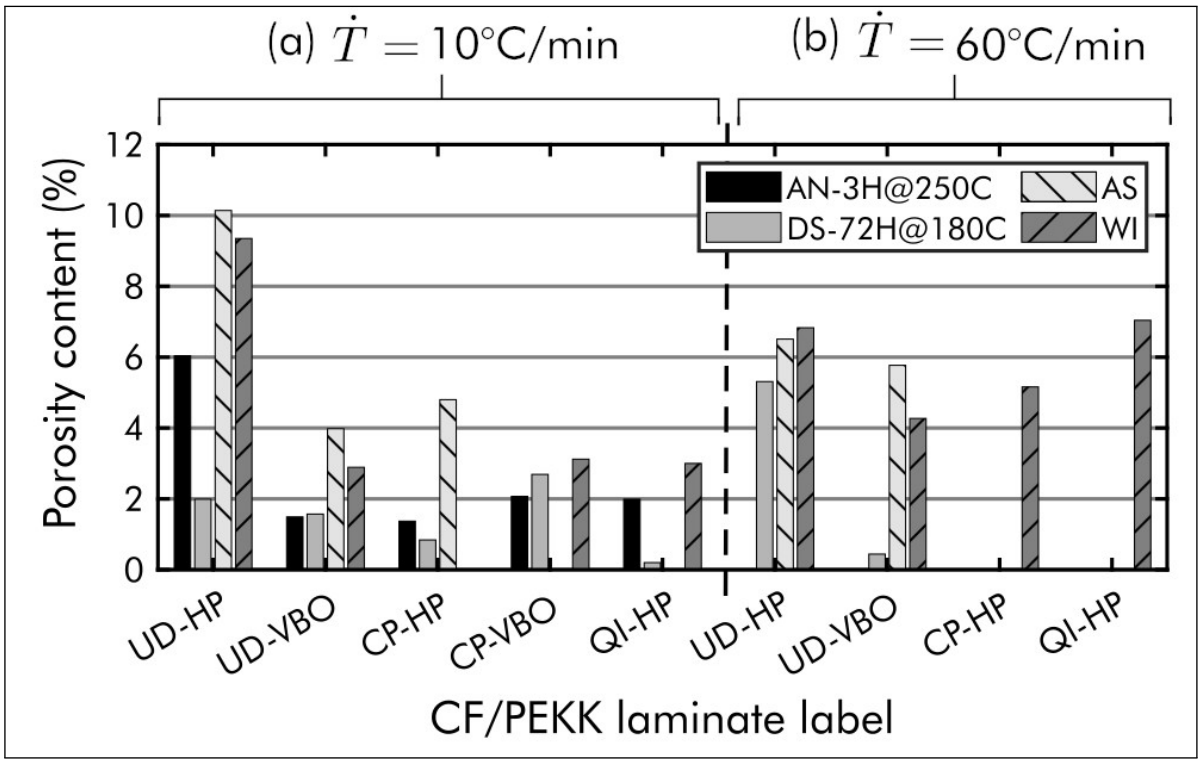

Figure 7.5: Final porosity content of some deconsolidated samples at 10 °C/min (a) and at 60 °C/min (b) under No Counter Pressure (NCP).

of VBO samples (Figure 7.5 b). The post-process micrographs thus supported the post-process thickness measurements analysis regarding the heating rate dependence of the deconsolidation driving mechanism but does not highlighted an effect of moisture contrary to the post-process thickness measurements.

Effect of plies orientation Figure 7.5 (a) shows a decrease of the porosity content in HP samples at 10 °C/min as layup goes from UD to CP to QI. This supports the post-process thickness measurements results which also show a dependence of HP samples deconsolidation on the plies orientation at lower heating rates. However, contrary to the thickness measurements which suggests that this effect is only applicable to WI samples, the micrographs show that this effect is rather extendable to other preconditioning treatments (AS, DS-72H@180C and AN-3H@250C).

Effect of pre-consolidation process There is a significant difference (Δ%Porosity = 6 %) between the porosity content of wet (AS and WI) HP samples and wet VBO samples at 10 °C/min (Figure 7.5 a). However, at 60 °C/min, this difference is more marked

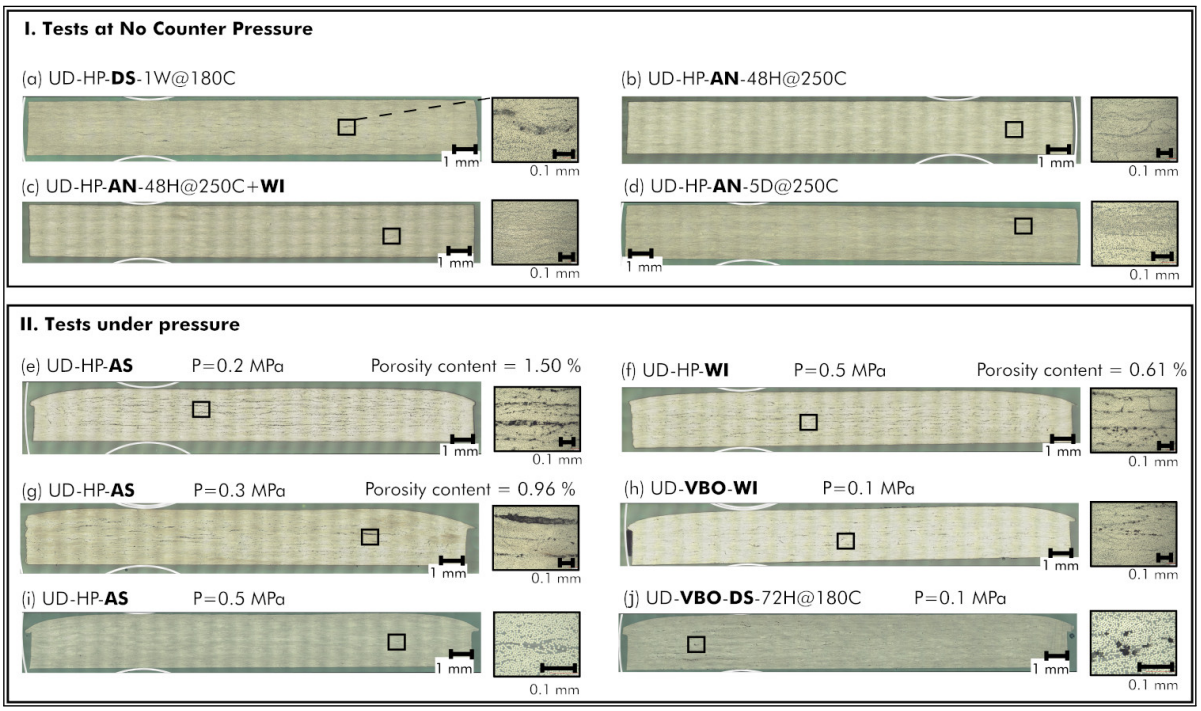

Figure 7.6: Post-process micrographs of UD-HP samples with different preconditioning treatments tested at 10 °C/min under No Counter Pressure (a-d) and under different counter pressure (e-j). Objective magnification ×200 and resolution 1.55^2 µm^2/pixel.

only for dried samples (Δ%Porosity = 5 %) than for wet samples (Δ%Porosity = 2 %). This suggests, again, that the pre-consolidation process has an effect on the samples deconsolidation, but this effect depends on the heating rate and the initial preconditioning. This distinction was not raised by the post-process thickness measurements.

Effect of annealing Figure 7.5 (a) shows that there is not a huge difference (Δ%Porosity = 0.41 %) between the final porosity content of dried (DS-72H@180C) and annealed (AN-3H@250C) samples in most of the tests conditions (UD-VBO, CP-HP, CP-VBO). In some cases (UD-HP and QI-HP), the final porosity content in AN-3H@250C samples is even higher than in DS-72H@180C samples. This confirms that the annealing at 250 °C for 3 hours is not effective to relax the residual stresses. For the other annealing pretreatments (AN-48H@250C and AN-5D@250C) and the long drying at 180 °C for 1 week (DS-1W@180C), the porosity content was lower than the measurement limit (Figure 7.6 a, b, d). This suggests that deconsolidation does not occur with these preconditioning treatments.

Residual stresses have thus a significant impact on TPCs deconsolidation, as indicated by the post-process thickness measurements analysis. In addition, the micrograph of the samples annealed and then stored in distilled water (AN-48H@250C+WI) also shows a porosity content below the measurement limit (Figure 7.6 c). This clearly indicates that moisture is not the driving factor of deconsolidation.

Effect of pressure The application of a counter pressure during the deconsolidation tests leads to a low final porosity content ($< 2\,\%$) in the samples (Figure 7.6 e-j). However, only the VBO samples tested under 0.1 MPa (Figure 7.6 f, h) and the AS UD-HP samples tested under 0.5 MPa (Figure 7.6 i) show a porosity content below the measurement limit. This means that a minimum counter pressure of 0.1 MPa was sufficient to prevent deconsolidation in the case of VBO samples whereas 0.5 MPa is required in the case of HP samples. This observation supports the important impact of the pre-consolidation process on TPCs deconsolidation.

Finally, the post-process analysis through micrographs and thickness measurements agree on the heating-rate dependence of TPCs deconsolidation. They also agree on the major contribution of residual stresses on deconsolidation. However, although both analysis agree on the important impact of the pre-consolidation process, their conclusions diverge on the validity domain of this effect. The final porosity content analysis indicates that the effect of pre-consolidation process depends on the heating rate and initial preconditioning, while the post-process thickness measurements suggests that this effect does not depend on either of these two parameters.

Moreover, their conclusions also diverge on moisture effect. The post-process thickness measurements shows a sensitivity of deconsolidation to moisture content while the porosity content analysis shows none. However, by considering the pores morphology and distribution in the deconsolidated UD-HP and UD-VBO samples for example, there is a clear difference between the wet (AS and WI) and dried (DS-72H@180C) or annealed (AN-3H@250C) samples (Figure 7.7). In wet samples, pores are larger and mainly located in the subsurface of the samples (Figure 7.7 a-d, i-l) whereas in dried or annealed samples pores are smaller and homogeneously located in the middle of the samples (Figure 7.7 e-h, m-n). The same distribution was observed on the CP and QI laminates which post-process micrographs are provided as supplementary materials (Appendix 7.A). This suggests that moisture may have an effect on deconsolidation, especially on the pores spatial distribution in the composite laminates.

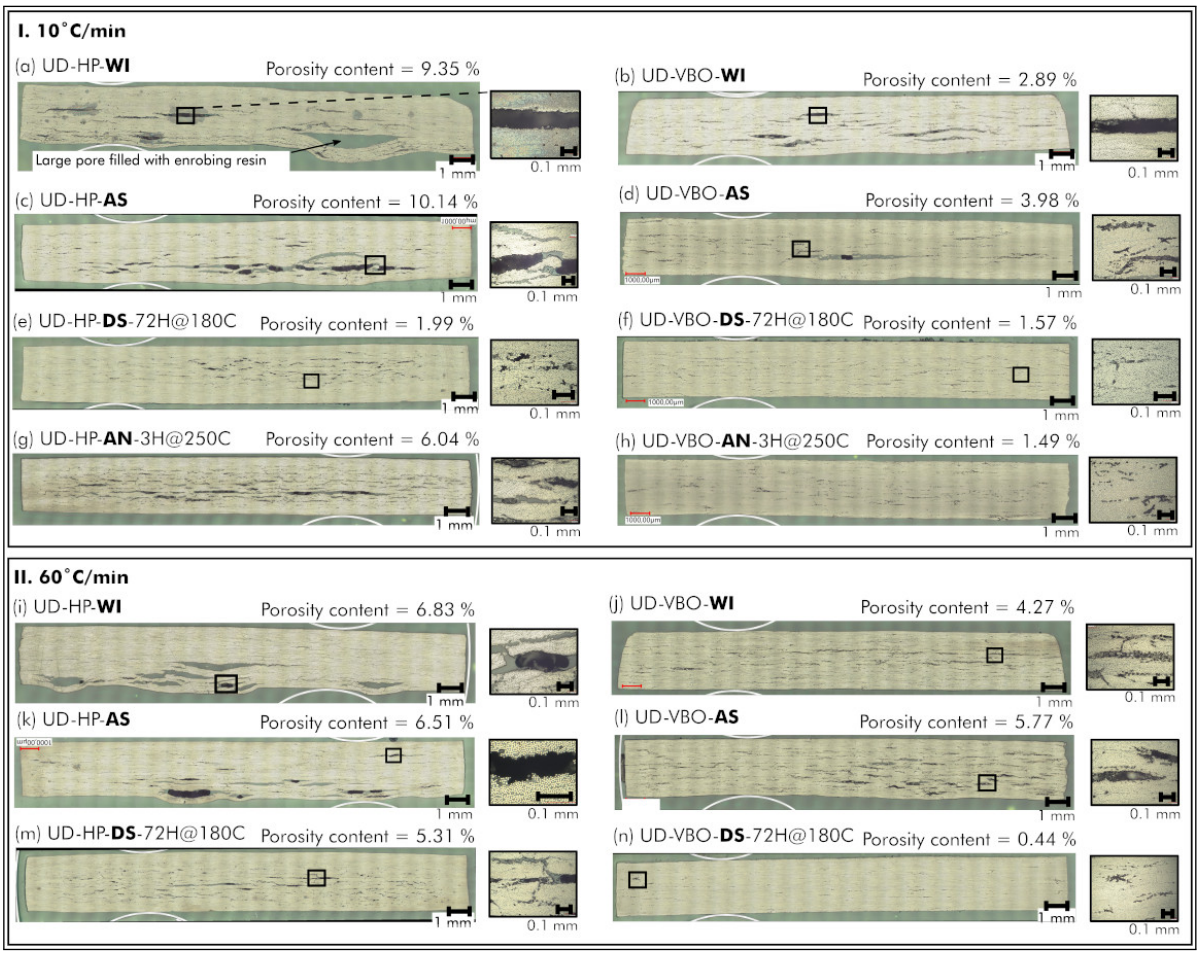

Figure 7.7: Micrographs of deconsolidated UD-HP and UD-VBO samples. After the experiments, the pores morphology and distribution are different between dried (DS-72H@180C) or annealed (AN-3H@250C) samples and wet (AS and WI) samples. Objective magnification $\times 200$ and resolution 1.55^2 µm^2/pixel.

After these post-process analysis, residual stresses appear to be the driving factor of deconsolidation, since a complete or partial relaxation of these stresses during annealing or long drying duration allowed to prevent the phenomenon. Moisture seems to have a negligible effect on the pore growth during deconsolidation, since re-humidifying of completely annealed samples does not lead to a significant porosity content in the sample (Figure 7.6 c). Moisture effect is thus probably limited to the pores location in the composite laminates.

However, as well as the post-process thickness measurement is influenced by shrinkage during cooling, the laminate micro-structure also changes significantly during heating (pore closure or splitting). These micro-structure changes during the compos-

ite laminate processing were highlighted in a previous study by a real-time *in situ* observation of the composite micro-structure evolution by synchrotron X-ray micro-tomography [21]. The final micrographs may be affected by these micro-structural changes during heating. It is thus necessary to characterize deconsolidation online during heating in order to have a deep insight about the involved mechanisms and then validate the results of the post-process micrographs.

CODEC bench was used for this purpose because it enables the deconsolidation to be monitored in real-time during the whole temperature and pressure cycle. The online measurements results, are subsequently analyzed to better understand the mechanisms involved during high-performance TPCs deconsolidation.

7.3.2 Online measurements analysis

Three data were obtained during each deconsolidation experiment on CODEC device (Figure 7.8 a): the copper hot plate temperature (TCc); the sample upper face temperature ($TC2$) and the sample deconsolidation strain ε_D, at the two measurement points calculated from the distance measurements.

Given the unilateral heating in CODEC, deconsolidation is expected to start at the hottest bottom side of the samples. In order to estimate the samples lower face temperature $TC1$, the experimentally measured temperatures TCc and $TC2$ were used as boundary condition in a thermal model developed and validated in Amedewovo *et al.* [16]. $TC1$ is estimated as the average of the simulated temperature field over a thickness corresponding to the three first plies [16].

The deconsolidation strain of the samples can then be plotted versus the lower face temperature (Figure 7.8 b). Unlike the post-process analysis, the sample behavior during heating can be observed thanks to the online and continuous strain measurement. As shown on Figure 7.8, the deconsolidation strain of the sample during heating is much higher than the final strain. The difference $\Delta\varepsilon_D$ between the maximum strain reached by the sample during heating and its final strain after cooling is about 0.14 m/m. The deconsolidation strain evolution observed on Figure 7.8 b is consistent with the one observed during real-time microtomography [21].

The sample behavior during heating can be divided into three stages visible in Figure 7.8 b.

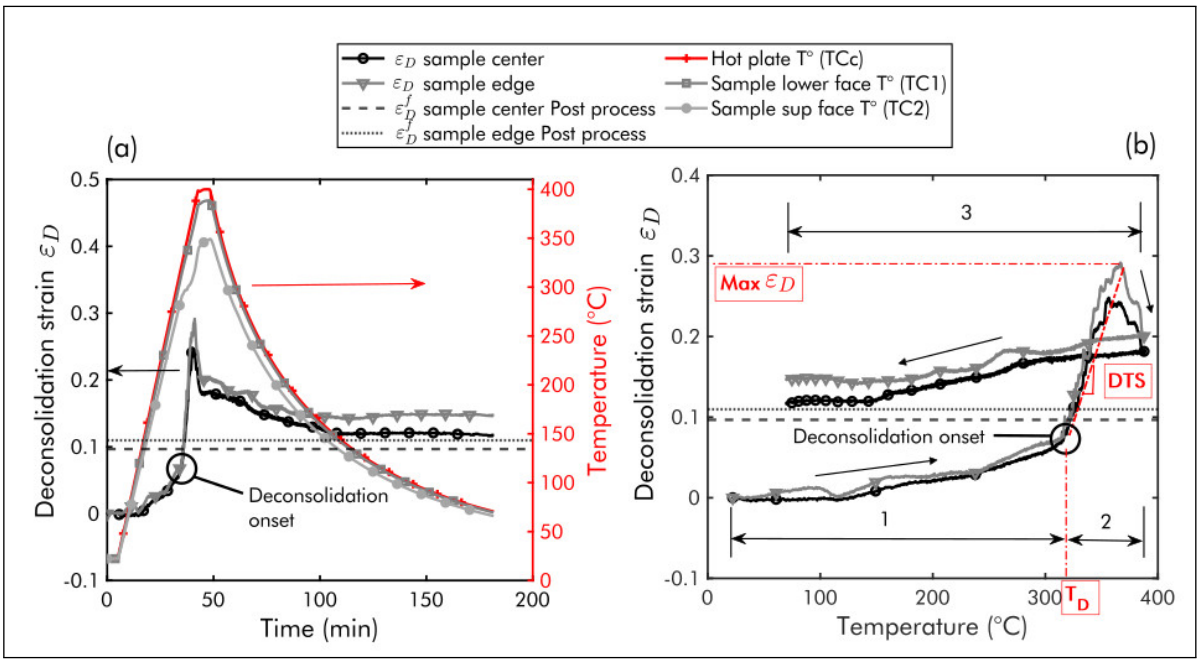

Figure 7.8: Continuous and online deconsolidation monitoring. Through thickness deconsolidation strain ε_D vs time (a) and deconsolidation strain ε_D vs the sample lower face temperature ($TC1$) estimated with the thermal model (b) of a quasi isotropic ($[0/90/+45/-45]_{2S}$) laminate sample consolidated in Hot Press and stored in water at 23 °C for 1 year and then heated at 10 °C/min under No Counter Pressure (NCP).

1. During stage 1, samples experience thermal expansion as the temperature increases until deconsolidation occurs. From that point, a significant slope change is observed on the deconsolidation strain curve.

2. In stage 2, the samples experience deconsolidation which generally extends during the dwell. During this stage, the deconsolidation strain increases significantly (from $\varepsilon_D = 0.07$ to 0.29) and at a strain rate of $\dot{\varepsilon}_D \approx 0.67 \times 10^{-3}$ s^{-1}. This strain increase is followed by a subsequent strain decrease until the beginning of cooling. The strain increase stage corresponds to the pore growth stage and the subsequent strain decrease corresponds to the pore splitting or closure stage during deconsolidation [21]. By observing the evolution of the sample upper face temperature $TC2$, it can be noted that the deconsolidation onset coincides with a regime change in the sample thermal behavior. This regime change can be explained by a decrease in the effective thermal conductivity of the material due to the appearance of large pores. Temperature measurement can thus be a way to detect the deconsolidation onset.

3. In stage 3 corresponding to the cooling step, samples undergo shrinkage due to the polymer matrix crystallization and thermal shrinkage. By comparing the curves obtained at the two measurement points, it can be seen that the maximum difference (Max $\Delta\varepsilon_D$) is 0.05. This difference highlights the heterogeneous nature of deconsolidation in unidirectional prepreg-based laminates. As clear from micrographs (Figure 7.7), macro-pores on the heated side are likely to create macroscopic motion that are recorded by the laser sensors on the top surface.

Furthermore, thanks to the online measurement with CODEC, several characteristic magnitudes related to the dynamic deconsolidation phenomenon could be quantified. These are for instance (Figure 7.8 b): deconsolidation temperature T_D (°C), maximum deconsolidation strain (Max ε_D), Deconsolidation's Thermal Sensitivity (DTS) ($°C^{-1}$) and deconsolidation rate (s^{-1}) [16]. These characteristic magnitudes are temperature and time-related coefficients. In order to identify the predominant factor during deconsolidation, between temperature and time, specific deconsolidation experiments were carried out on UD-HP samples.

7.3.3 Time and temperature-dependence of deconsolidation

The time and temperature-dependence of deconsolidation was first investigated by performing deconsolidation experiments with longer dwell times on UD-HP DS-72H@180C samples (Figure 7.9 a). During these experiments the samples were heated at 60 °C/min up to 380 °C then maintained at this temperature for two different dwell times: 5 min and 25 min. Figure 7.9 (a) shows that dwell time extension has no impact on the deconsolidation strain evolution. Indeed, after 5 min during the dwell, the deconsolidation strain decreases up to a stationary state which remains roughly constant until cooling onset.

Since the strain does not increase during the dwell, the time-dependence during the pore growth seems negligible from these tests. However, after reaching its maximum value (deconsolidation peak) during ramp-up, the deconsolidation strain does not instantly remain constant but rather gradually decreases before reaching a stationary state. This suggests that pore splitting which lead to strain decrease is time-dependent. This statement is further supported by a second experiment.

The second experiment consisted in heating UD-HP AS and DS-72H@180C samples at 60 °C/min up to different dwell temperatures: 312 °C, 322 °C, 338 °C, 370 °C, and

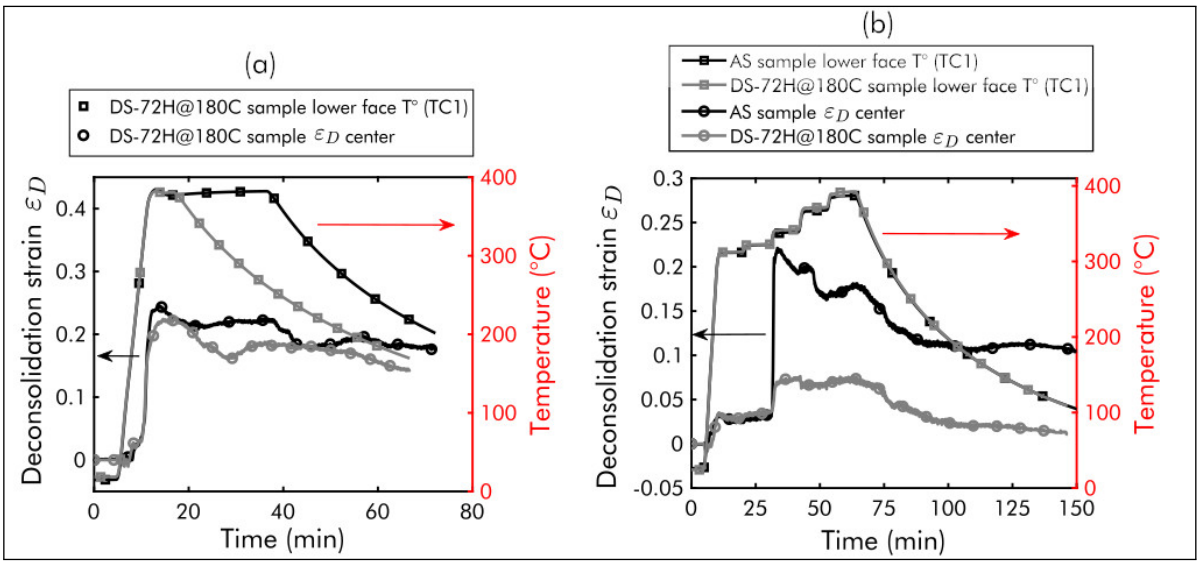

Figure 7.9: Through thickness deconsolidation strain ε_D vs time of DS-72H@180C UD-HP samples tested with two different dwell times at 60 °C/min (a) and deconsolidation strain ε_D vs time of DS-72H@180C and AS UD-HP samples also tested at 60 °C/min but with different dwell temperatures (b).

390 °C (Figure 7.9 b). The dwell time at each temperature was 10 min. Before deconsolidation, the AS and DS-72H@180C samples strain progress in the same way. The strain is almost constant during the first two temperature dwells at 312 °C and 322 °C. Thereafter, deconsolidation occurs during the ramp-up between 322 °C and 338 °C for both samples, leading to a brutal increase ($\dot{\varepsilon}_D \approx 0.25 \times 10^{-2}\,\mathrm{s}^{-1}$) of the samples strain in a short period of time (<2 min). No further deconsolidation is observed in the following increases of temperature. To the contrary, when the temperature is again maintained at 390 °C, the deconsolidation strain of AS samples decreases. Further increase of the temperature does not lead to a significant increase of the deconsolidation strain.

These results show that deconsolidation is initiated at a certain specific temperature but once the mechanism is started, there is no longer any dependence on temperature. Regarding pore splitting, it seems to depend on both time and temperature. It is favored by a softening of the polymer with increasing temperature. The absence of splitting stage with DS-72H@180C samples is probably due to the non appearance of large pores (see Figure 7.7 e, m) which is reflected by the low maximum strain (Max $\varepsilon_D = 0.08\,\mathrm{m/m}$). The initial drying before the tests followed by subsequent dwell at high temperatures (>300 °C) may prevent large pores appearance.

Both experiments show that the whole deconsolidation process is time and temperature-dependent. However, this study mainly focuses on understanding the driving mechanisms of pore growth during deconsolidation. For this reason, only the growth stage during the deconsolidation experiments were further investigated. As shown by the stopped experiments, time effect can be neglected during the growth stage according to the low time scales (minutes). Consequently, only temperature-related characteristic magnitudes such as T_D, DTS, and Max ε_D were selected for the deconsolidation tests results analysis.

7.3.4 Deconsolidation tests results

As for the post-process measurements, the effect of the different factors studied (moisture, plies orientation, *etc.*) on the deconsolidation characteristic magnitudes are examined in this section.

7.3.4.1 Deconsolidation onset temperature

Figure 7.10 shows the onset temperature of deconsolidation T_D of the deconsolidated samples at both heating rates and under No Counter Pressure (NCP). At 10 °C/min, deconsolidation occurs after the melting onset (310 °C) in most samples (Figure 7.10 a). At a high heating rate (60 °C/min), deconsolidation starts earlier (around 300 °C) before the melting onset, mainly in wet (AS and WI) samples (Figure 7.10 b).

Effect of moisture There is no significant difference ($\Delta T_D \leq$2 °C) between the deconsolidation temperature of dried (DS-72H@180C) and AS samples at 10 °C/min. This difference becomes substantial ($\Delta T_D \geq$10°C) in most cases at 60 °C/min. In fact, the average difference ΔT_D between the samples tested at 10 °C/min and 60 °C/min is about 10 °C with dried samples (DS-72H@180C) and 20 °C with AS samples. First, this means that increasing the heating rate leads to an overall decrease of the deconsolidation temperature. Second, the presence of moisture induces an accelerated onset of deconsolidation at high heating rates. Figure 7.10 (WI samples) shows that this accelerated onset in presence of moisture also occurs at low heating rates (10 °C/min) when the initial moisture content is high (0.2 wt.% in our case). Indeed, at both heating rates, the deconsolidation temperature drops by at least 10 °C with increasing moisture content from 0.01 wt.% in AS samples to 0.2 wt.% in WI samples.

Effect of plies orientation Plies orientation does not have a significant effect on deconsolidation temperature at 10 °C/min. The difference ΔT_D between UD samples

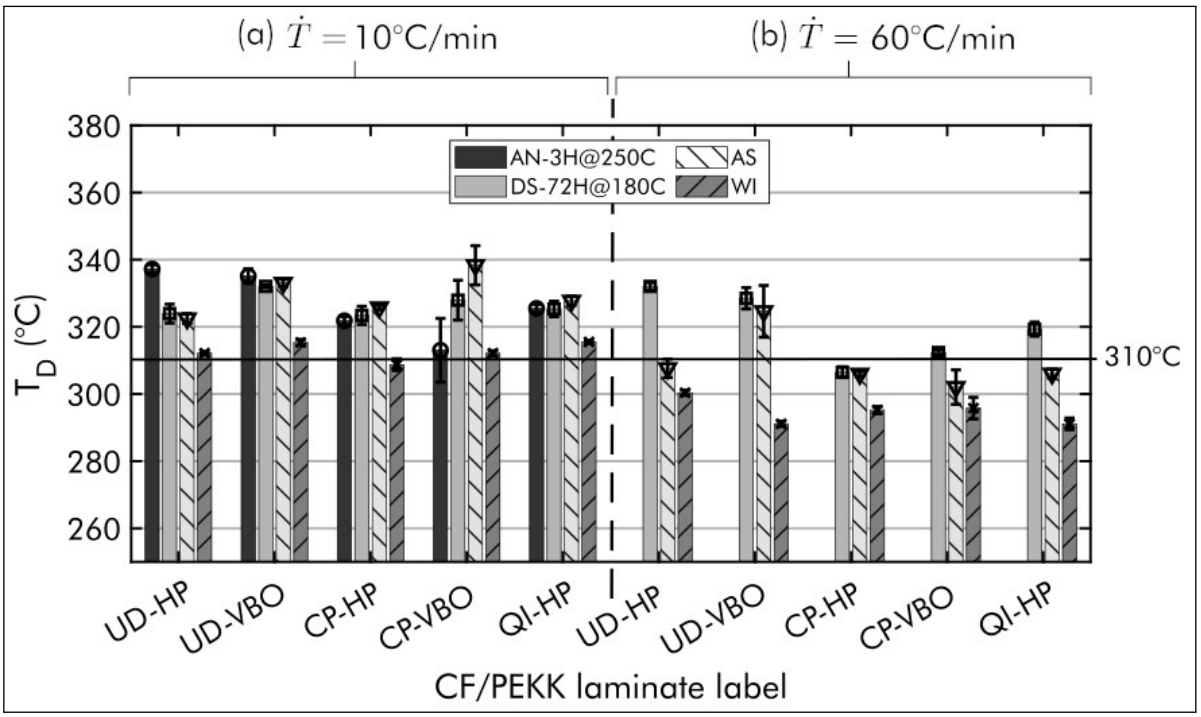

Figure 7.10: Deconsolidation onset temperature T_D of the deconsolidated laminates at two different heating rates and under No Counter Pressure (NCP).

and CP or QI samples at this heating rate is less than 5 °C regardless of the preconditioning treatment and the pre-consolidation process. A non negligible plies orientation effect ($\Delta T_D \geq$20 °C) is only noticed at 60 °C/min, on dried HP samples. In these dried HP samples, the deconsolidation temperature decreases at high heating rate when all the plies of the laminate are not oriented in the same direction. This suggests that plies orientation may affect, at high heating rate, the deconsolidation onset in HP laminates depending on their initial preconditioning.

Effect of pre-consolidation process At both heating rate, the difference ΔT_D between HP and VBO samples exceeds 10 °C only in DS-72H@180C and AS UD samples. Deconsolidation occurs earlier in the UD-HP samples compared to UD-VBO samples. This means that the pre-consolidation process may have an effect on the deconsolidation onset, depending on the plies orientation in the composite laminate.

Effect of annealing In most cases, samples annealing for 3 hours at 250 °C does not lead to a considerable change in deconsolidation onset temperature, compared to the DS-72H@180C samples. Any data regarding the other annealing or long drying

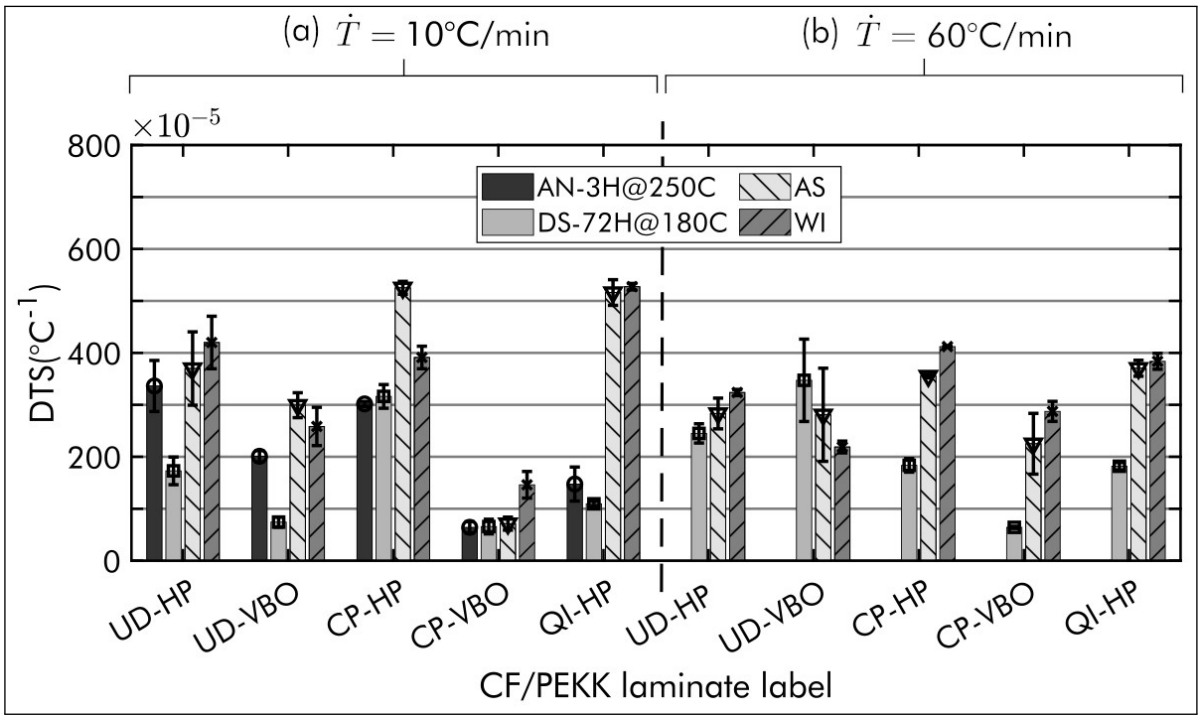

Figure 7.11: Deconsolidation's Thermal sensitivity of the deconsolidated laminates at two different heating rates and under No Counter Pressure (NCP).

pretreatments (AN-48H@250C, DS-1W@180C, *etc.*) was not plotted on Figure 7.10 because deconsolidation does not occur during the experiments with these groups of sample.

From a global point of view at this stage, deconsolidation onset depends mainly on moisture content and heating rate. The presence of moisture or increasing of the heating rate accelerates the deconsolidation onset. Other minor factors such as plies orientation or pre-consolidation process can also influence the deconsolidation onset but only in some specific cases. For example, deconsolidation may occur earlier in UD-HP laminates compared to UD-VBO samples laminates.

7.3.4.2 Deconsolidation's thermal sensitivity

The Deconsolidation's Thermal Sensitivity (DTS) is the sensitivity of the deconsolidation strain ε_D to a temperature variation ΔT. Figure 7.11 shows the DTS related to the deconsolidation experiments performed at both heating rates (10 °C/min and 60 °C/min) under No Counter Pressure (NCP).

Effect of moisture Increasing moisture content does not lead to a major change in the deconsolidation dynamics at both heating rates and in all the testing conditions. The difference ΔDTS between AS and WI samples is in average around $40 \times 10^{-5}\,°C^{-1}$. In some cases (UD-VBO and CP-HP), the DTS of AS samples is even higher than WI samples one (Figure 7.11 a). This observation suggests that moisture does not influence the dynamic deconsolidation behavior of the samples during deconsolidation.

Effect of plies orientation For both heating rates, Figure 7.11 shows a non negligible ($\Delta DTS \geq 100 \times 10^{-5}\,°C^{-1}$) effect of the plies orientation on the deconsolidation dynamics. In VBO samples, DTS decreases when the plies are crossed, regardless of the preconditioning treatment. This is not the case for HP samples where DTS evolution depend mainly on the preconditioning treatment. In wet samples (AS and WI), DTS of CP and QI samples is in average higher or equal to those of UD samples, regardless of the heating rate. However, in dried samples, DTS decreases in general as the samples go from UD to CP to QI. This means that the effect of plies orientation on the deconsolidation dynamics depends on the pre-consolidation process. With a pre-consolidation by VBO, deconsolidation dynamics is more severe in UD samples. This is also the case of HP consolidation, if the samples are pre-dried or annealed. In wet samples, CP and QI samples experience a more severe deconsolidation dynamic than UD ones.

Effect of pre-consolidation process For the same preconditioning treatment there is a significant difference ($\Delta DTS \geq 100 \times 10^{-5}\,°C^{-1}$) between the DTS of HP and VBO samples at both heating rates. In fact, DTS of VBO samples are in majority lower than HP samples one. This means that the deconsolidation dynamics is considerably affected by the sample pre-consolidation process.

Effect of annealing DTS of DS-72H@180C samples are mainly low compared to the wet (AS and WI) samples ones, showing that initial pre-drying significantly slows the deconsolidation dynamics. The same effect is mainly observed with the short time

annealing (3 hours) at 250 °C (Figure 7.11 a). However, DTS increases considerably after annealing in some cases (UD-HP and UD-VBO). This supports the non-effectiveness of this annealing treatment to fully relax residual stresses as suggested in Section 7.3.1.

At this stage, the online measurements results show that the deconsolidation dynamic behavior during heating is not significantly affected by moisture content. It is rather influenced by the plies orientation, the pre-consolidation process and initial pre-drying. For laminates consolidated in HP, the deconsolidation dynamics is more severe in dried UD laminates compared to CP and QI laminates, and inversely in wet samples. Deconsolidation dynamics is also more pronounced in HP laminates compared to VBO laminates. Finally, initial pre-drying reduces the deconsolidation dynamics.

7.3.4.3 Maximum deconsolidation strain

DTS solely is not sufficient to highlight the mechanisms involved during deconsolidation, even if it shows the influencing factors of its dynamics. It is also necessary to take into account the maximum deconsolidation strain ε_D reached by the sample during heating. Figure 7.12 shows the maximum deconsolidation strain reached by the samples at both heating rates (10 °C/min and 60 °C/min) under No Counter Pressure (NCP).

Effect of moisture As for DTS, the increase in moisture content does not lead to a significant increase of Max ε_D (Figure 7.12 a, b). The Max ε_D difference between AS and WI samples is in average about 0.02 m/m. This supports that the samples strain evolution during deconsolidation stage is not related to moisture effect.

Effect of plies orientation There is no substantial difference between the UD and the CP or QI samples for both consolidation process (HP and VBO) and regardless of the heating rate (Figure 7.12 a, b). For example, the difference of Max ε_D between UD and CP samples initially consolidated by HP and VBO is respectively 0.02 m/m and 0.03 m/m. This means that plies orientation does not have an effect on the maximum magnitude of deconsolidation strain during heating, in the tested conditions.

Effect of pre-consolidation process At both heating rates, the Max ε_D of HP samples are higher than VBO samples one (Figure 7.12 a, b). The difference of Max ε_D between HP and VBO samples exceeds in average 0.1 m/m. Pre-consolidation process thus has an important impact on the sample maximal strain during deconsolidation.

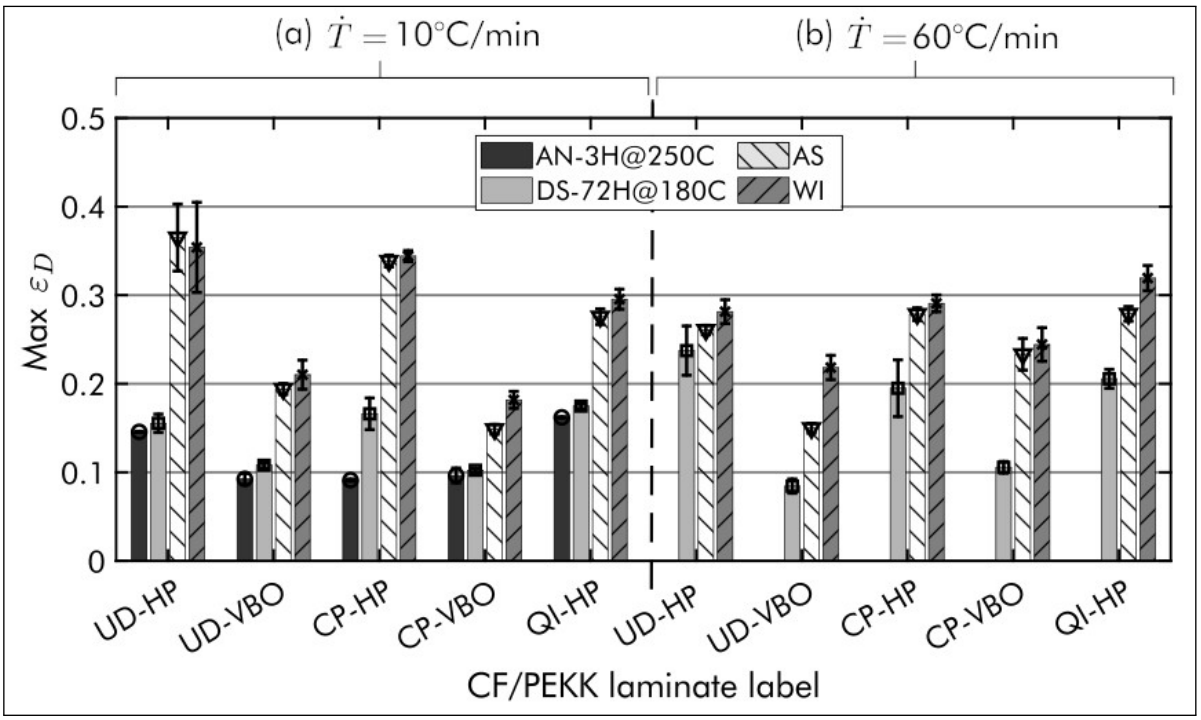

Figure 7.12: Maximum deconsolidation strain of the deconsolidated laminates at two different heating rates and under No Counter Pressure (NCP).

Effect of annealing The DS-72H@180C samples mainly have a low Max ε_D compared to the wet samples (Figure 7.12 a, b). However, there is not a considerable difference (ΔMax ε_D $\leq$0.03 m/m) between the short time annealed samples (AN-3H@250C) and the dried samples (DS-72H@180C). The difference of Max ε_D between both group of sample is inferior to 0.03 m/m. Again, the short time annealing (AN-3H@250C) was thus not effective to prevent deconsolidation in contrary to the long time drying (DS-1W@180C) and annealing (AN-48H@250C and AN-5D@250C).

The maximum magnitude of deconsolidation strain during heating is thus mainly driven by the initial pre-consolidation process and is affected by initial pre-drying or annealing. The maximum magnitude of deconsolidation strain is higher in HP laminates compared to VBO laminates. Initial drying of the samples leads to a reduction of the maximum deconsolidation strain. Finally full relaxation of residual stresses through long duration drying/annealing at high temperature ($\geq$ 180 °C) allows to prevent deconsolidation.

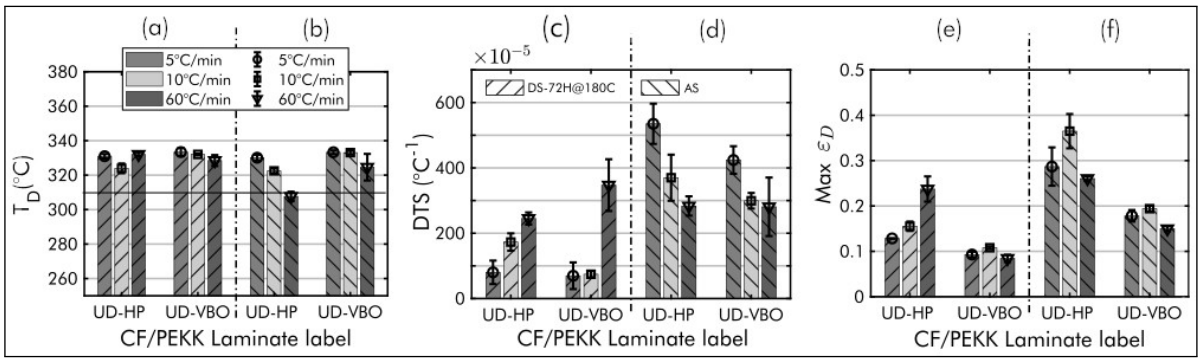

Figure 7.13: Effect of heating rate on deconsolidation characteristic magnitudes of DS-72H@180C (a, c, e) and AS (b, d, f) UD-HP and UD-VBO samples tested under No Counter Pressure (NCP).

7.3.4.4 Effect of heating rate

In order to check if the results obtained at 10 °C/min and 60 °C/min can be extrapolated to other heating rates, deconsolidation tests were performed at 5 °C/min on dried (DS-72H@180C) and wet (AS) UD-HP and UD-VBO samples under No Counter Pressure. Figure 7.13 shows the comparison between the different heating rates results for all the analyzed deconsolidation characteristic magnitudes.

Deconsolidation onset temperature Heating rate does not have a significant effect on the deconsolidation onset ($\Delta T_D \leq 5$ °C) in dried UD samples (Figure 7.13 a). The trend of decreasing deconsolidation temperature with increasing heating rate is only observed with AS samples (Figure 7.13 b). In fact, the difference ΔT_D between the T_D obtained at 5 °C/min and 10 °C/min is low (5 °C) compared to the difference between the one obtained at 10 °C/min and 60 °C/min (12 °C). These results show that the general trend observed not only on UD samples but also on CP and QI samples (see Figure 7.10 in Section 7.3.4.1) can be extrapolated to other heating rates.

Deconsolidation thermal sensitivity The experiments at 5 °C/min validate the effect of heating rate on deconsolidation dynamics. In the dried samples (DS-72H@180C), DTS increases with increasing heating rate (Figure 7.13 c). The opposite trend is observed in the case of AS samples, *i.e.* DTS decreases with increasing heating rate (Figure 7.13 d). This supports the non negligible effect of the initial pre-drying or annealing effect on the deconsolidation dynamics (see Section 7.3.4.2).

Maximum deconsolidation strain In dried UD-VBO samples, heating rate has not a significant effect (ΔMax ε_D $\leq$0.03 m/m) on the maximum deconsolidation strain (Figure 7.13 e). Conversely, Max ε_D increases with increasing heating rate in dried UD-HP samples (Figure 7.13 e). This different behavior between dried UD-HP and UD-VBO supports, again, the pre-consolidation process effect on the maximum deconsolidation strain (see Section 7.3.4.3).

When the samples are initially wet (AS), the Max ε_D obtained at 5 °C/min is bounded on the lower side by the Max ε_D obtained at 60 °C/min and on the upper side by the one at 10 °C/min (Figure 7.13 f). This indicates that there is a competition between the phenomena involved in deconsolidation which depends on the heating rate.

Depending on the initial preconditioning (dried or wet) and pre-consolidation process, the heating kinetics of the samples may significantly affect the onset, dynamics and amplitude of deconsolidation during CF/PEKK processing. For instance, in wet samples (AS) pre-consolidated in Hot Press, increasing heating rate from 10 °C/min to 60 °C/min decreases the onset temperature of deconsolidation, its dynamic and its maximum magnitude.

7.3.4.5 Effect of pressure

Up to this stage, only the online measurements obtained during the tests without counter pressure (NCP) were analyzed. To investigate the effect of pressure, deconsolidation tests were performed only on UD-HP samples at 10 °C/min under different counter pressure already mentioned in Table 7.4 (see Section 7.2.3.2). During these experiments, the pressure was maintained throughout the heating cycle. Figure 7.14 shows the influence of pressure on the deconsolidation characteristic magnitudes. The tests performed under 0.5 MPa for UD-HP samples and 0.1 MPa for UD-VBO samples were not added on Figure 7.14 because they did not produce deconsolidation. As already shown by the micrographs analysis (see Section 7.3.1.2), 0.1 MPa was sufficient to prevent deconsolidation in UD-VBO samples while for UD-HP samples, a minimum pressure of 0.5 MPa was required.

Deconsolidation onset temperature Regardless of the initial preconditioning, the samples tested under pressure have a higher deconsolidation temperature T_D. These temperatures were estimated with the thermal model by considering the change of thermal contact resistance with the application of pressure [16]. The temperature

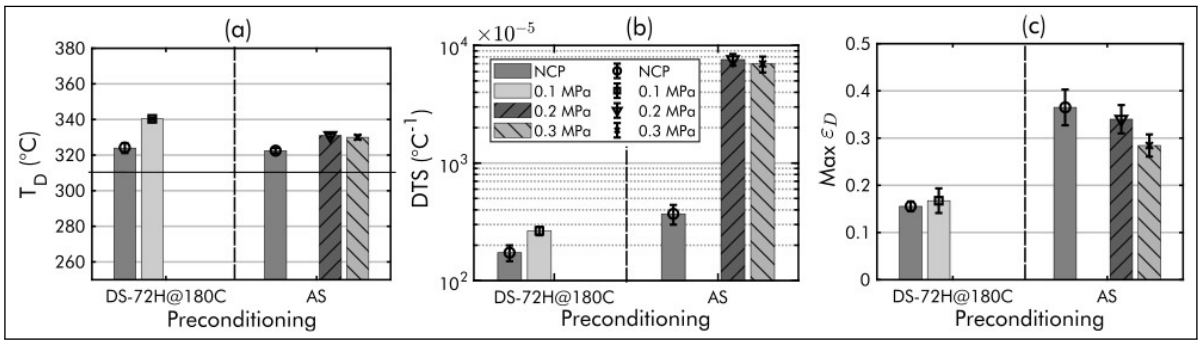

Figure 7.14: Effect of pressure on deconsolidation temperature T_D (a), deconsolidation's thermal sensitivity DTS (b) and the maximum deconsolidation strain Max ε_D (c) of AS and DS-72H@180C UD-HP samples tested at 10 °C/min under different counter pressure.

difference ΔT_D between the samples tested under counter pressure and under NCP is about 17 °C for dried samples and 10 °C for wet samples (Figure 7.14 a). However, increasing the counter pressure from 0.2 MPa to 0.3 MPa on AS samples does not result in a significant change ($\Delta T_D = 1$ °C) in the deconsolidation temperature. This observation shows that the application of a counter pressure during heating causes a shift in the deconsolidation temperature to a higher temperature (330 °C for AS and 340 °C for DS) which is almost insensitive to a subsequent pressure variation.

Deconsolidation thermal sensitivity There is a significant difference between the samples tested without counter pressure (NCP) and under counter pressure. In dried (DS-72H@180C) samples, DTS was multiply by two ($\times 2$) under 0.1 MPa, compared to the test without counter pressure (Figure 7.14 b). In AS samples, it is multiply by twenty ($\times 20$). On the one hand, this confirms that the lowering effect of initial pre-drying on the deconsolidation dynamics is also valid when the sample is under counter pressure. On the other hand, this observation shows that the application of pressure further accentuates the deconsolidation dynamics.

Maximum deconsolidation strain Below 0.3 MPa, a counter pressure application does not reduce significantly (ΔMax $\varepsilon_D \leq 0.02$ m/m) the samples maximum deconsolidation strain (Figure 7.14 c). The deconsolidation strain is significantly reduce from 0.3 MPa but only 0.5 MPa allowed to prevent deconsolidation. Consequently, there is a threshold between 0.3 MPa and 0.5 MPa below which deconsolidation of UD-HP laminates cannot be avoided. In the case of UD-VBO, 0.1 MPa was enough to avoid de-

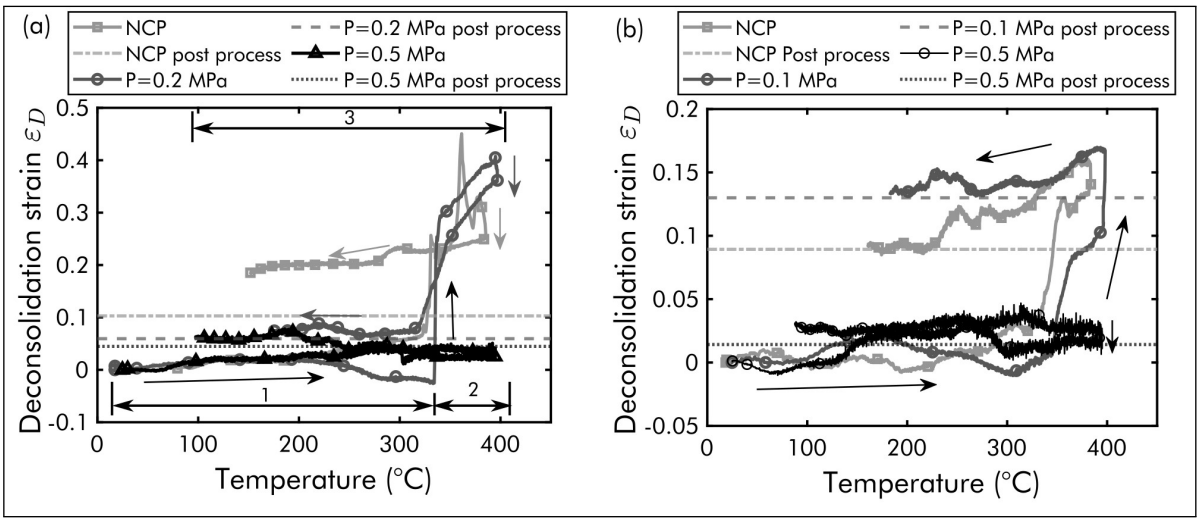

Figure 7.15: Through thickness deconsolidation strain ε_D at the center of a wet AS (a) and dried DS-72H@180C (b) UD-HP samples subjected to different counter pressure vs temperature (sample lower face temperature estimated with the thermal model).

consolidation of dried (DS-72H@180C) and wet (WI) samples. This supports, again, the important impact of the pre-consolidation process on the maximum deconsolidation strain during the heating stage.

In addition to the effect on the characteristic magnitudes, pressure also has an effect on the overall behavior of the samples during deconsolidation. This behavior is illustrated in Figure 7.15 with dried (DS-72H@180C) and wet (AS) samples. As described earlier in Section 7.3.2, the samples initially experiments roughly the same thermal expansion (stage 1). When no counter pressure is applied in the case of AS samples (Figure 7.15 a), a gradual evolution of the strain during deconsolidation is observed (stage 2). One notices the successive appearance of different peaks which correspond to a sequential appearance of large pores [21]. After this growth phase, the sample strain decreases until the cooling stage (stage 3) where the strain variation is no longer significant ($\Delta\varepsilon_D \approx 0.07\,\mathrm{m/m}$) compared to the deconsolidation stage ($\Delta\varepsilon_D \approx 0.45\,\mathrm{m/m}$). This behavior is consistent with the real-time microtomography during the same experiment [21].

When a counter pressure is applied, the sample behavior is different. During deconsolidation (stage 2), the sample strain increases rather fast at first and then gradually. Again, this growth phase is followed by a strain decrease. This time, the strain decreases significantly ($\Delta\varepsilon_D \approx 0.29\,\mathrm{m/m}$) before the sample solidification. Consequently,

although 0.2 MPa is not sufficient to prevent deconsolidation, it allows to re-consolidate the sample before cooling. This explains the low final porosity content observed on the post-process micrographs (see Figure 7.6 in Section 7.3.1.2). In the case of DS samples (Figure 7.15 b), 0.1 MPa was not sufficient to re-consolidate the samples before cooling. These observations show that even if low pressures (P$\leq$0.3 MPa) are sometimes not sufficient to prevent deconsolidation, they can in some cases re-consolidate the laminate, if the latter is held in the melt for sufficient duration.

7.4 Discussion

As highlighted in a previous study [21], the deconsolidation process in unidirectional prepreg-based TPC laminates includes 3 steps. The first step is pore nucleation which occurs after the glass transition temperature ($T_g \approx 160\,^{\circ}C$) before deconsolidation onset and extends throughout the heating stage of the laminates. The second step is pore growth which also starts after T_g but in a limited extent. The pore growth is more substantial when the composite reaches the onset temperature of deconsolidation. Finally, the last step is pore splitting or closure where the pores formed during the growth step, collapse and/or split into small-sized pores before cooling. The following sections discuss the influence of moisture, residual stresses and processing conditions on the deconsolidation process.

7.4.1 Influence of moisture

7.4.1.1 Nucleation

The final micrographs analysis performed in this study, clearly shows an effect of moisture on the pores spatial distribution in the laminates. In wet samples, the pores are mainly located on the laminates subsurface (Figure 7.7 a-d, i-l). In dried samples, the pores are instead mainly located in the middle of the laminates (Figure 7.7 e-h, m-n). Moreover, the online measurement show that deconsolidation occurs earlier in wet samples (Figure 7.10). These results are consistent with the *in situ* real-time microtomography and support the nucleating effect of moisture during the deconsolidation process [21]. Indeed, the moisture stored in wet samples during the preconditioning in ambient conditions or in water results from moisture transport mechanisms [15]. The moisture transport in the composite laminates starts from their boundaries then extends to the core due to the gradient of moisture concentration. Moisture is therefore

more concentrated near the sample surface, compared to the middle. Due to the very low moisture diffusion coefficient identified in a previous work [15], reaching a steady homogeneous moisture distribution may take a very long time.

In addition, moisture may be stored in the composites in two forms, namely "*weakly bonded*" water and "*strongly bonded*" water [15]. The "weakly bonded" water represents the water molecules stored in the free volumes within the composite laminates and the water molecules which form a single hydrogen bond with the polymer matrix. The "strongly bonded" water corresponds to the water molecules which form a double hydrogen bond with the polymer matrix. The free volumes may be nano or micro-pores located within the polymer matrix, at the fiber-matrix interfaces, or at the interplies.

During drying, the "weakly bonded" water desorbs from the composite but a high thermal energy is required to desorb the "strongly bonded" water. The thermogravimetric tests performed in a previous study from 140 °C to 300 °C revealed that during drying at 180 °C, only "weakly bonded" water is fully desorbed out of the composite samples [15]. This means that residual moisture, under a strongly bonded form always remains in the dried samples. As shown in [15] the amount of strongly bonded water with respect to the weakly bonded one may not be negligible due to the very small amount of moisture uptake in those materials.

It is assumed that there is no other residual volatiles apart from moisture in the dried samples. Other source of volatiles may be the additives used in prepreg manufacturing. However, the boiling point of these additives are often lower than the melting temperature (T_m) of the thermoplastic matrix. This results in the evaporation of most additives during the pre-consolidation step of the laminates. For this reason, the further drying at 180 °C has probably removed any residual volatiles from additives. Residual moisture bonded to the polymer matrix may thus explain the homogeneous distribution of the pores in the middle part of the dried samples.

The nucleating effect of moisture may also explain the accelerated onset of deconsolidation in wet samples compared to dried samples. As highlighted with the *in situ* microtomography in a previous study, compared to dried samples, the initial moisture content leads to a higher porosity content mainly located at the laminate interplies right before the deconsolidation onset [21]. These initial pores may weaken the interplies and thus lead to an early start of deconsolidation. Apart from the nucleating

effect, moisture may also affect the composite thermal and viscoelastic properties [23] and thus lead to an accelerated onset of deconsolidation. This has to be further checked in our case.

7.4.1.2 Growth

The micrographs and online measurements show that moisture has a negligible influence on the growth stage. An increase in moisture content neither lead to an increase in the final porosity content (Figure 7.5), nor does change the dynamics of deconsolidation (Figure 7.11) or the maximum strain (Figure 7.12). Moreover, deconsolidation does not occur after re-humidifying of annealed samples (Figure 7.6 c). These results suggest that moisture evaporation and/or diffusion is not the driving force of the pore growth during CF/PEKK laminates deconsolidation. In fact, to drive pore growth, moisture should diffuse into the nucleated pores to increase their interior pressure. The pores would then grow when the composite could no longer withstand this interior pressure. According to this phenomenological description, the increase in moisture content should lead to an increase in deconsolidation strain, since the pressure build-up inside the pores would be higher due to the higher moisture concentration.

This behavior is not observed in CF/PEKK laminates probably due to the very low moisture diffusion coefficient and the low moisture uptake in this material system. For example at 300 °C, moisture diffusivity D in CF/PEKK is estimated at $0.66 \times 10^{-9}\,\mathrm{m^2/s}$ [15] which is significantly low compared to its thermal diffusivity α which is about $0.26 \times 10^{-6}\,\mathrm{m^2/s}$ [24]. The ratio α/D between the thermal diffusivity and moisture diffusivity is thus 394 showing that moisture transport in CF/PEKK is extremely low compared to heat transport. This means that depending on the rate during the heating of wet samples, only some negligible amount of moisture probably desorbs out of the laminates during ramp-up. For example, a high heating rate may not allow a significant moisture desorption during ramp-up, compared to a low heating rate. A higher heating rate thus lead to a significant residual moisture at the deconsolidation onset, facilitating more pore nucleation. This may influence the early start of deconsolidation at high heating rates. However, the residual amount of moisture after desorption during ramp-up, may not have enough time to cause a pressure build-up inside the nucleated pores during deconsolidation at high heating rates.

7.4.2 Influence of residual stresses

All the results highlight the significant impact of pre-consolidation process on CF/PEKK deconsolidation. During HP consolidation process, the laminates were subjected to a high pressure (4 MPa) and rather fast cooling rate (10 °C/min). In addition to the fiber bed compaction, thermal and crystallization shrinkage and eventually the skin-core thermal gradient during cooling [25, 26] may lead to a complex three-dimensional residual stresses state stored in the laminates [27]. Subsequent re-heating of the consolidated laminates may lead to complex residual stresses loading phenomena causing the laminates deconsolidation.

Deconsolidation does not occur after re-humidifying in liquid water of annealed samples at 250 °C for 48 hours (Figure 7.6 c). Moreover, a drying at 180 °C for 1 week allowed to prevent deconsolidation (Figure 7.6 a), showing that the absence of deconsolidation in the annealed samples is not due to possible re-crystallization effects. Residual stresses thus appear to be the *driving force* of CF/PEKK laminates deconsolidation. Since the laminates were subjected to a low pressure (0.1 MPa) and a low cooling rate ($\approx$ 2 °C/min) during VBO processing, the residual stresses stored in VBO laminates are low compared to HP ones. This may explain the lower deconsolidation dynamics (Figure 7.11) and maximum strain (Figure 7.12) in VBO samples compared to HP samples. Since stress relaxation is enhanced over the material glass transition temperature ($T_g \approx$ 160 °C), some residual stresses may relax during the drying at 180 °C for 72 hours. This may explain the lower deconsolidation dynamics (Figure 7.11) and maximum strain (Figure 7.12) in dried samples compared to wet samples which were unable to relax their initial residual stresses before the experiments.

7.4.3 Influence of processing conditions

Apart from moisture and residual stresses, the laminates behavior during heating may also be significantly affected by some processing parameters such as plies orientation, heating rate and pressure.

Effect of plies orientation First, the results show a negligible impact of plies orientation on the maximum deconsolidation strain (Figure 7.12), suggesting that the residual stresses responsible of deconsolidation do not depend on plies orientation. It is however well known that the difference in orientation of plies induces internal stresses due to anisotropic shrinkage. This thus excludes as the origin of deconsolidation, the

residual stresses formed at *macromechanical level* on a ply-to-ply scale (see Figure 2.13 in Chapter 2) due to a difference in the transverse and longitudinal ply Coefficient of Thermal Expansion (CTE). In addition, the maximum deconsolidation strain of UD samples consolidated in VBO is lower than the Hot-Press consolidated one, and the pores are mainly located at the interplies. This also eliminates the residual stresses formed on the *micromechanical level* due to the mismatch in CTE between the fibers and the matrix CTE. Otherwise, the intraply pores should be also significant. We did prove here that those unavoidable stresses do not play a role on deconsolidation. We can therefore assume that the residual stresses responsible for deconsolidation are related to a fourth group of stress that are formed at the ply scale but are extrinsic, *i.e.* related to the consolidation process. The differences between VBO and HP suggest that these stresses are mainly related to consolidation pressure but further investigations are needed to confirm this.

Effect of heating rate In dried HP samples, increasing heating rate leads to increasing deconsolidation dynamics (Figure 7.13 c) and maximum strain (Figure 7.13 e). Since the same behavior was not observed in VBO samples, this cannot be attributed to thermal gradient effects. This behavior may be due to stress relaxation during ramp-up. Compared to a higher heating rate, a lower heating rate may allow the laminates to relax some residual stresses during ramp-up before deconsolidation onset.

However, a different behavior was observed in wet samples. The deconsolidation dynamics (Figure 7.13 d) and maximum strain (Figure 7.13 f) rather decrease with increasing heating rate. This may be attributed to a coupled effect of moisture and residual stresses at lower heating rates. Although the residual stresses are lower at deconsolidation onset (due to relaxation at low heating rates), the porosity content at the onset is much higher in wet samples due to moisture effect [21]. Consequently, a combination of the residual stresses and moisture effects, may lead to a higher deconsolidation strain at low heating rates in wet samples. This coupled effect on the pore growth was not observed in dried samples because of their low initial moisture content ($\ll 0.01\,\%$).

Effect of pressure A low counter pressure of 0.1 MPa was sufficient to prevent deconsolidation in wet VBO laminates while HP laminates required a minimum counter pressure of 0.5 MPa. This difference is explained by the low residual stresses stored in VBO laminates, compared to HP laminates.

7.5 Conclusion

Deconsolidation has a detrimental effect on TPC laminates. However, its understanding is still under investigations. In this work, the deconsolidation behavior of CF/PEKK was characterized experimentally.

The mechanisms involved during deconsolidation have been investigated through a parametric study. UniDirectional (UD), Cross-Ply (CP) and Quasi Isotropic (QI) laminates were consolidated in a Hot Press (HP) and by Vacuum Bag Only (VBO), in order to identify the effect of plies orientation and pre-consolidation process on deconsolidation. In order to analyze the influence of moisture and residual stresses, the consolidated laminates were subjected to different preconditioning treatments leading to several moisture content and residual stress level. Deconsolidation were characterized by post-process measurements (thickness measurements and micrographs) and online measurements on CODEC device. The online measurements allowed to quantify deconsolidation of CF/PEKK laminates under various conditions of heating rates and counter pressure representative of CF/PEKK processing.

The deconsolidation tests results show the complexity of the deconsolidation phenomenon which depends on several factors which effects are coupled. The post-process analysis limited the understanding of the phenomenon because of pore splitting during heating and shrinkage during cooling which respectively affect the final microstructure and thickness of the laminate. However, thanks to the online measurements using the CODEC device, the contribution of each factor on the CF/PEKK laminates deconsolidation was highlighted.

The results confirm that residual stresses are the driving forces of pore growth during CF/PEKK laminates deconsolidation. Moisture has a nucleating effects but does not affect the pore growth because of the slow moisture transport kinetic and low moisture uptake in this material system. However, results suggest an effect of moisture on CF/PEKK laminates thermal and viscoelastic properties which can lead to an accelerate onset of deconsolidation but further research is required to confirm this.

Results also reveal that the onset temperature of deconsolidation T_D depends mainly on moisture content (nucleating effects), heating rate and counter pressure. At low heating rates ($\leq$10 °C/min), deconsolidation occurs after the melting onset around

320 °C in dried samples and 310 °C when the moisture content is high (≈ 0.2 %). Increase in heating rate decreases the deconsolidation onset temperature which drop from 310°C at 10 °C/min to 300 °C at 60 °C/min.

Conversely, increase in counter pressure shifts the deconsolidation onset to higher temperature (over 330 °C). After the deconsolidation onset, the sample strain due to pore appearance and growth, depends mainly on the initial level of residual stresses stored in the CF/PEKK laminates. A higher level of residual stresses leads to a higher deconsolidation strain during heating. The plies orientation in the laminate have a negligible influence of the sample strain magnitude during heating but may affect the dynamics of pore growth. The samples strain is more sensitive to temperature variation in CP and QI when the laminates are not pre-dried.

Two means were used to prevent deconsolidation in this study, namely the application of sufficient counter pressure to counteract the residual stress loadings or long drying at temperatures above the glass transition temperature to relax residual stresses before processing. With VBO laminates, a minimum counter pressure of 0.1 MPa was sufficient while the HP laminates required 0.5 MPa to avoid deconsolidation. Regardless of the pre-consolidation process, a drying at 180 °C for 1 week or at 250 °C for 48 hours also allowed to prevent deconsolidation without having to apply a counter pressure.

It is suggested that the overall deconsolidation process in high-performance unidirectional prepreg-based TPC laminates is a coupled effect of two mechanisms: moisture evaporation and/or diffusion, thermomechanical stresses related to residual stresses or thermal gradients. The predominant mechanism during processing, will depend on the moisture-related properties of the material system (moisture diffusivity and maximum uptake) and the processing conditions. In this study, according to the laminates thickness, the thermal gradients in the samples were not high enough to highlight their effect on deconsolidation. In very thick samples, rapid heating may cause severe thermal gradients and also generate thermomechanical stresses in the laminates. In CF/PEKK laminates, deconsolidation results from the competition between thermomechanical forces (related to residual stresses) and the resistance exerted by the composite which depends on its thermo-viscoelastic properties and the external counter pressure.

This paper demonstrates that apart from applying a minimum counter pressure that prevents deconsolidation, minimizing residual stresses in pre-consolidated laminates could also be a way to avoid subsequent deconsolidation. Certainly, an annealing or

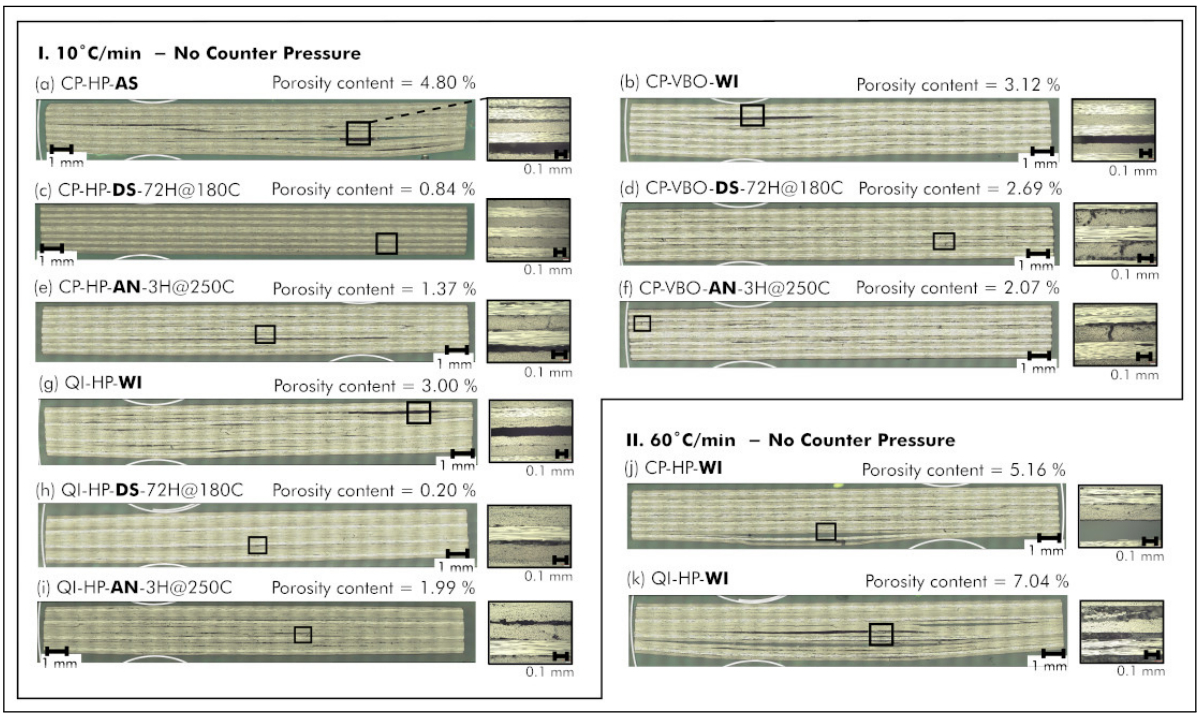

Figure 7.16: Post-process micrographs of deconsolidated CP-HP, CP-VBO and QI-HP samples tested at 10 °C/min (a-i) and 60 °C/min (j-k). The pores are mainly located at the interplies. Objective magnification ×200 and resolution 1.55^2 µm^2/pixel.

long drying step to relax stresses is not desirable, since it is time and energy consuming and takes away the benefit of rapid processing of TPC laminates. However, optimizing the laminates consolidation cycles in order to minimize residual stresses could be an alternative to avoid this additional step.

7.A Supplementary materials

Figure 7.16 shows some final micrographs of CP-HP, CP-VBO and QI-HP samples after the deconsolidation experiments at two different heating rates (10 °C/min, 60 °C/min).

References

[1] P. O. Hagstrand, F. Bonjour, and J. A. Månson, "The influence of void content on the structural flexural performance of unidirectional glass fibre reinforced polypropylene composites," *Composites Part A: Applied Science and Manufacturing*, vol. 36, pp. 705–714, 5 2005 (cit. on p. 201).

[2] H. Shi, I. F. Villegas, and H. E. Bersee, "Strength and failure modes in resistance welded thermoplastic composite joints: Effect of fibre-matrix adhesion and fibre orientation," *Composites Part A: Applied Science and Manufacturing*, vol. 55, pp. 1–10, 2013 (cit. on p. 201).

[3] X. Liu and F. Chen, "A Review of Void Formation and its Effects on the Mechanical Performance of Carbon Fiber Reinforced Plastic," *Engineering Transactions*, vol. 64, pp. 33–51, 2016 (cit. on p. 201).

[4] Y. Leterrier and C. G'sell, "Formation and Elimination of Voids During the Processing of Thermoplastic Matrix Composites," *Polymer Composites*, vol. 15, pp. 101–105, 2 1994 (cit. on p. 202).

[5] S. Roychowdhury, J. W. Gillespie, and S. G. Advani, "Volatile-induced void formation in amorphous thermoplastic polymeric materials: I. Modeling and parametric studies," *Journal of Composite Materials*, vol. 35, pp. 340–366, 4 2001 (cit. on p. 202).

[6] H. Shi, I. F. Villegas, and H. E. Bersee, "Analysis of void formation in thermoplastic composites during resistance welding," *Journal of Thermoplastic Composite Materials*, vol. 30, pp. 1654–1674, 12 2017 (cit. on p. 202).

[7] T. K. Slange, L. L. Warnet, W. J. Grouve, and R. Akkerman, "Deconsolidation of C/PEEK blanks: on the role of prepreg, blank manufacturing method and conditioning," *Composites Part A: Applied Science and Manufacturing*, vol. 113, pp. 189–199, 2018 (cit. on p. 202).

[8] M. Lu, L. Ye, and Y. W. Mai, "Thermal de-consolidation of thermoplastic matrix composites-II. "Migration" of voids and "re-consolidation"," *Composites Science and Technology*, vol. 64, pp. 191–202, 2 2004 (cit. on p. 202).

[9] L. Ye, Z. R. Chen, M. Lu, and M. Hou, "De-consolidation and re-consolidation in CF/PPS thermoplastic matrix composites," *Composites Part A: Applied Science and Manufacturing*, vol. 36, pp. 915–922, 7 2005 (cit. on p. 202).

[10] J. Wolfrath, V. Michaud, and J.-A. E. Månson, "Deconsolidation in glass mat thermoplastic composites: Analysis of the mechanisms," *Composites Part A: Applied Science and Manufacturing*, vol. 36, pp. 1608–1616, 12 2005 (cit. on p. 202).

[11] V. Donadei, F. Lionetto, M. Wielandt, A. Offringa, and A. Maffezzoli, "Effects of blank quality on press-formed PEKK/carbon composite parts," *Materials*, vol. 11, 7 2018 (cit. on p. 202).

[12] C.-C. M. Ma and S.-W. Yur, "Environmental effects on the water absorption and mechanical properties of carbon fiber reinforced PPS and PEEK composites. Part II," *Polymer Engineering & Science*, vol. 31, no. 1, pp. 34–39, 1991 (cit. on p. 202).

[13] C.-C. M. Ma, C.-L. Lee, M.-J. Chang, and N.-H. Tai, "Hygrothermal behavior of carbon fiber-reinforced poly (ether ether ketone) and poly (phenylene sulfide) composites. I," *Polymer composites*, vol. 13, no. 6, pp. 448–453, 1992 (cit. on p. 202).

[14] K.-M. Lee, S.-J. Park, T. Yu, S.-J. Park, and Y.-H. Kim, "Experimental prediction of internal defects according to defect area on NDI via water absorption behavior," *International Journal of Modern Physics B*, vol. 35, no. 14n16, p. 2 140 021, 2021 (cit. on p. 202).

[15] L. Amedewovo, A. Levy, B. de Parscau du Plessix, L. Orgéas, and S. Le Corre, "Online characterization of moisture transport in a high-performance carbon fiber-reinforced thermoplastic composite at high temperatures: Identification of diffusion kinetics," *Composites Part B: Engineering*, vol. 256, p. 110 629, 2023 (cit. on pp. 202, 207, 234–236).

[16] L. Amedewovo, A. Levy, B. de Parscau du Plessix, J. Aubril, A. Arrive, L. Orgéas, and S. Le Corre, "A methodology for online characterization of the deconsolidation of fiber-reinforced thermoplastic composite laminates," *Composites Part A: Applied Science and Manufacturing*, vol. 167, p. 107 412, 2022 (cit. on pp. 202–203, 206, 208, 211, 215, 220, 222, 231).

[17] T. K. Slange, "Rapid Manufacturing of Tailored Thermoplastic Composites by Automated Lay-up and Stamp Forming," Ph.D. dissertation, University of Twente, 2019 (cit. on p. 202).

[18] H. Perez-Martin, P. Mackenzie, A. Baidak, C. M. Ó. Brádaigh, and D. Ray, "Crystallinity studies of PEKK and carbon fibre/PEKK composites: A review," *Composites Part B: Engineering*, vol. 223, p. 109 127, 2021 (cit. on p. 203).

[19] J. Avenet, "Assemblage par fusion de composites à matrice thermoplastique: caractérisation expérimentale et modélisation de la cinétique d'auto-adhésion hors équilibre," Ph.D. dissertation, Université de Nantes (UN), 2021 (cit. on p. 203).

[20] H. Pérez-Martín, P. Mackenzie, A. Baidak, C. M. Ó. Brádaigh, and D. Ray, "Crystallisation behaviour and morphological studies of PEKK and carbon fibre/PEKK composites," *Composites Part A: Applied Science and Manufacturing*, p. 106 992, 2022 (cit. on p. 203).

[21] L. Amedewovo, L. Orgéas, B. de Parscau du Plessix, N. Lefevre, A. Levy, and S. Le Corre, "Deconsolidation of carbon fiber-reinforced PEKK laminates: 3D real-time *in situ* monitoring with synchrotron X-ray microtomoghraphy," In preparation (cit. on pp. 204, 215, 220–221, 233–235, 238).

[22] I. Arganda-Carreras, V. Kaynig, C. Rueden, K. W. Eliceiri, J. Schindelin, A. Cardona, and H. S. Seung, "Trainable Weka Segmentation: a machine learning tool for microscopy pixel classification," *Bioinformatics*, vol. 33, pp. 2424–2426, 15 2017 (cit. on p. 215).

[23] M. Coulson, L. Quiroga Cortés, E. Dantras, A. Lonjon, and C. Lacabanne, "Dynamic rheological behavior of poly (ether ketone ketone) from solid state to melt state," *Journal of Applied Polymer Science*, vol. 135, no. 27, p. 46 456, 2018 (cit. on p. 236).

[24] M. Coulson, E. Dantras, P. Olivier, N. Gleizes, and C. Lacabanne, "Thermal conductivity and diffusivity of carbon-reinforced polyetherketoneketone composites," *Journal of Applied Polymer Science*, vol. 136, no. 38, p. 47 975, 2019 (cit. on p. 236).

[25] J. Favre, "Residual thermal stresses in fibre reinforced composite materials, a review," vol. 1, no. 1, pp. 37–53, 1988 (cit. on p. 237).

[26] P. P. Parlevliet, H. E. Bersee, and A. Beukers, "Residual stresses in thermoplastic composites—A study of the literature—Part I: Formation of residual stresses," *Composites Part A: Applied Science and Manufacturing*, vol. 37, no. 11, pp. 1847–1857, 2006 (cit. on p. 237).

[27] M. M. Shokrieh, *Residual stresses in composite materials*. Woodhead publishing, 2014 (cit. on p. 237).

CHAPTER 8

GENERAL CONCLUSION AND PERSPECTIVES

Contents

8.1 Objective and scope reminder

Deconsolidation is a major concern regarding the current ambitions to develop Out Of Autoclave (OOA) consolidation techniques and welding technologies for high-performance ThermoPlastic Composites (TPCs) in large aircraft structures. Although the phenomenon is well identified industrially, it has been the subject of very few studies with regard to high-performance TPCs. Several questions about deconsolidation remained unanswered. For example, what is the physical origin of deconsolidation? What are the mechanisms involved during deconsolidation? When and where does deconsolidation occur? *etc.* So many questions that there is currently no predictive model of high-performance TPCs deconsolidation which was experimentally validated (at the best of the author knowledge). The objective of this thesis was thus to provide an in-depth understanding of the physical origin of deconsolidation and its driving mechanisms, which will supply physically motivated pore growth model and allow a better control of TPCs processing. Several experimental studies have been performed to achieve this goal. The investigations were carried out on a high-performance TPC used industrially in the aerospace sector (CF/PEKK provided by Toray Advanced Composites).

8.2 Main results overview

After reviewing the literature (Chapter 3), two main hypotheses emerged to explain the physical origin of deconsolidation: the presence of *moisture* and/or the stored *residual stresses* after laminates pre-consolidation. However, the focus of this thesis was not only to study the contribution of these two factors, but also to consider the influence of the *pre-consolidation method* and the *process parameters* during post-processing (shaping or welding) such as heating rate, pressure, dwell time and plies orientation in the laminates.

8.2.1 Moisture transport in CF/PEKK laminates

First, in order to properly decouple the effect of moisture from the effect of residual stresses, a study was performed on moisture transport mechanisms in CF/PEKK (Chapter 4). A new ThermoGravimetric Analysis (TGA) device called Online Moisture Ingress CHAracterization (OMICHA) bench has been developed and validated purposely (Figure 8.1 a). The device allows to continuously measure weight variation of large composite samples (up to 150 mm $\times$ 150 mm $\times$ 10 mm with

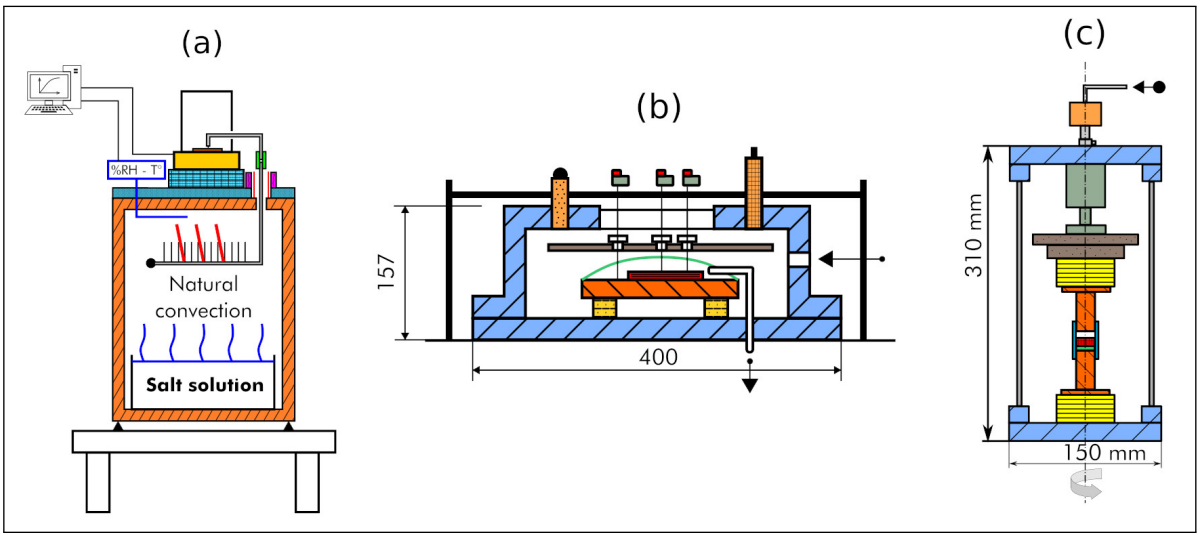

Figure 8.1: Experimental benches developed in this work. Schematic view of (a) Online Moisture Ingress CHAracterization (OMICHA) bench, (b) COmposite DEconsolidation Characterization (CODEC) bench and (c) *In situ* COmposite DEcconsolidation Tomography Observation (InCODETO).

a weight up to 36 g) under controlled and high temperature (up to 330 °C) and/or humid environment, with a relative error of 0.03 % (for samples weighing more than 1 g). The desorption tests carried out at high temperatures (from 140 °C to 300 °C), using the OMICHA device, reveal that moisture may be stored in CF/PEKK laminates in two forms: "weakly bonded water" and " strongly bonded water". This results in two diffusion mechanisms which were highlighted by the thermogravimetric experiments.

Moisture desorption is either Fickian ($T \leq$200 °C) or Non-Fickian ($T \geq$250 °C) depending on the heating temperature T. This dual behavior was described, with a good correlation, by a dual stage model. Furthermore, CF/PEKK laminates have low moisture diffusivities D_1 at high temperatures. D_1 ranges from 14.46×10^{-12} m^2/s at 140 °C to 660.49×10^{-12} m^2/s at 300 °C. In comparison, CF/PEKK laminate thermal diffusivity is about 0.26×10^{-6} m^2/s at 300 °C.

Based on these results, the samples were dried for 72 hours at 180 °C to study the effect of residual stresses solely. The effect of moisture was highlighted with two group of samples stored in ambient conditions (AS) for 5 months (moisture content: 0.01 wt.%) or immersed in distilled water (WI) at room temperature ($\approx$ 23 °C) for

1 year (moisture content: 0.2 wt.%). Other preconditioning conditions were also used to highlighted residual stresses effect, namely long drying for 1 week at 180 °C or annealing for 3 hours, 48 hours and 5 days at 250 °C.

8.2.2 Development and validation of CODEC

Following the initial preconditioning of the samples, deconsolidation tests were performed on the preconditioned samples. These tests consisted in applying a temperature cycle to the samples under or without counter pressure P. In order to be representative of the processing cycles of high-performance TPCs and also to better control the experiment conditions (temperature, heating rate $\dot{T}$, counter pressure), a new ThermoMechanical Analysis (TMA) device named COmposite DEconsolidation Characterization (CODEC) bench (Figure 8.1 b) has been developed (Chapter 5). CODEC allows to characterize deconsolidation *in situ* through continuous and online strain measurement of large samples (up to 150 mm $\times$ 50 mm), under industrial conditions (Max $T = 450$ °C, Max $\dot{T} = 60$ °C/min, Max $P = 1$ MPa) with a relative error of $\pm$ 2 %.

The first results obtained using CODEC reveals that *post-process measurements* solely (thickness and micrographs after experiment) are not representative of the micro and macrostructural changes that occur in the composite during heating. The continuous and online measurements performed in CODEC, showed that the maximum deconsolidation strain (Max ε_D) of the sample during heating is much higher (about 60 %) than the final strain measured using post-process techniques. The results clearly showed that post-process measurements solely are not suitable to understand the development of pores during processing. From the continuous and online strain measurement, the dynamics of deconsolidation as well as its onset conditions (T,P, *etc.*) and its magnitude (Max ε_D) have been characterized. However, strain measurement is a macroscopic measurement at the sample scale.

8.2.3 Real-time synchrotron X-ray tomography of CF/PEKK laminates during processing

In order to validate that the strain measurements actually correlate with the pore growth within the composite, a study was performed on the micro-structural changes that take place in the laminates during deconsolidation (Chapter 6). A specific device called *In situ* COmposite DEconsolidation Tomography Observation (InCODETO) bench was developed for this purpose (Figure 8.1 c). The device allows to apply a

temperature and pressure cycle (Max $T = 450\,°C$, Max $\dot{T} = 2\,°C/s$, Max $P = 1.12\,MPa$) representative of TPCs processing, on small samples of 20 mm diameter, while enabling synchrotron X-ray microtomography observation. The InCODETO bench was installed in the X-ray microtomograph of the ID19 beamline at the European Synchrotron Radiation Facilities (ESRF Grenoble, France).

The deconsolidation experiments using InCODETO were performed on small Uni-Directional (UD) and Cross-Ply (CP) samples initially dried (72H@180C) or stored in distilled water at room temperature ($\approx 23\,°C$) for 3 months (moisture content: 0.1 wt.%). Analysis of the tomographic scans performed at a resolution of $3.81^3\ \mu m^3/voxel$, reveals that the entire out-of-plane strain observed during deconsolidation is completely driven by the pore growth. This validated the reliability of the macro-scale strain measurements to reflect the porosity content evolution during deconsolidation. However, this correlation between strain and porosity content is only true during deconsolidation. In fact, the tomographic observations showed that the porosity content is almost constant during cooling even though the strain decreases due to shrinkage.

Furthermore, the tomographic observations showed that regardless of the initial preconditioning or plies orientation in the laminates, the deconsolidation process includes 3 stages: *nucleation*, *growth* and *splitting*. The nucleation stage begins before deconsolidation onset, after the material glass transition temperature (T_g) (160 °C) and results in the appearance of small rod-like and blade-like pores, which are mostly less than 30 µm long and oriented parallel to the fiber's principal axis. The nucleation extends throughout the composite heating stage.

Regarding the pore growth stage, it also begins after T_g but is severely limited before deconsolidation onset. For instance, the porosity content does not exceed 0.2 % and the pore lengths a few hundreds micrometers (between 100 µm and 230 µm), before deconsolidation. However, pore growth is significantly enhanced at the deconsolidation onset, leading to the formation of large rod-like, blade-like and disk-like pores (length $\gg 1\,mm$) oriented parallel to the fibers. During deconsolidation, the pores grow like crack propagation in a solid and lead to a decohesion at the interplies. The growth goes in both directions but the in-plane growth is much higher than the out-of-plane one. The tomograms analysis suggests that the pores mainly grow by *coalescence* through interface failure between neighboring pores, under thermomechanical loadings.

Once the composite laminates reached their maximum strain at the end of the growth stage, the large pores collapse or split into small pores due to the elastic recovery of the fiber bed (that were initially buckled during pore growth) and the effect of gravity or an external counter pressure. This is the splitting stage. In our test conditions, a re-consolidation pressure of 0.1 MPa allowed to reduce the porosity content from 13 % to 0.6 %.

The tomographic observations reveal that the 3 stages of the deconsolidation process occurs mainly at the interplies. Regardless of the initial preconditioning (dry or wet) pore nucleation always occurs, meaning that both residual stresses and moisture are involved in the nucleation process. However, the presence of moisture accelerates the nucleation. Moreover, deconsolidation occurs earlier in wet samples compared to dried ones, suggesting an effect of moisture on the composite thermal and viscoelastic properties. Although this study at the fibers scale allowed to identify the involved mechanisms that occur in the composite during processing, it does not clearly highlight the driving force of deconsolidation.

8.2.4 Parametric study of the mechanisms involved during deconsolidation

Following the study at the fibers scale, an extensive parametric study was performed at the laminates scale, on the driving mechanisms of deconsolidation (Chapter 7). The effect of moisture, residual stresses, pre-consolidation process, ply orientation, heating rate, dwell time and pressure were investigated. The laminates were initially manufactured by Hot Press Consolidation (HPC) and Vacuum Bag Only Consolidation (VBOC) with three different stacking sequence, namely UD, CP and Quasi Isotropic (QI). The samples (size: 125 mm $\times$ 25 mm $\times$ 2.90 mm) were then subjected to different preconditioning treatment according to the strategy defined after the study on moisture transport in CF/PEKK (see Section 8.2.1). The deconsolidation experiments were performed on the CODEC device at three different heating rates (5 °C/min, 10 °C/min, 60 °C/min), two different dwell times (5 min, 25 min) and under No Counter Pressure (NCP) or applied counter pressure (from 0.1 MPa to 0.5 MPa).

The results of the parametric showed that residual stresses are the driving forces of pore growth during deconsolidation in CF/PEKK laminates. A drying for 72 hours at 180 °C or annealing for 3 hours at 250 °C did not allow to avoid deconsolidation. Instead, a long drying for 1 week at 180 °C or annealing for 48 hours at 250 °C allowed to relax

the residual stresses and thus prevent deconsolidation without the application of any counter pressure. When residual stresses are not relaxed before post-processing, a counter pressure can be applied. In this study, a minimum counter pressure of 0.5 MPa was sufficient to prevent deconsolidation during heating of Hot Press-consolidated laminates. However, a lower counter pressure ($<$0.5 MPa) can reduce the porosity content (re-consolidation) after deconsolidation but does not guarantee an acceptable final porosity content (%Porosity$<$1 %).

Regarding moisture, the results reveal that it affects the pore nucleation (thermodynamic phenomenon) and does not significantly influence the pore growth (kinetic phenomenon) due to the low moisture diffusivity and moisture uptake in CF/PEKK laminates. Moreover, the results obtained at 10 °C/min showed that deconsolidation occurs earlier (T_D =310 °C) when the initial moisture weight content of the laminates is higher or equal to 0.2 %, suggesting that moisture may affect the thermal and viscoelastic properties of CF/PEKK laminates. In samples initially dried or with a low moisture content (around 0.01 wt.%), deconsolidation occurs in the melting zone (T_D $\geq$320 °C). However, increasing the heating rate from 10 °C/min to 60 °C/min lowered the onset temperature by 10 °C.

Furthermore, the parametric study also showed that the deconsolidation process is affected by the pre-consolidation process and post-processing conditions. For instance, a low counter pressure of 0.1 MPa was sufficient to prevent deconsolidation in the laminates manufactured by VBOC, unlike Hot Press-consolidated laminates. Moreover, the maximum strain (Max ε_D) of the laminates during deconsolidation is significantly low with VBOC laminates. With respect to post-processing conditions, Max ε_D is not influenced by the plies orientation or the dwell duration. The pore growth during deconsolidation is mainly temperature-dependent. It occurs almost instantly and can last less than 1 min. However, the splitting stage which determine the final porosity content is time-dependent. When no counter pressure was applied during the heating, a minimum of 5 min was required to achieve a steady state of the sample strain. A longer dwell time has therefore no significant influence on the final porosity content.

8.3 Perspectives

8.3.1 Short-term

- The results of this thesis provide insights into the phenomenology of deconsolidation. We now know the physical origin (why), the occurrence conditions (when), the mechanisms involved (how) and where deconsolidation occurs during CF/PEKK laminates post-processing (shaping or welding). Now the first question that arises is whether the described phenomenology is applicable to other polymers of the PolyArylEtherKetone (PAEK) family and other fiber architecture (woven fabrics). Additional experiments with another polymer matrix of the PAEK family or high performance woven fabric composites, would provide an answer to this question.
- Deconsolidation appears to be a result of the competition between thermomechanical forces (related to residual stresses) and the resistance exerted by the composite which depends on its thermo-viscoelastic properties and the external counter pressure. Although the results suggest an effect of moisture on a reduction of the composite thermo-viscoelastic properties, a characterization of moisture effect on these properties would confirm or refute this hypothesis.

8.3.2 Mid-term

- This study indicated that the appearance and growth of pores during deconsolidation may affect the effective thermal conductivity k_{eff} of the composite laminates. It would thus be interesting to characterize this evolution of k_{eff} as a function of the porosity content ϕ. Since the porosity content changes significantly throughout the processes (welding or thermostamping), this relationship $k_{eff}(\phi)$ would improve the temperature fields of the laminates estimated by simulation. This would allow a more accurate temperature control of the laminates during processing.
- On the industrial level, this thesis work provides three possible ways to prevent deconsolidation. The first option is to dry the composite at a temperature higher than T_g in order to relax the post-consolidation residual stresses (24 hours at 250 °C or 1 week at 180 °C). The second option is to apply sufficient counter

pressure to counteract the residual stress loadings (0.1 MPa for VBOC laminates and 0.5 MPa for HPC ones). The third option is to minimize the residual stresses by optimizing the laminates consolidation cycles. For example, VBOC allows to minimize residual stresses, thus reducing to 0.1 MPa the minimum counter pressure required to prevent deconsolidation.

8.3.3 Long-term

Based on the phenomenology described in this work, a predictive model of deconsolidation could be developed. This model should take into account not only the initial moisture content and distribution in the laminates but also the amount of residual stresses stored after pre-consolidation.

- Regarding the initial moisture content, it can be predicted knowing the evolution of moisture diffusivity D as function of temperature T, and the relation between moisture content at saturation M_∞ and the relative humidity RH. $D(T)$ was provided in this work. Additional thermogravimetric experiments could be performed at different relative humidity to identify $M_\infty(RH)$.
- With respect to the initial amount of residual stresses, it would be interesting to quantify it with a numerical model (viscoelastic model for example). This would require a characterization of the viscoelastic properties of the composite and its crystallization kinetics.
- Finally, the pore growth could be predicted by a thermo-viscoelastic model coupled with moisture diffusion and pore nucleation phenomena. Furthermore, the studies carried out in this work have produced a lot of data that can be used to improve phenomenological models (from the literature) in a relevant way. They can take into account: moisture diffusion as obtained in Chapter 4, a more realistic pore geometry as observed in Chapter 6 and they can be validated on a large range of parameters with experimental data (Chapter 6 and 7).

"This page left intentionally blank"

CHAPTER 9

EXTENDED SUMMARY IN FRENCH

Contents

9.1 Introduction

9.1.1 Contexte et motivation

Les émissions de CO_2 de l'aviation commerciale n'ont cessé d'augmenter au cours des dernières années, approchant les 1 milliards de tonnes de CO_2 par an [1]. Cela représente environ 2 % de toutes les émissions d'origine humaine. Entre 2004 et 2022 (avant COVID[1]), les émissions du secteur ont augmenté de près de 50 % [1]. Dans un contexte d'activité croissante dans le monde, ces émissions pourraient encore augmenter de plus de 50 %, pour atteindre environ 2 milliards de tonnes de CO_2 si aucune mesure n'est prise [2]. Le principal défi de l'aviation dans les prochaines années réside donc dans sa décarbonation, afin de répondre aux enjeux de la transition écologique et aux attentes des passagers en matière de mobilité durable. Dans cette optique, l'industrie aéronautique et les compagnies aériennes ont décidé de prendre le taureau par les cornes il y a plusieurs années en s'engageant à réduire leur contribution au réchauffement climatique, avec un objectif extrêmement ambitieux à l'horizon 2050 : diviser par deux les émissions de carbone du secteur par rapport à 2005, c'est à dire zéro émissions nettes (équilibre entre la quantité de gaz à effet de serre produite et la quantité retirée de l'atmosphère).

Outre les carburants aéronautiques durables (Sustainable Aviation Fuels, SAF en anglais) ou les nouvelles technologies de moteurs et d'avions, la réduction de poids est un facteur non négligeable de réduction de la consommation de carburant et des émissions de CO_2. Celà a conduit à une popularité accrue (malgré leur coût généralement élevé) des *matériaux composites* dans les pièces de haute performance qui doivent être légers. Par rapport aux matériaux plus conventionnels tels que les alliages d'aluminium ou de titane, les matériaux composites ont de meilleures propriétés spécifiques (rapport entre les propriétés mécaniques et la densité). L'amélioration continue des constituants du composite (matrice et renfort) a donné naissance à des matériaux composites de haute performance, aux propriétés thermomécaniques et à la résistance chimique améliorées, capables de remplacer les matériaux conventionnels dans les structures primaires. Cela se reflète dans les dernières générations d'avions tels que l'Airbus A350 XWB [3] et le Boeing 787 Dreamliner [4] dans lesquels la moitié du poids total est constituée de matériaux composites.

[1] COVID est une épidémie que le monde a connue vers la fin de 2019 et qui se poursuit à ce jour.

Outre l'aspect environnemental, l'utilisation de matériaux composites présente également un avantage économique important. Par exemple, les coûts d'assemblage peuvent représenter jusqu'à 50 % du coût d'une cellule d'avion. Les composites offrent la possibilité de réduire considérablement la quantité de travail d'assemblage et de fixations, car les pièces détaillées peuvent être combinées en un seul assemblage par moulage [5]. De plus, les composites ne se corrodent pas et leur résistance à la fatigue est exceptionnelle. La corrosion des alliages d'aluminium représente un coût important et un problème de maintenance constant pour les avions commerciaux. La résistance à la corrosion des composites peut donc permettre de réaliser d'importantes économies sur les coûts de maintenance. Cependant, les composites ont des coûts de matières premières élevés et généralement des coûts de fabrication et d'assemblage élevés. Par conséquent, pour répondre à la demande croissante de matériaux composites, leurs procédés de fabrication doivent être optimisés en réduisant les temps de cycle, les coûts énergétiques, *etc*.

9.1.2 Composites à matrice thermoplastique pour des applications structurelles aéronautique

Les matériaux composites, notamment les plastiques renforcés de fibres de carbone (CFRP en anglais), sont classés en deux catégories selon le type de matrice polymère (thermodurcissable ou thermoplastique). Les époxydes sont actuellement la matrice polymère traditionnelle utilisée dans de nombreuses structures haute performance, notamment pour les applications aéronautiques ou aérospatiales. Cependant, les fabricants ont manifesté un intérêt croissant pour l'introduction de plus en plus de composites à matrice thermoplastique (TPC en anglais) dans les structures des avions au cours de ces dernières années. Cet intérêt est illustré par le démonstrateur de fuselage multifonctionel (MFFD en anglais) réalisé en TPC et qui est l'une des plus grandes ($8\,\mathrm{m} \times 4\,\mathrm{m}$) aérostructures ThermoPlastic Composite (TPC) au monde, développée dans le cadre du projet Clean Sky 2 STUNNING mené par Airbus [6] (voir Figure 1.1 dans le chapitre 1). Cet intérêt est motivé par les avantages considérables qu'offrent les TPCs en termes d'assemblage, de réparabilité et de fabrication automatisée à haute cadence.

Cependant, la plupart des procédés de mise en œuvre des stratifiés TPC haute performance sont toujours en cours de développement. Le thermo-estampage de pièces à géométrie complexe n'est pas encore totalement maîtrisé. La consolidation *in situ*

n'est pas encore totalement maîtrisée et nécessite souvent une étape de consolidation ultérieure en autoclave. La consolidation de pièces épaisses uniquement sous bâche à vide en étuve est également en étude. En ce qui concerne le soudage, qui représente le principal avantage des TPCs, la plupart des procédés de soudage ne sont pas encore assez matures pour être industrialisés. Toutefois, plusieurs efforts de recherche et développement sont consacrés à une bonne maîtrise de la fabrication à haute cadence des TPCs, en particulier des procédés de soudage.

9.1.3 Problématique de déconsolidation

La mise en œuvre des stratifiés TPC préconsolidés (formage ou soudage) comprend le réchauffage, la reconsolidation et le refroidissement. Durant la première étape, les stratifiés préconsolidés sont réchauffés au-dessus de leur température de fusion (T_f). Le réchauffage peut être *global* (thermoestampage ou co-consolidation), ou *localisé* uniquement à l'interface de soudure (soudage par fusion). Pendant la reconsolidation, une contre-pression est appliquée pour mettre en forme le composite ou pour assurer un contact intime à l'interface de soudure. Les pièces composites formées ou assemblées sont ensuite refroidies pour figer leur état. Bien que le principe semble simple, l'applicabilité des stratifiés TPC est actuellement limitée par le phénomène de *déconsolidation*.

La déconsolidation fait référence à l'apparition et la croissance de pores pendant le réchauffage des stratifiés. Elle se produit lorsqu'aucune ou une faible contre-pression est appliquée pendant le réchauffage, ce qui est le cas pour la plupart des procédés de soudage ou de thermoformage. Par conséquent, il est parfois nécessaire d'appliquer une contre-pression de valeur généralement inconnue tout au long du procédé, afin d'empêcher la déconsolidation. Cela complique considérablement l'application du thermoformage ou du soudage sur des pièces épaisses ou à géométrie complexe. Le problème est que la présence de pores dans les composites dégrade fortement leur résistance mécanique [7–9]. Pour cette raison, les pièces dont le taux de porosité dépasse un seuil défini (1 % dans l'aéronautique) sont généralement rejetées.

9.1.4 Objectifs de la thèse

Bien que la problématique de déconsolidation soit bien identifiée industriellement, sa modélisation et les solutions optimales pour l'éviter sont aujourd'hui peu étudiées. Afin de prévenir la déconsolidation et d'optimiser la qualité des pièces produites, il

est nécessaire d'améliorer notre compréhension des causes et des mécanismes qui régissent le phénomène. L'objectif de cette thèse est donc de fournir une compréhension approfondie de l'origine physique de la déconsolidation et de ses mécanismes moteurs. Pour atteindre cet objectif, les conditions thermo-mécaniques de la consolidation et de la déconsolidation doivent être soigneusement contrôlées et analysées à l'échelle macroscopique (ou du stratifié) et microscopique (ou des fibres). De nouvelles techniques expérimentales seront donc développées dans cette étude afin de caractériser finement les conditions de déconsolidation (température, contre-pression, teneur en humidité, vitesse de chauffage, *etc.*) aux échelles macroscopique et microscopique. L'impact des conditions de fabrication des stratifiés (processus de consolidation, préconditionnement) sera également analysé pour comprendre l'effet d'une éventuelle redistribution/relaxation des contraintes résiduelles sur la déconsolidation. L'investigation portera sur un TPC haute performance utilisé industriellement dans le secteur aéronautique. Il s'agit d'un pré-imprégné unidirectionel (UD) à base de fibres de carbone renforcées de PolyEtherCetoneCetone (PEKK en anglais) avec une masse surfacique de fibres (FAW) de 194 g/m^2 et une épaisseur théorique de 0.185 mm, fourni par Toray Advanced Composites.

9.2 Synthèse des principaux résultats

Après une revue de la littérature (Chapitre 3), deux hypothèses principales ont émergé pour expliquer l'origine physique de la déconsolidation : la présence de *humidité* et/ou des *contraintes résiduelles* stockées après la préconsolidation des stratifiés. Cependant, l'objectif de cette thèse n'est pas seulement d'étudier la contribution de ces deux facteurs, mais aussi de considérer l'influence de la méthode de préconsolidation (presse ou étuve) et des paramètres procédé pendant la mise en œuvre (formage ou soudage) tels que la vitesse de chauffage, la contre-pression, le temps de palier et l'orientation des plis dans les stratifiés.

9.2.1 Transport de l'humidité dans les stratifiés CF/PEKK

Tout d'abord, afin de découpler correctement l'effet de l'humidité de celui des contraintes résiduelles, une étude a été réalisée sur les mécanismes de transport de l'humidité dans les CF/PEKK (Chapitre 4). Pour ce faire, un nouveau dispositif d'Analyse ThermoGravimétrique (ATG) appelé banc OMICHA a été développé et validé (voir Figure 8.1 a dans le Chapitre 8). Le dispositif permet de mesurer en

continu la variation de masse d'échantillons composites de grande taille (jusqu'à 150 mm × 150 mm × 10 mm avec une masse allant jusqu'à 36 g) dans un environnement contrôlé, à haute température (jusqu'à 330 °C) et/ou humide, avec une erreur relative de 0.03 % (pour les échantillons pesant plus de 1 g). Les essais de désorption réalisés à hautes températures (de 140 °C à 300 °C), à l'aide du dispositif OMICHA, révèlent que l'humidité peut être stockée dans les stratifiés CF/PEKK sous deux formes : "eau faiblement liée" et "eau fortement liée". Il en résulte deux mécanismes de diffusion qui ont été mis en évidence par les expériences thermogravimétriques.

La désorption de l'humidité est soit Fickienne ($T \leq 200\,°C$) soit Non-Fickienne ($T \geq 250\,°C$) en fonction de la température de chauffage T. Ce double comportement a été décrit, avec une bonne corrélation, par un modèle dit "dual stage". Par ailleurs, les stratifiés CF/PEKK présentent de faibles diffusivités d'humidité D_1 à hautes températures. La valeur D_1 varie de $14.46 \times 10^{-12}\,m^2/s$ à 140 °C à $660.49 \times 10^{-12}\,m^2/s$ à 300 °C. En comparaison, la diffusivité thermique du stratifié CF/PEKK est d'environ $0.26 \times 10^{-6}\,m^2/s$ à 300 °C.

En se basant sur ces résultats, les échantillons ont été séchés pendant 72 heures à 180 °C pour éliminer l'effet de l'humidité afin d'étudier uniquement l'effet des contraintes résiduelles. Quant à effet de l'humidité, il a été mis en évidence avec deux groupes d'échantillons stockés dans des conditions ambiantes (AS) pendant 5 mois (teneur en humidité : 0.01 wt. %) ou immergés dans de l'eau distillée (WI) à température ambiante ($\approx$ 23 °C) pendant 1 année (teneur en humidité : 0.2 wt.%). D'autres conditions de préconditionnement ont également été utilisées pour mettre en évidence l'effet des contraintes résiduelles, à savoir un séchage long pendant 1 semaine à 180 °C ou un recuit pendant 3 heures, 48 heures et 5 jours à 250 °C.

9.2.2 Développement et validation de CODEC

Après le préconditionnement initial des échantillons, des tests de déconsolidation ont été réalisés sur les échantillons préconditionnés. Ces tests ont consisté à appliquer un cycle de température aux échantillons avec ou sans contre-pression P. Afin d'être représentatif des cycles de mise en œuvre des TPCs haute performance et également mieux contrôler les conditions d'essai (température, vitesse de chauffe $\dot{T}$, contre-pression), un nouveau dispositif d'Analyse ThermoMécanique (TMA en anglais) nommé banc CODEC (voir Figure 8.1 b dans le Chapitre 8) a été développé (Chapitre 5). CODEC permet de caractériser la déconsolidation *in situ* par la mesure continue et en

ligne de la déformation d'échantillons de grande taille (jusqu'à 150 mm × 50 mm), dans des conditions industrielles (Max $T = 450\,^{\circ}\mathrm{C}$, Max $\dot{T} = 60\,^{\circ}\mathrm{C/min}$, Max $P = 1\,\mathrm{MPa}$) avec une erreur relative de $\pm\,2\,\%$. Les premiers résultats obtenus à l'aide de COmposite DEconsolidation Characterization (CODEC) révèlent que les *mesures post-processus* seules (épaisseur et micrographies après expérience) ne sont pas représentatives des changements micro et macrostructuraux qui se produisent dans le composite pendant le chauffage. Les mesures continues et en ligne effectuées dans CODEC, ont montré que la déformation maximale de déconsolidation (Max ε_D) de l'échantillon pendant le chauffage est beaucoup plus élevée (environ 60 %) que la déformation finale mesurée à l'aide des techniques de post-traitement. Les résultats montrent clairement que les mesures post-processus seules ne sont pas appropriées pour comprendre le développement des pores pendant le traitement. La mesure continue et en ligne de la déformation a permis de caractériser la dynamique de la déconsolidation ainsi que ses conditions de déclenchement (T, P, *etc.*) et son ampleur (Max ε_D). Cependant, la mesure de la déformation est une mesure macroscopique à l'échelle de l'échantillon.

9.2.3 Tomographie en temps réel par rayons X synchrotron de stratifiés CF/PEKK durant la mise en œuvre

Afin de valider que les mesures de déformation correspondent réellement à la croissance des pores dans le composite, une étude a été réalisée sur les changements microstructuraux qui ont lieu dans les stratifiés pendant la déconsolidation (Chapitre 6). Un dispositif spécifique appelé banc InCODETO a été développé dans ce but (voir Figure 8.1 c dans le Chapitre 8). Ce dispositif permet d'appliquer un cycle de température et de pression (Max $T = 450\,^{\circ}\mathrm{C}$, Max $\dot{T} = 2\,^{\circ}\mathrm{C/s}$, Max $P = 1.12\,\mathrm{MPa}$) représentatif des procédés de mise en œuvre des TPCs, sur de petits échantillons de 20 mm de diamètre, tout en permettant l'observation par microtomographie aux rayons X synchrotron. Le banc InCODETO a été installé dans le microtomographe à rayons X de la ligne de faisceau ID19 de l'European Synchrotron Radiation Facilities (ESRF Grenoble, France).

Les expériences de déconsolidation à l'aide de InCODETO ont été réalisées sur de petits échantillons d'unidirectionels (UD) et d'empilements croisés (CP) initialement séchés (72H@180C) ou stockés dans de l'eau distillée à température ambiante ($\approx 23\,^{\circ}\mathrm{C}$) pendant 3 mois (teneur en humidité : 0.1 wt.%). L'analyse des scans tomographiques réalisés à une résolution de $3.81^3\ \mu\mathrm{m}^3/\mathrm{voxel}$, révèle que la totalité de la déformation hors plan observée pendant la déconsolidation est entièrement due à la croissance

des pores. Ceci a validé la fiabilité des mesures de déformation à l'échelle macro pour refléter l'évolution du taux de porosité pendant la déconsolidation. Cependant, cette corrélation entre déformation et taux de porosité n'est vraie que pendant la déconsolidation. En effet, les observations tomographiques ont montré que le taux porosité est presque constant pendant le refroidissement, même si la déformation diminue en raison du retrait.

En outre, les observations tomographiques ont montré qu'indépendamment du préconditionnement initial ou de l'orientation des plis dans les stratifiés, le processus de déconsolidation comprend 3 étapes : *nucléation*, *croissance* et *effondrement*. L'étape de nucléation commence avant le début de la déconsolidation, après que le matériau ait atteint sa température de transition vitreuse T_g (160 °C) et se traduit par l'apparition de petits pores en forme de bâtonnets ou de lames, dont la longueur est généralement inférieure à 30 µm et orientés parallèlement à l'axe principal des fibres. La nucléation s'étend tout au long de l'étape de chauffage du composite.

En ce qui concerne la phase de croissance des pores, elle commence également après glass transition temperature (T_g) mais est fortement limitée avant le début de la déconsolidation. Par exemple, le taux de porosité ne dépasse pas 0.2 % et la longueur des pores quelques centaines de micromètres (entre 100 µm et 230 µm) avant la déconsolidation. Cependant, la croissance des pores est significativement accélérée au début de la déconsolidation, conduisant à la formation de grands pores en forme de bâtonnets, de lames et de disques (longueur $\gg$ 1 mm) orientés parallèlement aux fibres. Pendant la déconsolidation, les pores se développent comme une propagation de fissure dans un solide et conduisent à une décohésion aux interfaces interplis. La croissance se fait dans les deux directions mais la croissance dans le plan est beaucoup plus importante que celle hors-plan. L'analyse des tomogrammes suggère que les pores se développent principalement par *coalescence* par rupture d'interface entre les pores voisins, sous un chargement thermomécanique.

Une fois que les stratifiés composites ont atteint leur déformation maximale à la fin de la phase de croissance, les grands pores s'effondrent ou se subdivisent en petits pores en raison du retour élastique des fibres (qui étaient initialement déformées pendant la croissance des pores) et de l'effet de la gravité ou d'une contre-pression externe. C'est le stade de l'effondrement. Dans nos conditions d'essai, une pression de re-consolidation de 0.1 MPa a permis de réduire le taux de porosité de 13 % à 0.6 %.

Les observations tomographiques révèlent que les 3 étapes du processus de déconsolidation se produisent principalement aux interfaces entre les plis. Quel que soit le préconditionnement initial (sec ou humide), la nucléation des pores se produit toujours, ce qui signifie que les contraintes résiduelles et l'humidité sont toutes deux impliquées dans le processus de nucléation. Cependant, la présence d'humidité accélère la nucléation. De plus, la déconsolidation se produit plus tôt dans les échantillons humides que dans les échantillons secs, ce qui suggère un effet de l'humidité sur les propriétés thermiques et viscoélastiques du composite. Bien que cette étude à l'échelle des fibres ait permis d'identifier les mécanismes qui se produisent dans le composite pendant la mise en œuvre, elle ne met pas clairement en évidence la force motrice de la déconsolidation.

9.2.4 Étude paramétrique des mécanismes impliqués dans la déconsolidation

Après l'étude à l'échelle des fibres, une étude paramétrique approfondie a été réalisée à l'échelle des stratifiés, sur les mécanismes pilotant la déconsolidation (Chapitre 7). Les effets de l'humidité, des contraintes résiduelles, du procédé de pré-consolidation, de l'orientation des plis, de la vitesse de chauffage, du temps de palier et de la pression ont été étudiés. Les stratifiés ont été initialement fabriqués par consolidation sous presse (HPC) et en étuve sous bâche à vide (VBOC) avec trois séquences d'empilement différentes, à savoir UD, CP et quasi isotropique (QI). Les échantillons (taille: 125 mm $\times$ 25 mm $\times$ 2.90 mm) ont ensuite été soumis à différents traitements de préconditionnement selon la stratégie définie après l'étude sur le transport de l'humidité dans le CF/PEKK (voir section 9.2.1). Les essais de déconsolidation ont été réalisées sur le dispositif CODEC avec trois vitesses de chauffage différentes (5 °C/min, 10 °C/min, 60 °C/min), deux temps de palier différents (5 min, 25 min) et sans (NCP) ou avec une contre-pression appliquée (de 0.1 MPa à 0.5 MPa).

Les résultats de l'étude paramétrique ont montré que les contraintes résiduelles sont les forces motrices de la croissance des pores pendant la déconsolidation des stratifiés CF/PEKK. Un séchage de 72 heures à 180 °C ou un recuit de 3 heures à 250 °C n'ont pas permis d'éviter la déconsolidation. En revanche, un long séchage de 1 semaine à 180 °C ou un recuit de 48 heures à 250 °C ont permis de relaxer les contraintes résiduelles et donc d'empêcher la déconsolidation sans l'application d'une quelconque contre-pression. Lorsque les contraintes résiduelles ne sont pas relaxées avant la mise en

œuvre, une contre-pression peut être appliquée. Dans cette étude, une contre-pression minimale de 0.5 MPa était suffisante pour empêcher la déconsolidation pendant le chauffage des stratifiés consolidés sous presse à chaud. Cependant, une contre-pression plus faible ($<$0.5 MPa) peut réduire le taux de porosité (re-consolidation) après déconsolidation mais ne garantit pas un taux de porosité final acceptable (%Porosité$<$1 %).

En ce qui concerne l'humidité, les résultats révèlent qu'elle affecte la nucléation des pores (phénomène thermodynamique) et n'influence pas significativement la croissance des pores (phénomène cinétique) en raison de la faible diffusivité de l'humidité et de la teneur en humidité dans les stratifiés CF/PEKK. En outre, les résultats obtenus à 10 °C/min ont montré que la déconsolidation se produit plus tôt (T_D =310 °C) lorsque la teneur en humidité initiale des stratifiés est supérieure ou égale à 0.2 %, ce qui suggère que l'humidité peut affecter les propriétés thermiques et viscoélastiques des stratifiés CF/PEKK. Dans les échantillons initialement séchés ou ayant une faible teneur en humidité (environ 0.01 wt.%), la déconsolidation se produit dans la plage de fusion (T_D $\geq$320 °C). Cependant, l'augmentation de la vitesse de chauffage de 10 °C/min à 60 °C/min a diminué la température de démarrage de 10 °C.

En outre, l'étude paramétrique a également montré que le processus de déconsolidation est affecté par le procédé de pré-consolidation et les conditions de mise en œuvre. Par exemple, une faible contre-pression de 0.1 MPa était suffisante pour empêcher la déconsolidation dans les stratifiés fabriqués par VBOC, contrairement aux stratifiés consolidés sous presse à chaud. De plus, la déformation maximale (Max ε_D) des stratifiés pendant la déconsolidation est significativement faible avec les stratifiés Vacuum Bag Only Consolidation (VBOC). En ce qui concerne les conditions de mise en œuvre, la déformation maximale (Max ε_D) n'est pas influencée par l'orientation des plis ou la durée de palier. La croissance des pores pendant la déconsolidation dépend principalement de la température. Elle se produit presque instantanément et peut durer moins de 1 min. Cependant, l'étape d'effondrement qui détermine la taux de porosité final dépend du temps. Lorsqu'aucune contre-pression n'a été appliquée pendant le chauffage, un minimum de 5 min a été nécessaire pour atteindre un état stable de la déformation de l'échantillon. Un temps de palier plus long n'a donc pas d'influence significative sur le taux de porosité final.

References

[1] IATA. "Carbon dioxide emissions from commercial aviation worldwide from 2004 to 2022 (in million metric tons)." (2023), [Online]. Available: https://www.statista.com/statistics/1186820/co2-emissions-commercial-aviation-worldwide/ (visited on 2023) (cit. on p. 256).

[2] O. Wyman. "Projected CO_2 emissions from the aviation industry between 2022 and 2050, by scenario (in billion metric tons)." (2022), [Online]. Available: https://www.statista.com/statistics/1189613/projected-co2-emission-aviation-worldwide/ (visited on 2023) (cit. on p. 256).

[3] "Airbus A350 Family." (2013), [Online]. Available: https://www.airbus.com/en/products-services/commercial-aircraft/passenger-aircraft/a350-family (visited on 2022) (cit. on p. 256).

[4] "Boeing 787 Family." (2013), [Online]. Available: https://www.boeing.com/commercial/787/by-design/#/advanced-composite-use (visited on 2022) (cit. on p. 256).

[5] F. C. Campbell, *Lightweight materials: understanding the basics*. ASM international, 2012 (cit. on p. 257).

[6] "Multi-Functional Fuselage Demonstrator." (2023), [Online]. Available: https://www.jeccomposites.com/news/the-largest-thermoplastic-aerostructures-successfully-manufactured-as-part-of-the-multi-functional-fuselage-demonstrator-project/ (visited on 2023) (cit. on p. 257).

[7] D. Saenz-Castillo, M. Martín, S. Calvo, F. Rodriguez-Lence, and A. Güemes, "Effect of processing parameters and void content on mechanical properties and NDI of thermoplastic composites," *Composites Part A: Applied Science and Manufacturing*, vol. 121, pp. 308–320, 2019 (cit. on p. 258).

[8] M. L. Costa, S. f. M. De Almeida, and M. C. Rezende, "The influence of porosity on the interlaminar shear strength of carbon/epoxy and carbon/bismaleimide fabric laminates," *Composites Science and Technology*, vol. 61, no. 14, pp. 2101–2108, 2001 (cit. on p. 258).

[9] M. R. Wisnom, T. Reynolds, and N. Gwilliam, "Reduction in interlaminar shear strength by discrete and distributed voids," *Composites Science and Technology*, vol. 56, no. 1, pp. 93–101, 1996 (cit. on p. 258).

"This page left intentionally blank"

Titre : Etude du phénomène de déconsolidation dans les matériaux composites à matrice thermoplastique en relation avec le procédé de consolidation

Mots clés : Composite thermoplastique, porosité, contrainte résiduelle, humidité, soudage

Résumé : Le phénomène de déconsolidation se produit dans un composite thermoplastique lorsque celui-ci est réchauffé au-delà d'une certaine température. Si un confinement mécanique insuffisant est appliqué pendant ce chauffage, il peut alors apparaître des pores sous différentes formes (bulles, fissures, délaminages, *etc.*) qui vont dégrader très fortement la tenue mécanique des pièces. Ce problème est particulièrement important dans les procédés continus tels que la dépose de bandes, ou plus particulièrement le soudage, car les pièces à assembler sont chauffées, au moins localement, au-delà de leur température de fusion. Il est ainsi parfois nécessaire d'appliquer une certaine contrepression, de valeur mal connue, tout au long du processus de soudage. Ceci complique sensiblement la mise en œuvre de ces technologies. La compréhension de la déconsolidation, sa modélisation et les solutions optimales pour y remédier sont aujourd'hui peu étudiées, bien que le phénomène soit désormais bien identifié industriellement. Ce travail de thèse s'intéresse donc à la compréhension de l'origine physique de la déconsolidation ainsi que les différents mécanismes en jeu depuis l'apparition des pores jusqu'à leur croissance, à l'aide d'études expérimentales. Pour se faire, trois dispositifs innovants ont été développés (OMICHA, CODEC, InCODETO), permettant de caractériser finement aux échelles macro et méso les conditions thermomécano-diffusif de la déconsolidation. Les résultats fournissent la compréhension physique nécessaire pour une modélisation du phénomène et une meilleure maîtrise des procédés de soudage par fusion.

Title: Study of Thermoplastic Matrix Composites Deconsolidation Phenomenon by Considering the Consolidation Process

Keywords: Thermoplastic composite, porosity, residual stress, moisture, welding

Abstract: Deconsolidation occurs in a thermoplastic composite when it is heated above a certain temperature. If a low mechanical constraint is applied during this heating, pores may appear in various forms (bubbles, cracks, delamination, etc.) which will severely degrade the mechanical strength of the parts. This problem is particularly important in continuous processes such as *in situ* consolidation, or welding, since the parts being joined are heated, at least locally, above their melting temperature. Therefore, it is sometimes necessary to apply a counter pressure, of unknown value, throughout the welding process. This complicates significantly the implementation of these technologies. The understanding of deconsolidation, its modeling and the optimal solutions to prevent it are little study today, although the phenomenon is now well identified industrially. This thesis is thus interested in understanding the physical origin of deconsolidation as well as the different mechanisms involved from the appearance of pores to their growth, through experimental investigations. To do so, three innovative experimental benches have been developed (OMICHA, CODEC, InCODETO), allowing to finely characterize at macro and meso scales the thermomechanical-diffusive conditions of deconsolidation occurence. The results provide the physical understanding necessary for a modeling of the phenomenon and a better control of fusion welding processes.